Experimental Testing of Realistically Sized and Loaded FRP-Confined Prismatic Reinforced Concrete Columns

Coonan, Rachel

Award date:
2016

Awarding institution:
University of Bath

Experimental Testing of Realistically Sized and Loaded FRP-Confined Prismatic Reinforced Concrete Columns

Rachel Mary Coonan

A thesis submitted for the Degree of Doctor of Philosophy

University of Bath

Department of Architecture and Civil Engineering

October 2016

[BLANK PAGE]

ABSTRACT

An investigation into the achievable gain in axial strength capacity of FRP-confined prismatic reinforced concrete columns compared to unconfined columns when subject to axial and axial-flexural loading has been performed. An experimental test matrix of small-, medium-, and large-scale specimens addressed; size effect, load eccentricity and cross-sectional aspect ratio, allowing for detailed study of the cross-sectional behavioural mechanics and generation of an analytical model capturing the evolution of the cross-sectional behaviour.

Experimental results demonstrated that an increase in axial capacity of 48% was achievable in axially loaded specimens, but was limited by cross-sectional geometry, and inevitable second order effects, that were more extensive with increasing load eccentricity. There was a corresponding reduction in confinement effectiveness, thus more FRP plies or straps are required when subject to large bending. Furthermore, with increasing load eccentricity, there is a beneficial increase in lateral deformation capacity. All specimens of rectangular cross-section benefit from FRP-confinement but this decreases with increasing aspect ratio. Lastly, experimental testing highlighted the importance of debonding, as the side length of the specimen between corners increases, small areas to the whole side of the specimen detached.

Confinement of prismatic columns is achieved using the resistance generated in the FRP jacket as the concrete laterally expands, generating confining stresses at the convex corners under axial loading. Analysis of FRP strains at mid-height of the specimen show the formation of a cruciform shape originating at the corners, along the diagonals of the cross-section. As eccentric load is applied, the strains evolve into the higher compressive region, moving the effectively confined area over into this compressive region. Variation of the cross-sectional aspect ratio also dictates a change in effectively confined area, with higher strains generated next to the shorter side lengths. This complex behaviour necessitates research into large-scale specimens as the size effect does not encourage scaling of results from small-scale testing.

ACKNOWLEDGEMENTS

The research presented in this thesis was undertaken at the Department of Architecture and Civil Engineering at the University of Bath between September 2007 and September 2010. The research was gratefully funded by the Engineering and Physical Sciences Research Council (EPSRC). Similarly, the author would like to extend gratitude to the associated partners of the project; the Building Research Establishment and the Fibre Reinforced Polymer supplier, BASF.

The author would like to thank all those who have been instrumental in facilitating with this research, specifically the project supervisors, Dr Antony Darby and Prof Tim Ibell. Mention should be made to the laboratory staff at the University of Bath, who have spent considerable hours on various aspects of the project construction and testing. Specifically, Will Bazely, who accompanied the author to the BRE Watford facility for all specimen testing, and Brian Purnell, whose extensive experience in construction was invaluable.

Lastly, the author would also like to thank her parents for their never-ending support, especially during the write-up of the thesis and to her father for willingly assuming the role of editor! The author also extends thanks to her family, her partner, Stuart Wright, who has been incredibly encouraging, understanding and reassuring during the write-up of the thesis, and her daughter Molly, an adorable bundle of joy. The most inspirational person in this whole journey has been the author's Grandfather, Nicholas MacRae, an engineer himself, who has had continual curiosity in this research and is the reason for the author's interest in engineering in the first place.

Rachel Coonan

1st August 2016

TABLE OF CONTENTS

LIST OF TABLES

CHAPTER 2

CHAPTER 3

CHAPTER 4

CHAPTER 5

LIST OF FIGURES

CHAPTER 3

CHAPTER 4

CHAPTER 5

NOMENCLATURE

A_c	Area of concrete
A_e	Effectively confined area
A_g	Gross cross-section area
A_{ol}	Area of overlap in rectangular cross-section
A_s	Area of longitudinal tensile steel
b	Width of section
D	Diameter of circular column
d_c	Depth to concrete block in design
d_s	Depth to steel over cross-section
E_c	Design modulus of elasticity of concrete
E_{cm}	Secant modulus of elasticity of concrete
$E_{c,eff}$	Effective modulus of elasticity of concrete
E_{fd}	Design elastic modulus of FRP
E_{fk}	Characteristic elastic modulus of FRP
E_s	Modulus of elasticity of steel (typical 200GPa)
$\bar{E}_{fs}$	Secant modulus of FRP jacket material determined from tensile coupon tests
E_0	Secant modulus of concrete … Ecm
E_2	Slope of linear portion of confined concrete stress-strain curve
e_i	Nominal eccentricity of load on column
e_2	Lateral deflection due to second order effects for slender columns
f_c	Concrete strength capacity in design
$f_{c,uc}$	Concrete strength capacity in design, unconfined area
$f_{c,A}$	Concrete strength capacity in design, area A
$f_{c,B}$	Concrete strength capacity in design, area B
f_{c0}	Unconfined concrete compressive stress
f_{cc}	Confined concrete axial compressive strength
f_{cc}^*	Peak axial stress of concrete under constant confining pressure f_l
f_{ccd}	Design confined concrete compressive strength

f_{ck}	Characteristic compressive cylinder strength of concrete
f_{ctk}	Characteristic tensile strength of concrete (ideally derived from insitu pull-off tests)
f_{ctm}	Mean concrete tensile strength
f_{cu}	Characteristic compressive cube strength of concrete
f_{fd}	Design tensile strength of FRP
f_{fk}	Characteristic tensile strength of FRP
f_{fr}	Strength of FRP jacket material, determined from FRP coupon tests
f_{fu}	FRP ultimate tensile strength
f_l	Effective confining pressure
f_r	Equivalent confining pressure
f_{yd}	Design yield strength of longitudinal reinforcement
f_{yk}	Characteristic yield strength of longitudinal reinforcement
g_s	Shape factor [TR55 (2005)]
H	Height of column
H_{corbel}	Height of column including corbels
h	Overall depth of section
I_c	Second moment of area of uncracked concrete section
K_r	Correction factor depending on axial load
K_φ	Factor considering creep
k_e	Confinement effectiveness factor
k_1	Confinement effectiveness coefficient
k_{s1}	Shape factor
k_2	Strain enhancement coefficient
k_{s2}	Shape factor
k_ε	FRP efficiency factor
l_0	Effective length of column
l_{ol}	Length of overlapping region [TR55 (2005)]
M_{Ed}	Design ultimate moment
M	Moment in specimen
N	Ultimate axial load on column
N_0	Theoretical axial capacity of column under concentric loading
n_f	Number of FRP plies
P	Allowable load in design of corbels
R_c	Corner radius of prismatic column
r	Radius of gyration
r_m	Moment ratio
s	Spacing of steel stirrups

s_d	Standard deviation
t_f	Thickness of FRP laminate
T	Total thickness of FRP
x	Depth of neutral axis
x_g	Distance between strain gauges
α	Angle of failure in corbel design
β	Angle between the principal fibres of the FRP and a line perpendicular to the longitudinal axis of the member
Υ	Design cracking of corbel
γ_{mc}	Partial safety factor for concrete
δ_1	Relative displacement vector
ε_c	Axial strain in concrete
ε_{c2}	Axial strain in unconfined concrete at peak stress
ε_{cc}	Confined concrete axial strain
$\varepsilon_{cc,max}$	Maximum concrete strain in confined rectangular columns
ε_{cc}^*	Peak strain of concrete under constant confining pressure f_l
ε_{co}	Axial strain in concrete at peak stress
ε_{cu}	Axial strain of concrete at failure
ε_{ccu}	Confined concrete ultimate axial strain
ε_{fd}	Design ultimate strain of FRP
ε_{fe}	Effective FRP strain
$\varepsilon_{h,debond}$	Strain at which FRP wrap debonds
$\varepsilon_{h,rup}$	Hoop rupture strain of FRP
ε_j	Hoop tensile strain in FRP at failure
ε_{ju}	Ultimate tensile rupture strain
ε_s	Strain in stirrups for design
ε_t	Position of transition region between parabola and straight line for confined concrete
ε_y	Yield strain of steel
H	Dilation ratio of concrete
η_u	Limiting dilation ratio at failure
μ	Poisson's ratio
μ_s	Secant dilation ratio
μ_t	Tangent dilation ratio
λ	Slenderness ratio
λ_{crit}	Critical slenderness ratio for strengthened sections
λ_{lim}	Limiting slenderness ratio for strengthened sections
ρ_f	Ratio
ρ_ε	Confinement strain ratio

ρ_k	Confinement stiffness ratio
ρ_{sc}	Ratio of longitudinal steel in cross-section
σ_c	Axial stress of confined concrete
σ_{g1}	Stress at strain gauge
σ_l	Stress longitudinal
$\emptyset_s$	Steel bar diameter
$\tau_{lim,c}$	Limiting longitudinal shear stress in concrete
Φ	Internal angle of friction of concrete
φ_{ef}	Effective creep coefficient

CHAPTER 1

INTRODUCTION

1.1. BACKGROUND

This chapter introduces the use of fibre composites as a strengthening mechanism for structurally deficient reinforced concrete (RC) columns of prismatic cross-section. It highlights the benefits and concerns of this strengthening technique, and the aspects requiring further development. Furthermore, the objectives of this research project and the methodology adopted for testing are described.

1.2. BACKGROUND TO STRENGTHENING RC COLUMNS

It is widely known that when concrete exceeds ultimate strength under compression, the load-carrying capacity reduces progressively as the deformation increases. The deformational response exhibits a trend similar to that of a triaxial stress-strain relationship, which consists of a two phase response, initially ascending linearly until reaching ultimate strength, followed by a gradually descending response, referred to as softening, Figure 1-1.

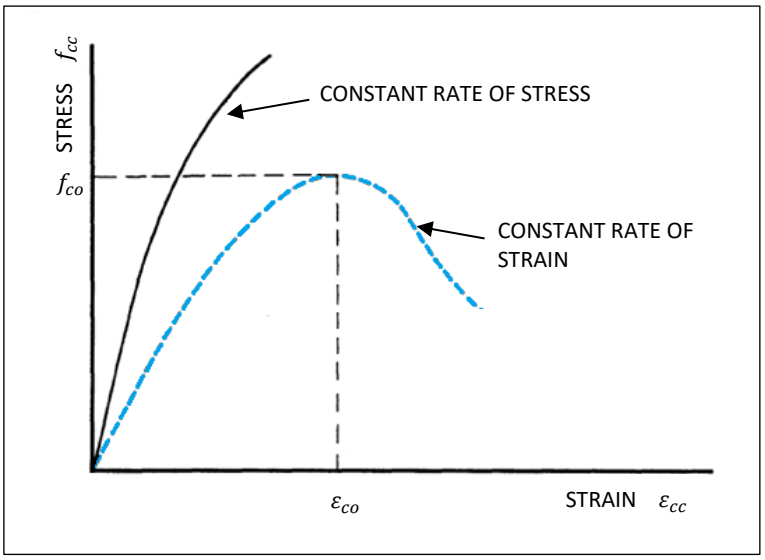

Figure 1-1: Stress-strain curve of unconfined concrete [Popovic (1973)]

Popovic (1973) established the stress-strain curve of concrete and demonstrated two responses; a stress controlled loading process (top curve in Figure 1-1) and a controlled constant rate of strain response, (bottom curve in Figure 1-1). Generally, testing of concrete specimens is displacement controlled thus the strain response is representative.

1.2.1. STRENGTHENING OF RC COLUMNS

Strengthening of deteriorating RC structures has long been necessary, often in response to aging, change in use and/or loading, damage, poor design, flaws in construction, and environmental conditions. To mitigate premature failure, strengthening techniques for RC columns adopted over the last few decades, are primarily in the form of steel jacketing, section enlargement, or dowelling in additional reinforcement. These techniques, although proven, have restrictions in their deployment of use; most significantly being the requirement of additional space, whether temporary for implementation or permanent for expansion. Frequently, the necessary space for expansion is not readily available, thus research into the use of fibre composites for external strengthening has progressed and has been implemented with increasing regularity since the millennium, Teng et al. (2003).

FRP is a light-weight, flexible alternative to steel or concrete, requiring minimal space for application or permanent expansion, and no bolted anchorage to the concrete. FRP is rapidly becoming a more popular choice in construction as the high strength-to-weight ratio

and non-corrosive properties makes it a feasible alternative. Some aspects of external FRP strengthening are still in their infancy subsequently limiting wider use. Direct application of a FRP wrap to prismatic columns is one such area, with further understanding of the mechanics of confinement required.

Fundamental knowledge validating research into strengthening of concrete columns for axial strength gain is well known [Richart et al. (1928), Manders et al. (1988)] and has developed from steel confinement over the last few decades, to using fibre composites in place of the former steel ties or spirals. FRP strengthening has become a popular means of column retrofit, in particular for circular columns where there is a greater comprehension of behaviour than that of prismatic columns, owing to the relatively simpler behavioural mechanics involved.

1.2.2. FIBRE COMPOSITES

Fibre composites are suitable for external strengthening due to their intrinsic properties, specifically, the high strength-to-weight ratio, simple installation and good resistance to corrosion.

FRP, a high strength and elastic modulus advanced fibre composite, comprising of a fibre material impregnated with an associated resin matrix and applied using a manual lay-up application process, was first experimented with in the 1980s [Fardis and Khalili (1982)]. The application of FRP to concrete columns has developed significantly faster in earthquake-prone regions because of the improved ductile response in the treated columns.

The advantages of retrofit of a RC column with a FRP jacket include: increased ductility as the concrete fails at a substantially greater strain; increased axial strength capacity due to the restriction on lateral expansion; greater stability against potential buckling of the longitudinal reinforcement; and flexibility and ease of application due to lighter material and no specialist equipment required for application in confined areas [Nanni (1995), TR55 (2005)]. However, with FRP jacketing, the quality control of application is harder to ascertain, and the durability and environmental stability have yet to be monitored over the long-term.

1.2.3. FRP CONFINEMENT

Structural columns when wrapped with FRP develop a considerable increase in strength and ductility due to the confinement of the concrete [Lam and Teng (2003b), Rocca et al. (2005), Wang et al. (2012)]. As the column is axially loaded in compression, confinement is achieved by utilising the resistance to lateral expansion provided by the FRP jacket as it goes into tension around the perimeter of the column, in the hoop direction. For circular columns, this confining force occurs around the whole perimeter due to the curvature of the FRP wrap providing an inwards component of force. Under concentric loading, lateral expansion is uniform generating a uniform strain distribution in the FRP, thus resulting in a uniform confining force and the confinement of the RC column can effectively increase the strength capacity by up to 300% (although serviceability criteria is likely to prevent this level of strengthening being achievable in practice) [Pesiki et al. (2001), Lam and Teng (2002), Teng and Lam (2004), Jiang and Teng (2007)].

For FRP-confined prismatic RC columns, the effect of confinement cannot be captured as simply as with circular columns and as such, an increase in capacity of up to 40% is considered attainable [Lam and Teng (2003b)]. This reduction is primarily due to the flat sides of the columns reducing the confining forces that can be generated from the curved area. Hence, the capacity gain for concentrically loaded columns can vary significantly depending on additional parameters of the research, most particularly, the size of the corner radius. As pure axial loading is not common in industry, the effect of axial-flexural loading on the generation of cross-sectional confinement requires comprehensive understanding. Research has been limited, with the effect of size yet to be fully captured. The addition of a flexural element to the loading reduces the increase in axial strength capacity attainable [Parvin and Wang (2001), Hadi and Widiarsa (2012), Maaddawy (2009)] and the point at which this technique is no longer beneficial needs to be ascertained.

In terms of circular and prismatic cross-sections, especially small-scale, the experimental test database is reasonably extensive. Load applied through testing in laboratory conditions is not truly representative of loading experienced on an authentic column in service requiring rehabilitation, hence there is low confidence in the use of this technique. A clearer understanding of the structural mechanics behind the effective use of this external FRP-confinement is required, in order to take advantage of the potential strength increase available.

1.2.4. EFFECTIVELY CONFINED AREA

The distribution of stress over the cross-section of a prismatic column is not explicitly known and is dependent on several factors. It is postulated that under concentric loading the FRP jacket goes into tension as the concrete laterally expands, generating confining forces only at the convex corners. Assuming sufficient strain is generated, these confining forces produce an effectively confined area forming a cruciform shape on the diagonals i.e. from corner to corner, where the region is assumed to be defined by a set of parabolic curves. The area outside this is deemed to be unconfined. There are many variables which alter the shape of the effectively confined area, specifically of interest to the author is the change in shape with; axial-flexural load application, and increase in cross-sectional aspect ratio.

A flexural effect in the columns can be induced by many factors including vertical misalignment, unbalanced moments, or lateral loading, hence it is necessary to test for eccentric loading. Typically, such columns carry a moment as well as an axial load, and it is not clear what form the confined area might take in such situations, where the lateral strain is not uniform. In eccentrically loaded specimens, the highly stressed concrete is located along an unconfined face of the column due to the non-uniform lateral expansion of the concrete caused by variation in axial strain. Furthermore, the strain in the FRP on the tension side of a column is substantially smaller than the equivalent strains on the compression side of the column. The ultimate strength increase of an eccentrically loaded prismatic column is postulated to be significantly less than a concentrically loaded column due to the change in stress distribution over the cross-section.

In square specimens, it is assumed that the parabolas are at 45 degrees to the sides of the cross-section, however, with an increase in the cross-sectional aspect ratio of a column, this is not explicitly known. It is debated as to whether the angle at which the parabolas leave the flat sides of the column follow the diagonals or remain at 45 degrees with respect to the sides [Lam and Teng (2003b), TR55 (2005)]. With increasing cross-sectional aspect ratio, the variance in confinement increases dramatically, thus it is essential to determine the cross-sectional behaviour accurately. Furthermore, eccentrically loading a column inevitably reduces the load capacity and it is postulated that the effectively confined area migrates into the area of higher compressive stress to satisfy the mechanics of equilibrium. This combined with an increase in cross-sectional aspect ratio has yet to be fully understood.

1.2.5. RESEARCH TO DATE

Research to date has been of two main paths; experimental, and analytical. Experimental research has focused on two broad aspects; column testing, and material testing. With reference to column testing, the majority of tests carried out have been on small-scale, concentrically loaded specimens, the results of which are often used as the basis for validating design models. Many of the specimens have no internal reinforcement and are relatively short, thus they do not exhibit potential slenderness effects. It brings into question the validity of using these design models for design of large-scale columns especially where there is the potential of axial-flexural loading. These concerns are fundamental to prismatic columns due to the non-uniformity of the confining stresses. Accordingly, while the current effectively confined area approach is a practical simplification which produces reasonable results under concentric load conditions, it may not adequately represent the mechanics of behaviour and perhaps should not be extrapolated to non-concentric load conditions.

An additional aspect not entirely addressed within testing of circular columns is the potential of debonding of the FRP jacket, primarily occurring on the flat sides of prismatic specimens. Debonding occurs due to the resulting variation in stress in the FRP around the columns' perimeter, specifically along the flat sides between the corners where resulting longitudinal shear stresses are acting between the FRP and the concrete. Thus the bond between the concrete and FRP can be compromised if the stresses are large enough and it is possible that debonding of the FRP will occur, especially where load is applied at a large eccentricity, thus this needs to be addressed.

Analytical models have been developed from the results of experimental testing, providing in many instances an accurate approach to design small-scale, concentrically loaded columns. These models do not reasonably predict the behaviour of large-scale or eccentrically loaded specimens in all instances, hence with the addition of a more extensive results database, a more accurate model will be presented.

It is evident that there are many aspects of research into FRP-confinement of prismatic columns that would benefit from further insight and development. The research performed and presented in this thesis concentrates on the behaviour of medium- and large-scale specimens, expanding the specimen database available for development of analytical models. This research has been carried out primarily at the University of Bath (UoB), with

experimental testing of medium- and large-scale specimens performed at the Building Research Establishment, Watford (BRE).

1.3. AIMS & OBJECTIVES

Research into behavioural mechanics and the subsequent use of FRP-confinement for prismatic columns has not progressed at the same rate as that for circular columns primarily due to the more complex confinement mechanics. Consequently, there is a lack of literature, including industry guidance to enable greater confidence in the use of FRP-confinement in industry.

The principal aim of this research is to ascertain if a reasonable gain in strength capacity is achievable with FRP-confinement of realistically sized and loaded prismatic RC columns. This research aim is divided into detailed objectives, specifically:

1. To establish the effect of column size upon the strength capacity increase and failure modes of FRP-confined prismatic columns
2. To establish the effect of cross-sectional aspect ratio and load eccentricity upon the evolution of the effectively confined area, and the resulting strength enhancement of FRP-confined prismatic columns
3. To develop a rational model for predicting the strength of realistically dimensioned FRP-confined prismatic columns subject to concentric and eccentric loading capturing the mechanics of the behaviour.

This research project has global significance due to the limited, and largely empirical guidance on strengthening prismatic columns currently available. Consequently, the results of this project are considered to be immediately beneficial in providing a sound basis for developing rational design guidance. This research improves the understanding of FRP-confinement of prismatic columns within the profession, leading to safe, efficient, and practical strengthening methodologies.

1.4. THESIS APPROACH

This thesis comprises of six chapters, as follows:

1. INTRODUCTION

2. LITERATURE REVIEW AND BACKGROUND RESEARCH

   Details the relevant work performed to date, relating to FRP-confined prismatic concrete columns and demonstrates the areas that would benefit from further research.

   Initial background work using FEM to verify postulated behaviour of the shape and movement of the effectively confined area is presented in this chapter.

3. TEST DESIGN AND METHODOLOGY

   Details the design of the test specimens and methodology adopted for laboratory testing, for both specimens and materials.

4. TEST RESULTS

   Presents and analyses results of the testing as detailed in Chapter 3 and compares with the current design guidance TR55 (2011) and others research.

5. ANALYTICAL MODELLING

   Presents an adaptation of an existing analytical model to encompass the effect of cross-sectional aspect-ratio and load eccentricity. This new model is further compared with other researchers test results.

6. DISCUSSION AND CONCLUSIONS

   This chapter discusses the results from experimental testing and analytical modelling. The implications of this work, as well as the recommendations for future work are conveyed.

The direction of this research project has focused on characterising the behaviour of prismatic columns and establishing the mechanics of behaviour over the cross-section. Supplementary information on this research is included in the appendices.

CHAPTER 2

LITERATURE REVIEW AND BACKGROUND RESEARCH

2.1. INTRODUCTION

Over the past few decades, research into the behaviour of composite materials for rehabilitation of deficient structures has seen a significant increase. An aspect of this research that has had specific focus and direction is the use of FRP as an external strengthening mechanism through confinement of reinforced concrete columns when the current or foreseeable state of the structure is unable to sustain the required loading. Research has focused on composites for the purpose of strengthening due to the adaptability of both the material and the application technique for differing use and location.

Confinement of concrete by external jacketing is an effective strengthening technique owing to the initiation of FRP lateral confining pressure as the concrete approaches peak capacity, thus forcing the concrete into a triaxial state of stress that is maintained; consequently increasing the ultimate strength and strain capacity of the column. Initially, the lateral restraint of concrete expansion under loading developed from the use of optimally spaced steel stirrups, and then further progressed to fibre composites. This chapter outlines the progression of research in the field of FRP-confinement of concrete columns and highlights the aspects of the research that would benefit from further insight.

Furthermore, background work using Finite Element Modelling (FEM) to establish the shape of the effectively confined area of prismatic columns is presented. The FEM created simulates the movement of the effectively confined area of prismatic specimens subjected

to axial or axial-flexural loading and confirms postulated views on the shape and movement of the effectively confined area.

2.2. STRENGTHENING OF RC COLUMNS

Natural change of use and decay of a structure act to the detriment of the concrete's structural integrity and thus necessitate the development and adaptation of strengthening techniques where traditional strengthening methods are not feasible. Traditional techniques most commonly used over the years are; steel retrofitting (grout injected steel jacket) and section enlargement (construction of an additional reinforcement cage around an existing column which is then in-filled with concrete). These methods, although appropriate and successful in a vast number of cases, are limiting in certain instances, most commonly due to constraints with space and duration of application. Hence the use of fibre reinforced polymers (FRP) to increase the strength capacity was developed off the back of steel retrofitting, as it demonstrates similar confinement mechanics by utilising the resistance to lateral expansion of the concrete under compressive loading. The design calculation, methodology and application technique differs.

FRP jacketing has proved a suitable alternative to steel due to its intrinsic properties, specifically, the high strength-to-weight ratio, simple installation and good resistance to corrosion. Initially research into the application of FRP wraps to concrete columns developed significantly faster in earthquake prone regions due to the increased flexural capacity available in the columns [Chaallal and Shahawy (2000)]. The primary focus of this research however has not been on the axial capacity of the structure. For axial strengthening, development of FRP strengthening of concrete columns originated with circular columns, with experimental testing being carried out to determine the increase in axial strength capacity of RC columns when wrapped with FRP and the subsequent behaviour of the confinement mechanics with focus on testing of small cylinders. Analytical models were established from this work and where possible, correlated against previous testing, initially that of steel confinement. Further development of these models focused on specific parameters along with comparisons through experimentation varying attributes such as concrete strength, FRP detail (architecture, type, wrap direction), and corner radius.

2.3. BEHAVIOURAL MECHANICS OF FRP-CONFINED COLUMNS

Axial loading a circular FRP-confined column, generates a circumferential uniform confining pressure originating from the FRP jacket, which resists the lateral (radial) expansion of the column; and as such this induces the concrete core into a state of multi-axial compression, concurrently improving both the deformation and strength capacity in the circular column. Compaction of the concrete aggregate (through a combination of particle sliding, crushing of the aggregate and void compaction, dependent on the angle of internal friction) initially provides an elastic resistive response against the axial load and once the capacity of the concrete is almost reached, the FRP-confinement is induced.

Confinement provided by an FRP wrap to a concrete core is passive (the confining pressure from the jacket is induced by and increases with the expansion of the concrete core) rather than active (where the external force applies a known lateral pressure to the concrete, and can be controlled to an extent in response to the applied load). This confinement changes to active confinement with the cracking of the concrete core as dilation occurs, generating a continuously increasing lateral confining pressure. It is widely known that when subject to axial compression, concrete can demonstrate a linear volumetric compaction or reduction up to 90% of the peak stress, after which non-linear hardening through further expansion or dilation occurs up to peak stress, causing the concrete to become unstable, which can be negated with FRP-confinement. Active confinement has its uses when establishing the load-extension curves of the specimen but it is essential to remember that it does not represent the behaviour of concrete where the confining stress comes from the surface of the concrete, as the confining pressure from the jacket is induced by and increases with the expansion of the concrete core.

2.3.1. FRP-CONFINED CIRCULAR COLUMNS

When a concrete column of circular cross-section is loaded in compression, the confinement from FRP, oriented in the hoop direction, displays an approximately bilinear stress–strain response, Figure 2-1. The initial portion of this curve follows that of unconfined concrete as the FRP jacket has minimal influence at this point. The effect of the FRP jacket is dual as observed by Issa and Karam (2004). Firstly there is an increase in the peak stress of the confined column with respect to the unconfined specimen, Figure 2-1. As the axial stress in

the concrete increases with the lateral expansion of the concrete core, a subsequent reduction in the stiffness is evident. At the unconfined concrete peak strain, typically around 0.002, the fissured material causes the FRP to engage and activate fully, limiting the stiffness degradation in the concrete as the FRP starts to behave plastically. Secondly, in the stress-strain response after the transition point is reached and the slope of this second region is dependent upon the stiffness of the FRP, with post-peak ductility of the confined column forming a pseudo-ductile plateau as the concrete is restrained by the FRP jacket. If the stiffness from the FRP-confinement is low, the stress-strain plot can demonstrate a descending branch, with peak load greater than the ultimate load and high stiffness produces an ascending portion as shown in Figure 2-1.

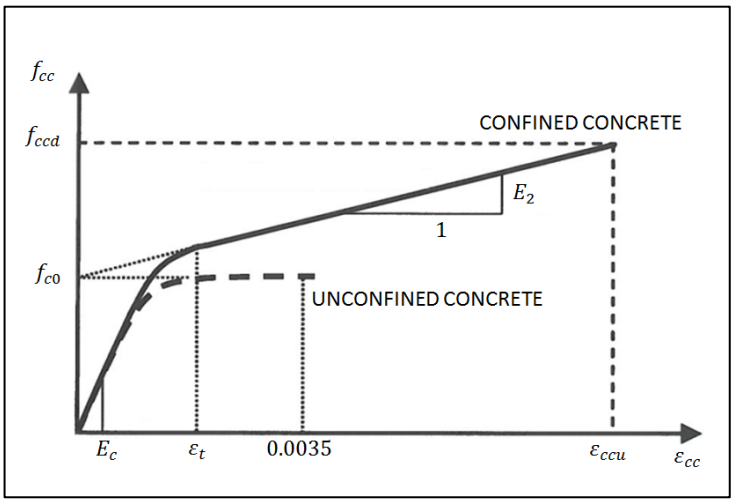

Figure 2-1: Bilinear stress-strain response of circular RC columns [Lam and Teng (2003b)]

As the FRP jacket only engages with the concrete as it starts to exceed its elastic range, the initial strain conditions are negligible in the confinement of the column, unlike that experienced with flexural strengthening. Thus theoretically the FRP jacket can only increase the ultimate limit state capacity, hence the serviceability limit state loading condition which ensures that the behaviour remains elastic is not altered. Consequently, this technique is of no benefit to columns with only a marginal increase in loading that is already anticipated in the initial design criteria.

FRP-confinement of circular columns under concentric loads can significantly increase the compressive strength and the ultimate axial compressive strain, therefore sustaining the lifespan of the specimen, Teng and Lam (2004). With axial-flexural load application, the

improvement in axial and deformation capacity is substantial, Bisby and Ranger (2010). This extensive experimental research of FRP-confined of circular columns under axial and axial-flexural load conditions has enabled the development of analytical models, which give a reasonably accurate estimate of the behaviour [Fam et al. (2003), Ranger and Bisby (2007).

2.3.1.1. PROGRESSION TO BEHAVIOURAL ANALYSIS OF PRISMATIC COLUMNS

A significant amount of research into FRP-confinement has been dedicated to characterising the behaviour of circular columns, however RC columns are regularly of prismatic cross-section. Prismatic columns are generally accepted to be less efficient in confinement, due to the more complicated, non-uniform confinement mechanics, as the higher stress concentrations develop at the corners [Chaallal & Shahawy (2000)]. A large scope of research work has room for significant development in this area.

Mitigation of the prismatic shape effect is achieved by rounding the corners of the columns and applying appropriate shape factors in many design models. Research into optimisation of the shape and size of the corners, has demonstrated that square columns rupture prematurely if the corner radius is too small, so the edge is effectively snapping the FRP jacket. The other extreme, optimal strength enhancement occurs with an annular cross-section, so as there are no flat sides, strain distribution is uniform, refer Figure 2-2. Hence smoothing the edges of square cross-sections has a significant role in delaying rupture of the FRP jacket and as such the efficiency of the FRP confinement is directly related to the radius of the cross-section edges [Al-Salloum (2007)]. It is evident that circular columns experience full confinement over the cross-section (under concentric loading) but as the cross-section becomes prismatic, with decreasing corner radius, the confined area subsequently decreases, Barrington et al. (2011).

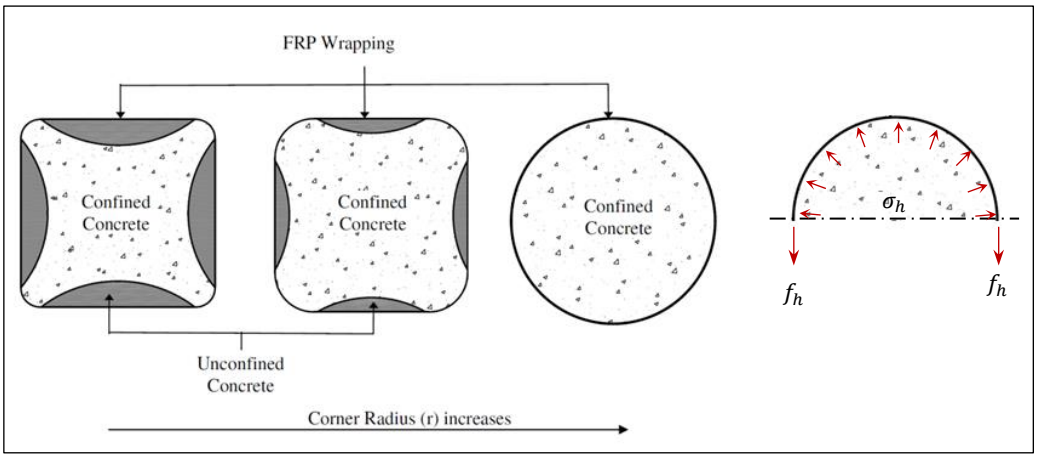

Figure 2-2: Effect of corner radius on the concrete confinement [Al-Salloum (2007)], with circular stress distribution demonstrated

Circular columns can achieve approximately a 300% increase in capacity due to cross-sectional shape whereas prismatic columns have a strength enhancement of nearer 50% [Mirmiran et al. (1998), Rochette and Labossière (2000), Pessiki et al. (2001), Campione et al. (2003), Chaallal et al. (2003), Mukherjee et al. (2004)]. This has been established in general from smaller scale specimens and it is postulated that the relative increase in strength capacity will be less for large-scale specimens as there is doubt in the ability to scale up the these results.

2.3.2. FRP-CONFINED PRISMATIC COLUMNS

Ultimate capacity of the confined concrete in terms of compressive strength and maximum axial strain is directly related to the lateral pressure generated by the confinement mechanisms [Turgay et al. 2009]. As the confining pressure for prismatic columns only occurs at the convex corners, there is a difference in behaviour with circular specimens. When a concentric load is applied, the FRP jacket goes into tension, confining pressure is generated at the convex corners, and a cruciform shaped area forms along the diagonals, see Figure 2-3, left image. This cruciform is assumed to be of a concrete strength equal to that of an equivalent circular column and outside the cruciform, at the flat sides of the cross-section, negligible or no confinement of the concrete is generated. Therefore if the pressure is reduced due to flat sides and small corner radii, the achievable increase in compressive strength is reduced also. This behaviour has been developed from that generally assumed

to occur with steel confined columns [Park and Paulay (1975), Mander et al. (1988) Cusson and Paultre (1995)].

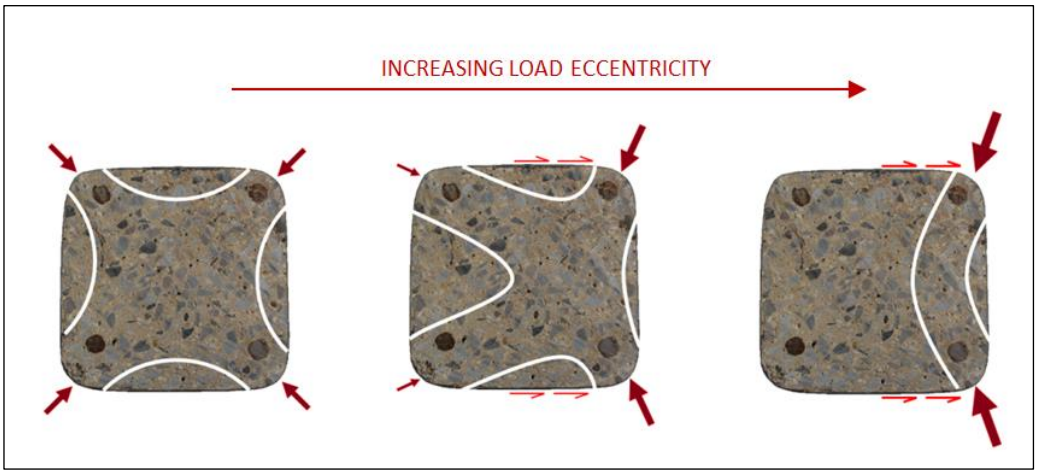

Figure 2-3: Confining forces at the corners generating the effectively confined area for concentric loading, with postulated movement into the compressive side of the column for increasing load eccentricity

It is debated whether the parabolas intersect the side faces at 45 degrees or at an angle in line with the diagonals. Lam and Teng (2003b) assume an angle of 45 degrees in their model, regardless of the aspect ratio of the column. However, when evaluating the concentric and eccentric behaviour, a more reasonable approximation of the parabolic behaviour is that the initial start of the parabola follows that of the diagonals, regardless of aspect ratio, to better capture the force distribution in the corners, generated from the FRP jacket. This is evident in the strains measured at the corners of the cross-section, that once translated into forces do not show an even concentration around the corners. Furthermore, this gives more flexibility when addressing the behaviour over the cross-section of prismatic specimens subject to eccentric loading.

Author and supervisor postulate that as the eccentricity of load increases, the effectively confined area of the column moves into the compressive region, refer Figure 2-3. The application of eccentric loading loses the symmetry of loading and the uniform stress generated at the corners, as there is no longer uniform axial strain in these sections of the jacket. This alteration of confining forces at the corners generates large shear stresses along the side of the column, with the possibility of the occurrence of debonding as the FRP jacket reaches failure strain levels.

The shape and movement of the effectively confined area again differs with the increase in the aspect ratio of the column. As the square cross-section becomes rectangular, there is an increase in length along one side, which increases the unconfined region along this side, generating a size effect not found in circular columns. The shape of the effectively confined area is thus a function of the flat side dimensions of the cross-section and the corner radius. As the flat sides of the specimen increase in length, the size is proportionally enlarged, and it cannot be assumed that the confinement mechanics behave in the same manner. Furthermore, the uneven distribution of strain over the cross-section is increased with eccentric loading, Figure 2-4.

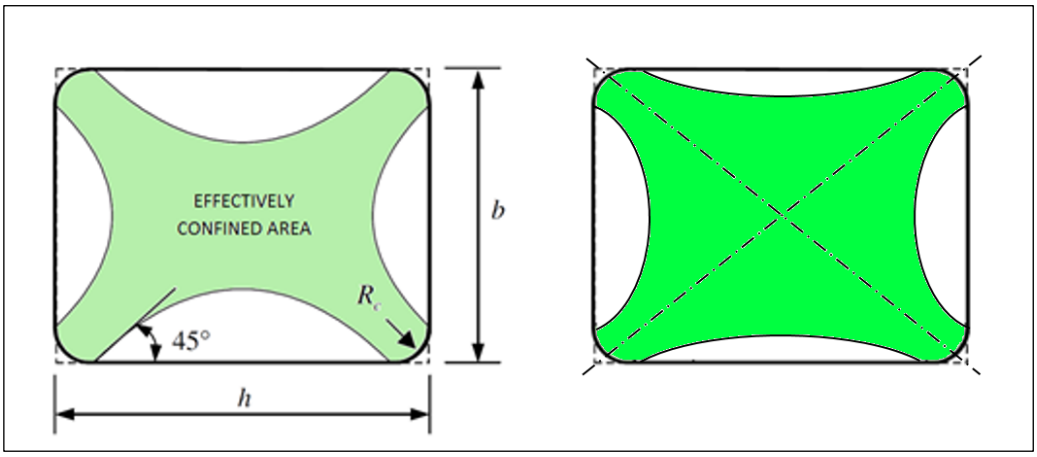

Figure 2-4: Effectively confined area of a rectangular column, parabolas at 45 degrees [Lam and Teng (2003b)], and in line with the diagonals [Author and supervisor postulation]

As the lateral confining pressure varies across the two axes of a rectangular column, there have been many theories postulated on the effectively confined area. Assuming that the angle of the parabolas is the same as that of the diagonals, it is generally accepted that an area of lesser confinement will occur where the parabolas overlap in columns with very large cross-sectional aspect ratios.

2.4. EXPERIMENTAL TESTING

Extensive experimental testing has been carried out on annular cross-sections with either pure axial compressive loading applied or a combined axial-flexural loading (popular for seismic testing). The experimental database is less populated for prismatic cross-sections, with the majority of results limited to small-scale specimens. Small-scale testing has focused on many parameters: significant work on cross-sectional change from circular to square including the shape of the corner radius; development of models, both design and analytical; FRP architecture, layering, application; concrete detail and strength but this has yet to be tested on scaled up versions.

To evaluate and compare the experimental testing performed on prismatic specimens, parameter selection has been necessary. The parameters omitted were selected as the results could not necessarily be extrapolated for comparison with the experimental work presented in this thesis, and these are detailed below:

- Composite Material Type; with the exception of large-scale rectangular specimens with increasing cross-sectional aspect ratio due to the limited research on specimens or this shape and size, thus allowing for a greater overview on the cross-sectional mechanics
- Fibre Architecture layout; generally data is only presented for unidirectional application in the hoop direction, as other orientations have been seen to be beneficial in axial or flexural capacities depending on the load conditions, but this would not give a reasonable comparison against the experimental testing in this research
- Plain Concrete; tends to be used in small-scale specimens and as such not necessary for this research as the small-scale prismatic RC database is reasonably extensive
- Extreme conditions; including but not limited to: fire, blast, and seismic loading, which are best evaluated on large-scale specimens subjected to axial-flexural loading once the fundamental behaviour is fully understood
- Extreme geometry; limits on parameters were essential hence aspects such as; very tall, slender columns, Tao and Yu (2008), or excessively large cross-section aspect ratios that presented wall-type behaviour were not included

Only FRP-confined columns using a wet lay-up method are considered, other confinement methods are not addressed here. The data referring to cylinders and prisms is vast and although essential to understanding the behaviour of concrete/FRP interaction, the results are not included in detail here as they cannot be extrapolated sufficiently well enough for practical design and use due to postulated size effects. They also do not address effects such as slenderness, which are necessary as the size becomes realistic. Furthermore, these small-scale results are often used to verify design models; accordingly care should be taken here in ensuring the validity when scaling up.

A summary of the papers included in the review of experimental research into prismatic columns confined with FRP are detailed in Table 2-1.

Table 2-1: Summary of research presented in Table 2-2, in relation to selected parameters of this research

AUTHOR	ASPECTS COVERED	SIZE EFFECT	LOAD PROFILE	ASPECT RATIO
CHAALLAL AND SHAHAWY (2000)	SMALL-SCALE RECTANGULAR, ECCENTRIC LOADING		Y	Y
PESSIKI ET AL. (2001)	LARGE-SCALE SPECIMENS	Y		
LAM AND TENG (2003B)	SMALL-SCALE SQUARE AND RECTAGULAR SPECIMENS	Y		Y
PROTA ET AL. (2003)	SMALL-SCALE RECTANGLUAR SPECIMENS			Y
ROCCA ET AL (2005)	SIZE EFFECT FOR SQUARE AND RECTANGULAR SPECIMENS	Y		Y
AL-SALLOUM (2007)	CORNER RADIUS FOCUS	Y		
MONTI AND NISTICO (2008)	SMALL-SCALE SQUARE AND RECTANGULAR SPECIMENS	Y		Y
EL MAADDAWY (2009)	SMALL-SCALE, ECCENTRIC LOADING		Y	
SADEGHIAN ET AL. (2010)	SMALL-SCALE RECTANGULAR SPECIMENS, ECCENTRIC LOADING			Y
TURGAY ET AL. (2010)	FRP WRAPPING FOCUS	Y		
WU AND WEI (2010)	SHORT SQUARE AND RECTANGULAR PRISMS			Y
BARRINGTON ET AL. (2011)	CORNER RADIUS FOCUS	Y		
DE LUCA ET AL. (2011)	GFRP WRAPPED			Y
HADI AND WIDIARSA (2012)	SMALL-SCALE, ECCENTRIC LOADING		Y	
WANG ET AL. (2012)	MEDIUM-SCALE SPECIMENS	Y		
MICELLI AND MODARELLI (2013)	RECTANGULAR SPECIMENS			Y
SONG ET AL. (2013)	SMALL-SCALE, ECCENTRIC LOADING		Y	

The set of experimental research directly related to this research is presented in detail in Table 2-2.

Table 2-2: Experimental testing on prismatic cross-sections (part 1 of 11)

AUTHOR ID	SPECIMEN GEOMETRY						MATERIAL DATA					LOAD PROFILE		RESULTS			
	BREDTH	WIDTH	HEIGHT	HEIGHT INC. CORBELS	ASPECT RATIO	CORNER RADIUS	FRP DETAIL (No. WRAPS)	NOMINAL PLY THICKNESS	ULTIMATE TENSILE STRAIN AT RUPTURE	PLAIN OR REINFORCED CONCRETE	UNCONFINED COMP. CUBE STRENGTH	LOAD ECCENTRICITY	LOADING NOTES	PEAK LOAD	PEAK COMP. STRESS	AXIAL STRAIN AT PEAK LOAD	FAILURE MODE[†]
	b mm	h mm	H mm	H_{corbel} mm	h/b	R_c mm					f_{cu} MPa	e_i mm		N kN	f_{cc} MPa	ε_{cc}	
Chaallal and Shahawy (2000)																	
BC-0L-E0	200	350	2100	3500	1.75	0	0	N/A	N/A	RC	25	0		1877	U/K	U/K	C-C
BC-2L-E0	200	350	2100	3500	1.75	0	2	0.5	0.014	RC	25	0		2411	U/K	U/K	FRP-R
BC-0L-E3	200	350	2100	3500	1.75	0	0	N/A	N/A	RC	25	75		1228	U/K	U/K	C-C
BC-2L-E3	200	350	2100	3500	1.75	0	2	0.5	0.014	RC	25	75		1334	U/K	U/K	FRP-R
BC-0L-E6	200	350	2100	3500	1.75	0	0	N/A	N/A	RC	25	150		712	U/K	U/K	CORBEL
BC-2L-E6	200	350	2100	3500	1.75	0	2	0.5	0.014	RC	25	150		827	U/K	U/K	C-B
BC-0L-E12	200	350	2100	3500	1.75	0	0	N/A	N/A	RC	25	300		310	U/K	U/K	C-C
BC-2L-E12	200	350	2100	3500	1.75	0	2	0.5	0.014	RC	25	300		440	U/K	U/K	C-B
BC-0L-E16	200	350	2100	3500	1.75	0	0	N/A	N/A	RC	25	400		240	U/K	U/K	C-C
BC-2L-E16	200	350	2100	3500	1.75	0	2	0.5	0.014	RC	25	400		356	U/K	U/K	FRP-RB
NOTES:	Test set-up differed from many tests, columns were on side, and hydrallic jack applied through use of a rig																
Pessiki et al. (2001)																	
0	152	152	610	N/A	1.00	38	0	N/A	N/A	RC	U/K	0		U/K	U/K	0.0021	U/K
1	152	152	610	N/A	1.00	38	1	U/K	0.015	RC	U/K	0		U/K	U/K	0.0133	U/K
2	152	152	610	N/A	1.00	38	2	U/K	0.015	RC	U/K	0		U/K	U/K	0.017	U/K
S1	458	458	1830	N/A	1.00	38	0	N/A	N/A	RC	U/K	0		U/K	U/K	0.0019	C-S
S4	458	458	1830	N/A	1.00	38	3	U/K	0.015	RC	U/K	0		U/K	U/K	0.0021	FRP-R
NOTES:	Large corner radius for small-scale specimens resulted in similar results to the circular specimens tested alongside, attributed to the relative size of the corner radius to cross-section dimensions Proposed shape factor and strain effifiency factor from results, addresses dilation ratio																

Table 2-2 (contd.): Experimental testing on prismatic cross-sections (part 2 of 11)

AUTHOR ID	SPECIMEN GEOMETRY						MATERIAL DATA					LOAD PROFILE		RESULTS			
	BREDTH	WIDTH	HEIGHT	HEIGHT INC. CORBELS	ASPECT RATIO	CORNER RADIUS	FRP DETAIL (No. WRAPS)	NOMINAL PLY THICKNESS	ULTIMATE TENSILE STRAIN AT RUPTURE	PLAIN OR REINFORCED CONCRETE	UNCONFINED COMP. CUBE STRENGTH	LOAD ECCENTRICITY	LOADING NOTES	PEAK LOAD	PEAK COMP. STRESS	AXIAL STRAIN AT PEAK LOAD	FAILURE MODE[†]
	b mm	h mm	H mm	H_{corbel} mm	h/b	R_c mm					f_{cu} MPa	e_i mm		N kN	f_{cc} MPa	ε_{cc}	
Lam and Teng (2003b)																	
S1R15	150	150	600	N/A	1.00	15	1	0.165	U/K	PC	42.1	0		U/K	35	U/K	U/K
S1R25	150	150	600	N/A	1.00	25	1	0.165	U/K	PC	42.1	0		U/K	39	U/K	U/K
S2R15	150	150	600	N/A	1.00	15	2	0.33	U/K	PC	42.1	0		U/K	50	U/K	U/K
S2R25	150	150	600	N/A	1.00	25	2	0.33	U/K	PC	42.1	0		U/K	62	U/K	U/K
S3R15	150	150	600	N/A	1.00	15	3	0.495	U/K	PC	30	0		U/K	62	U/K	U/K
S3R25	150	150	600	N/A	1.00	25	3	0.495	U/K	PC	30	0		U/K	66	U/K	U/K
S4R15	150	150	600	N/A	1.00	15	4	0.66	U/K	PC	30	0		U/K	64	U/K	U/K
S4R25	150	150	600	N/A	1.00	25	4	0.66	U/K	PC	30	0		U/K	81	U/K	U/K
S5R15	150	150	600	N/A	1.00	15	5	0.825	U/K	PC	51.9	0		U/K	83	U/K	U/K
S5R25	150	150	600	N/A	1.00	25	5	0.825	U/K	PC	51.9	0		U/K	95	U/K	U/K
R4R15	150	225	600	N/A	1.50	15	4	0.66	U/K	PC	51.9	0		U/K	49	U/K	U/K
R4R25	150	225	600	N/A	1.50	25	4	0.66	U/K	PC	51.9	0		U/K	52	U/K	U/K
NOTES:	Failure images in the paper show rupture of the FRP at or near midheight of the specimen, however this is for one square and one rectangular specimen only FRP overap length of 150mm																
Prota et al. (2003)																	
B-1	115	420	1500	N/A	3.65	20	0	N/A	N/A	RC	12	0		1072	U/K	N/A	C-C
B-2	115	420	1500	N/A	3.65	20	0	N/A	N/A	RC	12	0		1068	U/K	0.00417	C-C
S-1	115	420	1500	N/A	3.65	20	3 @[0°]	NR	4.66	RC	12	0		1397	U/K	0.00618	FRP-R
S-2	115	420	1500	N/A	3.65	20	3 @[0°]	NR	4.66	RC	12	0		1388	U/K	0.00517	FRP-R
S-3	115	420	1500	N/A	3.65	20	3 @[0°]	NR	4.66	RC	12	0		1348	U/K	0.00522	FRP-R
NOTES:	GFRP used in this series of tests, application varied with longiduinally oriented fibres as well Unconfined concrete compressive stress, f'_c = 12MPa																

Table 2-2 (contd.): Experimental testing on prismatic cross-sections (part 3 of 11)

AUTHOR ID	SPECIMEN GEOMETRY						MATERIAL DATA					LOAD PROFILE		RESULTS			
	BREDTH	WIDTH	HEIGHT	HEIGHT INC. CORBELS	ASPECT RATIO	CORNER RADIUS	FRP DETAIL (No. WRAPS)	NOMINAL PLY THICKNESS	ULTIMATE TENSILE STRAIN AT RUPTURE	PLAIN OR REINFORCED CONCRETE	UNCONFINED COMP. CUBE STRENGTH	LOAD ECCENTRICITY	LOADING NOTES	PEAK LOAD	PEAK COMP. STRESS	AXIAL STRAIN AT PEAK LOAD	FAILURE MODE[†]
	b mm	h mm	H mm	H_{corbel} mm	h/b	R_c mm					f_{cu} MPa	e_i mm		N kN	f_{cc} MPa	ε_{cc}	
Rocca et al (2005)																	
B1	317.5	635	1371.6	N/A	2.00	0	0	N/A	N/A	RC	28	0		5920	U/K	U/K	C-S
B2	317.5	635	1371.6	N/A	2.00	0	7	U/K	0.93	RC	28	0		7446	U/K	U/K	FRP-R
B3	317.5	635	1371.6	N/A	2.00	0	2	U/K	0.93	RC	28	0		6330	U/K	U/K	FRP-R
C1	457.2	457.2	1016	N/A	1.00	0	0	N/A	N/A	RC	28	0		6739	U/K	U/K	C-SB
C2	457.2	457.2	1016	N/A	1.00	0	4	U/K	0.93	RC	28	0		7379	U/K	U/K	FRP-RB
C3	457.2	457.2	1016	N/A	1.00	0	2	U/K	0.93	RC	28	0		7086	U/K	U/K	FRP-R
D1	647.7	647.7	1371.6	N/A	1.00	0	0	N/A	N/A	RC	28	0		13259	U/K	U/K	C-SB
D2	647.7	647.7	1371.6	N/A	1.00	0	5	U/K	0.93	RC	28	0		15319	U/K	U/K	FRP-RB
D3	647.7	647.7	1371.6	N/A	1.00	0	2	U/K	0.93	RC	28	0		14029	U/K	U/K	FRP-R
E1	323.85	323.85	685.8	N/A	1.00	0	0	N/A	N/A	RC	28	0		2673	U/K	U/K	C-SB
E2	323.85	323.85	685.8	N/A	1.00	0	2	U/K	0.93	RC	28	0		3972	U/K	U/K	FRP-RB
E3	323.85	323.85	685.8	N/A	1.00	0	4	U/K	0.93	RC	28	0		4123	U/K	U/K	FRP-R
F1	323.85	323.85	1371.6	N/A	1.00	0	0	N/A	N/A	RC	28	0		3447	U/K	U/K	C-SB
F2	323.85	323.85	1371.6	N/A	1.00	0	2	U/K	0.93	RC	28	0		3839	U/K	U/K	FRP-RB
F3	323.85	323.85	1371.6	N/A	1.00	0	4	U/K	0.93	RC	28	0		3830	U/K	U/K	FRP-RB
G1	914.4	914.4	1981.2	N/A	1.00	0	0	N/A	N/A	RC	28	0		28165	U/K	U/K	C-S
G2	914.4	914.4	1981.2	N/A	1.00	0	8	U/K	0.93	RC	28	0		30847	U/K	U/K	FRP-RB
H1	635	1270	2743.2	N/A	2.00	0	0	N/A	N/A	RC	28	0		27578	U/K	U/K	C-SB
H2	635	1270	2743.2	N/A	2.00	0	19	U/K	0.93	RC	28	0		31136	U/K	U/K	FRP-R
NOTES:	FRP is Mapewrap C UNI-AX 300/40																

Table 2-2 (contd.): Experimental testing on prismatic cross-sections (part 4 of 11)

AUTHOR ID	SPECIMEN GEOMETRY						MATERIAL DATA				LOAD PROFILE		RESULTS			
	BREDTH	WIDTH	HEIGHT	HEIGHT INC. CORBELS	ASPECT RATIO	CORNER RADIUS	FRP DETAIL (No. WRAPS)	NOMINAL PLY THICKNESS	ULTIMATE TENSILE STRAIN AT RUPTURE	PLAIN OR REINFORCED CONCRETE	UNCONFINED COMP. CUBE STRENGTH	LOAD ECCENTRICITY	LOADING NOTES	PEAK LOAD	PEAK COMP. STRESS	AXIAL STRAIN AT PEAK LOAD	FAILURE MODE[†]
	b mm	h mm	H mm	H_{corbel} mm	h/b	R_c mm					f_{cu} MPa	e_l mm		N kN	f_{cc} MPa	ε_{cc}	
Al-Salloum (2007)																	
S-r5 -1uc	150	150	500	N/A	1.00	5	0	N/A	N/A	PC	32-35	0		U/K	U/K	0.0337	C-Sh
S-r5 -1c	150	150	500	N/A	1.00	5	1	1.20	U/K	PC	32-35	0		U/K	U/K	0.1176	FRP-R
S-r5 -2uc	150	150	500	N/A	1.00	5	0	N/A	N/A	PC	32-35	0		U/K	U/K	0.0337	C-Sh
S-r5 -2c	150	150	500	N/A	1.00	5	1	1.20	U/K	PC	32-35	0		U/K	U/K	0.1176	FRP-R
S-r25-1uc	150	150	500	N/A	1.00	25	0	N/A	N/A	PC	32-35	0		U/K	U/K	0.0307	C-Sh
S-r25-1c	150	150	500	N/A	1.00	25	1	1.20	U/K	PC	32-35	0		U/K	U/K	0.6949	FRP-R
S-r25-2uc	150	150	500	N/A	1.00	25	0	N/A	N/A	PC	32-35	0		U/K	U/K	0.0307	C-Sh
S-r25-2c	150	150	500	N/A	1.00	25	1	1.20	U/K	PC	32-35	0		U/K	U/K	0.6949	FRP-R
S-r38-1uc	150	150	500	N/A	1.00	38	0	N/A	N/A	PC	32-35	0		U/K	U/K	0.0207	C-Sh
S-r38-1c	150	150	500	N/A	1.00	38	1	1.20	U/K	PC	32-35	0		U/K	U/K	0.7907	FRP-R
S-r38-2uc	150	150	500	N/A	1.00	38	0	N/A	N/A	PC	32-35	0		U/K	U/K	0.0207	C-Sh
S-r38-2c	150	150	500	N/A	1.00	38	1	1.20	U/K	PC	32-35	0		U/K	U/K	0.7907	FRP-R
S-r50-1uc	150	150	500	N/A	1.00	50	0	N/A	N/A	PC	32-35	0		U/K	U/K	0.0998	C-Sh
S-r50-1c	150	150	500	N/A	1.00	50	1	1.20	U/K	PC	32-35	0		U/K	U/K	1.1147	FRP-R
S-r50-2uc	150	150	500	N/A	1.00	50	0	N/A	N/A	PC	32-35	0		U/K	U/K	0.0998	C-Sh
S-r50-2c	150	150	500	N/A	1.00	50	1	1.20	U/K	PC	32-35	0		U/K	U/K	1.1147	FRP-R
CYL-1uc	150	150	500	N/A	1.00	75	0	N/A	N/A	PC	32-35	0		U/K	U/K	0.0616	C-Sh
CYL-1c	150	150	500	N/A	1.00	75	1	1.20	U/K	PC	32-35	0		U/K	U/K	0.9699	FRP_R
CYL-2uc	150	150	500	N/A	1.00	75	0	N/A	N/A	PC	32-35	0		U/K	U/K	0.0616	C-Sh
CYL-2c	150	150	500	N/A	1.00	75	1	1.20	U/K	PC	32-35	0		U/K	U/K	0.9699	FRP-R

NOTES: Axial strain at ultimate load is stated for each specimen type, as opposed to each specific specimen

Table 2-2 (contd.): Experimental testing on prismatic cross-sections (part 5 of 11)

AUTHOR ID	SPECIMEN GEOMETRY						MATERIAL DATA					LOAD PROFILE		RESULTS			
	BREDTH	WIDTH	HEIGHT	HEIGHT INC. CORBELS	ASPECT RATIO	CORNER RADIUS	FRP DETAIL (No. WRAPS)	NOMINAL PLY THICKNESS	ULTIMATE TENSILE STRAIN AT RUPTURE	PLAIN OR REINFORCED CONCRETE	UNCONFINED COMP. CUBE STRENGTH	LOAD ECCENTRICITY	LOADING NOTES	PEAK LOAD	PEAK COMP. STRESS	AXIAL STRAIN AT PEAK LOAD	FAILURE MODE[†]
	b mm	h mm	H mm	H_{corbel} mm	h/b	R_c mm					f_{cu} MPa	e_i mm		N kN	f_{cc} MPa	ε_{cc}	
Monti and Nistico (2008)																	
200 x 200UW	200	200	1400	N/A	1.00	20	0	N/A	N/A	PC	21.48	0		670	U/K	U/K	U/K
200 x 200UW*	200	200	1400	N/A	1.00	20	0	N/A	N/A	PC	21.48	0		490	U/K	U/K	U/K
200 x 200UW800	200	200	800	N/A	1.00	20	0	N/A	N/A	PC	21.48	0		600	U/K	U/K	U/K
200 X 200 W	200	200	1400	N/A	1.00	20	1*	U/K	0.52	PC	21.48	0		855	U/K	U/K	U/K
200 x 200W870	200	200	870	N/A	1.00	20	1*	U/K	0.52	PC	21.48	0		800	U/K	U/K	U/K
200 x 200WL	200	200	1400	N/A	1.00	20	0	N/A	N/A	PC	21.48	0		1180	U/K	U/K	U/K
200 X 200WL*	200	200	1400	N/A	1.00	20	0	N/A	N/A	PC	21.48	0		940	U/K	U/K	U/K
200 x 200WL870	200	200	1400	N/A	1.00	20	0	N/A	N/A	PC	21.48	0		1200	U/K	U/K	U/K
200 x 300UW	200	300	1400	N/A	1.50	20	0	N/A	N/A	PC	21.48	0		1000	U/K	U/K	U/K
200x300W	200	300	1400	N/A	1.50	20	1*	U/K	0.52	PC	21.48	0		1180	U/K	U/K	U/K
200 x 300WL	200	300	1400	N/A	1.50	20	0	N/A	N/A	PC	21.48	0		1600	U/K	U/K	U/K
200 x 400UW	200	400	1400	N/A	2.00	20	0	N/A	N/A	PC	21.48	0		1380	U/K	U/K	U/K
200 x 400W	200	400	1400	N/A	2.00	20	2	U/K	0.52	PC	21.48	0		1600	U/K	U/K	U/K
200 x 400WL	200	400	1400	N/A	2.00	20	0	N/A	N/A	PC	21.48	0		2000	U/K	U/K	U/K
NOTES:	* two layers of FRP at the top and bottom of the specimen HM CFRP Straps used Looks at the degredation of the transverse elastic modulus, which indicated that the concrete had become anisotropic																

Table 2-2 (contd.): Experimental testing on prismatic cross-sections (part 6 of 11)

AUTHOR ID	SPECIMEN GEOMETRY						MATERIAL DATA					LOAD PROFILE		RESULTS			
	BREDTH	WIDTH	HEIGHT	HEIGHT INC. CORBELS	ASPECT RATIO	CORNER RADIUS	FRP DETAIL (No. WRAPS)	NOMINAL PLY THICKNESS	ULTIMATE TENSILE STRAIN AT RUPTURE	PLAIN OR REINFORCED CONCRETE	UNCONFINED COMP. CUBE STRENGTH	LOAD ECCENTRICITY	LOADING NOTES	PEAK LOAD	PEAK COMP. STRESS	AXIAL STRAIN AT PEAK LOAD	FAILURE MODE[†]
	b mm	h mm	H mm	H_{corbel} mm	h/b	R_c mm					f_{cu} MPa	e_i mm		N kN	f_{cc} MPa	ε_{cc}	
El Maaddawy (2009)																	
UW-e1	125	125	500	1200	1.00	0	none	0.38	0.013	RC	28.5	37.5		215	U/K	U/K	C-C
UW-e2	125	125	500	1200	1.00	0	none	0.38	0.013	RC	28.5	54		165	U/K	U/K	C-C
UW-e3	125	125	500	1200	1.00	0	none	0.38	0.013	RC	28.5	71		145	U/K	U/K	C-CY
UW-e4	125	125	500	1200	1.00	0	none	0.38	0.013	RC	28.5	107.5		92	U/K	U/K	C-CY
FW-e1	125	125	500	1200	1.00	0	full	0.38	0.013	RC	28.5	37.5		295	U/K	U/K	FRP-RB
FW-e2	125	125	500	1200	1.00	0	full	0.38	0.013	RC	28.5	54		205	U/K	U/K	FRP-RS
FW-e3	125	125	500	1200	1.00	0	full	0.38	0.013	RC	28.5	71		157	U/K	U/K	FRP-RS
FW-e4	125	125	500	1200	1.00	0	full	0.38	0.013	RC	28.5	107.5		95	U/K	U/K	FRP-RS
PW-e1	125	125	500	1200	1.00	0	partial	0.38	0.013	RC	28.5	37.5		275	U/K	U/K	FRP-RB
PW-e2	125	125	500	1200	1.00	0	partial	0.38	0.013	RC	28.5	54		200	U/K	U/K	FRP-RS
PW-e3	125	125	500	1200	1.00	0	partial	0.38	0.013	RC	28.5	71		150	U/K	U/K	FRP-RS
PW-e4	125	125	500	1200	1.00	0	partial	0.38	0.013	RC	28.5	107.5		93	U/K	U/K	FRP-RS
NOTES:	Concrete compressive cylinder strength, f'_c = 28.5 +/- 2.5MPa Full length of the specimen, including corbels was 1200mm, with corbels of 250x250mm cross-section The total moment is based on the primary moment caused by the inital eccentricity and the secondary momentl caused by the lateral midheight displacement at failure (P-delta)																
Sadeghian et al. (2010)																	
U200	200	300	2700	N/A	1.50	15	none	N/A	N/A	RC	40	200		337	U/K	U/K	C-C
U300	200	300	2700	N/A	1.50	15	none	N/A	N/A	RC	40	300		156	U/K	U/K	C-C
S200-L2T	200	300	2700	N/A	1.50	15	3 @ (90°)2/0	0.90	U/K	RC	40	200		491	U/K	U/K	FRP-R
S200-L4T	200	300	2700	N/A	1.50	15	5 @ (90°)4/0	0.90	U/K	RC	40	200		600	U/K	U/K	FRP-R
S300-L2T	200	300	2700	N/A	1.50	15	3 @ (90°)2/0	0.90	U/K	RC	40	300		284	U/K	U/K	FRP-R
S300-L4T	200	300	2700	N/A	1.50	15	5 @ (90°)4/0	0.90	U/K	RC	40	300		356	U/K	U/K	FRP-R
S300-DD'	200	300	2700	N/A	1.50	15	2@ ±45°	1.80	U/K	RC	40	300		238	U/K	U/K	FRP-R
NOTES:	Specimen S200-L4T did not fail in the FRP due to the limitation of actuator capacity Peak load was the ultimate load at which the FRP failed																

Table 2-2 (contd.): Experimental testing on prismatic cross-sections (part 7 of 11)

AUTHOR ID	SPECIMEN GEOMETRY						MATERIAL DATA					LOAD PROFILE		RESULTS			
	BREDTH	WIDTH	HEIGHT	HEIGHT INC. CORBELS	ASPECT RATIO	CORNER RADIUS	FRP DETAIL (No. WRAPS)	NOMINAL PLY THICKNESS	ULTIMATE TENSILE STRAIN AT RUPTURE	PLAIN OR REINFORCED CONCRETE	UNCONFINED COMP. CUBE STRENGTH	LOAD ECCENTRICITY	LOADING NOTES	PEAK LOAD	PEAK COMP. STRESS	AXIAL STRAIN AT PEAK LOAD	FAILURE MODE[†]
	b mm	h mm	H mm	H_{corbel} mm	h/b	R_c mm					f_{cu} MPa	e_i mm		N kN	f_{cc} MPa	ε_{cc}	
Turgay et al. (2010)																	
C1	200	200	1000	N/A	1.00	25	none	N/A	N/A	RC	18.08	0		U/K	U/K	U/K	U/K
C2	200	200	1000	N/A	1.00	25	partial*	0.17	0.015	RC	18.08	0		U/K	U/K	U/K	U/K
C3	200	200	1000	N/A	1.00	25	1	0.17	0.015	RC	18.08	0		U/K	U/K	U/K	U/K
C4	200	200	1000	N/A	1.00	25	partial*	0.17	0.015	RC	18.08	0		U/K	U/K	U/K	U/K
C5	200	200	1000	N/A	1.00	25	2	0.17	0.015	RC	18.08	0		U/K	U/K	U/K	U/K
NOTES:	* partial wrap at top and bottom of specimen Low concrete strength dictated by the capacity of the testing rig Images of failure methods available in the paper, but annotation as to which specimens is not																
Wu and Wei (2010)																	
0S-1.0	150	150	300	N/A	1.00	30	0	N/A	N/A	PC	30	0		U/K	34	N/A	U/K
0R-1.25	150	188	300	N/A	1.25	30	0	N/A	N/A	PC	30	0		U/K	34	N/A	U/K
0R-1.5	150	225	300	N/A	1.50	30	0	N/A	N/A	PC	30	0		U/K	36	N/A	U/K
0R-1075	150	263	300	N/A	1.75	30	0	N/A	N/A	PC	30	0		U/K	37	N/A	U/K
0R-2.0	150	300	300	N/A	2.00	30	0	N/A	N/A	PC	30	0		U/K	35	N/A	U/K
1S-1.0	150	150	300	N/A	1.00	30	1	0.17	1.84	PC	30	0		U/K	41	0.0105	FRP-R
1R-1.25	150	188	300	N/A	1.25	30	1	0.17	1.84	PC	30	0		U/K	39	0.0067	FRP-R
1R-1.5	150	225	300	N/A	1.50	30	1	0.17	1.84	PC	30	0		U/K	38	0.0051	FRP-R
1R-1075	150	263	300	N/A	1.75	30	1	0.17	1.84	PC	30	0		U/K	38	0.0043	FRP-R
1R-2.0	150	300	300	N/A	2.00	30	1	0.17	1.84	PC	30	0		U/K	37	0.0043	FRP-R
2S-1.0	150	150	300	N/A	1.00	30	2	0.33	1.84	PC	30	0		U/K	60	0.0204	FRP-R
2R-1.25	150	188	300	N/A	1.25	30	2	0.33	1.84	PC	30	0		U/K	51	0.0148	FRP-R
2R-1.5	150	225	300	N/A	1.50	30	2	0.33	1.84	PC	30	0		U/K	44	0.0142	FRP-R
2R-1075	150	263	300	N/A	1.75	30	2	0.33	1.84	PC	30	0		U/K	41	0.0049	FRP-R
2R-2.0	150	300	300	N/A	2.00	30	2	0.33	1.84	PC	30	0		U/K	39	0.0043	FRP-R
NOTES:	FRP overlap of 150mm in the middle of the longer side																

Table 2-2 (contd.): Experimental testing on prismatic cross-sections (part 8 of 11)

AUTHOR ID	SPECIMEN GEOMETRY						MATERIAL DATA				LOAD PROFILE		RESULTS			
	BREDTH	WIDTH	HEIGHT	HEIGHT INC. CORBELS	ASPECT RATIO	CORNER RADIUS	FRP DETAIL (No. WRAPS)	NOMINAL PLY THICKNESS	ULTIMATE TENSILE STRAIN AT RUPTURE	PLAIN OR REINFORCED CONCRETE	UNCONFINED COMP. CUBE STRENGTH	LOAD ECCENTRICITY	LOADING NOTES	PEAK LOAD	PEAK COMP. STRESS	AXIAL STRAIN AT PEAK LOAD	FAILURE MODE†
	b mm	h mm	H mm	H_{corbel} mm	h/b	R_c mm					f_{cu} MPa	e_l mm		N kN	$f_{\alpha c}$ MPa	$\varepsilon_{\alpha c}$	
Barrington et al. (2011)																	
U00-1	150	150	450	N/A	1.00	3	1	0.12	1.7	PC	25 / 30	0		709	32	U/K	U/K
U00-2	150	150	450	N/A	1.00	3	1	0.12	1.7	PC	25 / 30	0		738	33	U/K	U/K
U00-3	150	150	450	N/A	1.00	3	1	0.12	1.7	PC	25 / 30	0		702	31	U/K	U/K
U25-1	150	150	450	N/A	1.00	25	1	0.12	1.7	PC	25 / 30	0		734	33	U/K	U/K
U25-2	150	150	450	N/A	1.00	25	1	0.12	1.7	PC	25 / 30	0		684	31	U/K	U/K
U25-3	150	150	450	N/A	1.00	25	1	0.12	1.7	PC	25 / 30	0		720	33	U/K	U/K
U50-1	150	150	450	N/A	1.00	50	1	0.12	1.7	PC	25 / 30	0		647	32	U/K	U/K
U50-2	150	150	450	N/A	1.00	50	1	0.12	1.7	PC	25 / 30	0		620	31	U/K	U/K
U50-3	150	150	450	N/A	1.00	50	1	0.12	1.7	PC	25 / 30	0		707	35	U/K	U/K
U75-1	150	150	450	N/A	1.00	75	1	0.12	1.7	PC	25 / 30	0		573	32	U/K	U/K
U75-2	150	150	450	N/A	1.00	75	1	0.12	1.7	PC	25 / 30	0		637	36	U/K	U/K
U75-3	150	150	450	N/A	1.00	75	1	0.12	1.7	PC	25 / 30	0		584	33	U/K	U/K
W00-1	150	150	450	N/A	1.00	3	1	0.12	1.7	PC	25 / 30	0		806	36	U/K	U/K
W00-2	150	150	450	N/A	1.00	3	1	0.12	1.7	PC	25 / 30	0		852	38	U/K	U/K
W00-3	150	150	450	N/A	1.00	3	1	0.12	1.7	PC	25 / 30	0		844	38	U/K	U/K
W25-1	150	150	450	N/A	1.00	25	1	0.12	1.7	PC	25 / 30	0		848	39	U/K	U/K
W25-2	150	150	450	N/A	1.00	25	1	0.12	1.7	PC	25 / 30	0		849	39	U/K	U/K
W25-3	150	150	450	N/A	1.00	25	1	0.12	1.7	PC	25 / 30	0		899	41	U/K	U/K
W50-1	150	150	450	N/A	1.00	50	1	0.12	1.7	PC	25 / 30	0		879	43	U/K	U/K
W50-2	150	150	450	N/A	1.00	50	1	0.12	1.7	PC	25 / 30	0		870	43	U/K	U/K
W50-3	150	150	450	N/A	1.00	50	1	0.12	1.7	PC	25 / 30	0		910	45	U/K	U/K
W75-1	150	150	450	N/A	1.00	75	1	0.12	1.7	PC	25 / 30	0		854	48	U/K	U/K
W75-2	150	150	450	N/A	1.00	75	1	0.12	1.7	PC	25 / 30	0		886	50	U/K	U/K
W75-3	150	150	450	N/A	1.00	75	1	0.12	1.7	PC	25 / 30	0		924	52	U/K	U/K

NOTES: Strain measurements using GeoPIV software, as coded by White et al. (2003)

Table 2-2 (contd.): Experimental testing on prismatic cross-sections (part 9 of 11)

AUTHOR ID	SPECIMEN GEOMETRY						MATERIAL DATA					LOAD PROFILE		RESULTS			
	BREDTH	WIDTH	HEIGHT	HEIGHT INC. CORBELS	ASPECT RATIO	CORNER RADIUS	FRP DETAIL (No. WRAPS)	NOMINAL PLY THICKNESS	ULTIMATE TENSILE STRAIN AT RUPTURE	PLAIN OR REINFORCED CONCRETE	UNCONFINED COMP. CUBE STRENGTH	LOAD ECCENTRICITY	LOADING NOTES	PEAK LOAD	PEAK COMP. STRESS	AXIAL STRAIN AT PEAK LOAD	FAILURE MODE[†]
	b mm	h mm	H mm	H_{corbel} mm	h/b	R_c mm					f_{cu} MPa	e_i mm		N kN	f_{cc} MPa	ε_{cc}	
De Luca et al. (2011)																	
S-1-control	610	610	304	N/A	1.00	25.4	0	N/A	N/A	RC	46.625	0		9870	U/K	U/K	U/K
S-1-5GA	610	610	304	N/A	1.00	25.4	5	1.23	4.7	RC	60.75	0		N/A	U/K	U/K	U/K
S-1-2GB	610	610	304	N/A	1.00	25.4	2	1.18	4.5	RC	46.375	0		9790	U/K	U/K	U/K
R-1-control	508	737	304	N/A	1.45	25.4	0	N/A	N/A	RC	60	0		U/K	U/K	U/K	U/K
R-1-5GA	508	737	203	N/A	1.45	25.4	5	1.23	4.7	RC	70.5	0		5050	U/K	U/K	U/K
R-0.5-control	356	508	203	N/A	1.43	25.4	0	N/A	N/A	RC	43.375	0		5050	U/K	U/K	U/K
R-0.5-5GA	356	508	203	N/A	1.43	25.4	5	1.23	4.7	RC	67.25	0		6490	U/K	U/K	U/K
R-0.5-2GB	356	508	203	N/A	1.43	25.4	2	1.18	4.5	RC	58	0		5360	U/K	U/K	U/K
R-0.5-5GB	356	508	203	N/A	1.43	25.4	5	2.95	4.5	RC	62.125	0		6860	U/K	U/K	U/K
NOTES:	GFRP used in this series of tests																
Hadi and Widiarsa (2012)																	
0C0	200	200	800	N/A	1.00	34	0	N/A	N/A	RC	79.5	0		3248	U/K	U/K	C-SB
0C25	200	200	800	N/A	1.00	34	0	N/A	N/A	RC	79.5	25		1950	U/K	U/K	C-SB
0C50	200	200	800	N/A	1.00	34	0	N/A	N/A	RC	79.5	50		1336	U/K	U/K	C-SB
0B	200	200	800	N/A	1.00	34	0	N/A	N/A	RC	79.5	bending		241	U/K	U/K	C-SB
1HC0	200	200	800	N/A	1.00	34	1	0.45	U/K	RC	79.5	0		3279	U/K	U/K	FRP-R
1HC25	200	200	800	N/A	1.00	34	1	0.45	U/K	RC	79.5	25		2076	U/K	U/K	FRP-R
1HC50	200	200	800	N/A	1.00	34	1	0.45	U/K	RC	79.5	50		1433	U/K	U/K	FRP-R
1HB	200	200	800	N/A	1.00	34	1	0.45	U/K	RC	79.5	bending		247	U/K	U/K	FRP-R
3HCO	200	200	800	N/A	1.00	34	3	1.35	U/K	RC	79.5	0		3585	U/K	U/K	FRP-R
3HC25	200	200	800	N/A	1.00	34	3	1.35	U/K	RC	79.5	25		2269	U/K	U/K	FRP-R
3HC50	200	200	800	N/A	1.00	34	3	1.35	U/K	RC	79.5	50		1534	U/K	U/K	FRP-R
3HB	200	200	800	N/A	1.00	34	3	1.35	U/K	RC	79.5	bending		260	U/K	U/K	FRP-R
1V2HC0	200	200	800	N/A	1.00	34	2 (w strips)	0.90	U/K	RC	79.5	0		3522	U/K	U/K	FRP-R
1V2HC25	200	200	800	N/A	1.00	34	2 (w strips)	0.90	U/K	RC	79.5	25		2296	U/K	U/K	FRP-R
1V2HC50	200	200	800	N/A	1.00	34	2 (w strips)	0.90	U/K	RC	79.5	50		1533	U/K	U/K	FRP-R
1V2HB	200	200	800	N/A	1.00	34	2 (w strips)	0.90	U/K	RC	79.5	bending		518	U/K	U/K	FRP-R
NOTES:	Axial strain at ultimate load is stated for each specimen type, as opposed to each specific specimen																

Table 2-2 (contd.): Experimental testing on prismatic cross-sections (part 10 of 11)

AUTHOR ID	SPECIMEN GEOMETRY						MATERIAL DATA				LOAD PROFILE		RESULTS			FAILURE MODE[†]
	BREDTH	WIDTH	HEIGHT	HEIGHT INC. CORBELS	ASPECT RATIO	CORNER RADIUS	FRP DETAIL (No. WRAPS)	NOMINAL PLY THICKNESS	ULTIMATE TENSILE STRAIN AT RUPTURE	PLAIN OR REINFORCED CONCRETE	UNCONFINED COMP. CUBE STRENGTH	LOAD ECCENTRICITY	LOADING NOTES	PEAK LOAD	PEAK COMP. STRESS	AXIAL STRAIN AT PEAK LOAD	
	b mm	h mm	H mm	H_{corbel} mm	h/b	R_c mm					f_{cu} MPa	e_l mm		N kN	f_{cc} MPa	ε_{cc}	
Wang et al. (2012)																	
S1H1L0M	305	305	915	N/A	1.00	30	0	N/A	N/A	RC	U/K	0		U/K	32	0.373	C-SB
S1H2L0M	305	305	915	N/A	1.00	30	0	N/A	N/A	RC	U/K	0		U/K	35	0.412	C-SB
S1H1L1M	305	305	915	N/A	1.00	30	1	0.17	U/K	RC	U/K	0		U/K	35	0.428	FRP-R
S1H1L2M	305	305	915	N/A	1.00	30	2	0.33	U/K	RC	U/K	0		U/K	35	0.434	FRP-R
S1H1L2C	305	305	915	N/A	1.00	30	2	0.33	U/K	RC	U/K	0	Cyclic	U/K	34	0.387	FRP-R
S1H1L3M	305	305	915	N/A	1.00	30	3	0.50	U/K	RC	U/K	0		U/K	37	0.428	FRP-R
S1H1L3C	305	305	915	N/A	1.00	30	3	0.50	U/K	RC	U/K	0	Cyclic	U/K	37	0.487	FRP-R
S1H2L1M	305	305	915	N/A	1.00	30	1	0.17	U/K	RC	U/K	0		U/K	31	0.53	FRP-R
S1H2L2M	305	305	915	N/A	1.00	30	2	0.33	U/K	RC	U/K	0		U/K	36	0.416	FRP-R
S1H2L3M	305	305	915	N/A	1.00	30	3	0.50	U/K	RC	U/K	0		U/K	37	0.529	FRP-R
S1H1L2D1	305	305	915	N/A	1.00	30	2	0.33	U/K	RC	U/K	0		U/K	35	0.452	FRP-R
S1H1L2D2	305	305	915	N/A	1.00	30	2	0.33	U/K	RC	U/K	0		U/K	36	0.432	FRP-R
S1H1L3D2	305	305	915	N/A	1.00	30	3	0.50	U/K	RC	U/K	0		U/K	37	0.449	FRP-R
S1H1L3D2	305	305	915	N/A	1.00	30	3	0.50	U/K	RC	U/K	0		U/K	35	0.456	FRP-R
S2H1L0M	204	204	612	N/A	1.00	20	0	N/A	N/A	RC	U/K	0		U/K	30	0.364	C-SB
S2H2L0M	204	204	612	N/A	1.00	20	0	N/A	N/A	RC	U/K	0		U/K	33	0.406	C-SB
S2H1L1M	204	204	612	N/A	1.00	20	1	0.17	U/K	RC	U/K	0		U/K	36	0.704	FRP-R
S2H1L1P	204	204	612	N/A	1.00	20	1	0.17	U/K	RC	U/K	0		U/K	33	0.485	FRP-R
S2H1L1C	204	204	612	N/A	1.00	20	1	0.17	U/K	RC	U/K	0	Cyclic	U/K	34	0.535	FRP-R
S2H1L2M	204	204	612	N/A	1.00	20	2	0.33	U/K	RC	U/K	0		U/K	35	0.633	FRP-R
S2H1L2P	204	204	612	N/A	1.00	20	2	0.33	U/K	RC	U/K	0		U/K	38	0.921	FRP-R
S2H1L2C	204	204	612	N/A	1.00	20	2	0.33	U/K	RC	U/K	0	Cyclic	U/K	35	0.797	FRP-R
S2H2L1M	204	204	612	N/A	1.00	20	1	0.17	U/K	RC	U/K	0		U/K	33	0.465	FRP-R
S2H2L1C	204	204	612	N/A	1.00	20	1	0.17	U/K	RC	U/K	0	Cyclic	U/K	34	0.654	FRP-R
S2H2L2M	204	204	612	N/A	1.00	20	2	0.33	U/K	RC	U/K	0		U/K	34	0.652	FRP-R
S2H2L2C	204	204	612	N/A	1.00	20	2	0.33	U/K	RC	U/K	0	Cyclic	U/K	36	0.801	FRP-R

NOTES:
FRP overlap of 150mm near the corners
Average compressive cylinder strength at 28 days was 23.9MPa and actual at time of testing was 25.5MPa
Specimens D1 and D2 were subject to different levels of loading prior to application of the FRP, this predamage was applied through cycling the compressive axial load five times with each cycle readhing up to 40% and 80% of the confined RC column capacity respectively

Table 2-2 (contd.): Experimental testing on prismatic cross-sections (part 11 of 11)

AUTHOR ID	SPECIMEN GEOMETRY						MATERIAL DATA					LOAD PROFILE		RESULTS			
	BREDTH	WIDTH	HEIGHT	HEIGHT INC. CORBELS	ASPECT RATIO	CORNER RADIUS	FRP DETAIL (No. WRAPS)	NOMINAL PLY THICKNESS	ULTIMATE TENSILE STRAIN AT RUPTURE	PLAIN OR REINFORCED CONCRETE	UNCONFINED COMP. CUBE STRENGTH	LOAD ECCENTRICITY	LOADING NOTES	PEAK LOAD	PEAK COMP. STRESS	AXIAL STRAIN AT PEAK LOAD	FAILURE MODE†
	b mm	h mm	H mm	H_{corbel} mm	h/b	R_c mm					f_{cu} MPa	e_i mm		N kN	f_{cc} MPa	ε_{cc}	
Micelli and Modrelli (2013)																	
NP1	150	300	150	N/A	2.00	25	0	N/A	N/A	PC	28	0		U/K	25	U/K	C-C
CP1	150	300	150	N/A	2.00	10	2	0.33	1.5	PC	28	0		U/K	32	U/K	FRP-R
CP2	150	300	150	N/A	2.00	25	1	0.17	1.5	PC	28	0		U/K	36	U/K	FRP-R
CP3	150	300	150	N/A	2.00	25	2	0.33	1.5	PC	28	0		U/K	42	U/K	FRP-R
NP6	200	400	150	N/A	2.00	25	0	N/A	N/A	PC	28	0		U/K	18	U/K	C-C
CP6	200	400	150	N/A	2.00	25	1	0.17	1.5	PC	28	0		U/K	30	U/K	FRP-R
CP7	200	400	150	N/A	2.00	25	2	0.33	1.5	PC	28	0		U/K	34	U/K	FRP-R
NOTES:	Short prisms, CP1 had a small corner radius of 10mm to simulate a wrong prepertion of column geometry																
Song et al. (2013)																	
SSP-1-1	100	100	300	N/A	1.00	10	1	0.13	U/K	PC	30	0		U/K	366	U/K	FRP-R
SSP-1-2	100	100	300	N/A	1.00	10	2	0.26	U/K	PC	30	0		U/K	431	U/K	FRP-R
SSP-1-3	100	100	300	N/A	1.00	10	3	0.39	U/K	PC	30	0		U/K	560	U/K	FRP-R
SSP-2-1	150	150	450	N/A	1.00	15	1	0.13	U/K	PC	30	0		U/K	686	U/K	FRP-R
SSP-2-2	150	150	450	N/A	1.00	15	2	0.26	U/K	PC	30	0		U/K	816	U/K	FRP-R
SSP-2-3	150	150	450	N/A	1.00	15	3	0.39	U/K	PC	30	0		U/K	1017	U/K	FRP-R
SSR-1	250	250	1000	N/A	1.00	25	1	0.17	U/K	RC	30	20		U/K	1214	U/K	FRP-R
SSR-2	250	250	1000	N/A	1.00	25	1	0.17	U/K	RC	30	60		U/K	1015	U/K	FRP-R
SSR-3	250	250	1000	1500	1.00	25	1	0.167	U/K	RC	30	100		U/K	568	U/K	FRP-R
SSR-4	250	250	1000	1500	1.00	25	1	0.167	U/K	RC	30	150		U/K	390	U/K	FRP-R
Notes:	FRP overlap of 100mm																

† Failure mode

C-S	Concrete spalling
C-C	Concrete crushing
C-CY	Concrete crushing, yielding steel
C-Sh	Concrete shear
C-SB	Concrete spalling, steel buckle
FRP-R	FRP rupture
FRP-RB	FRP rupture, bursting of concrete
FRP-RS	FRP rupture & yielding of steel
FRP-RB	FRP rupture, steel buckle

Table 2-2 demonstrates the limited availability of test specimens of large-scale, prismatic cross-section, especially subject to eccentric loading. For comparison purposes, small-scale specimens from Pessiki et al. (2001), Prota et al. (2003), El Maaddawy (2009), Al-Salloum (2007), and Barrington et al (2011) are included in view of the parameters varied and studied and so allow for good comparison with the test matrix presented in Chapter 3.

2.4.1. SIZE EFFECT

The research into the strength capacity gain in medium- and large-scale columns of prismatic cross-section subjected to concentric loading has been covered by Rochette and Labossière (2000), Pessiki et al. (2001), Lam and Teng (2003b), Rocca et al. (2005), Monti and Nistico (2008), and Wang et al. (2012). This research backs up the postulated theory that due to the existence of a size effect, it is not ideal to scale the results from small-scale specimens. This size effect can primarily be attributed to the length increase of the flat sides of the column cross-section on larger specimens.

Pessiki et al. (2001) tested small- and large-scale, FRP-confined prismatic columns however failed to provide an adequate comparison of the results in terms of size effect. The research demonstrates that for the large-scale specimens, the increase in capacity from the tests was not adequate to assume a large increase in load or deformation capacity, and that a large region along the flat sides of the cross-section showed little confinement. Furthermore, the research verified that there is minimal confinement in the concrete next to these flat sides and as such the stress-strain response differed significantly from that of circular columns, demonstrating a descending second region of the relatively bilinear response. Circular columns tend to demonstrate an increasing second region of the bilinear response, refer Figure 2-5. Thus in this instance there would be insufficient capacity for strength enhancement; this is corroborated by Lam and Teng (2003b).

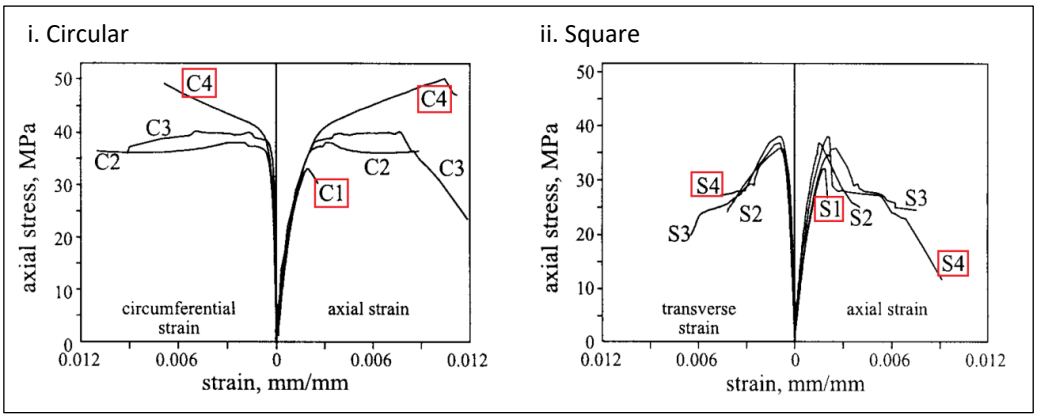

† Specimens denoted C1 and S1 are unconfined, Specimens denoted C4 and S4 are confined with 3 plies of CFRP

Figure 2-5: Axial stress-strain behaviour of large-scale specimens for i. circular columns and ii. square columns [Pessiki et al. (2001)]

Failure of specimens through rupture of the FRP jacket at a load higher than the unconfined specimens was commonly found, Pessiki et al. (2001), Rocca et al. (2005), Monti and Nistico (2008), Turgay et al. (2010) and Wang et al. (2012). However, beyond this, the variables in the research leave the specimen field sparse for comparison, specifically where a full set of FRP-confined specimens and corresponding unconfined control specimens are available for comparison.

With increase in specimen size and a subsequent increase in the lateral deflection at mid-height, the P-Delta effects require attention. Even though the loading is in theory solely axial, in reality, geometric imperfections and loading variance mean that there is some element of bending in these columns. It is essential to address the slenderness to determine the potential for buckling and second order effects, to establish the capacity of the specimen. Due to the bilinear behaviour of the stress-strain curves, once unconfined concrete capacity is reached, and the FRP engages, the stiffness of the column has dropped and as such, the slenderness of the FRP-confined column reduces. This is captured in Teng and Jiang (2009) revised critical slenderness for FRP-confined circular columns:

$$\lambda_{crit} = \frac{\lambda_{lim}}{\frac{f_{ccd}}{f_{co}}(1+0.06\rho_{\varepsilon})} \qquad (2\text{-}1)$$

where: $\rho_{\varepsilon} = \frac{\varepsilon_{h,rup}}{\varepsilon_{c2}}$ is the strain ratio

This equation encompasses the strain ratio and demonstrates that the increase in capacity without a corresponding increase in flexural stiffness, generates a lower critical stiffness

ratio. To further negate this, if a FRP-confined column is deemed to be slender, design is advised to take second order effects into consideration, TR55 (2011). Hadi (2006a) observed that the theoretical ultimate capacity of the columns did not take the bending element into consideration and as such, overstates the capacity. The significance is that the structure that has been designed without taking into consideration second order effects, and is now comparatively weaker in compression due to part of the axial capacity supporting the unconsidered moment. Thus the structure is required to adapt to abnormal loads before full redundancy, redistributing these unanticipated bending moments to other elements.

Strain in the FRP jacket was captured by Wang et al. (2012) when testing medium-scale specimens. The results of this demonstrated that in general, the strains in the wrap are higher in the middle as opposed to the corners. This result could do with being verified as the gauges were positioned on the corners with only one in-between each corner, hence a large portion of the behaviour of the FRP around the circumference has not been captured.

2.4.2. LOAD ECCENTRICITY

The research performed to date into medium- and large-scale columns of square cross-section, subject to eccentric loading have been covered by Chaallal and Shahawy (2000), Tao and Yu (2008), El Maaddawy (2009) and Song et al. (2013). FRP-confined columns have shown that as the load eccentricity is increased the flexural stiffness decreased as the stiffness enhancement of the axial load was diminishing. Testing on eccentrically loaded prismatic columns has been somewhat sparse, with more of the studies being focused on circular specimens. The form of the specimen and the application of the load can vary significantly.

Experimental results have demonstrated a general decrease in strength capacity as the eccentricity of the load increases [Chaallal and Shahawy (2000), Tao and Yu (2008), Midday (2009), Bisby and Ranger (2010), Song et al. (2013)]. Typical failure of the columns is in a flexural mode with large lateral deflections, and minimal or no strength increase obvious for unidirectional confined columns. Fundamentally, FRP-confinement has been found to significantly increase the deformability of columns, especially slender columns but provide minimal strength gains.

Chaallal and Shahawy (2000) studied eccentrically loaded beam columns as well as addressing the orientation of the fibres. Interestingly, they found that the curvature of the FRP-confined specimens was greater than that of the unconfined specimens. And as such they demonstrated the usefulness in flexure of the columns. When the flexure was controlled, the strengthened beam-columns demonstrated a higher flexural stiffness.

FRP-confined specimens are able to experience higher moment capacities as well as large deflections beyond the yielding stress of the steel, Chaallal and Shahawy (2000). The larger the applied eccentricity, the larger the mid-span deflections. Tao and Yu (2008) further backed these results with the behaviour of eccentrically loaded slender columns, with a height of 3000mm and cross-section 150mm square behaving in a similar manner. This emphasised the ductility available in the specimens when FRP confinement is utilised, as seen in Figure 2-6, where the ratio of applied load to the ultimate axial load can be seen to produce large deflections even at peak load. Specimen BS-3R was subject to a 100mm load eccentricity. Tao and Yu (2008) specimens were wrapped with both unidirectional and bidirectional fibre orientation, and for unidirectional fibre orientation, the strength capacity increase was negligible if indeed any at all. However bidirectional fibre orientation proved to be more effective, due to the support to axial and bending capacity simultaneously and demonstrated 29-62% increase, as opposed to no obvious increase for unidirectional.

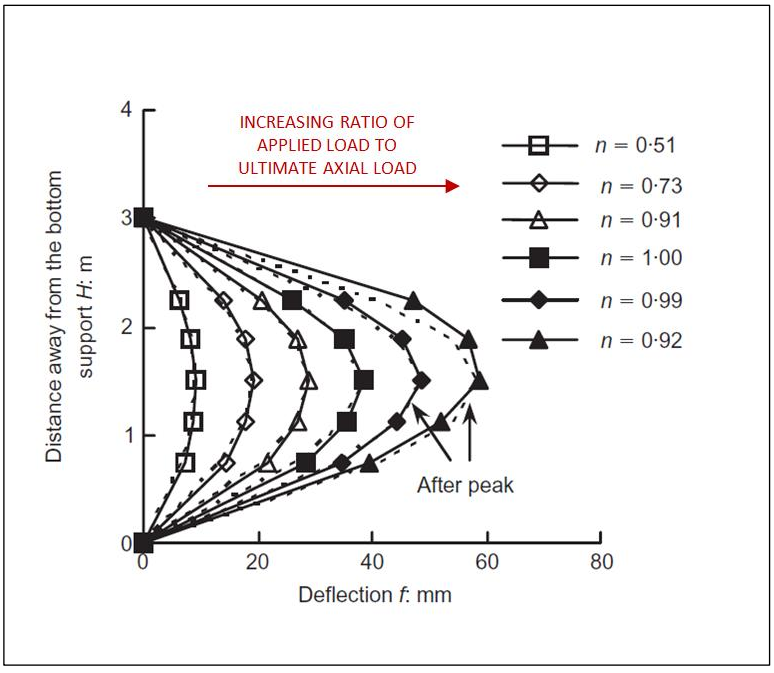

Figure 2-6: Column deflection with increasing load level, specimen BS-3R [Tao and Yu (2008)]

Slenderness of the FRP-confined columns is susceptible to an increase in the size of the transverse steel reinforcement, with increased size increasing the ductility of the column but not the ultimate strength, Turgay et al. (2010). This is useful to consideration in the design of reinforcement for existing columns.

With small-scale eccentrically loaded columns, the strength gain from FRP-confinement is found to be inversely proportional to the eccentricity ratio, El Maaddawy (2009). The results may be slightly exaggerated due to the sheer size of the corbel end sections, Figure 2-7, with the mass being so much that it could be causing a premature pulling in the rebar generating a yield failure in the reinforcement of the column and inducing a larger bending moment. El Maaddawy (2009) further studied the difference with fully and partially wrapped columns and verified the postulated theory that partially wrapped specimens had lower strength capacity.

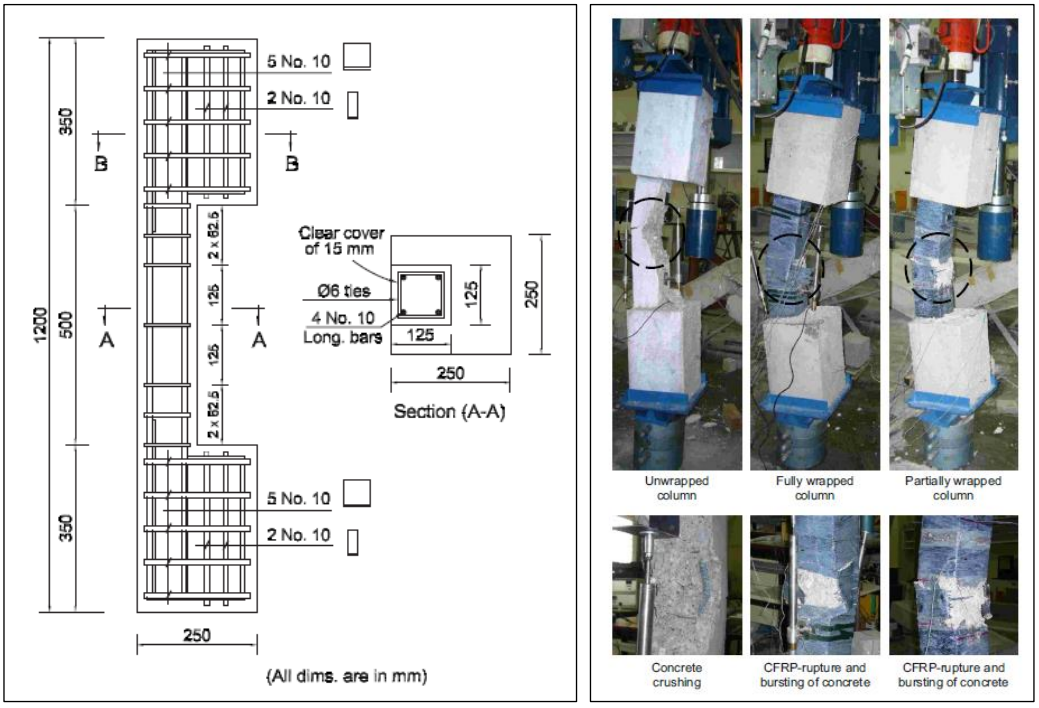

Figure 2-7: Eccentrically loaded columns with corbel ends, from left; specimen details and failure modes, El Maaddawy (2009)

Specimens of larger size have seen results demonstrating that the axial capacity increase over the unconfined equivalent is small but the deformation capacity increase is significant as the FRP jacket postpones rupture of the concrete and reinforcement. As the number of FRP plies used increases, or more optimally, FRP straps placed around a lesser number of

FRP sheets, this maximum compressive load that it could sustain increases linearly [Hadi and Widiarsa (2012) and Song et al. (2013)]. However as the load eccentricity increases, the sustained maximum compressive load decreases linearly.

Axial-flexural loading is commonly found in structures such as buildings and bridge piers. There is limited research on axial-flexural behaviour in FRP-confined columns, especially when taking into consideration the difficulty or reluctance to scale up results due to the size effect. Research conducted into the behaviour of FRP-confined columns in seismically active regions may hold an insight into this, but in many instances, the parameters varied and observed are not necessarily those chosen for addressing the potential strength capacity gain. Thus, the limiting aspect in this field of research is the size of the eccentrically loaded specimens and the lack of corresponding control specimens for those that have been tested.

2.4.3. CROSS-SECTIONAL ASPECT RATIO

The research performed to date into columns of rectangular cross-section have been covered by, Lam and Teng (2003b), Prota et al. (2003), Rocca at al. (2005), Youssef et al. (2007), Sadeghian (2010), Wu and Wei (2010), De Luca et al. (2011) and Micelli and Modarelli (2013). De Luca et al. (2011) used GFRP reinforcement for strengthening.

Fundamentally, as the cross-sectional aspect ratio of a prismatic column increases, the benefit from confinement of the column reduces [Rochette and Labossière (2000), Chaallal et al. (2003), Lam and Teng (2003b), Toutianji et al. (2010), Wu and Wei (2010) and Micelli and Modarelli (2013)] and the ultimate axial strain decreases, due to the longer flat sides that can sustain little or no loading. Lam and Teng (2003b) further demonstrated that an aspect ratio of greater than 1:2.6 (0.38), along with sharp corners can induce negative confinement, demonstrated by an overlap in the parabolic curves, Figure 2-8.

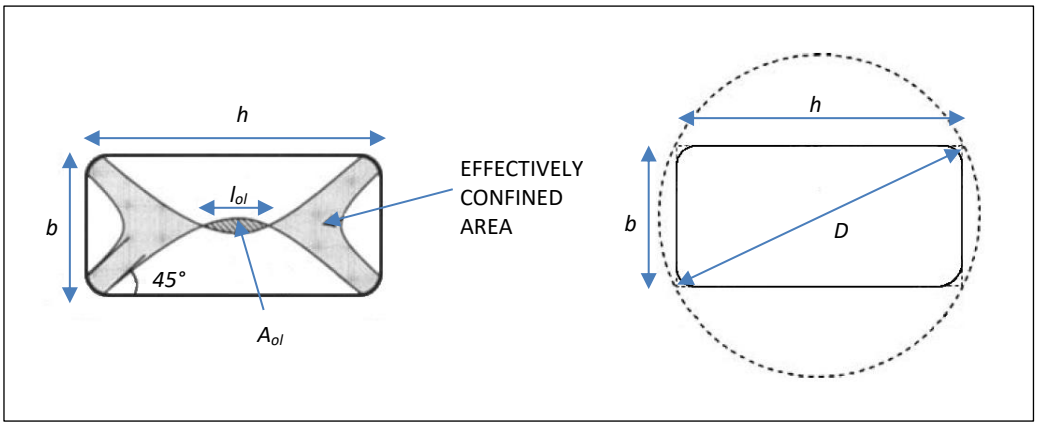

Figure 2-8: Area of overlap in confinement in large aspect ratio cross-sections [TR55 (2005)]

When examining the research on varying cross-sectional aspect ratio, often unconfined control specimens of concentric loading are omitted, thus making the comparison difficult. In particular, Chaallal and Shahawy (2000) tested medium-scale, eccentrically loaded specimens but the lack of an unconfined control specimen meant there was little to reference the change in behaviour between unconfined and FRP-confined. Furthermore, these specimens were tested as beam-columns with varying fibre architecture in the FRP jacket, thus they are omitted from detailed comparison with the experimental research presented in this thesis and are for specific reference only in this work.

Deviation from postulated behaviour and existing test results was evident with Chaallal et al. (2003), small-scale rectangular columns of various aspect ratios. These specimens were subject to concentric loading only. The results of this testing demonstrated that as the cross-sectional aspect-ratio of the columns increased, so too did the strength capacity. This is contrary to the testing of other researchers as confinement was found to be far more effective in terms of strength capacity for square cross-sections than rectangular, and as the aspect ratio increased, there was a reduction in the strength gain and effectiveness of confinement, until there was no significance in confinement for an aspect ratio of greater than 2.0 [Wu and Wei (2010), Micelli and Modarelli (2013)].

In terms of the stress-strain curve, if the second portion is ascending, there is deemed to be sufficient confinement. However, due to the mechanics of confinement, a descending branch was found instead for prismatic columns [Youssef et al. (2007), De Luca et al. (2011)]. This was due to the larger side dimensions and lower area of confinement in the specimens. The effectiveness was higher for square cross-section, the dilation ratio was smaller along

the diagonals than the two transverse directions as opposed to rectangular specimens where the dilation ratio was higher along the short or transverse directions but smaller on the long side length. Thus it is essential that this is addressed in the stress-strain modelling when used to design rectangular columns.

Other research into large cross-sectional aspect ratios includes Maalej et al. (2003) and Toutanji et al. (2010) who focused the research on large-scale (defined as field size), RC columns confined with FRP. The variables in the research were the aspect ratio and the corner radii. However, due to the sheer size of the longer flat sides, the relevance of the results is difficult to ascertain as the confinement mechanics of the specimens vary so significantly, with the area of confinement perhaps unable to meet from one end to the other. Toutanji et al. (2010) verified Lam and Teng (2003b) research showing that the confined strength decreased with larger aspect ratios due to the lack of confinement along the sides.

It became apparent through testing of rectangular specimens that a column with a large aspect ratio was influenced by a number for factors. Firstly, these specimens required a thicker FRP jacket to avoid degradation before FRP rupture, and secondly, the maximum axial strain at peak decreased with increasing aspect ratio, hence the confinement effectiveness similarly decreased with increasing aspect ratio [Wu and Wei (2010)]. Lastly, confinement effectiveness decreased with increase of concrete strength and this cannot be counteracted by increasing the number of wraps for strength gain [Micelli and Modarelli (2013)].

2.4.3.1. COMBINED CROSS-SECTIONAL ASPECT RATIO AND LOAD ECCENTRICITY

The research on columns of rectangular cross-section subjected to eccentric loading is even sparser and where this research is available, a control specimen of concentric loading is lacking.

Sadeghian et al. (2010) addressed the eccentricity of load alongside variation in the number of wraps and orientation of the FRP. All specimens were bidirectionally wrapped and as such do not lend to an accurate comparison in this research. The overall behaviour of these specimens was seen to be of similar nature to that of unidirectional wrapping; with large ductility evident and failure though rupture of the FRP alongside yielding of the reinforcing

longitudinal steel bars, producing a bilinear stress-strain curve. Particularly, when the fibre orientation in the FRP jacket was ±45 degrees, as opposed to the lateral and longitudinal combinations, optimal behaviour was demonstrated in terms of ductility/deformation improvement.

Additionally, when strengthened columns failed in a tension-controlled manner, the transverse layers did not demonstrate any confinement improvement on the compression side of the section. In this region, concrete behaviour is similar to the unconfined concrete. Thus it is essentially ineffective for use in strength enhancement through confinement.

However, within analysis of the results, cross-sectional confinement behaviour has not been examined in detail; hence the movement of the effectively confined area as a combination of both rectangular shape and load eccentricity is not explicitly understood.

2.4.4. EFFECT OF CORNER RADIUS DIMENSION

The size of the corner radius relative to the cross-sectional dimensions has a significant effect on strength capacity gain of FRP-confined columns [Al-Salloum (2007), Barrington et al. (2011)]. It has been well established that circular specimens provided more confinement than a prismatic equivalent as the whole circular cross-section is confined and as such, prismatic columns with larger radii, can generate greater confining forces at the corners. For square columns, an increase in efficiency in confinement as the corner radius increased in size and proximity due to the assumed parabolic arching action over the cross-section was established [Matthys et al. (2005)]. Furthermore, this was corroborated as Campione and Miraglia (2003), Rochette et al. (2000), Lam and Teng (2003b), Yang et al. (2004), Al-Salloum (2007), Barrington et al. (2011) all found that the effective stress increased as the corner radius-to-section width ratio increased, with sharp corners demonstrating significantly lower confinement capacity.

Examination of the stress-strain diagram for small-scale specimens of varying radii [Al-Salloum (2007)] illustrated increased axial and ductile capacity with larger corner radius, ultimately with the optimal being of circular cross-section, Figure 2-9. The initial portion of the bilinear curve was similar for specimens of all corner radii, however, beyond the transition zone, as the slope was a function of the ratio of corner radius to cross-section height, as this ratio was increased, consequently the performance improved.

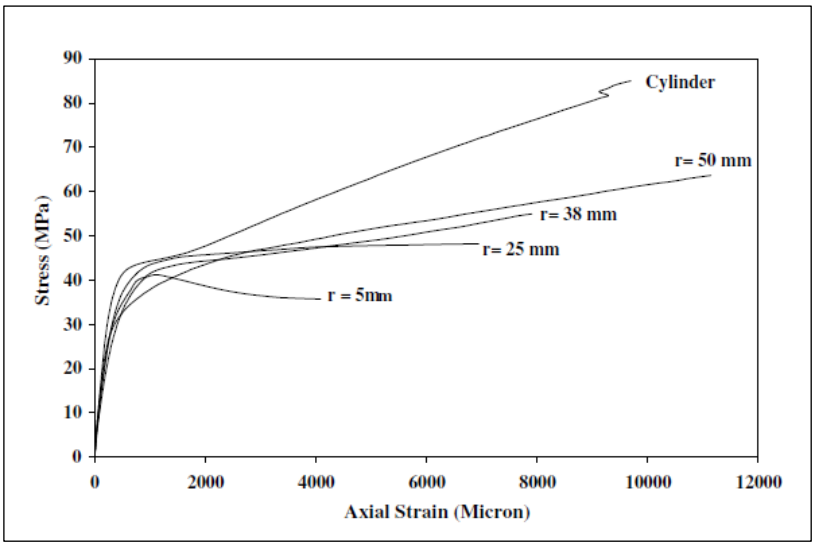

Figure 2-9: Stress-strain plot demonstrating the effect of corner radius on confined square columns, Al-Salloum (2007)

Research by Wang and Wu (2008), verified that the post peak slope of the stress-strain curve increased as the corner radius increased. Thus the increment of the effective confining strength was highly influenced by the corner radius and this gain in strength capacity was in direct proportion with the corner radius ratio.

Strain in the FRP jacket varies over the height of the specimen as well as in the transverse direction. To encapsulate the FRP behaviour over the height, Barrington et al. (2011) made use of GeoPIV software, already proven to have an excellent correlation with typically used foil strain gauges [Bisby and Take (2009)]. GeoPIV software interpreted readings using high resolution digital image correlation. The surface was prepared of uneven colour/texture and strain distributions from this were measured between pre-set cameras at predefined intervals.

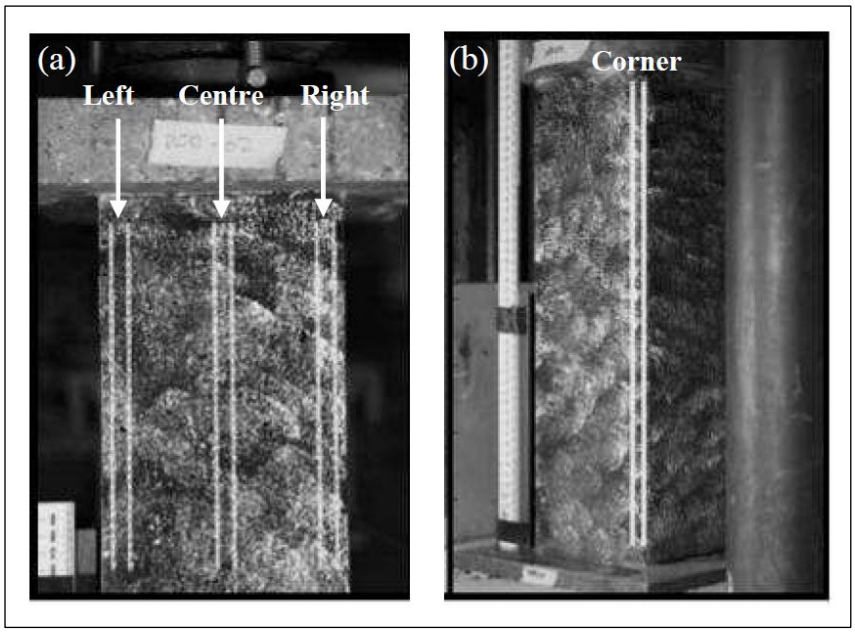

Figure 2-10: Digital image correlation photographs showing lines of pixel patch pairs for (a) flat face left, centre, and right strain measurements and (b) corner strain measurements [Barrington et al. (2011)]

Using software developed by White et al. (2003), an area for investigation was defined in the first image reviewed, Figure 2-10, and this was tracked throughout the following images selected for assessment. The selected area could be located anywhere within the field of view of the camera, and measurements in the selected area taken in any in-plane direction. Defining pairs of the selected areas, allowed for strains to be computed over any chosen gauge length, in any direction. This image correlation technique has a proven accuracy exceeding one tenth of one pixel [White et al. (2003)].

The strain data collected gave an excellent insight into the strain behaviour over the height of the specimen, Figure 2-11. Failure of the specimen occurred at mid-height, which was the location of highest strain as demonstrated by the failure photograph. The strains at each end of the specimens were similar irrespective of corner radii, but increased in the middle section with larger corner radius as anticipated.

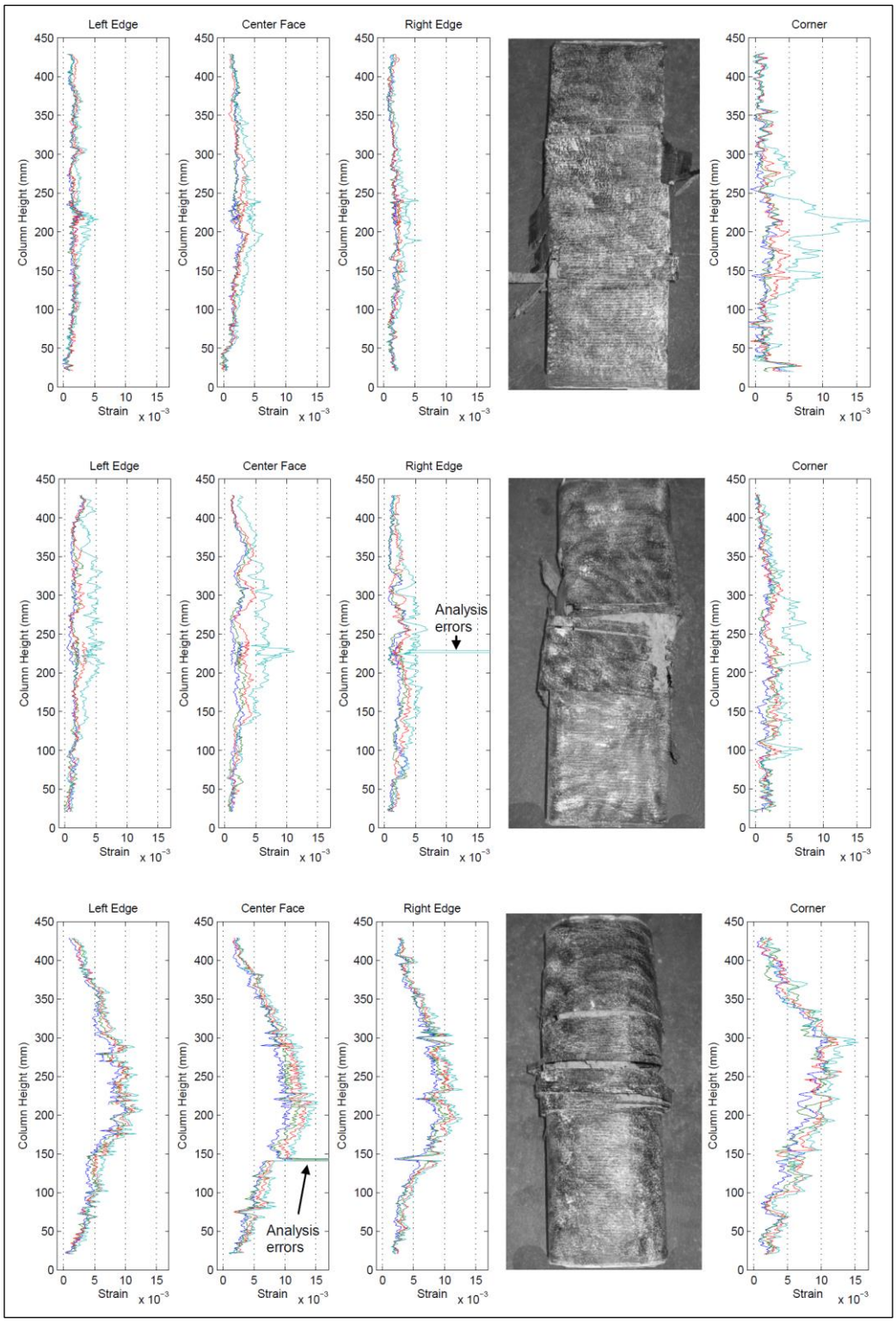

Figure 2-11: Hoop strain profiles near failure for corner radius of; top 3mm, middle 25mm and bottom 50mm, using GeoPIV software [Barrington et al. (2011)]

FRP strains were of consistent magnitude over the flat side between the corners (refer to Figure 2-10 for patch locations), and these strains increased with larger corner radius. It could not be fully ascertained from the data presented, if the left and right strain patches, Figure 2-10, were located within the corner radius and so were subject to consistent spacing relative to the width of the specimen, or were moved relative to the corner edge as the size of the corner radius increased. If the location of the gauge remained in the same location relative to the cross-section width, potential bending effects from the curvature of the surface could have registered in the gauges and had an influence on the results.

In terms of magnitude, the FRP ultimate strain was only observed in the circular specimens prior to failure, and not observed in prismatic specimens (also witnessed by Bisby and Take (2009)]. Furthermore, as the corner radii decreased, the magnitude of strain prior to failure also reduced. Thus there was a direct correlation between the sharpness of the corner and the failure strength of the FRP jacket [Karam & Tabbara (2004), Al-Salloum (2007)] as a smaller corner radius corresponded to a smaller hoop strain efficiency.

Failure of prismatic specimens tended to originate in close proximity to the corners due to the weak flexural rigidity of the FRP at the flat face [Cole and Belarbi (2001), Barrington et al. (2011)], enabling the specimen to bulge as lateral dilation of the concrete occurred under compression, subsequently causing higher localised hoop strains at the corners. Thus, the FRP coupon ultimate strain had evidently been a reasonable estimation of the FRP jacket failure strain for circular specimens but requires adaption to encompass the effects from the prismatic cross-section and the change from curved surface of the corners to the flat sides of the specimen.

Fundamentally, the effect of confinement on columns with sharp corners is insufficient to provide a reasonable strength increase in the specimens. However after peak load this confinement increases and is sufficient enough to increase the ductility in the specimens.

2.4.5. FURTHER EXPERIMENTAL STUDY OF FRP-CONFINED PRISMATIC COLUMNS

Numerous other parameters have been varied and analysed in experimental testing with respect to FRP-confined RC columns, and although not directly relating to the test parameters here, due to the relevance with interpretation of the results, these have been

studied. These parameters include; fibre direction of FRP jacket, number of FRP layers and the transverse steel reinforcement.

The application of the FRP jacket has received attention, with unidirectional, or bidirectional fibres an option, and the angle of placement also a variable. Fibres are often wrapped solely in the hoop direction for lateral restraint of the concrete, as when aligned unidirectionally along other axes are found to be of negligible benefit to the strength increase, instead aiding the flexural capacity when oriented towards the longitudinal direction [Mirmiran et al. (1998), Fitzwilliam and Bisby (2010)]. The optimum angle for application of unidirectional FRP for strength increase is between 0 degrees and 15 degrees as it has been observed that the pure axial strength of the section decreased as the winding angle increased and the flexural capacity increased with the winding angle up to 45 degrees [Chaallal and Shahawy (2000)]. Hence to achieve a gain in both strength and ductility, bidirectional fibres are often used.

Parvin and Wang (2001) demonstrated that as the use of external reinforcement of the column increased the load capacity of the column, the further increase in load capacity with the number of layers of external reinforcement was observed. This is analogous to circular columns. Lam and Teng (2003b) demonstrated an increase in ductility as the number of layers of FRP increased. Another option in confinement is to adopt straps over a layer of FRP confinement which proved to be as beneficial as a few more FRP plies and due to the reduction in material, a more cost effective method [Hadi and Widiarsa (2012)].

Adapting the amount of transverse steel reinforcement influenced the failure behaviour of FRP-confined specimens [Turgay et al. (2010)]. The longitudinal reinforcement did not have an effect on the ductility of the columns, however this was for short specimens, hence the results are of limited direct relevance.

2.5. FINITE ELEMENT MODELLING – BACKGROUND AND ANALYSIS

Finite Element Modelling (FEM) can facilitate with an accurate simulation and assessment of the formation and evolution of the effectively confined area, and the strain generated at the corners from which the resultant confining forces can be established. FEM is an idealisation of the structure or component, generated by a series of nodes linked by elements of finite size. Each node or element is defined by a set of descriptions, detailing material, boundary constraints, interaction specification and loading data.

In this research FEM has been utilised as a tool to analyse the distribution of confined stresses at the mid-height plane of the column, for a representative loading profile, as established in the experimental study. The simulations developed were numerically modelled using 3D hexahedral elements, adapting parameters of aspect ratio and load eccentricity on prismatic FRP-confined columns to validate postulated theory and enable comparison with the analytical model established from experimental results.

2.5.1. FEM BACKGROUND

FEM of a FRP-confined prismatic column cross-section to evaluate the effectively confined area has not been extensive. The relevant models are summarised in Table 2-3, in terms of material, geometry and boundary condition parameters.

Table 2-3: Details of FE Model Construction relevant to Authors Experimental Investigation (part 1 of 3)

CONCRETE MODEL	FRP MODEL	CONCRETE/FRP INTERACTION	BOUNDARY CONDITIONS
YANG ET AL. (2004)			
NOT SPECIFIED	TWO-NODE LINEAR TIMOSHENKO BEAM ELEMENTS	FINITE MOTION WITH NO SEPARATION	SYMMETRIC BCS APPLIED AT TWO CUT FACES PARALLEL TO AXIS OF COLUMN FORCE APPLIED AT ONE END OF THE FRP, OTHER RESTRAINED
PACKAGE: ABAQUS (1998)			
KARAM AND TABBARA (2005)			
ADINA BUILT IN MODEL (HYPO-ELASTIC, BASED ON UNIAXIAL STRESS-STRAIN RELATION) $E_c = 26\ GPa$ $\mu = 0.18$	LINEAR ELASTIC BEHAVIOUR TO FAILURE $E_{frp} = 105\ GPa$	CONCRETE AND FRP SHARED SAME NODES, THUS REPRESENTING A PERFECT BOND	NOT SPECIFIED
PACKAGE: ADINA NOTES: NEWTON ITERATIVE APPROACH USED f_c = 30MPa OCCURRING AT A STRAIN OF 0.002			
CHAKRABARTI ET AL. (2008)			
SOLID65 LINEAR, ELEMENTS, 8-NODED, CAPABLE OF PLASTIC DEFORMATION, CRACKING AND CRUSHING FOR CONCRETE. WILLIAM AND WARNKE FIVE PARAMETER FAILURE MODEL USED. $E_c = 4732.9765\sqrt{f_c}$ $f_t = 0.62276\sqrt{f_c}$ $\mu = 0.2$ LINK8 ELEMENTS FOR STEEL REINFORCEMENT $E_s = 200{,}000MPa$ $\mu = 0.3$	SOLID 64 LAYERED ELEMENTS, ASSUMED ORTHOTROPIC	NOT SPECIFIED	BOTTOM END OF COLUMN FIXED SYMMETRIC BCS APPLIED AT TWO CUT FACES PARALLEL TO AXIS OF COLUMN UNIFORM DISPLACEMENT ON THE TOP SURFACE IN AXIAL DIRECTION.
PACKAGE: ANSYS NOTES: ELASTIC MODULUS AND TENSILE STRENGTH ACCORDING TO ACI: 319, 1999 NEWTON-RAPHSON APPROACH TO NONLINEAR ANALYSIS USED			

Table 2-3 (contd.): Details of FE Model Construction relevant to Authors Experimental Investigation (part 2 of 3)

CONCRETE MODEL	FRP MODEL	CONCRETE/FRP INTERACTION	BOUNDARY CONDITIONS
DORAN ET AL. (2009)			
DRUCKER-PRAGER WITH EIGHT-NODED ISOPARAMETRIC SOLID ELEMENT WITH AN INCOMPATIBLE STRAIN FIELD	LINEAR ELASTIC THICK SHELL ELEMENTS	NOT SPECIFIED	DISPLACEMENT OF THE TOP SURFACE OF THE COLUMN
PACKAGE: NOT SPECIFIED NOTES: THIS PAPER BUILDS UPON WORK OF KOLSAL ET AL. (2009) HENCE IS IT NOT PRESENTED SEPARATELY HERE.			
YU ET AL. (2010)			
8-NODE SOLID ELEMENTS TO PRODUCE A CONCRETE DAMAGED PLASTICITY MODEL STRAIN HARDENING/ SOFTENING RULE AND FLOW RULE ARE VARIABLES.	4-NODE SHELL LINEAR ELASTIC WITH STIFFNESS IN THE HOOP DIRECTION ONLY	MESH TIE CONSTRAINT	BCS REPRESENTED AXIS-SYMMETRIC BEHAVIOUR
PACKAGE: ABAQUS NOTES: FEM PURPOSE WAS TO EVALUATE THE PLASTICITY MODEL, INCLUDING VARIATIONS IN STRAIN-HARDENING/SOFTENING AND FLOW-RULE.			
HAJSADEGHI ET AL. (2011)			
SOLID65, AN 8-NODED SOLID BRICK ELEMENT LINK8 FOR STEEL REINFORCEMENT	SHELL41, A 3D ELEMENT WITH MEMBRANE STIFFNESS BUT NO BENDING	NOT SPECIFIED	BCS REPRESENTED AXIS-SYMMETRIC BEHAVIOUR, CONCENTRIC LOADING, THUS QUARTER MODELLED
PACKAGE: ANSYS 5.4 (1995) NOTES: STEEL PLATES (SOLID45 ELEMENTS) WERE MODELLED AT THE TOP AND BOTTOM OF THE SPECIMEN FOR LOAD APPLICATION ON TOP, AND FIXED BC ON BOTTOM PLATE			
CSUKA AND KOLLÁR (2012)			
CONFINEMENT SENSITIVE PLASTICITY CONSTITUTIVE MODEL OF PAPANIKOLAOU AND KAPPAS (2007)	LAMINATED PLATE THEORY ASSUMING LINEAR ELASTIC BEHAVIOUR TO FAILURE	NOT SPECIFIED	ONE AXIS OF SYMMETRY
PACKAGE: NOT SPECIFIED NOTES: NOMINAL THICKNESS MODELLED			

Table 2-3 (contd.): Details of FE Model Construction relevant to Authors Experimental Investigation (part 3 of 3)

CONCRETE MODEL	FRP MODEL	CONCRETE/FRP INTERACTION	BOUNDARY CONDITIONS
MOSTOFINEJAD ET AL. (2015)			
DRUCKER-PRAGER PLASTICITY MODEL	ORTHOTROPIC MATERIAL, LINEAR ELASTIC UNTIL FAILURE USING TSAI-WU FAILURE CRITERION	NOT SPECIFIED	BCS REPRESENTED AXIS-SYMMETRIC BEHAVIOUR, CONCENTRIC LOADING, THUS QUARTER MODELLED AXIAL LOAD APPLIED TO TOP OF SPECIMEN
PACKAGE: NOT SPECIFIED NOTES: NOMINAL THICKNESS MODELLED			

FEM has focused on the effect of the corner radius, specifically in relation to the confinement generated. Yang et al. (2004) developed a simple experimental test device, Figure 2-12, that allowed for interchangeable corner sections, between 0 to 50.8mm radius (the side dimensions of the corner insert being 100mm by 100mm for 0mm corner radius), and applied the FRP jacket around the outside of the test device, as the effect of wrapping manifests in the radial stress. The results of this experiment were compared with the presented FEM.

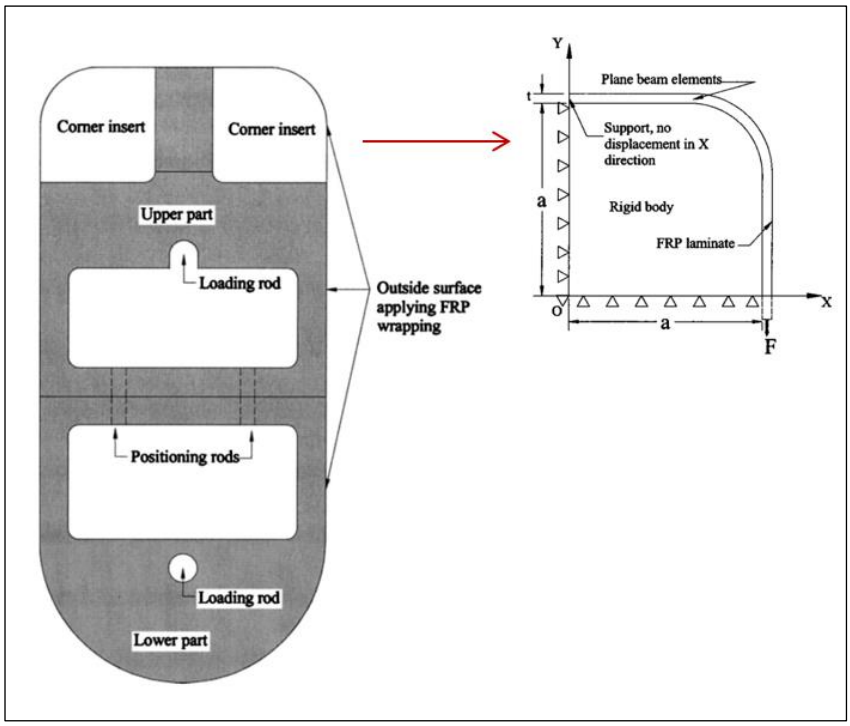

Figure 2-12: Test set-up, with FEM corner detail [Yang et al. (2004)]

To verify these experimental results, Yang et al. (2004) used ABAQUS to model a quarter of the cross-section (taking into account symmetry), with boundary conditions applied as per Figure 2-12. Reasonable agreement was found between the experimental and FEM results, with the identification of the stress concentration factor in the FEM results at the higher end of the test results.

FEM results agreed with experimental testing and other research [Barrington et al. (2011)] on changing size of corner radii, with the larger corner radius experiencing a greater strain in the FRP wrap. Another parameter varied was the number of FRP plies, and as this increased, so did the stress measured over the cross-section, again reflected with the FEM results.

Interestingly Yang et al. (2004) also considered the integrity of the corner inserts through a film applied over the corner radius which was peeled off post-testing and examined by the manufacturers. This demonstrated that the radial distribution around the corner of the smaller radius to be higher, and much more localised, Figure 2-13, due to the confined area being a function of the corner radius and confining efficiency, dependent on the distribution over the cross-section.

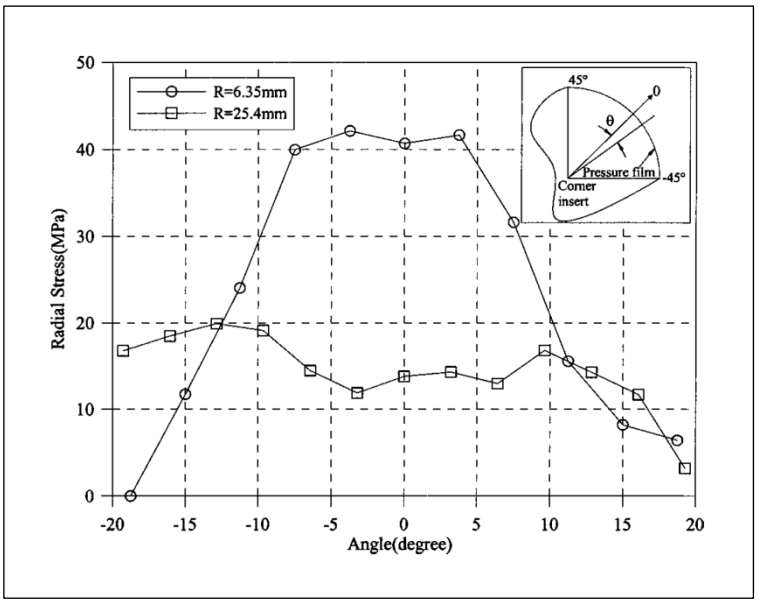

Figure 2-13: Radial stress distribution at the corners, established through experimental testing [Yang et al. (2004)]

When the step duration was controlled in FEM, the development and movement of the stress over the cross-section could be monitored. As the applied load increased, the stress clearly developed at the corners of the cross-section with minimal effect on the flat sides [Chakrabarti et al. (2008)], Figure 2-14.

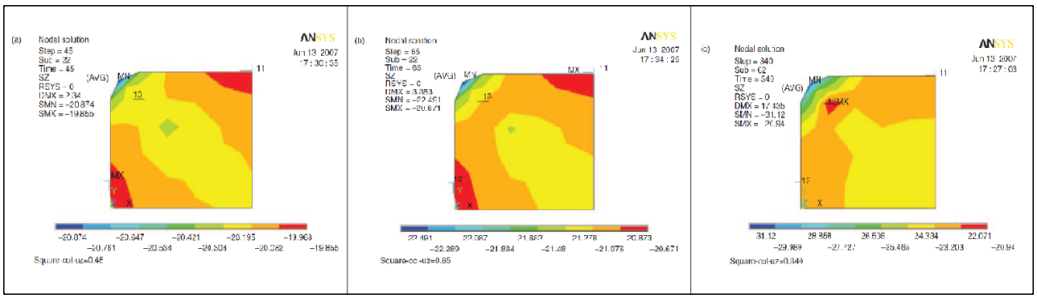

Figure 2-14: Axial stresses in the concrete at various stages of the analysis [Chakrabarti et al. (2008)]

This development was further corroborated by Yu et al. (2010). Teng et al. (2007) model, detailed in Section 2.6.1 was adopted to produce material parameters for the model, due to the ability to predict the entire axial stress-axial strain curve and lateral strain-axial strain curve. Hence it was useful in defining the flow rule and the hardening/softening rule. A further assumption for simplicity was that the concrete behaviour before peak stress can be

attributed to the plastic behaviour, and post peak stress was only due to concrete damage. Two approaches were used for exploring the flow rule of confined concrete were as follows:

- *Method I*

  This assumed an equivalent FRP-confined circular section, thus the hoop expansion was directly related to the confining pressure provided by the FRP jacket. Thus the flow rule was assumed to be the same for concrete over the whole section.

- *Method II*

  The effective confining pressure, along with the area strain, defined as the average of the two lateral strains were used, thus meaning the flow rule for concrete may be different for each point over a non-circular section.

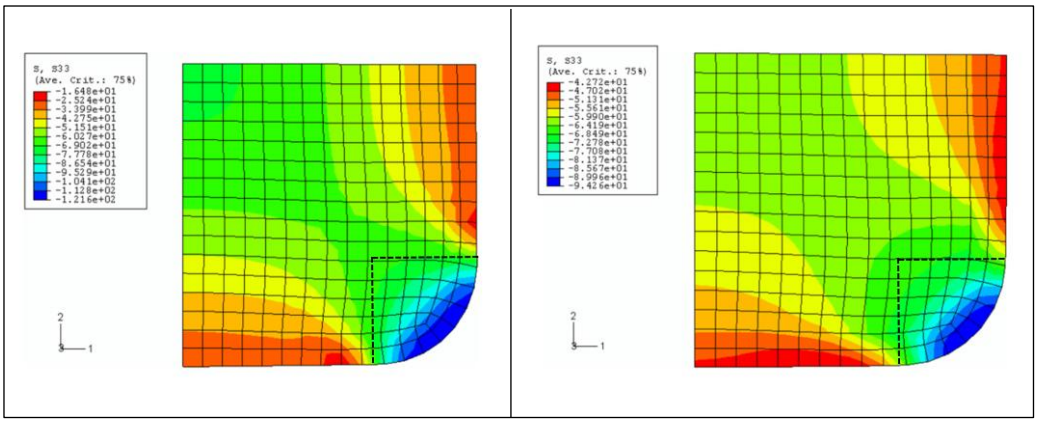

Figure 2-15: Axial stress distribution over cross-section with flow rule based on i. Method I, and ii Method II [Yu et al. (2010)]

The area of high confinement was similar in the corners, as annotated in Figure 2-15. The shape of the parabolas generated from the corner varied to a degree but not enough to warrant further analysis of these methods in this research, as relative to the corners, it is a region of low to medium confinement. Both methods demonstrated with reasonable accuracy the behaviour of the effectively confined area with minimal deviations, thus it can be used to establish the capacity of the specimen for the cross-section.

With a change in cross-section from square to rectangular, an inevitable change in the shape of the effectively confined area occurs with high concentration of the stress remaining in the corners for concentric loading, Figure 2-16 [Mostofinejad et al. (2013)].

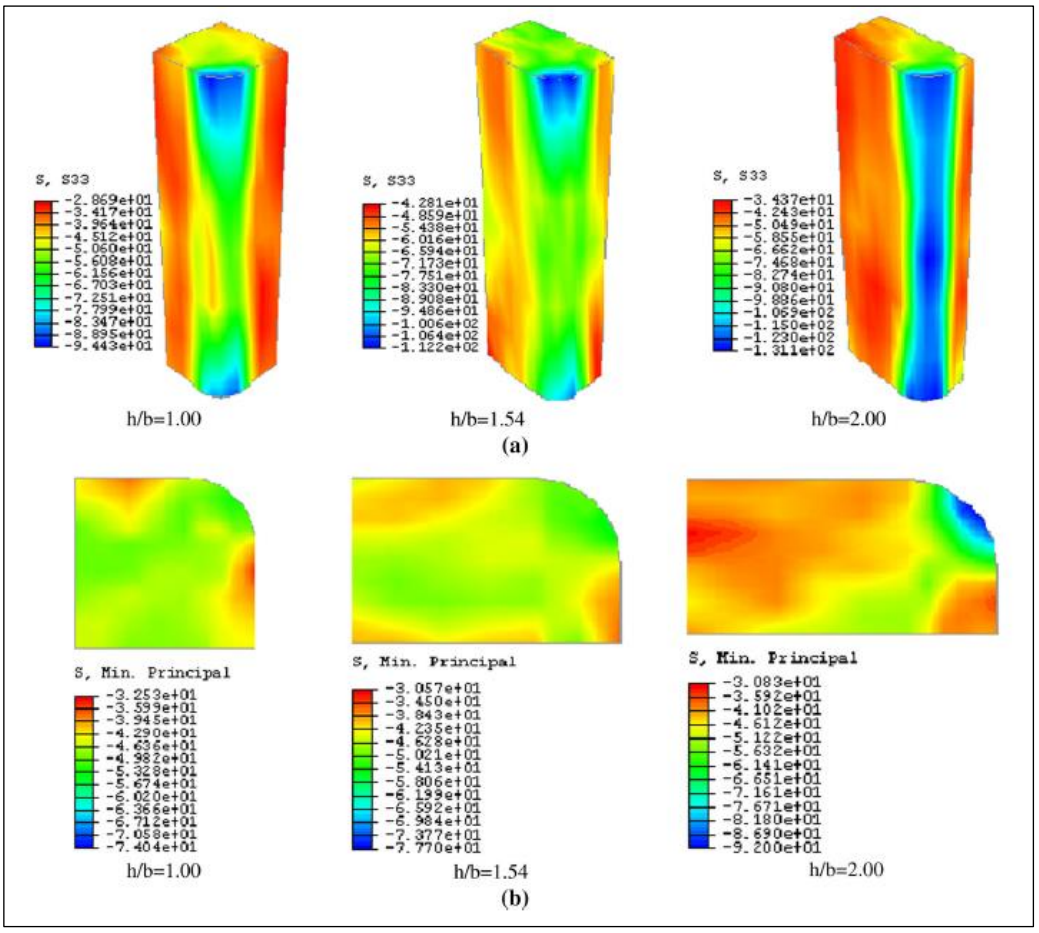

Figure 2-16: Rectangular cross-section stress distribution in specimens with a corner radius of 25mm and different aspect ratios; a. axial stress and b. lateral confining stress [Mostofinejad et al. (2013)]

The results required careful consideration as the mid-height section is more representative, away from ends where load application and/or boundary conditions are set. Furthermore, the results are not set within the same limits, hence direct comparison of stress plots is not feasible. From Figure 2-16, the stress had increased in the corners with increasing flat side length. Hajsadeghi et al. (2011) corroborated this movement of the confined area again into the corners, with a higher magnitude stress along the shorter sides, Figure 2-17.

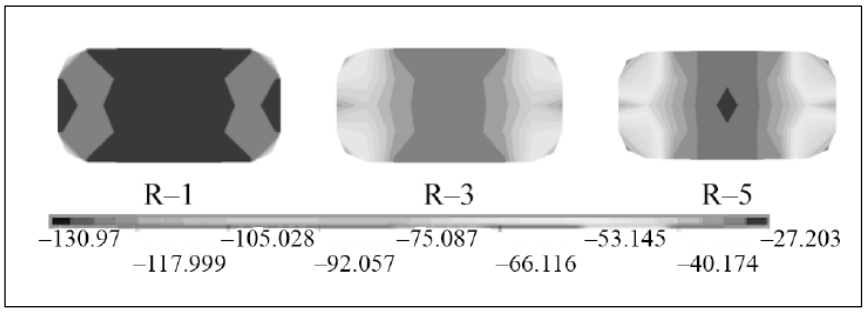

Figure 2-17: Rectangular cross-section contours of axial compressive stress of concrete at mid-height of rectangular columns [Hajsadeghi et al. (2011)]

The development of the effectively confined area has been modelled for square and rectangular specimens under concentric loading, however this is not a realistic representation of loading as there is usually a flexural component. To identify the movement of the effectively confined area under eccentric loading on square specimens, a FEM was developed and analysed.

2.5.2. FINITE ELEMENT MODEL

ABAQUS software suite (version 6.4) was selected as the most appropriate FEM package due to the detailed material models; specifically for concrete. Due to the nature of the analysis, ABAQUS/Standard; a general-purpose analysis programme that implicitly solves a system of equations at each increment of the analysis for either linear or nonlinear analyses was used. The model was created using a combination of coding and the graphical interface, ABAQUS/CAE, and run through the ABAQUS/Command, allowing for a greater selection of element and interaction definitions. Post simulation analysis was performed in ABAQUS/Viewer.

The key aspects focused on in FEM design were; the geometry and arrangement of the structure, the supports and constraints, and the loading conditions. As detailed in Table 2-3, numerous parameters have been studied extensively and varied to find the optimum representation for accurate comparison against test results [Yu et al. (2010)]. As the focus of this model is to evaluate the shape and movement of the effectively confined area as opposed to the stress and strain level, proven material definitions were adopted.

2.5.3. MODEL DESCRIPTION

The FRP-confined RC column was modelled as either a representative one quarter or one half of the cross-section, for concentrically and eccentrically loaded columns respectively, due to symmetry of geometry and load. This proportional modelling generated a reduction in simulation duration whilst not compromising evaluation of the behaviour of the effectively confined area. The FEM did not predict the behaviour to failure due to limitations inherent in the model, instigated to ensure focus was on the evolution of the effectively confined area as opposed to the failure mechanism of the FRP. Model generation fell into four main categories; the geometry, material definition, boundary conditions, and the simulation definition.

2.5.3.1. DISCRETIZED GEOMETRY

FEM geometry was defined by a series of finite elements, connected through shared nodes, with each element representing a discrete portion of the structure. The arrangement of these elements defined the mesh, an approximation of the actual geometry of the structure to a predetermined degree of accuracy. The geometry comprised of three distinct parts, each modelled with appropriate element type:

1. *CONCRETE*

   The concrete cross-section was modelled using eight-noded, reduced integration, solid continuum elements (C3D8R). Steel reinforcement was not deemed necessary for modelling as the focus was on the general shape and movement of the effectively confined area. The optimum size mesh applied used elements of approximately the maximum size of the aggregate to avoid over- or under-stating the results.

2. *FRP JACKET*

   A complex model for the FRP wrap was not necessary to observe the movement of the effectively confined area over the cross-section as the FRP provided confining pressure only. Thus, conservatively, a beam element (B31) was selected; a 2 node, as the length of the FRP in the model is significantly greater than the other dimension and as such, the stress in this direction (along the axis of the beam) was of the most significance.

3. *CONCRETE TO FRP CONTACT*

   Contact between the concrete and FRP was modelled using gap elements, but a closed contact definition. A perfect bond between concrete and FRP was assumed. The interfacial shear stresses were modelled using spring elements, an idealisation of axial components in a local direction.

FEM results were particularly sensitive to the model set-up, specifically the mesh density (too low or high and distorted results were likely to be produced). With optimal increase of the mesh density, the results of the analysis converge to a unique solution, and the time required for the analysis increased. It is imperative to note that the FEM solutions were an approximation of the actual results of the physical problem being simulated. Thus care was required in the approximations made in the model's geometry, material behaviour, boundary conditions, and loading to ensure a close replication of the physical problem.

The effect of size was not encompassed in the FEM as a unit geometry was modelled. As such, minimal change in the results were found when tested against a small-scale model with the evolution of the effectively confined area when varying the size. ABAQUS uses nominal sizing, defined by the input, hence for this model, metric SI system was adopted. The depth of the cross-sectional elements was a nominal unit depth.

2.5.3.2. MATERIAL MODELLING

Drucker-Prager failure criterion represented the concrete surface as it demonstrates preferable constitutive behaviour of frictional materials. The Drucker-Prager criterion is a smooth version of the Mohr-Coulomb yield surface, refer Figure 2-18, and the Mohr-Coulomb criterion assumes that failure is independent of the value of the intermediate principal stress but the Drucker-Prager model does not. This model had the following vertices in the deviatoric plane, Figure 2-18. The impact of this is that wherever the stress-state has two equal principal stress values, the flow direction can change significantly with little or no change in stress. It is a pressure dependent model for determining whether a material has failed or undergone plastic yielding. Drucker-Prager plasticity models are generally preferred for modelling constitutive behaviour of frictional materials.

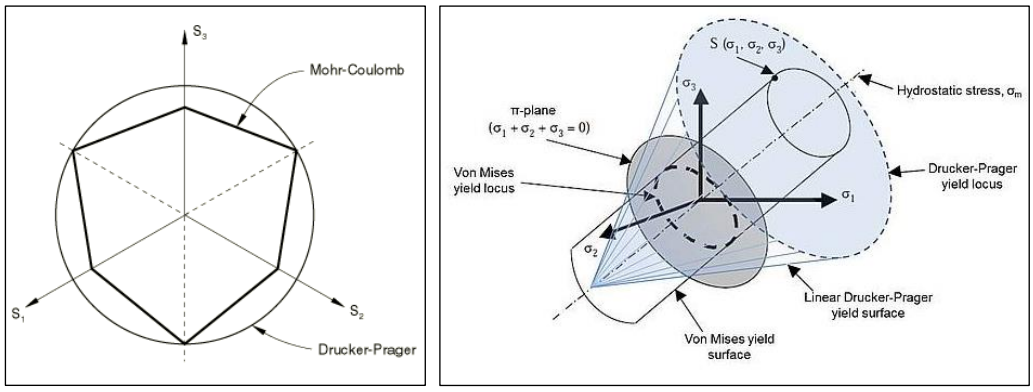

Figure 2-18: Mohr-Coulomb and Drucker-Prager model in the deviatoric plane [ABAQUS Analysis User's Manual] and Drucker Prager yield criteria [Dassault Systemes]

For the purposes of this research, assumptions made of concrete plasticity were:

1. A rigid perfectly-plastic collapse occurred, with all failing material reaching full strength (elastic deformations were negligible)
2. The modified Mohr-Coulomb failure criterion with a non-zero cut off was assumed for the concrete.
3. The internal angle of friction, φ, which reflects the slope of the yield surface in the stress space was assumed to be constant at 35 degrees for all combinations of stress. Typical variation of the angle constant is between 30 degrees and 40 degrees [Koksal et al. (2009)]. This was a crude estimation as studies have found that the internal angle of friction varies with increasing plastic deformation [Karabinis and Rousakis (2002), Karabinis et al. (2008), Yu and Zhou (2010)] with concrete behaviour under constant confinement not being accurately modelled for a constant angle of friction [Vermeer and de Borst (1984), Jiang and Wu (2012)]. However the behaviour of the concrete model under a constant angle of friction was satisfactory for a representation of the effectively confined area over the cross-section.
4. The hardening behaviour was defined explicitly with the compressive stress and corresponding absolute value of corresponding plastic strain.

The FRP was defined as an elastic-isotropic material with a Young's Modulus of 150GPa and Poisson's Ratio of 0.3. Beam elements were deemed appropriate for use as the behaviour of the FRP in the instance of this modelling is unidirectional and as such, behaviour was in

the lateral direction is only necessary. Hoop modulus, FRP thickness and rupture strain were 80.1GPa, 0.34mm & 1.3% respectively.

2.5.3.3. BOUNDARY CONDITIONS

The loads and boundary conditions assigned were particularly similar between models for the main part. Both the concrete and FRP were restrained through use of symmetry, ensuring that the internal section of the concrete could not move. Symmetry was on two axes for the concentrically loaded model, Figure 2-19, and one axis for the eccentrically loaded model.

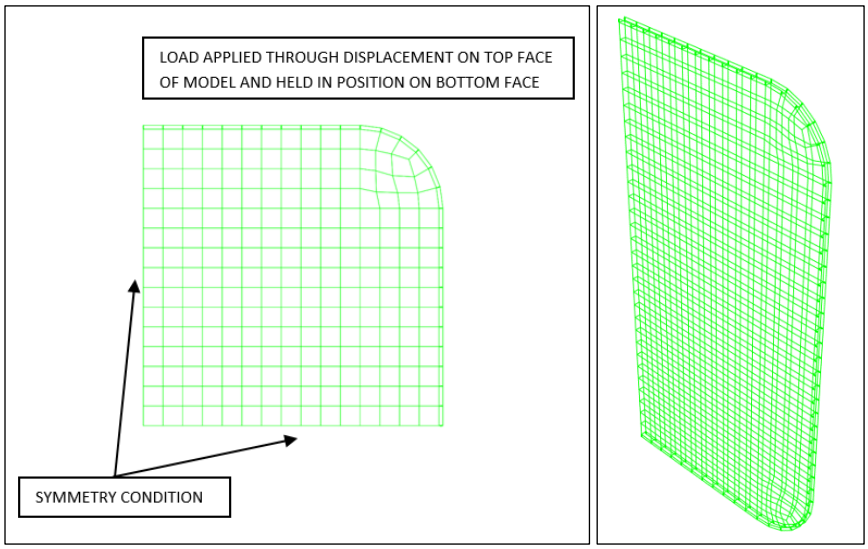

Figure 2-19: FEM boundary conditions, symmetry applied on the sides and displacement on top and bottom faces used to generate confinement, from left, concentrically loaded and eccentrically loaded models

Loading on the model was applied through use of the boundary conditions, to enable a controlled application, with a predefined end point. This was achieved through applying a vertically downwards displacement on the top surface, and for the eccentrically loaded model, it was linearly profiled appropriately over the cross-section.

2.5.3.4. SIMULATION

A static analysis was selected for this analysis, as monotonic loading was applied and the short-term evolution of the effectively confined area was required. Static analyses are useful

when inertia effects are not significant and as such can be neglected. The analysis can be linear or nonlinear and it ignores time dependent material effects but takes rate-dependent plasticity and hysteretic behaviour for hyper elastic materials into account.

Three types of output are stored in the output database; field output, history output and diagnostic information, and these were defined as required. The frequency of output was determined in terms of increments, number of intervals during the step, size of regular time intervals or time plots.

2.5.4. FINITE ELEMENT ANALYSIS RESULTS

The purpose of the FEM was to address the formation and movement of the effectively confined area, as opposed to producing accurate numerical results to back up the experimental testing. As ABAQUS provided a non-dimensional pre-model generation, and numerical results are not the focus, size effect was deemed irrelevant for the purposes of this write up. There was no significant change in the behaviour of the effectively confined area and to capture it, geometry or material parameters would require adaption, or substantially more complex modelling to capture accurate forces at the corners.

2.5.4.1. EFFECTIVELY CONFINED AREA – CONCENTRIC LOADING

The effectively confined area was postulated to generate at the convex corners of the prismatic cross-section and then form a cruciform shape over the diagonals with the higher concentration of stress expected to be at the corners. Looking at the stress plots in the out-of-plane direction, the results demonstrated the high concentration of stress, of a magnitude of approximately 100N/mm^2, dropping down to approximately 50N/mm^2 along the diagonals, Figure 2-20.

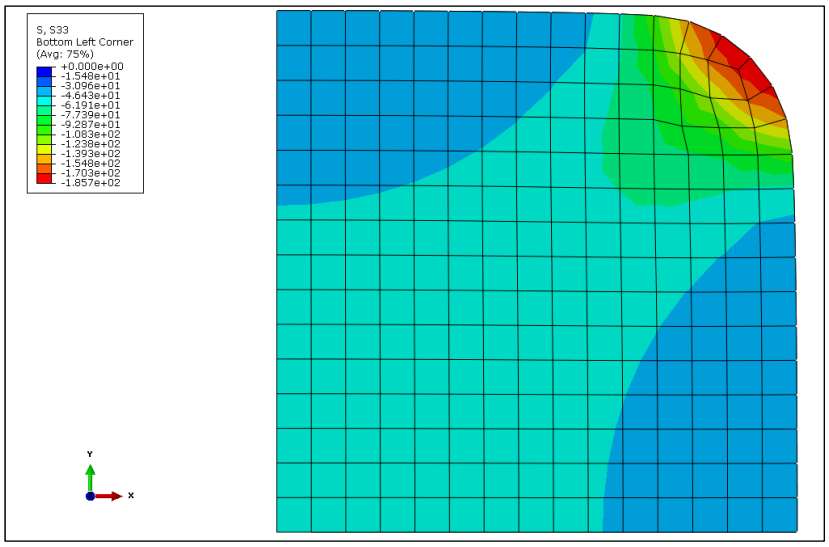

Figure 2-20: FEM Stress, out-of-plane stress plot of effectively confined area for concentric loading

The stress plotted in Figure 2-20 was in the out-of-plane principal direction (designated S33). With FEM, the values were arbitrarily attributed to the geometry and displacement to mimick the loading. The shape of the effectively confined area always followed the fundamental concept with the higher stress present at the corners. The magnitude of the stresses varied as expected with the different displacement conditions, representing different load eccentricities. However, to accurately address the stress magnitude a more detailed model of the FRP and concrete-to-FRP interaction would be advisable.

2.5.4.2. MIGRATION OF THE EFFECTIVELY CONFINED AREA

The effectively confined area, when compared with the concentrically loaded model, migrated into the region of higher compressive stress of the cross-section, Figure 2-21.

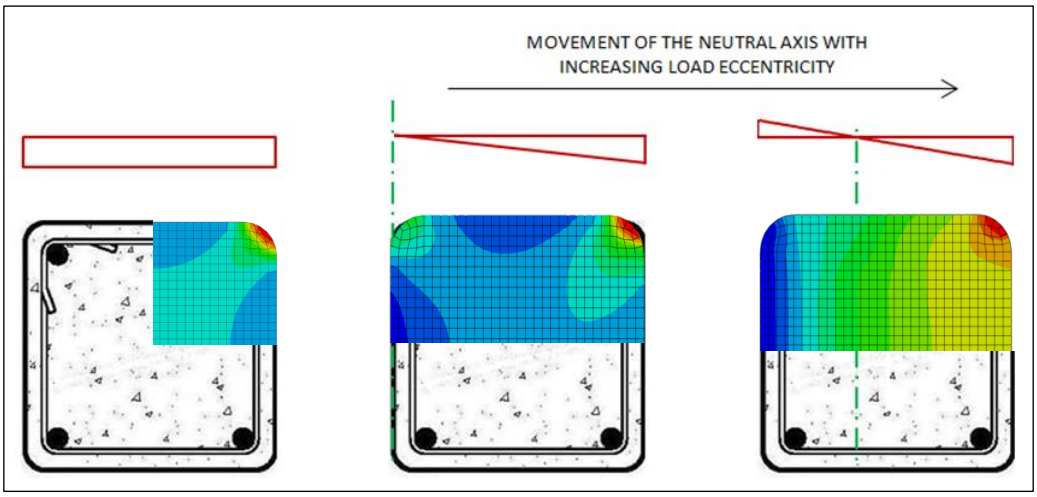

Figure 2-21: Movement of the effectively confined area into the higher compressive region of the cross-section, from left; concentric, eccentric profile no.1 (ECC1) and eccentric profile no.2 (ECC2) (load application profiles as identified in Figure 3-2)

Analysis of the strains measured around half of the cross-section, illustrated that the stress in the corners deviated from that of concentric loading and with the higher stress concentration being on the side of the column that the load was applied. The shape of the effectively confined area was then postulated to move towards this side of the cross-section. This was evident in the FEM strain plots, with minimal confinement at the sides of the specimens and progression of the cruciform shape into the middle. Furthermore, as the load eccentricity increased, the strain at the corner away from the point of application of the load reduced to near nothing, leaving that side of the column in minimal to no confinement.

2.5.5. FINITE ELEMENT MODELLING SUMMARY

FEM was employed to demonstrate the shape and movement of the effectively confined area over the prismatic cross-section as the load application went from purely axial to axial-flexural. The parameters inputted into the FEM ensured that the focus was on the migration of the area whilst replicating the strain profiles identified in the experimental test matrix.

The stress distribution over the cross-section illustrated the high confinement at the convex corners with the confinement forming along the cross-section diagonals, reducing towards the centre of the column. There was minimal or no confinement along the flat sides. When the load eccentricity was applied to the assembly, the area of high stress at the corners remains the same and of very similar shape with increasing applied eccentricity. However,

the rest of the confinement migrated to the side of the cross-section of applied eccentricity, leaving little confinement in the other side.

2.6. BEHAVIOURAL MODELLING

Prediction of the compressive behaviour of confined concrete is founded on the pioneering research of Richart et al. (1928), which focused on hydrostatically, triaxially confined concrete and demonstrated that both the strength and ductility of the concrete increased, with increasing confinement pressure. Richart et al. (1928) analysis was based on active confinement of concrete subject to constant hydrostatic pressure, and thus the confining pressure acting on the concrete was independent of its lateral expansion. The definition for the confined concrete strength and strain have been utilised as the base relation for establishing the strength capacity increase of concrete columns confined with a variety of materials:

$$f_{cc} = f_{co} + k_1 f_l \qquad (2\text{-}2)$$

where: k_1, the confinement effectiveness coefficient, is equal to 4.1 for Richart et al. (1928)

Initial adoption of Richart et al. (1928) strength capacity definition was for steel encased concrete tubes, primarily with an alteration to k_1. Modelling of passive confinement initially experienced with steel jackets with neither uniform nor constant confining stress, was mitigated when the steel confinement began to yield and a constant confining pressure was induced. Experimental work has since validated this expression for use with steel. Furthermore, these models were also developed to capture the properties of concrete and the corresponding behaviour so aspects such as the softening of concrete, which digresses from the elastic behaviour, were elaborated upon. The progression of modelling strength behaviour from Richart et al.'s (1928) fundamental research has led to design relying heavily on accurate stress-strain models.

Manders et al. (1988) adopted a slightly different approach, with the model is based on Popovic (1973) equation for longitudinal compressive concrete stress, where the tangent modulus depends on the peak stress and strain. A William and Warnke (1975) failure surface

for triaxial compression state with equal effective confining pressure was used, to give a confined compressive strength of:

$$f_{cc} = 2.254\sqrt{1 + 7.94\frac{f_l}{f_{co}}} - 2\frac{f_l}{f_{co}} - 1.254 \qquad (2\text{-}3)$$

When the confinement is provided by FRP, the confinement pressure is roughly constantly increasing and ideally failure only occurs with the FRP at its ultimate capacity. Thus a general assumption is that a specimen confined with FRP fails if the hoop stress exceeds the ultimate strength of the FRP. It must be noted that this is not the only governing factor as it assumes that the ultimate strength of various sections will be the same if the ultimate strength of the FRP is the same, regardless of stiffness. It differs from steel confinement in that the ultimate capacity is governed by FRP failure and not failure of the concrete.

Initial work to adapt steel-confinement models for applicability to FRP came from Fardis and Khalili (1982), who proposed that the lateral pressure, f_l, for circular columns, that is generated as the concrete starts to dilate and expand laterally when loaded, Figure 2-22, can be defined as follows:

$$f_l = \frac{2f_{fd}t_f}{d} \qquad (2\text{-}4)$$

Determination of the lateral confining pressure can quantify an initial insight into the confinement ability of the applied FRP jacket. This is easily achieved as it is a function of the cross-sectional geometry, FRP stiffness and the lateral expansion of the concrete.

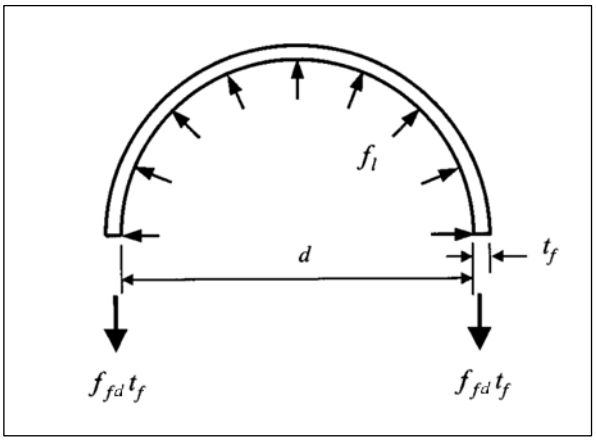

Figure 2-22: Confining action of FRP on circular cross-section [Lam and Teng (2002)]

As the FRP jacket resists the lateral expansion of the column, the concrete core is induced into a state of multi-axial compression; concurrently improving both the deformation and strength capacity. This confinement to the concrete core is passive and, as such, the confining pressure is highly dependent upon the relationship between the applied axial stress and the induced lateral strain. However, active confinement is necessary in establishing the load-extension curves of the FRP-confined specimen, but it must be noted that confining pressure varies continuously with the axial strain.

With the transition of cross-section shape from circular to prismatic, the edge sharpness influences the distribution of the confining stresses and subsequently reduces the compressive strength. Due to the flat sides and sharp edges, determination of the ultimate lateral strain is difficult and the interaction of the behaviour between the FRP and concrete is hard to establish in model form. Hence, stress-strain models have difficulty in precisely predicting this; therefore a realistic value for the lateral strain failure is not often able to be used.

Extensive development for prediction of the strength increase and behaviour of FRP-confined concrete columns has taken two distinct forms of models; analysis-oriented models which use an incremental process to determine the stress-strain curve, and design-oriented models which utilise relatively simple closed-form expressions, often ideal for design. Thus model selection is dependent on the use, and the results required at the end. It should be noted however that usually, the equations forming the basis of design-oriented models will often have originated in some manner from analysis-oriented models. Consequently, analysis-oriented models are discussed here first.

2.6.1. ANALYSIS-ORIENTED STRESS-STRAIN MODELS

To generalise, analysis-oriented models assume theoretical active confinement thus the basis of the model is that the axial stress and axial strain of concrete confined with FRP at a given lateral strain, are the same as those of the same concrete actively confined with a constant confining pressure equal to that supplied by the FRP jacket. Analysis-oriented models observe the response of the concrete and the FRP jacket individually as well as their interaction in an explicit manner. This is equivalent to assuming that the stress path of the confined concrete does not affect its stress–strain behaviour.

The analysis-oriented models addressed in this research are: Mirmiran and Shahawy (1996); Spoelstra and Monti (1999); Fam and Rizkalla (2001); Chun and Park (2002); Harries and Kharel (2002); Marques et al. (2004); Binici (2005) and Teng et al. (2007), due to the manner in which they approach modelling of FRP-confined prismatic columns.

An FRP-confined concrete stress-strain curve is generated through an incremental process with the resulting stress-strain curve crossing a series of stress-strain curves for the same concrete but of different levels of active confinement, Figure 2-23. As the use of an active-confinement model leads to a conceptual, effective model, this has been the popular method of establishing analysis-oriented models. Other approaches have been adopted [Harmon et al. (1998), Becque et al. (2003)] but the simplistic, yet accurate approach of the former have meant that it is these models that are assessed in this chapter.

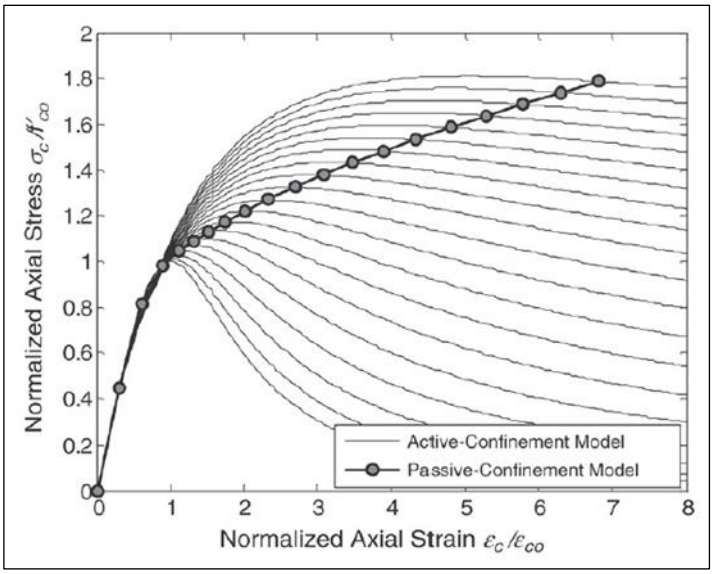

Figure 2-23: Active and passive confinement model [Jiang and Teng (2007)]

The active confinement stress-state induced in the concrete from the lateral reinforcement means that the axial load is carried by the concrete, thus the passive stress-strain behaviour can be established from the active behaviour. In Figure 2-23, for the ascending part of the stress-strain curve, the confining effect is negligible as the lateral expansion is small at this stage. This reflects the behaviour of unconfined concrete and as such, has the same stiffness. When the stress-strain curve starts to descend, the FRP jacket dominates behaviour, generating a multi-axial state of stress in the concrete core. From this series of active confinement stress-strain curves, the passive stress-strain curve is generated at the

point which it crosses this series of stress–strain curves for the same concrete strength with different confining pressure.

When determining an analysis-oriented model, the two key elements are; the active-confinement model and, the lateral-to-axial strain relationship (which defines the dilation property of the FRP-confined concrete). The procedure for finding this stress-strain curve of the model is:

1. For a specified axial strain, use the lateral-to-axial strain relationship to establish the lateral strain,
2. Using force equilibrium and radial displacement compatibility, establish the corresponding lateral confining pressure given by the FRP jacket,
   Steps 1 and 2 are an iterative approach required to achieve the correct lateral strain
3. From the axial strain and the active confinement model, the corresponding axial stress can be determined, establishing a point on the stress-strain curve of the FRP-confined concrete
4. Iterate steps 1 to 3 to generate the other points on the curve, shown in Figure 2-23.

The performance of this model is dependent on the peak stress and its corresponding axial strain, and the stress-strain equation used. The lateral-to-axial strain relationship is explicitly defined in many models and an educated choice on which to adopt is required. The performance of the model varies with and relies upon good selection and use of; the peak axial stress and the corresponding lateral-to-axial strain relationship, in addition to the stress-strain equation, so as to provide a unified treatment of the confined concrete. This is why the analysis-oriented models are more versatile in their use than design-oriented models.

2.6.1.1. LATERAL-TO-AXIAL STRAIN RELATIONSHIP

The lateral-to-axial strain relationship provides the connection between the response of the concrete core and the FRP-jacket but in a passive manner as it is not available in active confinement models. The lateral-to-axial strain relationship can be either explicitly or implicitly defined, and varies with researcher.

The lateral-to-axial strain equation applicable to unconfined, actively confined and FRP-confined concrete, proposed by Teng et al. (2007b) takes the following explicit form:

$$\frac{\varepsilon_c}{\varepsilon_{co}} = 0.85\left(1+\frac{\sigma_l}{f_{co}}\right)\left[\left(1+0.75\left(\frac{-\varepsilon_l}{\varepsilon_{co}}\right)\right)^{0.7} - exp\left(-7\left(\frac{-\varepsilon_l}{\varepsilon_{co}}\right)\right)\right] \quad (2\text{-}5)$$

The confining pressure, σ_l, is a constant pressure, representing active confinement although in reality the FRP jacket provides a passive confining pressure, dependent on the stiffness of the jacket. This generalisation provides accurate results, when compared with the author's experimental test programme.

$$\sigma_l = \frac{E_{fd}t_f\varepsilon_{fe}}{R} = \frac{E_{fd}t_f\varepsilon_l}{R} \quad (2\text{-}6)$$

Teng et al. (2007b) established the definition for lateral-to-axial strain through interpretation of the dilation properties of both unconfined and confined concrete as presented in Mirmiran and Shahawy (1996), Harries and Kharel (2002). The variation utilised by Mirmiran and Shahawy (1996) uses the tangent dilation ratio, μ_t, of the lateral-to-axial strain curve to link the lateral strain and axial strain, through a fractional function derived from their test results. The maximum value of tangent dilation ratio occurs when axial strain reaches ε_{co} but it cannot suppress lateral dilation at that early a stage. A limitation of this model is that some parameters are not clearly defined.

For Harries and Kharel (2002), the variation in the secant dilation ratio, μ_s, is described by a trilinear equation again based on their test results. Spoelstra and Monti (1999) explicitly consider the continuously increasing pressure caused by the FRP jacket, and show that the ultimate strain has a direct dependence on the maximum confinement pressure and the concrete modulus, whilst having an indirect dependence on the concrete strength. Thus the proposed lateral-to-axial strain relationship is:

$$\frac{\varepsilon_{cu}}{\varepsilon_{co}} = 2 + 1.25\,\overline{E_c}\,\varepsilon_{ju}\sqrt{f_{cu}} \quad (2\text{-}7)$$

Implicit expressions are used in Chun and Park, 2002, Marques et al. (2004), Binici (2005), and these expressions do not directly define the strain relationship in the model.

2.6.1.2. PEAK AXIAL STRESS (FAILURE POINT OF SPECIMEN)

The peak axial stress equation defines the failure surface of concrete as the point on the stress-strain curve of actively confined concrete. The five parameter multiaxial failure surface, detailed by William and Warnke (1975) is adopted in Mirmiran and Shahawy (1996), Spoelstra and Monti (1999), Fam and Rizkalla (2001) and Chun and Park (2002), and is following a curved form, reducing from a linear form in terms of stress as the confinement increases.

$$f_{cc}^{*} = f_{co}\left(2.254\sqrt{1+7.94\frac{f_l}{f_{co}}}-2\frac{f_l}{f_{co}}-1.254\right) \quad (2\text{-}8)$$

where: f_{cc}^{*}, is the peak axial stress of concrete under specific confining pressure, f_l

Mirmiran and Shahawy (1997), went on to propose another definition for the peak axial stress, f_{cc}, picked up by Harries and Kharel (2002), demonstrating significantly lower peak stress for the same confinement as Equation 2-8, with the variance increasing with the increasing confinement ratio.

$$f_{cc}^{*} = f_{co} + 4.269\, f_l^{\,0.587} \quad (2\text{-}9)$$

Marques et al. (2004), Binici (2005) and Teng et al. (2007) all proposed peak axial stress equations when compared, Figure 2-24, demonstrated close agreement. Marques et al. (2004) used the equation proposed by Razvi and Saatcioglu (1999):

$$f_{cc}^{*} = f_{co} + 6.7\, f_l^{\,0.83} \quad (2\text{-}10)$$

And this proved to be in close agreement with the Leon-Pramono criterion used by Binici (2005), which assumed the tensile strength of concrete is taken as 0.1 times its compressive strength.

$$f_{cc}^{*} = f_{co}\left(\sqrt{1+9.9\frac{f_l}{f_{co}}}+\frac{f_l}{f_{co}}\right) \quad (2\text{-}11)$$

Teng et al. (2007), defined the peak axial stress in a linear form, with the confining pressure factored based on test results:

$$f_{cc}^{*} = f_{co} + 3.5\, f_l \quad (2\text{-}12)$$

Lam and Teng (2007) provide a comparison of these equations, Figure 2-24i, demonstrating the variance in results, with the equation provided by Harries and Kharel (2002). Significantly, the conservatism in the stress and strain at peak load for the corresponding confinement ratio is deemed too much and as such, will not be included for comparison any further.

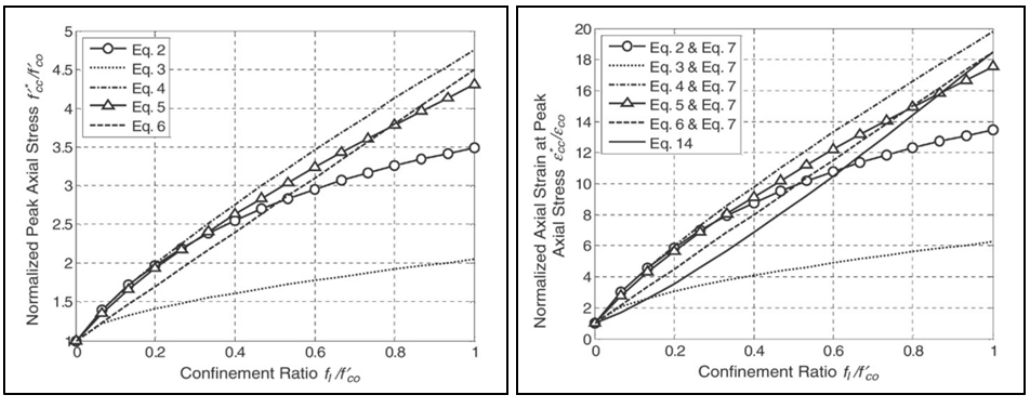

* Eq.2 is equation 2-6
Eq.3 is equation 2-7
Eq.4 is equation 2-8
Eq.5 is equation 2-9
Eq.6 is equation 2-10

^ Eq.2 & Eq.7 is equation 2-11
Eq.3 & Eq.7 is equation 2-11
Eq.4 & Eq.7 is equation 2-11
Eq.5 & Eq.7 is equation 2-11
Eq.6 & Eq.7 is equation 2-11
Eq.14 is equation 2-12

Figure 2-24: Comparison of: i. peak axial stress equations, ii. axial strain at peak axial stress [Jiang and Teng (2007)]

The corresponding axial strain for peak axial stress in all models barring Marques et al. (2004) is defined as:

$$\varepsilon_{cc}^* = \varepsilon_{co}\left[1 + 5\left(\frac{f_{cc}^*}{f_{co}} - 1\right)\right] \qquad (2\text{-}13)$$

This was initially proposed by Richart et al. (1928), with the key aspect of the effectiveness in axial strain being five times that of stress still being deemed relevant for these models. Marques et al. (2004) use a modified version of Equation 2-11, using a parameter from Razvi and Saatcioglu (1999) for $f_{co} > 40MPa$. This accounts for the reduced effectiveness in the enhancement of axial strain for high strength concrete.

Further to this, Jiang and Teng (2007) progressed this to propose an equation that separated the definition of strain enhancement from peak axial stress to combat through analysis of the active confinement relationship to give:

$$\frac{\varepsilon_{cc}^*}{\varepsilon_{co}} = 1 + 17.5\left(\frac{\sigma_l}{f_{co}}\right) \qquad (2\text{-}14)$$

From Figure 2-24, the refinement proposed by Jiang and Teng (2007) is in close agreement with the majority of the other results. Furthermore, this takes a slightly different form, with closer to linear behaviour as the confinement increases.

2.6.1.3. STRESS-STRAIN EQUATION

The stress-strain equation adopted in all models (except Harries and Kharel (2002) which is not included for further analysis) was originally proposed by Popovic (1973) and then adapted by Mander et al. (1988) for steel confined concrete.

$$\frac{\sigma_c}{f_{cc}^*} = \frac{(\varepsilon_c/\varepsilon_{cc}^*)r}{r-1+(\varepsilon_c/\varepsilon_{cc}^*)^r} \qquad (2\text{-}15)$$

where: $r = \frac{E_c}{E_c - f_{cc}^*/\varepsilon_{cc}^*}$

It is based on an elastic, perfectly plastic behaviour of the FRP jacket, thus assumes the confining pressure is constant after the concrete reaches its compressive strength and engages with the confining jacket.

A thorough study by Jiang and Teng (2007) into the analysis-oriented models demonstrated the accuracy of Teng et al. (2007) model, especially when the adaptation to the axial strain by Jiang and Teng (2007) is included. This model is compared with independent test data and can also be used for steel tube-confined concrete thus the model is widely applicable for a variety of confining materials.

2.6.2. DESIGN-ORIENTED STRESS-STRAIN MODELS

Design-oriented models utilise closed-form expressions directly derived from test results and treat the FRP-confined column as a single composite material, hence the convenience for design.

Generally, the basis of all design-oriented models is the definition for the compressive strength of confined concrete, previously having been defined by Samaan et al. (1998):

$$\frac{f_{cc}}{f_{co}} = 1 + k_1 \frac{f_l}{f_{co}} \qquad (2\text{-}16)$$

Lam and Teng (2003b) defined a model for rectangular columns, based on that created for circular cross-sections, Lam and Teng (2003a). This model has been selected for use due to its simplicity whilst providing reasonable accuracy, furthermore, the UK design guidance, TR55 (2005) is based on this model. More recently, the ACI-440.2R (2008) adopted this model with slight alterations. Lam and Teng's (2003b) model is based on the assumption that the axial stress and axial strain of confined concrete at a given lateral strain is the same as actively confined concrete with a constant confining pressure equal to that supplied by the FRP. In other words, the stress path does not affect the stress-strain behaviour. The model is especially useful as it adopts a simple form that reduces to that of unconfined concrete when no FRP is present. In circular specimens, the confining pressure is relatively constant around the circumference and thus, the maximum confining pressure is assumed as:

$$f_l = \frac{2E_{fd}\varepsilon_j t_f}{D} \qquad (2\text{-}17)$$

It is assumed here that ε_j be taken as the actual hoop rupture strain $\varepsilon_{h,rup}$ as measured in the FRP jacket, instead of the FRP ultimate tensile strain ε_{frp} as the rupture strain is regularly found to be smaller than that obtained from flat tensile coupon tests.

$$\varepsilon_{h,rup} = k_\varepsilon \varepsilon_{fd} \qquad (2\text{-}18)$$

k_ε, the FRP efficiency factor accounts for the difference between actual strain rupture and coupon test strain, as defined by Pessiki et al. (2001) and as it varies with shape type, an average value, defined by Lam and Teng (2003a), of 0.586 is used for circular columns but needs to be evaluated for prismatic sections.

Experimental investigation into the stress-strain curve for FRP-confined columns, has found that this relationship takes a bilinear form. The confining stress defined by Lam and Teng (2003b), takes the following form:

$$\sigma_c = \begin{cases} E_c\varepsilon_c - \frac{(E_c - E_2)^2}{4f_{co}}\varepsilon_c{}^2 & (0 \le \varepsilon_c \le \varepsilon_t) \\ f_{co} + E_2\,\varepsilon_c & (\varepsilon_t \le \varepsilon_c\, \varepsilon_{cu}) \end{cases} \qquad (2\text{-}19)$$

where: $\varepsilon_t = \frac{2f_{co}}{E_c - E_2}$, the slope of the straight second part

$E_2 = \frac{f_{co} - f_{co}}{\varepsilon_{cu}}$, is illustrated in Figure 2-25

The initial section of the stress strain curve follows stiffness of unconfined concrete into a parabolic form (affected to a small degree by the FRP jacket), and into the second stage, a straight line, indicating the FRP behaviour. Figure 2-25 shows the path of unconfined concrete at this point, where it softens slightly and fails at generally assumed ultimate axial strain of 0.0035.

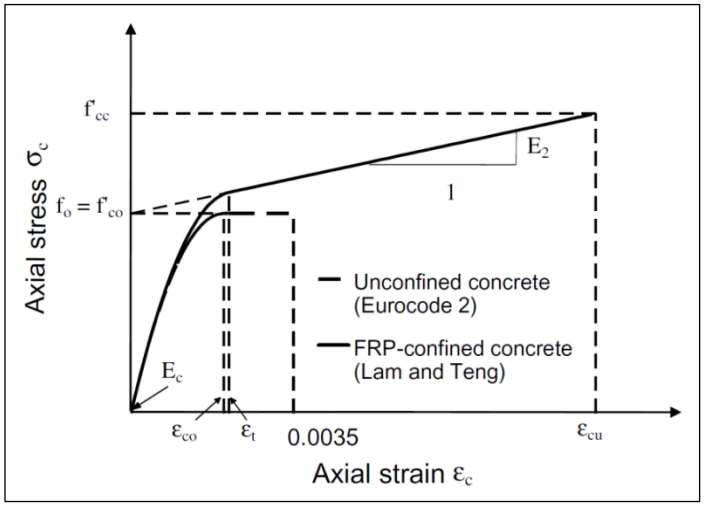

Figure 2-25: FRP-confined concrete stress-strain model [Lam and Teng (2003b)]

The second part of the FRP-confinement curve is ascending if the FRP is adequately confined, then the ultimate axial strain and compressive strength are reached simultaneously so both are enhanced. However, this branch can also be descending where the compressive strength of the concrete is reached before the FRP has opportunity to reach the ultimate strain and rupture. Subsequently, the ultimate strain of uniformly confined concrete, ε_{cu}, is given by:

$$\frac{\varepsilon_{cu}}{\varepsilon_{co}} = 1.75 + k_2 \frac{f_l}{f_{co}} \left(\frac{\varepsilon_{h,rup}}{\varepsilon_{co}}\right)^{0.45} \quad (2\text{-}20)$$

Many other models are available for design-oriented models, but provide little more accuracy for prismatic, uniformly confined specimens as Lam and Teng (2003b). Again, as TR55 (2005) uses Lam and Teng (2003a) as the basis for the derivation of the stress-strain behaviour, the prismatic version of this model is focused on in detail here.

2.6.3. LAM AND TENG'S (2003b) MODEL FOR PRISMATIC COLUMNS

To account for the prismatic cross-section and the lack of uniformity in the strain distribution in the FRP jacket, Lam and Teng (2003b) used an equivalent circular column of diameter *D*:

$$D = \sqrt{h^2 + b^2} \tag{2-21}$$

where: *D*, is the diagonal distance of the section, refer Figure 2-26, and inserted into Equation 2-15 in place of the actual diameter, *d*.

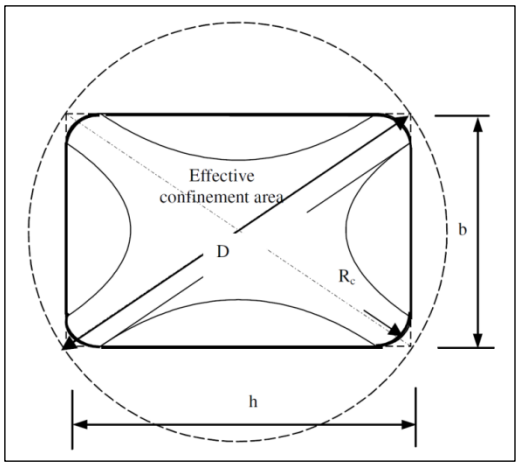

Figure 2-26: Shape factor for prismatic columns [Lam and Teng (2003b)]

The compressive strength of the confined concrete of the prismatic section is adapted from that defined for circular cross-sections and is predicted using the equation originally defined by Samaan et al. (1998) with the addition of a factor, k_{s1}:

$$\frac{f_{cc}}{f_{co}} = 1 + k_1 k_{s1} \frac{f_l}{f_{co}} \tag{2-22}$$

where: $k_1 = 6.0\, f_l{}^{-0.3}$, the confinement effectiveness coefficient, taken as 3.3

And the change to the axial strain includes a shape factor, k_2:

$$\frac{\varepsilon_{cu}}{\varepsilon_{co}} = 1.75 + k_2 k_{s2} \frac{f_l}{f_{co}} \left(\frac{\varepsilon_{h,rup}}{\varepsilon_{co}}\right)^{0.45} \tag{2-23}$$

The shape factors are defined by the effectively confined area and the aspect ratio and are essential in encompassing the change in the ratio of confinement as the aspect ratio of the

columns increases and subsequently, the confining area alters. For both shape factors, k_{s1} and k_{s2}, it is necessary that $h \geq b$.

$$k_{s1} = \left(\frac{b}{h}\right)^{\alpha} \frac{A_e}{A_c} \quad (2\text{-}24)$$

where: α , approximated as 2 based on experimental results for strength enhancement

$$k_{s2} = \left(\frac{b}{h}\right)^{\beta} \frac{A_e}{A_c} \quad (2\text{-}25)$$

where: β , approximated as 0.5 based on experimental results for strain enhancement

It is generally accepted that for the moment over the prismatic cross-section, only the area within the parabolas can be classed as confined by the FRP jacket, and that the area outside is not defined as such. This however, currently states that if the aspect ratio is greater than 2.62, it will be negative.

The proposed effective confinement area defined graphically by four parabolas and is of the form:

$$\frac{A_e}{Ac} = \frac{1 - \left(\left(\frac{b}{h}\right)(h-2R_c)^2 + \frac{\left(\frac{h}{b}\right)(b-2R_c)^2}{(3A_g)}\right) - \rho_{sc}}{1 - \rho_{sc}} \quad (2\text{-}26)$$

where: $A_g = bh - (4 - \pi){R_c}^2$

Through comparison with results, this model has shown reasonable accuracy for the purposes of design allowing close prediction of the stress-strain curves of prismatic columns when checked against experimental results. Furthermore it demonstrated that as the cross-sectional aspect ratio of the column increased, the strength in the column increased (relative to the equivalent unconfined specimen) but the axial ultimate strain decreased.

2.6.4. OTHER SIGNIFICANT DESIGN-ORIENTED MODELS

Lam and Teng's (2003b) model has been updated by Teng et al. (2007) and Teng et al. (2009). The key difference in the 2007 model showed a more widely applicable lateral strain equation and the Teng et al. (2009) adaption allowed more accurate prediction of the

descending branch of the stress strain equation. This is useful as accurate prediction of strength is crucial to design, especially where confinement may be weak and provide less of an increase in strength capacity than postulated.

Models developed over the past few decades have varied significantly in results and accuracy. A common variance are the values used for k_1 and k_2, which to generalise, is of a form either nonlinear in terms of f_l/f_{c0} or f_l, or it takes a linear description of the relationship between the confined strength and the lateral confining pressure.

The models studied are detailed in Table 2-4 and are described in terms of shape factor, compressive stress and ultimate axial strain.

Table 2-4: Design-Oriented Stress-Strain Models (part 1 of 2)

SHAPE FACTOR	COMPRESSIVE STRENGTH	ULTIMATE AXIAL STRAIN
MIRMIRAN AND SHAHAWY (1997)		
$k_s = \frac{2R_c}{D}$	$\frac{f_{cc}}{f_{co}} = 1 + k_1 \frac{f_l}{f_{co}}$ WHERE: $k_1 = 6.0\, f_l^{-0.3}$	THE DETAIL REQUIRED TO USE THIS EQUATION IS NOT PRESENT
NOTES: CONFINEMENT MODEL FOR FRP ENCASED CONCRETE TUBES *D* SHOULD BE THE LONGER SIDE LENGTH, LAM AND TENG, 2003B		
PESSIKI ET AL. (2001)		
STRAIN EFFICIENCY FACTOR USED TO ACCOUNT FOR DIFFERENCE WITH RUPTURE COUPON TEST STRAINS. $k_\varepsilon = k_{\varepsilon 1} k_{\varepsilon 2} = \frac{\varepsilon_{ju}}{\varepsilon_{jr}} \frac{\varepsilon_{jr}}{\varepsilon_{fd}}$	$f_{cc} = \frac{2n\overline{E_{fs}}}{D} \varepsilon_{fd} k_{\varepsilon 1} k_{\varepsilon 2}$	NOT SPECIFIED
NOTES: MODEL FOR CONCENTRICALLY LOADED SPECIMENS. STRAIN EFFICIENCY FACTORS USED IN PLACE OF SHAPE FACTOR IN COMPRESSIVE STRENGTH DEFINITION. k_s ORIGINALLY AS PER RESTREPOL AND DEVINO (1996).		
CAMPIONE AND MIRAGLIA (2003)		
$k_1 = 2$	$f_r = f_u \left[\left(1 - \frac{\sqrt{2}}{2} k_i \right) \frac{2r}{b_d} + k_i \frac{\sqrt{2}}{2} \right]$ WHERE $f_l = \frac{\sqrt{2} f_u t_j}{b} k_i$	$\frac{\varepsilon_{cu}}{\varepsilon_{co}} = 1 + \rho_{frp} \frac{1}{\varepsilon_{co}} \frac{{\sigma_j}^2}{E_{fd}} \frac{1}{f_{co} + f_l}$ WHERE: $\rho_{frp} = \frac{2[2(b - 2R_c) + \pi R_c] t_f}{b^2 - (4 - \pi){R_c}^2}$
NOTES: EVALUATES THE CONFINING PRESSURE IN THE ULTIMATE CONDITION OVERESTIMATED VALUES POSSIBLY DUE TO SHAPE/SIZE OF SPECIMENS TESTED. ASSUMES FRP RUPTURE. MODEL CHECKED AGAINST SPECIMENS SMALL & CONCENTRICALLY LOADED WITH NO CONFINED STRENGTH INCREMENT FOR PRISMATIC ELEMENTS. GOOD APPROACH		
YOUSSEF ET AL. (2007)		
NOT SPECIFIED	$\frac{f_{cc}}{f_c} = 0.5 + 1.225 \left(\frac{f_{lu}}{f_c} \right)^{\frac{3}{5}}$	$\varepsilon_{cc} = 0.004325 + 0.2625 \left(\frac{f_{lu}}{f_c} \right) \left(\frac{f_{ju}}{f_c} \right)^{0.5}$
NOTES: SEMI-EMPIRICAL MODEL BASED ON EXPERIMENTAL RESULTS FROM LARGE-SCALE ANNULAR AND PRISMATIC SPECIMENS UNDER CONCENTRIC LOAD FUNDAMENTAL FLAW HERE IS THAT THE EXPERIMENTAL RESULTS ARE NOT PUBLISHED. SEVERAL GENERAL SHAPE FACTORS PROPOSED AS OPPOSED TO ONE SPECIFIC FOR COMPRESSIVE STRENGTH EQUATION, REFER TO PAPER.		

Table 2-3 (contd.): Design-Oriented Stress-Strain Models *(part 2 of 2)*

SHAPE FACTOR	COMPRESSIVE STRENGTH	ULTIMATE AXIAL STRAIN
TENG ET AL. (2007)		
$k_1 = 3.5$	$\frac{f_{cc}^*}{f_{co}} = 1 + k_1 \frac{\sigma_l}{f_{co}}$	$\frac{\varepsilon_{cc}{}^*}{\varepsilon_{co}} = 1 + 17.5 \frac{\sigma_l}{f_{co} f_{co}}$
NOTES: THE UPDATE TO THIS MODEL IS A MORE ACCURATE DEFINITION OF THE LATERAL STRAIN, BASED ON NEW TEST INFORMATION AND A NEW FAILURE SURFACE DEFINED IN THE ACTIVE CONFINEMENT MODEL EQUIVALENT CIRCULAR COLUMN MODELLED WITH $D = \sqrt{h^2 + b^2}$		
EL MAADDAWY (2009)		
$k_s = \frac{\left[1 - \frac{(b-2R_c)^2 + (h-2R_c)^2}{3A_g}\right]}{(1-\rho_s)}$	$f_{cc} = f_c + (f_{co} - f_c)\left(\frac{1}{1 + e_i/h}\right)$	NOT SPECIFIED
NOTES: THIS MODEL INCLUDES A NONLINEAR SECOND ORDER ANALYSIS TO TAKE INTO ACCOUNT THE EFFECTS OF LOAD ECCENTRICITY THROUGH AN ADAPTED STRESS BLOCK. NO DEFINITION OF ULTIMATE STRAIN. THE MODEL IS BASED ON THE FOLLOWING DEFINITIONS PRIOR TO SECOND ORDER ANALYSIS. SHAPE FACTOR IS USED IN THE DEFINITION FOR f_l AND NOT THE COMPRESSIVE CONFINING STRENGTH.		
TOUTANJI ET AL. (2010)		
$k_1 = 4.0$ $k_{c2} = \left[\frac{2r}{D}\right]^{\gamma}$ $k_{c3} = \left[\frac{d}{b}\right]^{\eta}$ WHERE ϒ = 0.1 AND H = 0.13	$f_{cc} = f_{co} + k_1 k_{c2} k_{c3} f_l$	$\varepsilon_j = \beta \varepsilon_{fum}$
NOTES: A DESIGN-ORIENTED MODEL THAT TAKES INTO ACCOUNT THE CORNER RADIUS AND ASPECT RATIO THROUGH THE ADDITION OF TWO NEW FACTORS, k_{c1} AND k_{c2}. k_{e2} AND k_{e3} ADDRESS THE VARIATION IN CORNER RADIUS AND ASPECT RATIO RESPECTIVELY A REGRESSION ANALYSIS WAS PERFORMED ON THE LATERAL STRAIN IN THE FRP TO GIVE THE EFFECTIVE SHAPE FACTOR IS USED IN THE DEFINITION FOR f_l AND NOT THE COMPRESSIVE CONFINING STRENGTH.		
TURGAY ET AL. (2010)		
$k = \left(4.07\left(\frac{f_l}{f_{co}}\right) - 0.89\left(\frac{f_l}{f_{co}}\right)^2 + 0.807\right) f_{co}$	$\sigma_1 = \frac{\varepsilon_1 \left(4750\sqrt{f_{co}}\right)}{1 + \left(\frac{\left(4750\sqrt{f_{co}}\right)}{E_s} - 2\right)\frac{\varepsilon_1}{\varepsilon_{cc}} + \left(\frac{\varepsilon}{\varepsilon}\right.}$	$\varepsilon_{cc} = \varepsilon_{cc}\left(1 + k_2 \frac{f_l}{f_{co}}\right)$
NOTES: A PRACTICAL FAILURE SURFACE IS USED, BASED ON UNCONFINED COMPRESSIVE STRENGTH AND EXPRESSES THE CONFINED CONCRETE BEHAVIOUR USING A FAILURE CRITERION, ALL BASED ON KÖKSAL, 2006. THE EQUIVALENT CIRCULAR DIAMETER, $D = 2bh/(b+h)$		

El Maaddawy (2009) introduced a model to encompass the effects of the load eccentricity on the cross-sectional behaviour of the column through adaptation of Equations 2-14 and 2-18. The alterations included a ratio for the confinement effects. Note that there is no prediction as to the ultimate compressive strain in this model even though the strain profile over the cross-section is postulated to move significantly and as such, will impact the ultimate compressive strain. To encompass the effect of the load eccentricity, the stress block was adapted in an iterative manner to take in the effects of the equivalent stress block. Although this model tries to address the eccentricity a fundamental aspect that is not touched upon is the examination of the P-Delta effects, found to be inherent in any eccentrically loaded FRP-confined column if not excessively short.

The second order analysis demonstrated the aspects of the eccentric loading, Figure 2-27. The description of the specimens' curvature was detailed in terms of the moment and curvature individually, with the results of this approach being favourable when compared to Chaallal and Shahawy (2000). However although the model is unique in this use of second order effects to demonstrate the effect of eccentricity on the column, the comparison was done through computer programming and is therefore difficult to verify.

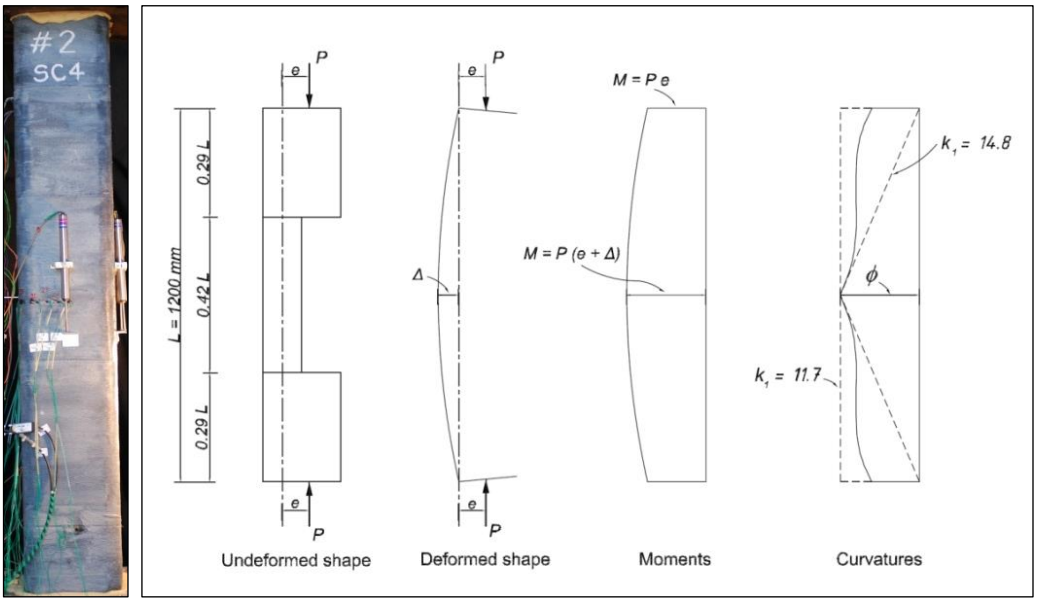

Figure 2-27: Specimen deformation in terms of moment and curvature when eccentrically loaded [El Maaddawy (2009)]

The comparison of Youssef et al. (2007) model with that of Lam and Teng (2003b) highlighted a discrepancy with the manner that Lam and Teng (2003b) model the initial

portion of the stress-strain curve, as the stiffness was noticeably greater than the experimental data, and nor did the concrete modulus relate well with this data. There was good correlation in the second portion of the curve. As the first portion is for unconfined concrete, this can be overlooked as the FRP jacket has not yet engaged at this point. They highlighted the overestimation by Mander et al. (1988) but this was to be expected in that the model was for steel-confined concrete, which with the active confinement generated, displays significantly different behaviour when addressing the strength capacity.

2.6.5. BEHAVIOURAL MODELLING SUMMARY

There are many design-oriented stress-strain models available that claim to accurately model the behaviour of FRP-confined columns. The key is to determine the most appropriate for the material and loading parameters in the design, then to take the one that is deemed the most accurate or appropriate for the specific research. This can be narrowed down slightly, and in the case of the research presented in this thesis, the model by Lam and Teng (2003b) was the immediate choice due to its accuracy and simplicity of use, in addition to being utilised as the base model for TR55 (2005) design. TR55 (2005) is no longer the current design guidance, having been superseded by TR55 (2011). However, during design, testing, and a large portion of the analysis, this was current and as such, this guidance will be evaluated initially, followed by the latest edition TR55 (2011).

However, analysis-oriented models tend to be the model of choice for more detailed analysis and design due to their increased versatility, adaptability to other confining materials and the accuracy of results. They are often used to supply data to design-oriented models.

2.7. DESIGN GUIDANCE

At the initiation of the research, and during design, testing and analysis to a large extent, the applicable design guidance was:

- Design Guidance for Strengthening Concrete Structures Using Fibre Composite Material (TR55), document no. Concrete Society Technical Report 55 (2005) [TR55 (2005)]
- Guide for the Design and Construction of Externally Bonded FRP Systems for Strengthening Concrete Structures, document no. ACI Committee 440.2R-02, 2002 [ACI (2002)]
- Externally Bonded FRP Reinforcement for RC Structures by the fédération international du béton (fib) (2001) [fib (2001)]
- Design and Construction of Building Components with Fibre-Reinforced Polymers, document no. S806-02 Canadian Standard Association (2002) [CSA (2002)]

During experimental design and testing, TR55 (2005) was the current UK design guidance and as detailed in the following sections, a very reasonable estimation of the behaviour relative to other models. This has subsequently been updated, TR55 (2011), post design and testing, and as such, both codes are reviewed, and referred to where appropriate. Specifically, experimental design is compared with the guidance used, TR55 (2005) and in evaluation of results, both editions of the design guidance are referenced. The other design guidance presented above has been reviewed for that revision, to demonstrate the choices made through the research, starting with design. As these codes were not pursued initially, the updated versions are not reviewed and focus has therefore remained with the UK guidance.

The similarities in the design philosophies of these codes lie in the use of a limit state design principle, which provides acceptable levels of safety against ultimate and serviceability limit states. The load combinations under consideration are used along with an applied amplification or reduction factor accounting for the probability of the load being greater than calculated. This gives a nominal capacity of the member. However the manner in which these are applied vary, with some applied material factors and others applying strength reduction factors to the nominal capacity. FRP reduction factors vary between codes and with material type, environment among other aspects.

2.7.1. TECHNICAL REPORT 55 (TR55) – UK BASED DESIGN GUIDANCE

TR55 (2005) adopts the model defined by Lam and Teng (2003a) due to its simplicity and accuracy in representing the behaviour for circular columns and adapts for practical design use. The code uses a limit state design approach of an elastic analysis with no redistribution (linear elastic until failure).

To account for the change in cross-section from circular to prismatic, a shape factor is applied to the equations defining the stress-strain behaviour. The key conditions for meeting the TR55 (2005) guidance using Lam and Teng (2003a) model are:

- Loading is concentric, or as near as reasonably practicable
- The smaller edge dimension of the prismatic cross-section is not greater than 200mm
- The aspect ratio is not greater than 1:1.5
- The corners have a minimum radius of 15mm

Contrary to Lam and Teng's (2003b) theory that the initial slopes of the parabolas that define the effectively confined area are 45 degrees from the side of the cross-section, TR55 (2005) takes the angle to be the same as that of the diagonals. Thus using this method, the likelihood of an overlapped region increases with increasing cross-sectional aspect ratio, due to the larger parabolas corresponding to the longer edge that may overlap, ergo reducing the level of confinement, Figure 2-8. As this area is not confined, it cannot be included in the effective area.

Thus the ratio of effectively confined to unconfined area is defined as:

$$\frac{A_e}{Ac} = \frac{1 - ((h-2R_c)^2 + (b-2R_c)^2 - 3A_{ol})/(3A_g) - \rho_{sc}}{1 - \rho_{sc}} \qquad (2\text{-}27)$$

where: $A_g = bh - (4 - \pi){R_c}^2$, the total cross-sectional area

$$A_{ol} = \begin{cases} 0 & 2b \geq (h-2R_c) \\ \frac{{l_{ol}}^3}{3(h-2R_c)} & 2b < (h-2R_c) \end{cases}$$

$l_{ol} = \sqrt{(h-2R_c)^2 - 2b(h-2R_c)}$, the length of the overlapping region

If $2b \geq (h - 2R_c)$ is the case, the overlapping region is required to be subtracted from the area as this area is in reality not confined and can lead to an overestimation of the capacity. As such, this will properly reflect the reduction in confinement with the increasing aspect ratio.

The shape factor, g_s, relates the confining pressure from the FRP wrap to that of a circular column of diameter D:

$$g_s = \frac{b}{h}\frac{A_e}{A_g} \tag{2-28}$$

Thus the equivalent confining pressure can be taken as:

$$f_{cc} = f_{co} + 2.0 g_s f_r \tag{2-29}$$

where: $f_{c0} = 0.67 f_{cu}/\gamma_{mc}$

This model takes the form for the compressive strength of the confined specimen:

$$f_{cc} = E_c \varepsilon_c - \frac{(E_c - E_2)^2}{4 f_{co}} {\varepsilon_{cc}}^2 \qquad 0 \leq \varepsilon_{cc} \leq \varepsilon_t \tag{2-30a}$$

$$f_{cc} = f_{co} + E_2 \varepsilon_{cc} \qquad \varepsilon_t < \varepsilon_{cc} \leq \varepsilon_{ccu} \tag{2-30b}$$

where: f_{cc}, the confined concrete axial compressive strength

$E_c = 5.5\sqrt{\frac{f_{cu}}{\gamma_{mc}}}$, the initial modulus of elasticity of the concrete

$E_2 = \frac{f_{cc} - f_{co}}{\varepsilon_{ccu}}$, slope of the linear portion of the stress-strain confined concrete curve

$f_{co} = \frac{0.67\, f_{cu}}{\gamma_{mc}}$, unconfined compressive concrete strength

$\varepsilon_t = \frac{2 f_{co}}{E_c - E_2}$, the position of transition region between parabola and straight line for confined concrete

It is essential to note that application of the model is only suitable if there is a corresponding increase in axial strain for the increase in axial stress. For low confinement, the ultimate strength may be less than the peak strength thus a condition of fulfilment of the TR55 (2005) is that the stress-strain model is only used when the following condition of Xiao and Wu (2000) is met:

$$\frac{2t_f E_{fd}}{D\,(f_{co})^2} > 0.183 \quad (2\text{-}31)$$

The ultimate design stress is defined as:

$$f_{ccd} = f_{co} + 0.05\left(\frac{2t_f}{D}\right)E_{fd} \quad (2\text{-}32)$$

Note that this is based on concrete compressive cube strength and a partial safety factor of 1.5. The ultimate strain is:

$$\varepsilon_{cu} = \varepsilon_{co}\left(1.75 + 12\left(\frac{2E_{fd}t_f}{E_0 D}\right)\left(\frac{0.6\varepsilon_{fd}}{\varepsilon_{co}}\right)^{1.45}\right) \quad (2\text{-}33)$$

where: $E_0 = \frac{0.67 f_{cu}}{\gamma_{mc}\varepsilon_{co}}$, the secant modulus of concrete

$\varepsilon_{co} = 2.4x10^{-4}\sqrt{\frac{f_{cu}}{\gamma_{mc}}}$, the axial strain in unconfined concrete at peak stress

Material factors are applied during the computation of the resistance but for research purposes these are defined as equal to 1.0.

2.7.2. LEADING NON UK BASED DESIGN GUIDANCE OPTIONS

The design guidance presented below was relevant at time of design and testing, and thus is compared with TR55 (2005).

2.7.2.1. ACI-440.2R (2008)

ACI 440 is a limit state design code, in accordance with ACI 318-99 and is for the design of non-slender, circular RC columns. It is based on the proofs of Spoelstra and Monti (1999) that the techniques for steel jacketing are applicable for FRP-confinement. It is based on Equation 2-2, but includes a multiplier for the unconfined compressive stress, to give:

$$f_{cc} = f_c\left[2.25\sqrt{1 + 7.9\frac{f_l}{f_c}} - 2\frac{f_l}{f_c} - 1.25\right] \quad (2\text{-}34)$$

The prismatic cross-sections are dealt with in the definition for the confining pressure from the FRP jacket by including an efficiency factor for the geometry, including the longitudinal steel reinforcement. Thus the effective lateral confining pressure is stated as:

$$f_l = \frac{k_s \rho_f \varepsilon_{fe} E_f}{2} \quad (2\text{-}35)$$

where: $k_s = 1 - \frac{(b-2R_c)^2+(h-2R_c)^2}{3bh(1-\rho_l)}$ and ϵ_{fe} is required to be within specific limits

ϵ_{fe} is the lesser of 0.004 and $0.75\epsilon_{fu}$ to mitigate debonding failure in the concrete at a lesser strain than the ultimate fibre strain

There is no explicit definition for the axial strain in columns with prismatic cross-section. It is recognised that although there is no increase in strength, the ductility of the column is improved significantly. Further recommendations are for an aspect ratio of less than 1.5 and the side dimensions greater than 36in to be neglected (unless experimental testing can verify).

2.7.2.2. FIB (2001)

This code is a limit state design with no plastic redistribution, refer to EC2 CEN1991 for more detail and is based on the Spoelstra and Monti (1999) model. The confined concrete strength is similar to ACI, 2002, with respect to Manders et al (1988) definition:

$$f_{cc}^* = f_c \left[2.254\sqrt{1 + 7.94\frac{f_l}{f_c}} - 2\frac{f_l}{f_c} - 1.254\right] \quad (2\text{-}36)$$

In this guidance the hoop strain at failure, is lower than that in the ACI (2002) definition.

$$\varepsilon_{ccu} = \varepsilon_{cc}^* \left(\frac{2\beta\varepsilon_{fu}\varepsilon E_{cc}}{E_c - E_{cc}}\right)^{1-E_{cc}/E_c} \quad (2\text{-}37)$$

fib (2001) does not give any appropriate reduction factors specified due to the lack of experimental data for prismatic cross-sectional columns available at time of publishing. The *fib (2001)* also gives a practical option to use which uses regression analysis on their model and only requires f_l as opposed to the calculation of f_{cc}^* and ε_{cc}^* from Manders et al. (1988) model, thus making it more readily useable.

2.7.2.3. CSA S806-02 (2002)

The Canadian design guidance *CSA S806-02* addresses prismatic columns, using an adapted version of Equation 2-1, with a shape factor $k_c = 0.25$, the maximum confined concrete compressive strength is:

$$f_{cc} = 0.85f_c + k_1 k_s f_l \quad (2\text{-}38)$$

There is no detail on the origin of this equation. It is a simplistic representation, changing linearly with a constant confinement stress, thus better representation is provided in the other design guidance documentation. The confinement stress has been derived through use of the equilibrium of forces in a circular columns, using an equivalent diameter, *D*, corresponding to the minimum side dimension.

$$f_l = \frac{2ntt_f f_{fe}}{D} \quad (2\text{-}39)$$

where: *D* is the lesser of *b* and *h*

f_{fe} is the lateral stress in the FRP jacket at failure and should be the lesser of $0.004E_f$ and $\phi_f f_{fu}$

There is no definition in this guidance as to the maximum useable axial strain.

Rocca et al. (2005) performed a comparison of the design guidance available using results from experimental testing. Specifically, the prismatic specimens were of different cross-sectional size, approximately medium-scale, with the sections being 300mm square and 320mm by 340mm rectangular. The unconfined concrete strength, $f_{cu} = 28MPa$ and the specimens were wrapped with 4 No. layers of CFRP.

The results from the comparison demonstrated that there is less of a gain in compressive strength with the rectangular cross-sections, as opposed to square (refer to Table 5-2, Rocca et al. (2005)). However, for CSA (2002), this was not the case, with a slight increase in strength available due to the computation of the equivalent circular cross-section (using the smaller of the prismatic cross-section sides for the diameter). Thus, it has been decided to neglect any further use of CSA (2002) as it does not appear to give feasible results alongside the others.

In this comparison, TR55 (2005) provides the lowest ratio for the predictive equations for the strength, but this is acceptable in that it is conservative. Also the strengthening ratio proves to have the closest results when compared to the experimental data. Hence, for the purposes of this research, TR55 (2005) guidance has been adhered to where possible so results can be aligned with UK standard practice.

2.7.3. UPDATES TO GUIDANCE, POST EXPERIMENTAL TEST DESIGN

The most relevant update in design guidance post experimental testing is the Concrete Society Technical Report 55 3rd Edition, TR55 (2011). In terms of axial strengthening, TR55 (2011) allows for the effects of debonding and the rupture of the FRP to be taken into consideration as well as inclusion of slenderness effects that have been found to be inherent in FRP-confined columns unless particularly short. Column slenderness is considered through use of interaction diagrams for all loading, concentric or eccentric; refer to Sections 8.2.3 and 8.2.4 of TR55 (2011) for further detail.

The major change for prismatic columns between TR55 (2005) and TR55 (2011) editions is the way in which the shape of the cross-section is dealt with. The explicitly defined shape factor g_s is no longer used and instead an effectiveness factor is defined from simple averaged confining stresses and corresponding equilibrium models. This effectiveness factor, k_e is:

$$k_e = \frac{R_c}{b}\left(1 + \frac{b}{h}\right) \tag{2-40}$$

The compressive stress has subsequently been updated and encompasses this effectiveness factor to give:

$$\frac{f_{ccd}}{f_{co}} = 1 + 5.25(k_e\rho_k - 0.01)\rho_e \tag{2-41}$$

where: $\rho_k = \frac{E_{fd}t_f}{\left(\frac{0.85f_{ck}}{\varepsilon_{c2}}\right)R_c}$

$$\rho_e = \frac{\varepsilon_{h,rup}}{\varepsilon_{c2}}$$

This is only valid however if there is sufficient stiffness in the structure to satisfy:

$$\rho_k \geq {}^{0.01}/_{k_e} \tag{2-42}$$

In addressing prismatic columns, TR55 (2011) specifies a limiting shear stress to encompass the shear stress that potentially develops between the concrete and FRP, as the FRP hoop strains reduce in certain sections due to a non-uniform distribution of strain around the FRP jacket, Figure 2-28. The limiting shear stress is defined as:

$$\tau_{lim,c} = 0.8\frac{f_{ctk}}{\gamma_c} \tag{2-43}$$

where: f_{ctk}, the characteristic concrete tensile strength is defined in BS EN 1992

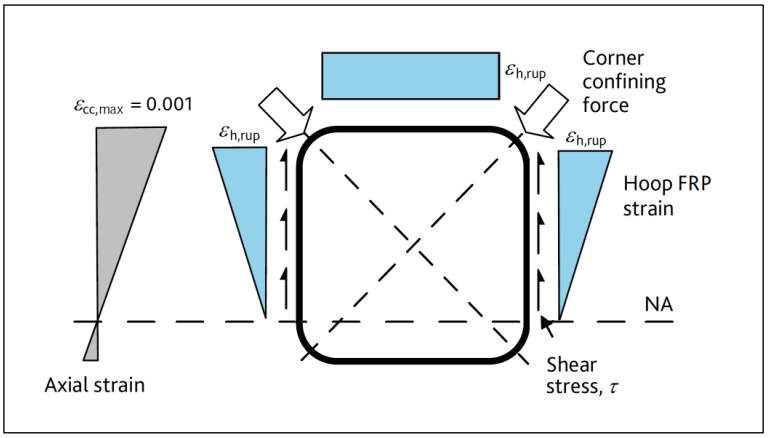

Figure 2-28: Behaviour of confining stresses over cross-section when subject to eccentric loadings [TR55 (2011)]

This definition captures potential debonding of the FRP jacket, therefore including the subsequent reduction in the confining force at the corners, through the strain at which debonding occurs, $\varepsilon_{h,debond}$ replacing $\varepsilon_{h,rup}$:

$$\varepsilon_{h,rup} = \varepsilon_{h,debond} = \tau_{lim,c}\frac{(h-2R_c)}{t_f E_{fd}} \tag{2-44}$$

Thus to establish the useable axial force following the methodology stated in TR55 (2011) Section 8.5.1, an interaction diagram consisting of four main points should be created:

1. The axial load corresponding to zero moment
2. The axial load and moment for neutral axis depth = *h* (or *b* if loaded on the minor axis)

3. The balance point where the longitudinal steel yields at the same time as the concrete reaches maximum strain
4. The moment corresponding to zero axial load

Once these points have been established, they can be joined by a straight line to get a representative curve. The interaction diagram proposed now takes debonding and potential second order effects into consideration, thus a more accurate representation of the concrete and FRP behaviour.

A further major design guidance update includes the change from British Standards to Eurocodes, specifically from BS 8110, Structural use of concrete to Eurocode 2, to BS EN 1992 Design of concrete structures, Part 1-1, General rules and rules for buildings (UK Annex). The Eurocodes address all concrete strengths in terms of cylinder strength and as such, it allows for comparison with TR55 (2011), which references BS EN 1992 is in terms of cylinder strength. For the design of concrete columns, the major difference with EC2 is the inclusion of a moment due to imperfection and the subsequent eccentricity due to imperfection. This has been further developed in TR55 (2011).

2.8. CONCLUDING REMARKS

Until recently, the main focus work on FRP-confined RC columns has been on circular specimens. However the progression of the testing and analysis has moved onto prismatic cross-sections, demonstrating that under favourable conditions, an increase in capacity is feasible. Experimental testing of concentrically loaded prismatic columns gives an increase in capacity when optimally wrapped, and shows that the confinement mechanics over the cross-section of the column takes a cruciform shape, following the diagonals from the corners. As the stress field over the cross-section is not uniform, the results obtained from circular columns cannot be applied to prismatic columns. The change in this shape with eccentric loading still has some ambiguity and would benefit from further analysis.

Analytical modelling has been extensively performed for circular specimens and often adopted for prismatic cross-sections with a shape factor applied. To date, these models are considered accurate for concentrically loaded square columns but work is required to ensure the viability of both rectangular and eccentrically loaded models. This is reflected in

the design guidance that takes a conservative approach, applying significant limitations to their use.

CHAPTER 3

TEST DESIGN AND METHODOLOGY

3.1. INTRODUCTION

Chapter 3 details the design, construction and testing of the experimental programme, developed to assess the achievable increase in strength capacity, and the confinement behaviour of FRP-confined columns. Specifically, this chapter includes; specimen design and material selection, construction methodology, test set-up, and immediate post-test analysis, thus enabling full comprehension of results. The test programme was realised using facilities at the Department of Architecture and Civil Engineering, University of Bath (UoB) and the Building Research Establishment, Watford (BRE) between January 2008 and August 2010.

3.2. TEST MATRIX CONCEPT

Design of the test matrix commenced with a review of previous test programmes, detailed in Chapter 2, Section 2.4, with specific focus on specimens of larger size (particularly in cross-sectional dimension) and/or the application of axial-flexural loading. Prior research into prismatic columns focused mainly on small-scale specimens with varying parameters, notably; specimen dimension, corner radii, concrete strength, load profile, and FRP type and application. Hence research into medium- and large-scale specimens is less extensive, and largely limited to an increase in cross-sectional dimension without the proportional increase in height, thus rendering the specimen behaviour that of short columns, and often subject solely to axial loading.

Through examination of the existing research, it was proposed that the experimental programme address three main parameters, producing an extensive test matrix:

Parameter 1: *Specimen Size*

Consisting of small-, medium- and large-scale specimens; the size of which was limited by the height (5m clearance), and capacity (10,000kN limit) of the BRE loading rig. Small-scale specimens were essential for comparison purposes with previous research.

Parameter 2: *Loading Profile*

Purely axial, and axial-flexural loads; the inclusion of concentric loads enabled an accurate comparison with previously tested small-scale specimens.

Parameter 3: *Aspect Ratio*

Cross-sectional aspect ratios of 1:1 to 1:2.5 on medium-scale specimens; allowed for the change in the confinement mechanics of medium-scale columns to be determined.

Note: *Corner Radius*

The corner radius was determined through literature review and selected as 20mm for small-scale specimens as an arbitrary reasonable value. Thus for medium- and large-scale specimens, this was scaled up accordingly along with the cross-section dimensions to give corner radii of 40mm and 60mm respectively.

The parameters were applied singularly and in particular combinations for unconfined and FRP-confined RC columns. Emphasis was placed on the behaviour and failure mechanism of the FRP in the design of specimens, to provide the necessary insight into the confinement mechanics of medium- and large-scale columns. Design standards and guidance where available were adhered to, allowing for a reasonable comparison between specimens both in this and previous research. The established test matrix is detailed in Table 3-1.

Table 3-1: Experimental Test Matrix

SPECIMEN GROUP	SPECIMEN ID	GEOMETRY					MATERIAL DATA						LOAD DATA		
		BREDTH b mm	WIDTH h mm	HEIGHT H mm	ASPECT RATIO	CORNER RADIUS R_c mm	CONCRETE STRENGTH f_{cu} N/mm^2	STD. DEVIATION	DIAMETER LONG. STEEL Φ_s mm	No. LONG BARS	LONG. STEEL RATIO ρ_{sc}	No. FRP WRAPS	STRAIN PROFILE	APPLIED ECCENTRICITY e_d mm	DESIGN STRENGTH CAPACITY N_D kN
SC	SC1	150	150	925	1.0	20	37.9	0.84	12	4	2.04	0	CON	0	828
	SC2	150	150	925	1.0	20	39.4	0.62	12	4	2.04	2	CON	0	995
	SC3	300	300	1850	1.0	40	24.4	1.37	25	4	2.22	0	CON	0	2582
	SC4	300	300	1850	1.0	40	24.4	1.37	25	4	2.22	4	CON	0	3480
	SC5	450	450	2400	1.0	60	42	1.64	25	8	1.97	0	CON	0	8290
	SC6	450	450	2400	1.0	60	24.4	1.37	25	8	1.97	6	CON	0	7548
SE	SE1	150	150	925	1.0	20	39.4	0.62	12	4	2.04	0	ECC1	12	696
	SE2	150	150	925	1.0	20	37.9	0.00	12	4	2.04	2	ECC1	8	851
	SE3	150	150	1250	1.0	20	37.9	0.00	12	4	2.04	0	ECC2	68	257
	SE4	150	150	1250	1.0	20	36.7	0.85	12	4	2.04	2	ECC2	34	540
	SE5	300	300	1850	1.0	40	42	1.64	25	4	2.22	0	ECC1	15	3901
	SE6	300	300	2450	1.0	40	42	1.64	25	4	2.22	4	ECC2	67	1052
	SE7	450	450	2400	1.0	60	42	1.64	25	8	1.97	0	ECC1	23	8497
	SE8	450	450	3300	1.0	60	24.4	1.37	25	8	1.97	6	ECC2	119	1832
RC/E	RC1	300	450	2400	1.5	40	35.3	0.00	25	6	2.20	0	CON	0	3840
	RC2	300	450	2400	1.5	40	24.4	1.37	25	6	2.20	4	CON	0	5410
	RC3	300	600	3200	2.0	40	35.3	1.00	25	8	2.20	0	CON	0	5130
	RC4	300	600	3200	2.0	40	24.4	1.37	25	8	2.20	4	CON	0	5510
	RE1	300	600	3200	2	40	24.4	1.37	25	8	2.20	4	ECC1	36	6432
	RE2	300	600	4200	2	40	35.3	1.00	25	8	2.20	4	ECC2	385	2454
	RE3	600	300	3200	2.0	40	24.4	1.37	25	8	2.20	4	ECC1	27	1899
	RE4	600	300	3600	2.0	40	35.5	1.64	25	8	2.20	4	ECC2	365	1654
	RC5	300	750	3750	2.5	40	35.3	1.00	25	10	2.20	0	CON	0	6420
	RC6	300	750	3750	2.5	40	24.4	1.37	25	10	2.20	4	CON	0	8180

The experimental programme consisted of 24 No. specimens; 6 No. small-scale, 14 No. medium-scale and 4 No. large-scale, categorised to allow for examination of key parameters individually and in set combinations.

Series 1 – Size Effect (SC)

Comprised Specimens: *Square cross-section subjected to axial load only*

Series Objective: *To address the effect of increasing size on the strength capacity of the column*

Variations: *Scaling – all specimens were uniformly scaled (in terms of geometry, reinforcing steel, FRP plies) where feasible, however there was a slight variation in the ratio of cross-sectional steel, due to standard rebar diameter*

Concrete strength – cast strength was not consistent due to several internal and external concrete mixes used due to the volume of concrete required, this is further discussed in Section 3.4.1.1

Table 3-2: Specimen Detail for Series SC – Size Effect

SPECIMEN ID	X-SEC	LENGTH	CONCRETE COMP. CUBE STRENGTH (WITH STANDARD DEVIATION)		# LONG. STEEL & DIAMETER	# FRP WRAPS	LOAD PROFILE	DESIGN LOAD
	mm	mm	N/mm²		mm			kN
SC1	150 | 150	925	39.4	0.62	4 NO. Ø 12	-	CONCENTRIC	816
SC2		925	37.9	0.84		2		995
SC3	300 | 300	1850	24.4	1.37	4 NO. Ø 25	-		2548
SC4		1850	24.4	1.37		4		3486
SC5	450 | 450	2400	42.0	1.64	8 NO. Ø 25	-		7811
SC6		2400	24.4	1.37		6		7562

Series 2 – Load Profile (SE)

Comprised Specimens: *Square specimen subjected to axial-flexural loads (specimens from Series SC included for comparison)*

Series Objective: *To address the change in behaviour of small-, medium- and large-scale columns as a load is applied at an eccentricity and the subsequent change in strength capacity*

Variations: *Scaling of rebar and concrete strength as detailed in Series SC*

Table 3-3: Specimen Detail for Series SE – Load Profile

SPECIMEN ID	X-SEC	LENGTH	CONCRETE COMP. CUBE STRENGTH (WITH STANDARD DEVIATION)		# LONG. STEEL & DIAMETER	# FRP WRAPS	LOAD PROFILE	DESIGN LOAD
	mm	mm	N/mm²		mm			kN
SC1	*150 | 150*	*925*	*37.9*	*0.84*	*4 NO. Ø 12*	*-*	*CONCENTRIC*	*816*
SC2		*925*	*39.4*	*0.62*		*2*		*995*
SE1	150 | 150	925	39.4	0.62	4 NO. Ø 12	-	ECC1	696
SE2		925	37.9	0.84		2		851
SE3		1250	37.9	0.84		-	ECC2	257
SE4		1250	36.7	0.85		2		540
SC4	*300 | 300*	*1850*	*24.4*	*1.37*	*4 NO. Ø 25*	*4*	*CONCENTRIC*	*3486*
SE5	300 | 300	1850	42.0	1.64	4 NO. Ø 25	4	ECC1	3729
SE6		2450	42.0	1.64		4	ECC2	2432
SC6	*450 | 450*	*2400*	*24.4*	*1.37*	*8 NO. Ø 25*	*6*	*CONCENTRIC*	*7811*
SE7	450 | 450	2400	42.0	1.64	8 NO. Ø 25	6	ECC1	8110
SE8		3300	24.4	1.37		6	ECC2	3633

Series 3 – Cross-Sectional Aspect Ratio (RC/E)

Comprised Specimens:	*Rectangular cross-section of varying aspect-ratio subjected to both axial and axial-flexural loading (specimens included from Series SC for comparison)*
Objective:	*To evaluate the change in confinement and cross-sectional behaviour with the increase in cross-sectional aspect ratio and subsequently the behaviour with axial-flexural loading applied in both the minor and major axes*
Variations:	*Cross-section design - deviation from the design specification was essential in order to increase the cross-sectional aspect ratio whilst remaining within constraints determined by material availability and rig capacity, this change is demonstrated in Figure 3-1*

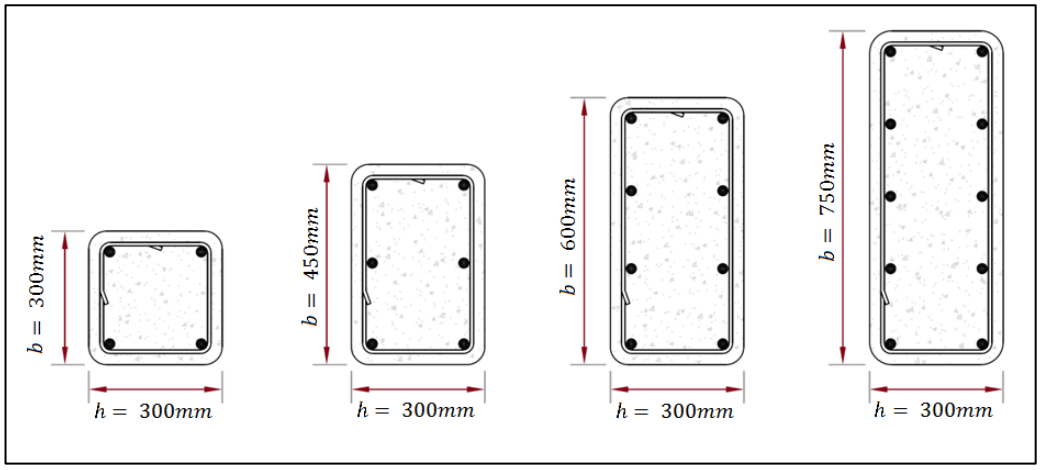

Figure 3-1: Variation in cross-sectional geometry for Series RC/E

Table 3-4: Specimen Detail for Series RC/E – Cross-Sectional Aspect Ratio

SPECIMEN ID	X-SEC	LENGTH	CONCRETE COMP. CUBE STRENGTH (WITH STANDARD DEVIATION)		# LONG. STEEL & DIAMETER	# FRP WRAPS	LOAD PROFILE	DESIGN LOAD
	mm	mm	N/mm²		mm			kN
SC3	*300 | 300*	*1850*	*24.4*	*1.37*	*4NO. Ø 25*	*-*	CONCENTRIC	*2548*
SC4		*1850*	*24.4*	*1.37*		*4*		*3486*
RC1	300 | 450	2400	24.4	1.37	6NO. Ø 25	-		4810
RC2		2400	35.3	1.11		4		5232
RC3	300 | 600	3200	24.4	1.37	8 NO. Ø 25	-		6424
RC4		3200	24.4	1.11		4		6627
RE1	300 | 600	3200	35.3	1.37		4	ECC1	5972
RE2		4200	35.3	1.37		4	ECC2	2526
RE3	600 | 300	3200	35.3	1.37		4	ECC1	4474
RE4		3600	35.3	1.37		4	ECC2	2196
RC5	300 | 750	3750	24.4	1.11	10 NO. Ø 25	-	CONCENTRIC	8038
RC6		3750	35.3	1.37		4		7651

3.3. DESIGN OF TEST SPECIMENS

Examination of pertinent literature revealed approximate dimensions for the small-scale control specimens' cross-section (150mm by 150mm) and height (625mm test section), from which scaled-up dimensions for medium- and large-scale specimens were determined. The corner radii of the specimens required adequate size to mitigate the risk of premature rupture of the FRP due to stress concentrations generated at sharp corners. Thus a corner radii that was 13% of the side dimension allowed adequate space for stirrups and the minimum concrete cover. Consideration was paid to the application of axial-flexural load, with the extreme eccentric profile (ECC2) used to move the compression zone so that it was theoretically in half of the cross-section. The two eccentric profiles established were: a strain profile with the neutral axis at one side of the cross-section, ECC1 in Figure 3-2, effectively putting approximately 75% of the cross-section in compression; and the neutral axis in the centre of the cross-section, thus theoretically almost half of the cross-section in compression so close to representing pure bending, ECC2 in Figure 3-2.

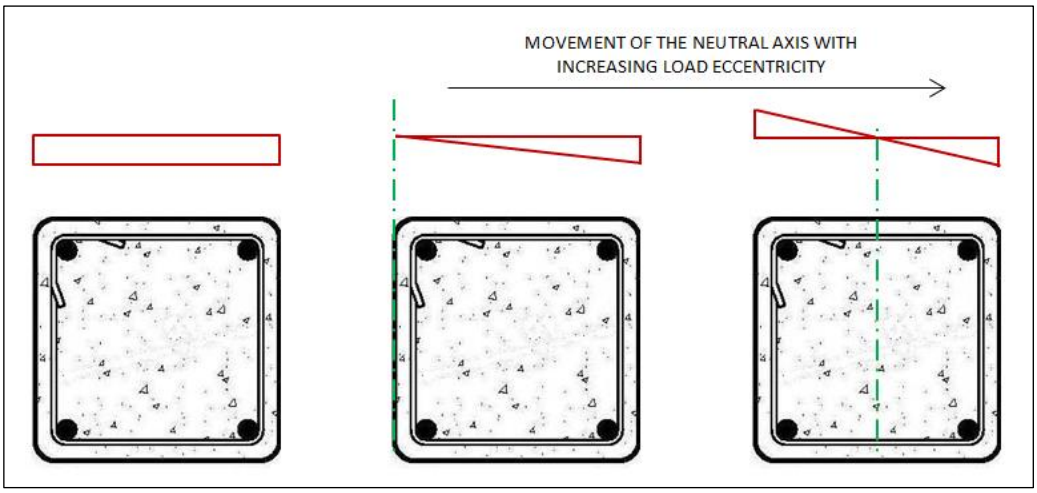

Figure 3-2: Stress profiles over the column cross-section for load application, left to right; concentric, ECC1 and ECC2

3.3.1. DESIGN OF AN UNCONFINED COLUMN

Unconfined specimen design was ultimately restricted by the test rig capacity of 10,000kN, including consideration of the feasible increase in capacity of FRP-confined specimens. All specimens were designed to be comparable to previous tests, refer to Table 2-1, to validate the results and develop an analytical model for design.

3.3.1.1. DESIGN FOR CONCENTRICALLY LOADED SPECIMEN (ID SC3)

For design of the unconfined control specimen, a 300x300mm cross-section was selected, with a 40mm corner radius and a test section height of 1250mm. For the concrete design, the ratio of longitudinal steel to cross-sectional area was determined to be 2% thus beneficially reducing the P-Delta effects without including a larger percentage of steel, and risking that it dominates behaviour. A design concrete strength capacity, f_{cu} of 30MPa ensured that the concrete did not dominate behaviour in the FRP-confined specimens. The cross-sectional dimensions are shown in Figure 3-3.

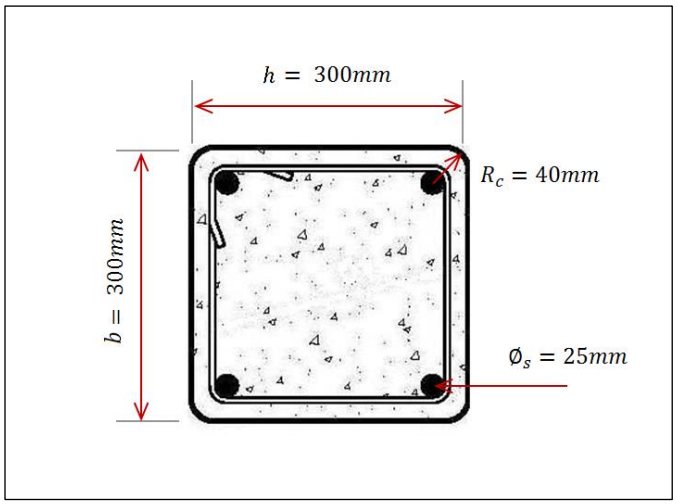

Figure 3-3: Cross-section dimensions for a medium-scale, concentrically loaded specimen

The axial strength, *N*, of an unconfined specimen under concentric loading is dependent upon on both the strength capacity concrete, f_{cu}, as well as the longitudinal steel, f_{yd}:

$$N = 0.67\, f_{cu}\, A_g + f_{yd}\, A_s \qquad (3\text{-}1)$$

Initial design of the specimens included 0.67 of the concrete compressive cube strength, and for accurate representation of the design at it has been included in the design calculations presented here. In design for research it is typical practice to remove all safety factors, however here it has been retained as it is not a safety factor. Instead it is due to the compressive concrete strength in a structure developing only 0.67 of the compressive cube strength, Figure 3-4 [BS8110]. Thus as the specimens are of a size representative of existing structures, it was deemed appropriate to retain this assumption on the development on the concrete strength for design.

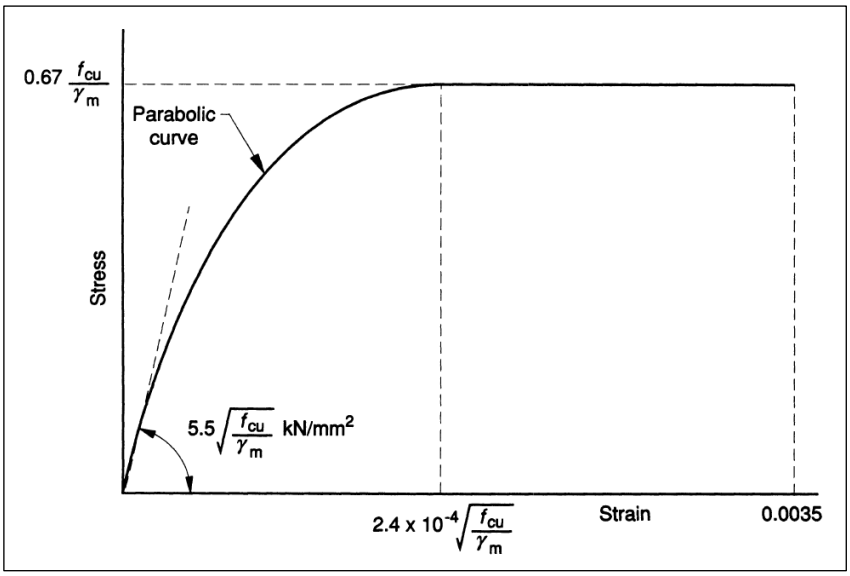

Figure 3-4: Design stress-strain curve for concrete in compression [BS8110 Figure 2-1]

Theoretically, for the axially loaded specimen there was no corresponding moment, thus the point of application of the load was on the centre point of the specimen. The minimal, but necessary steel reinforcement is illustrated in Figure 3-3, with the longitudinal bars and stirrups in accordance with BS8110-1: 1997 for the central section of the specimen. Specimen ends were extended and strengthened to ensure that the focus on behaviour and failure remained in the central section.

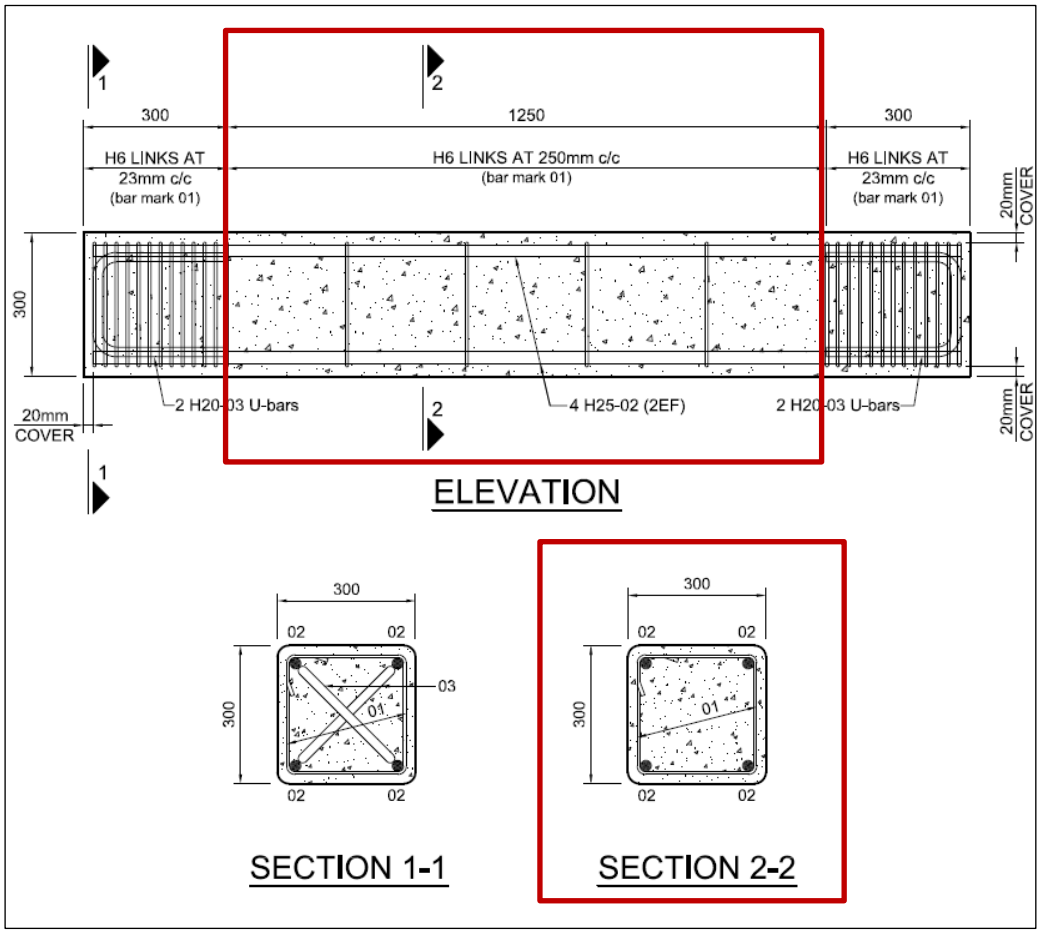

Figure 3-5: Medium-scale control specimen – Straight column (loading profile concentric and ECC1), red boxes highlighting test area with minimal reinforcement

Refer to Appendix A for detailed calculations.

3.3.1.2. DESIGN FOR ECCENTRICALLY LOADED SPECIMEN (THEORETICAL AT MEDIUM-SCALE)

For design of the unconfined axial-flexural loaded specimen, the strain profile to produce the greatest eccentricity is used. This profile has ε_{co} of 0.0035 to -0.0035, theoretically producing an even ratio of compression to tension over the cross-section, refer Figure 3-2. This placed the neutral axis at mid height of the cross-section.

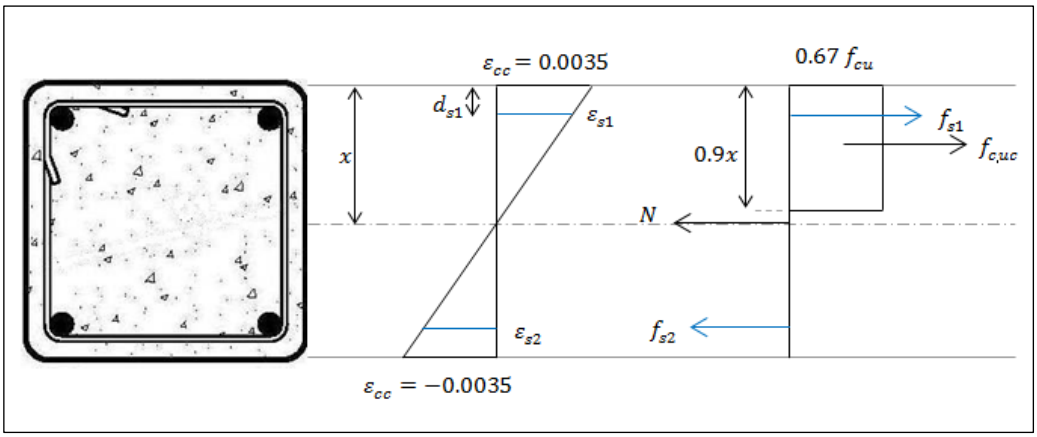

Figure 3-6: Stress profile over medium-scale cross-section for ECC2 load profile

The strain, ε_s, in the longitudinal steel is calculated as:

$$\varepsilon_s = \pm \frac{\varepsilon_{co}}{x} d_s \qquad (3\text{-}2)$$

The longitudinal steel capacity, f_s, due to the symmetry of the neutral axis was established using either Equation 3-3a if steel has not yielded ($\varepsilon_s < 0.0029$) or 3-3b if steel has yielded ($\varepsilon_s \geq 0.0029$), as appropriate:

$$f_s = \pm \frac{A_s}{2} \varepsilon_s E_s \qquad (3\text{-}3a)$$

$$f_s = \pm \frac{A_s}{2} f_{yd} \qquad (3\text{-}3b)$$

And the concrete capacity, f_c, used a nominal unconfined concrete strength of 30MPa:

$$f_{c,uc} = h\,(0.9x)0.67 f_{cu} \qquad (3\text{-}4)$$

From the steel and concrete capacity, the axial strength, *N*, was:

$$N = f_{s1} + f_{s2} + f_{c,uc} \qquad (3\text{-}5)$$

Subsequently the moment, *M*:

$$M = f_{s1} d_{s1} + f_{s1} d_{s2} + f_{c,uc} d_{c,uc} - N\,0.5b \qquad (3\text{-}6)$$

And the load eccentricity, e_i:

$$e_i = \frac{M}{N} \tag{3-7}$$

The load eccentricity necessary for ECC2 strain profile was determined to be 190mm (refer to Appendix A for detailed calculations). To adequately represent the loading profile, the point of application of the load measured from the centreline of the column exceeded the cross-sectional dimension, see Figure 3-7, thus corbelled end sections were necessary.

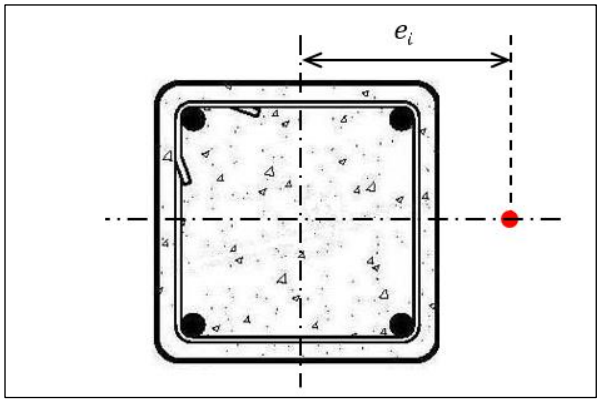

Figure 3-7: Theoretical point for load application for profile ECC2 on an unconfined specimen

The reinforcing steelwork for the corbelled specimen is illustrated in Figure 3-8.

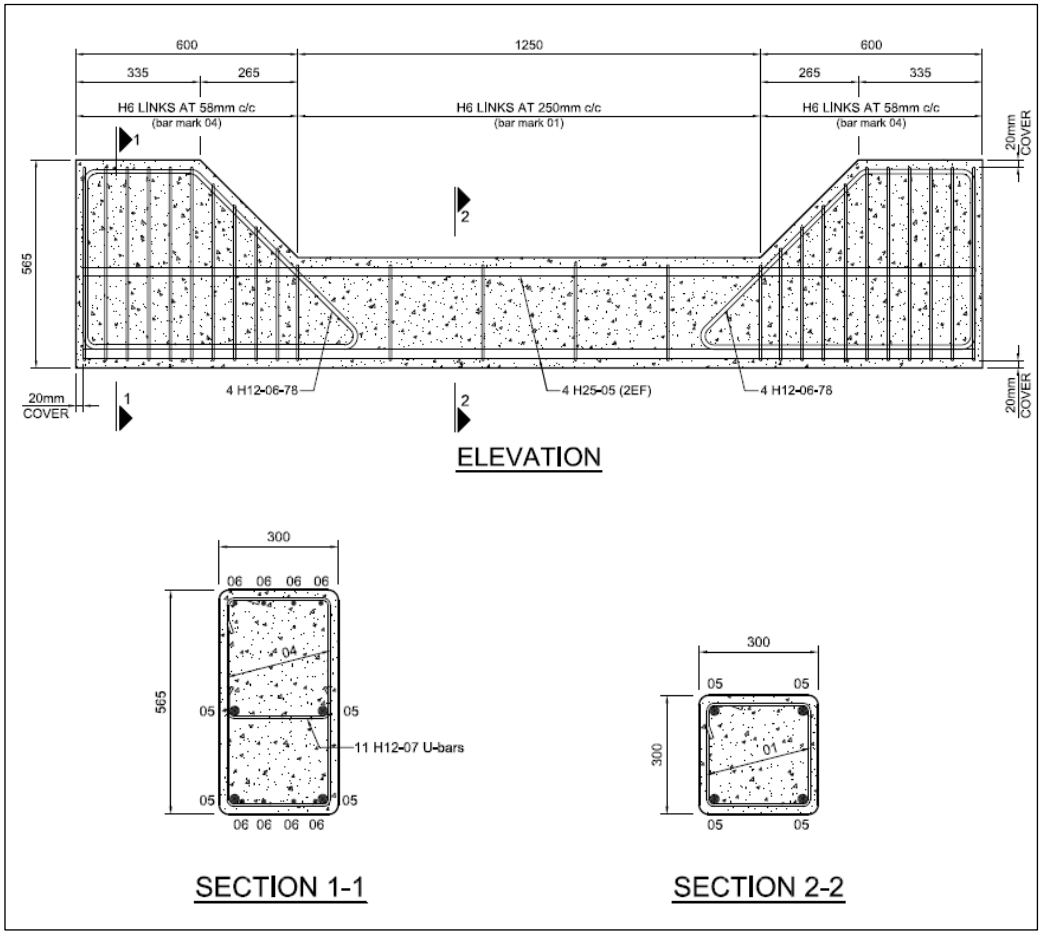

Figure 3-8: Medium-scale control specimen – Corbel column (loading profile ECC2)

Design of the corbels estimated the likely failure path from the edge of a 100mm steel loading plate centred at the calculated eccentricity. A minimum distance from the edge of the plate to the edge of the column of 100mm, was necessary to remove the possibility of premature failure at the corbel edge. Yield-line failure was established and the allowable load, *P*, determined as follows:

$$P\delta_1 = b\, d_c \tfrac{1}{2}(1 - \sin\alpha)\; x\; f_{cu}\; \gamma \qquad (3\text{-}8)$$

where: δ_1, the relative displacement vector, $\delta_1 = \frac{1}{\cos\alpha}$

Reinforcement steel quantity and size was ascertained iteratively through comparison of the load to generate yield-line failure and construction requirements to ensure integrity in design:

$$N_{\emptyset} = \pi \emptyset_s f_{yd} y \quad (3\text{-}9)$$

where: y, established through fundamental trigonometry

This was used as a template for other specimens and only altered in ratio where necessary. For steel rebar layout and sizing, refer to bar schedules in Appendix B.

3.3.2. DESIGN OF A FRP-CONFINED COLUMN

FRP confinement was applied in the hoop direction, thus the major considerations when designing the column was the tensile rupture of the FRP. At the time of specimen design there was no design standard governing the use of FRP for external confinement, so TR55 (2005) was referred to for guidance.

3.3.2.1. DESIGN FOR CONCENTRICALLY LOADED SPECIMEN (ID SC4)

To account for the influence of confinement on the cross-sectional behaviour, TR55 (2005) assumes a shape factor over the cross-sectional area of columns with non-square cross-sections. An effectively confined area is assumed by a set of parabolas, originating from the corners, with the area external to these parabolas being of negligible confinement, Figure 3-9. The shape of this cruciform is a function of the cross-section dimensions thus, as the cross-sectional aspect ratio changes, the effectively confined area adapts, with the potential of producing an overlap of lesser confinement in the centre, Figure 3-9, which the shape factor takes into account.

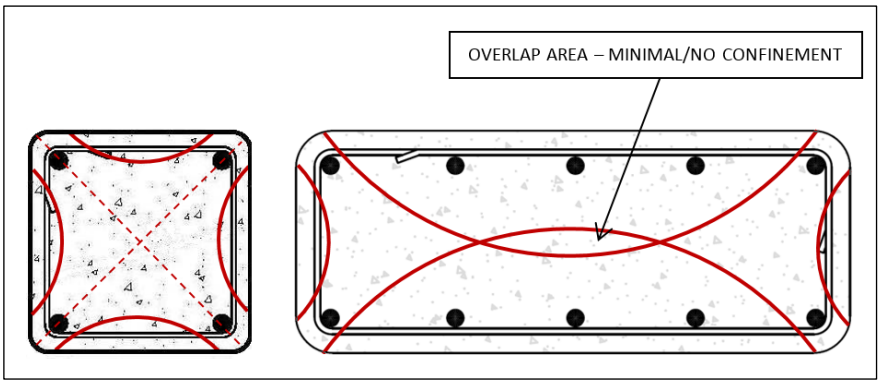

Figure 3-9: Assumed effectively confined area; left, square and right, large aspect-ratio rectangular specimens as demonstrated in TR55 (2005) Figure 34, assuming a 45 degree angle of the parabolas as per Lam and Teng (2003b)

TR55 (2005) uses an adapted version of Lam & Teng's (2003b) model to determine the effectively confined area, thus, the ratio of the effectively confined area to the cross-sectional area was determined as per Equation 3-10 (TR55 (2005) Equation 44):

$$\frac{A_e}{A_g} = \frac{1 - [(h - 2R_c)^2 + (b - 2R_c)^2 - 3A_{ol}]/(3A_g) - \rho_{sc}}{1 - \rho_{sc}} \qquad (3\text{-}10)$$

where: total cross-sectional area, $A_g = bh - (4 - \pi){R_c}^2$

ρ_{sc}, the ratio of longitudinal steel to the cross-section

A_{ol}, the area of overlap in the parabolas that must be subtracted if $2b < (h - r_c)$ is reached, is calculated from:

$$A_{ol} = \begin{cases} 0 & if \quad 2b \geq (h - 2r_c) \\ \frac{{l_{ol}}^3}{3\,(h - 2R_c)} & if \quad 2b < (h - 2r_c) \end{cases}$$

and length of the overlapping region is:

$$l_{ol} = \sqrt{(h - 2R_c)^2 - 2b(h - 2R_c)}$$

The shape factor (TR55 (2005) Equation 45) reflects the subsequent reduction in confinement as the aspect ratio of the column increases, relating the effective confining pressure to that provided by an FRP wrap of the same thickness of an equivalent circular column of diameter D (defined as $D = \sqrt{(b^2 + h^2)}$, the diagonal distance across the section, Lam & Teng (2003b):

$$g_s = \frac{b}{h}\frac{A_e}{A_g} \qquad (3\text{-}11)$$

Thus the equivalent confining pressure (TR55 (2005) Equation 46) was:

$$f_r = \frac{2\, f_{fd}\, t_f}{\sqrt{b^2 + h^2}} \quad (3\text{-}12)$$

where: t_f, the FRP thickness, 0.32mm for each wrap

f_{fd}, the design tensile strength of FRP

The unconfined compressive strength was established as per unconfined specimens:

$$f_{c0} = \frac{0.67\, f_{cu}}{\gamma_{mc}} \quad (3\text{-}13)$$

where: γ_{mc}, the concrete partial safety factor, 1.0 for design

And from the equivalent confining pressure and the shape factor, the strength of the confined rectangular column (TR55 (2005) Equation 47) was:

$$f_{cc} = f_{c0} + 2.0\, g_s\, f_r \quad (3\text{-}14)$$

Subsequently the specimen peak load was:

$$N = f_{cc}\, A_g + f_{yd}\, A_s \quad (3\text{-}15)$$

Theoretically, pure axial load is applied, thus there is no design moment.

Through design calculation, a theoretical increase in strength capacity for a concentrically loaded column was found to be around 45%.

3.3.2.2. DESIGN FOR ECCENTRICALLY LOADED SPECIMEN (ID SE6)

To account for the strain in the FRP, an adapted strain profile was applied to the specimen cross-section. The high level of confinement in the FRP along the topside of the column, especially at the corners induces high strains, a limiting value of ultimate axial compressive strain, $\varepsilon_{cc,max}$, of 0.01 is adopted (although lower than typically found in practice, it ensures that the concrete integrity is maintained). This was later incorporated into TR55 (2011) for design for combined axial compression and flexure (Section 8.4). However, on the opposite side of the cross-section, there is only concrete strain due to minimal/no strain in the FRP at the corners. The adapted stress block included two additional triangular elements to

closer resemble the actual curved stress profile, thus taking into consideration the further capacity of the concrete as the confinement was induced, Figure 3-10. The change in strains then pushed the location of the neutral axis back towards what is the tension side of the unconfined column (it is no longer at mid-height).

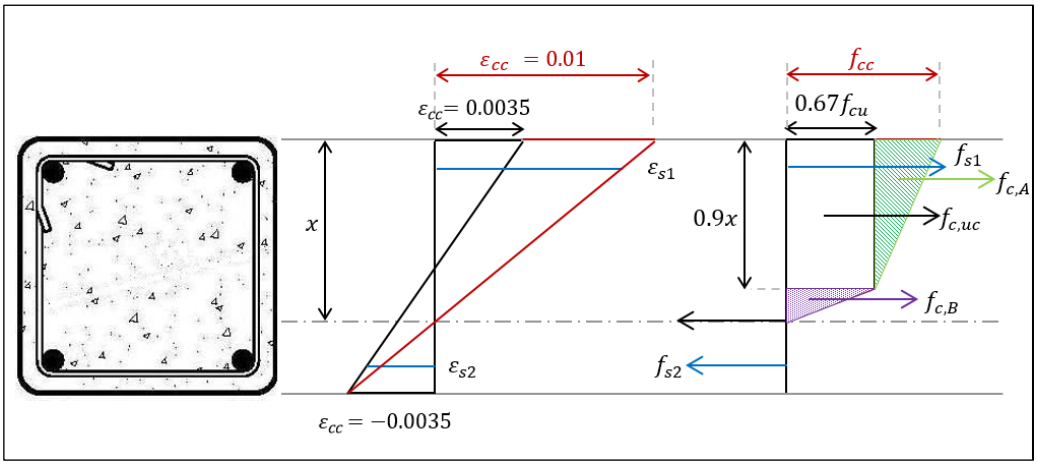

Figure 3-10: Stress profile variation over an FRP-confined specimen cross-section, load profile ECC2

To determine the load capacity of the FRP-confined, eccentrically loaded column, ε_s and f_s were calculated as per Equation 3-2 to Equation 3-3 for the unconfined specimen.

Determination of the stress block representing the concrete capacity deviated from the unconfined method as follows:

$$f_{c,uc} = h\ (0.9x)\ 0.67\ f_{cu} \quad (3\text{-}16)$$

$$f_{c,A} = h\ [0.5\ (f_{cc} - \ 0.67 f_{cu})\ 0.9x] \quad (3\text{-}17)$$

$$f_{c,B} = h\ [0.5\ (0.1x)\ 0.67\ f_{cu}] \quad (3\text{-}18)$$

Thus, from f_s and f_c, the axial strength in the column, *N*, was:

$$N = f_{s1} + f_{s2} + f_c + f_{c1} + f_{c2} \quad (3\text{-}19)$$

Subsequently the moment, *M*, was determined:

$$M = f_{s1}d_{s1} + f_{s1}d_{s2} + f_c d_c + f_{c1}d_{c1} + f_{c2}d_{c2} - N0.5b \quad (3\text{-}20)$$

And the eccentricity was applied at:

$$e_i = \frac{M}{N} \quad (3\text{-}21)$$

With an eccentricity of 103mm (refer to Appendix A for detailed calculations), the confined specimen was designed with corbelled end sections, ensuring that there was consistency in the small-scale unconfined and confined specimens. The design for the corresponding unconfined specimen was checked for the capacity of the confined specimen and if necessary adapted for larger bar diameter and/or quantity, and this design used for both unconfined and confined specimens. At the design stage, the increase in capacity due to confinement represented a 40% increase in peak strength capacity in the FRP-confined square columns.

3.4. METHODOLOGY AND SPECIMEN TESTING

The experimental programme took four main stages; material selection and testing, construction and strengthening of the specimens, testing, and post-test analysis.

3.4.1. MATERIAL SELECTION AND ANALYSIS

Material selection was governed by design specification, expense, and location. For the purpose of comparison with previous research and for ease of construction, reinforced concrete was selected to ensure that as far as possible failure would occur in the FRP jacket. All material testing was performed at the University of Bath.

3.4.1.1. REINFORCED CONCRETE

Concrete used in construction is often paired with steel reinforcement due to the relative ease of construction and the versatility of the combined materials. The constitutive parts enable it to be beneficial in both tension and compression. The reinforced concrete was normal strength concrete (NSC) to ensure that it did not dominate the behaviour of the test specimens, instead allowing the FRP to perform to its maximum capacity and fail.

The test region of the specimen can be seen in Figure 3-5, highlighted in the red box. Refer to Appendix B for the bar schedule for each specimen.

STEEL REINFORCEMENT

The steel reinforcement was designed to BS8110-1: 1997 where feasible. Grade S355 steel was used. The approaches to design varied depending upon location of reinforcement in the specimen:

1. *Central Section*
   Highlighted in Figure 3-5. Designed to BS8110-1: 1997, specifically the lateral restraint was using the maximum allowable spacing so as to provide minimal influence on the confinement behaviour of the FRP jacket.

2. *End Section*
   Greater quantity of steel used in the end sections. Stirrups were required to be significantly closer in spacing to ensure that concrete spalling was limited and failure did not occur at the ends.

Standard tensile pull out tests of the steel rebar were performed at the University of Bath. Each series of diameter consisted of three specimens and the average values of each taken, detailed in Table 3-5.

Table 3-5: Reinforcing Steel – Bar Strength Data

REBAR SIZE (mm)	YIELD STRENGTH (MPa)	STANDARD DEVIATION	ELASTIC MODULUS (GPa)	STANDARD DEVIATION	NO. OF TESTS
Ø 3mm (steel wire)	779	5.39	182	2.24	3
Ø 6mm	535	2.69	151	2.68	3
Ø 8mm	523	2.42	214	1.32	3
Ø 12mm	556	6.33	215	9.94	3
Ø 25mm	590	7.07	195	1.13	3

CONCRETE

Specimens were designed to a nominal concrete compressive cube strength of 30MPa. Small-scale specimens were constructed with material from the University of Bath and mixed on site as per conventional practice. The constituent parts and proportions for the 30MPa mix are detailed in Table 3-6. The concrete was prepared using a 0.3m^3 pan mixer, with one batch casting two columns and fifteen 100mm cubes for strength determination. The formwork was reused each time.

Table 3-6: Concrete Constituent Parts – University of Bath Mix

CONSTITUENT PART ǂ1	QUANTITY (PER m^3)	COMMENTS
COARSE AGGREGATE	870KG	10MM CRUSHED LIMESTONE LIMITED TO 10MM DUE TO THE HIGH CONCENTRATION OF STEEL IN END SECTIONS, POTENTIALLY RESTRICTING FLOW
FINE AGGREGATE	1020KG	COMBINATION SAND/GRIT, UNCRUSHED
ORDINARY PORTLAND CEMENT	355KG	CEM N CLASS, ENSURING BASE LINE COMPARISON
WATER	190KG	

ǂ1 Plasticiser was not used in the mix as the length of time required per cast meant that the risk of the concrete setting before all moulds were full was too high.

The volume of concrete required for the medium- and large-scale specimens necessitated that the mix was outsourced and poured at the UoB. Slump and cube tests were performed to establish the actual strength.

For all casts, concrete cubes were prepared as per BS8110-1: 1997 and cured under the same conditions as the specimens. At 7, 14 and 28 days, three cubes per cast were tested to evaluate the development of the compressive cube strength against predicted strength and to establish the actual 28 day compressive cube strength, refer Table 3-7. Cubes tests, as opposed to cylinder tests, were decided upon as the best strength testing method due to the small size and the lack of treatment necessary before testing, as well being the standard testing method in the UK and Europe.

Table 3-7: Concrete Cube 28 Day Strength

CUBE SERIES	28 DAY COMPRESSIVE CUBE STRENGTH				STANDARD DEVIATION
	CUBE 1	CUBE 2	CUBE 3	AVERAGE	
UOB-1	40.13	39.13	39.00	39.4	0.62
UOB-2	37.81	37.81	37.18	37.9	0.84
UOB-3	37.68	36.68	36.10	36.7	0.85
EXT-1	40.14	43.03	42.91	42.0	1.64
EXT-2	34.33	35.12	36.52	35.3	1.11
EXT-3	22.80	25.25	25.07	24.4	1.37

The variation in concrete strength in small-scale mixes was attributed to; the outdoor storage of the ingredients, and variation in aggregate size. Through study of the strength results, it was evident that weather was a significant factor, as after wet weather, there was additional interstitial water accumulated in the samples.

The external concrete mixes revealed a large variation in cube strength. A 30N concrete mix was ordered from the supplier but this was initially overestimated with the actual strength far exceeding an average strength of 30N, as is typical when supplying a mix to a building site. The over-strength was addressed for external mix two but still exceeded 30N with a large slump. Lastly, the third mix was closer in estimation to the required strength.

3.4.1.2. CARBON FIBRE REINFORCED POLYMER (CFRP)

The CFRP jacket consisted of a fibre matrix; Grafil 34-700 carbon fibre, a Sidakur 30 resin system, a thixotropic adhesive comprising two components mixed 1:3 ratio. The mechanical properties provided by the manufacturer state a tensile strength, f_{fd}, of 2572MPa and Young's Modulus, E_{fd}, of 137GPa for a 300gsm unidirectional fibre architecture.

The mechanical properties were verified through tensile coupon tests performed at UoB. Adherence to ASTM D3039-00 for coupon design was sought, dictating a length of 255mm and width of 18mm, coupons can be seen in Figure 3-11.

Before testing, the thickness of each sample was measured to account for the differing number of wraps and for variation application. The tests were performed on the 200kN,

load controlled Dartec rig, with mechanical properties established from load and displacement, adequate for the elastic/brittle response.

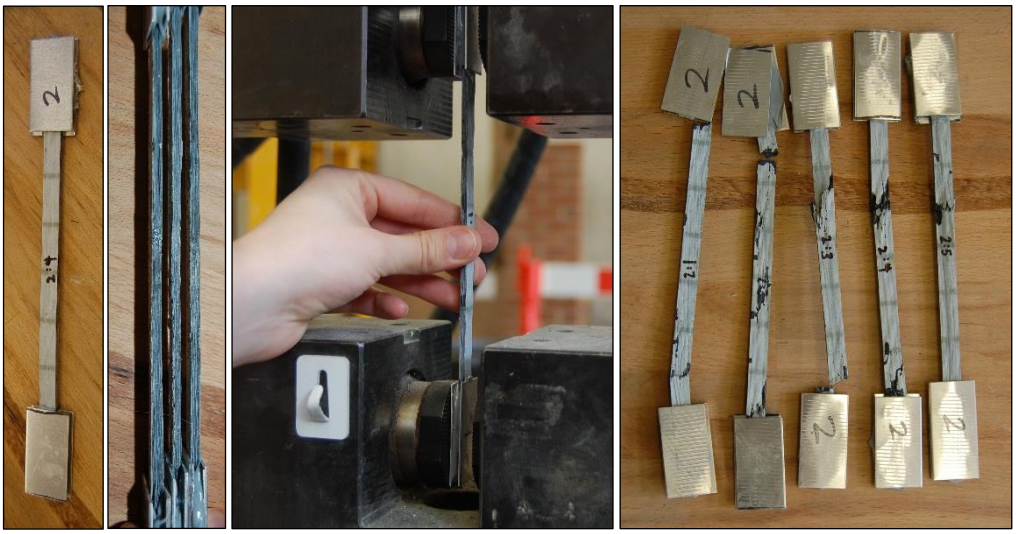

Figure 3-11: Testing method images for FRP coupons, left to right; initial coupon, thickness of coupons, placement in the testing rig, and failed specimens from one series

Initial testing was performed to establish if there was a variation in strength in between a fresh wet-layup sample and a sample from an undamaged area of the test specimen. No change in strength was evident, thus samples from undamaged areas of the specimens were used for the remaining coupon tests, results of which are found in Table 3-8.

Table 3-8: FRP Coupon Test Results – Failure Strength

FRP COUPON SERIES	NO. OF TESTS	THICKNESS (mm)	TENSILE STRENGTH (MPa)	YOUNG'S MODULUS (GPa)	RUPTURE STRAIN
1	5	3.56	2083	105	0.020
2	5	3.28	2348	120	0.020
3	5	3.23	3598	191	0.019

The average tensile strength and elastic modulus were found to be 2676MPa and 138GPa respectively, very close to that state by the manufacturer (Data sheet is included in Appendix B). Ultimate strain of the FRP is 2.0%.

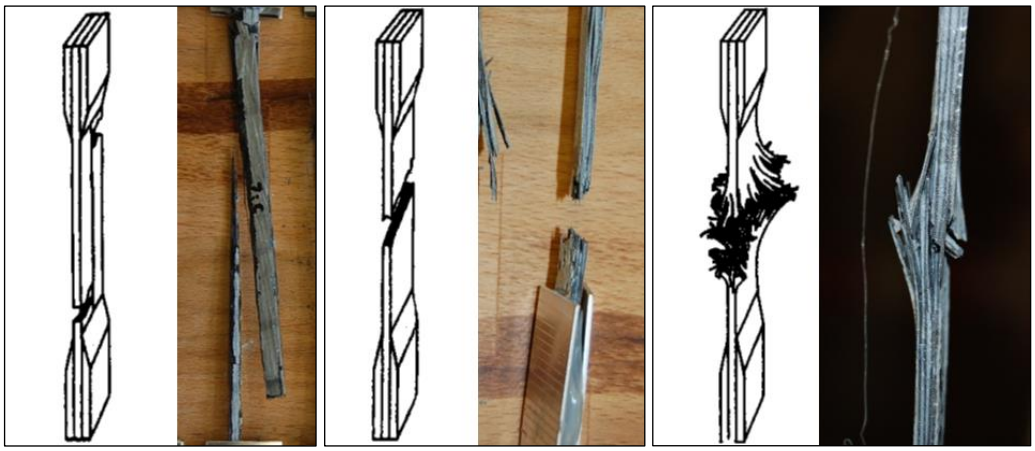

Figure 3-12: FRP tensile coupon failure modes [ASTM D3039] and test failure photograph; from left, longitudinal failure, lateral failure, and explosive failure

The three types of failure modes witnessed are illustrated in Figure 3-12, these being; longitudinal failure, lateral failure, and explosive failure. All failure methods were instantaneous compared to the duration of loading. Explosive failure was found to be the predominant failure method.

3.4.2. CONSTRUCTION AND STRENGTHENING OF SPECIMENS

Construction and strengthening of specimens was performed at the UoB. Exact real-world conditions could not be mimicked due to time and cost constraints, hence aspects such as settlement, weather, and decay to name a few, have not been addressed. However this is in concurrence with existing published test series.

3.4.2.1. SPECIMEN CONSTRUCTION

Construction of the specimens comprised of three main phases; preparation, assembly of steel, and concrete casting.

1. *PREPARATION*

   This phase included material specification and purchase, design and fabrication of the casting moulds, organisation of logistical requirements and substantial monitoring to ensure consistent preparation and testing.

2. *ASSEMBLY OF STEEL CAGES*

   Slight differences between the assembly of small-, medium- and large-scale specimens was necessary. The rebar was supplied 'straight' for small-scale columns hence required to be bent into shape on site, thus slightly increasing the margin of error in steel assembly. For the medium- and large-scale specimens, the rebar was supplied pre bent. The steel cages were tied together, structural welding was not performed.

3. *CASTING*

   Specimen moulds were cleaned, removing dust and contaminants before casting. The formwork was waxed, thus reducing the likelihood of the concrete sticking to the sides and the steel cages were placed on plastic feet in the correct moulds. Lifting tails were secured to the medium- and large-scale specimens (one on top of each column and two in the bottom end section at opposite sides). Space constraints required that the casting of the specimens occurred in several batches. Specimens were covered with plastic sheeting to reduce the escape of moisture and cured for 28 days.

Figure 3-13: Casting of a set of specimens using an external mix

Figure 3-14: Slump testing of concrete

3.4.2.2. STRENGTHENING (FRP APPLICATION)

There are a few methods of FRP application; dry, pre-impregnated or preformed shell (primarily used in new structures). The FRP (supplied by BASF) comprised a dry roll fabric and a two part epoxy resin. Application of the FRP jacket required particular conditions and application technique. Specifically, application required a dry environment, on dry specimens within an ambient temperature range, alongside careful preparation of the concrete surface, resin and fibre material.

Preparation of the cast specimens was three phase: grit blasting to remove excess cement/dust that had settled on the surfaces from casting exposing a sound, clean surface for the resin to bond to; corner chamfering to form the corner radius determined in design; and cleaning along with surface 'set-up' so that the surfaces were thoroughly cleaned with a damp sponge and strain gauge wires tucked away, before CFRP strengthening could commence. Failure to do so risked a weak or non-existent bond between CFRP and concrete.

Figure 3-15: FRP Application – Specimen preparation, from left; removing all excess cement/dust after grit blasting, and positioning on trestles with wires tucked away

The FRP jacket was applied so that the fibres were running in the transverse direction to the longitudinal axis of the column to provide lateral restraint to the concrete core. The number of wraps on each column varied depending on scale, refer to Table 3-1. The fibre wrap was supplied in 510mm wide rolls, cut to appropriate length and where necessary, additional cuts made in the end sections to accommodate lifting point and extruding wires from the strain gauges in the end sections. It was necessary to have a slight overlap of the FRP wraps

and to minimise extra strengthening, this was placed on opposite sides for the even numbers of wraps. It was essential to consider the location of the lap joints to minimise impact on rupture failure.

A wet lay-up application technique was used, as follows:

1. The surface was coated with a layer of the epoxy resin marginally wider than the fibre sheet to ensure 100% contact, Figure 3-17.
2. The fibre sheet was placed on the resin with the edge starting on the flat side, just after the corner radius on the designated side and wrapped round in the transverse direction in a continuous manner until it reached the start of the fibre sheet, Figure 3-18. An arbitrary overlap length of 100mm as per standard practice was used to ensure adequate confinement. At this point the wrap was smoothed down with brushes to ensure that there were no air bubbles present that could compromise the integrity of the wrap.
3. The fibre sheet on the column was coated with resin and wrapped round repeating this process until all the pre-cut fibre sheet was used and secured to the specimen with a coating of resin.
4. This procedure was repeated for a second layer, starting at the opposite side of the column to the original layer and going in the counter direction, Figure 3-19.
5. As the width of the fibre roll was less than the column length, this process was repeated as many times as necessary without overlapping fibre sheets at the circumferential seam, Figure 3-20.

No CFRP was applied with fibres in the longitudinal direction of the column.

Figure 3-16: FRP Application – Preparation of the resin coating using Sidakur two part epoxy resin

Figure 3-17: FRP Application – Step 1, coating the surface with a layer of epoxy resin (note, for medium- and large-scale specimens, it was deemed prudent to cover the whole specimen with FRP)

Figure 3-18: FRP Application – Steps 2 & 3, placing of the fabric sheet, coating with resin and repeating around the cross-section of the column

Figure 3-19: FRP Application – Step 4, placing of the next fabric sheet, ensuring that it starts on the opposite side to the previous layer

Figure 3-20: FRP Application – Step 5, repetition of steps 1 to 4 until the length of the specimen is covered in FRP

3.4.3. TESTING PROCEDURE

Testing of the specimens was performed on three loading rigs in two locations; at the UoB and the BRE. Test set-up in terms of placement of the specimen, instrumentation and loading were consistent where feasible. Material tests and small-scale specimen tests was performed at the UoB. Medium- and large-scale specimens could not be tested at UoB owing to the limited capacity and dimensions of the testing rig.

3.4.3.1. INSTRUMENTATION

Data collection was primarily through use of strain gauges and linear-variable displacement transducers (LVDTs) mounted around the specimens. Strain gauges measured the axial strain in the longitudinal rebar, facilitating in the evaluation of the authentic strain profile. Strain gauges were also affixed on the CFRP wrap in the transverse (hoop) direction.

STRAIN GAUGES

In order to ascertain fully the behaviour of the column, strain gauges were applied to the longitudinal steel on both sides of one set of bars along the axis of loading, Figure 3-21. Further gauges were applied in the hoop direction of the FRP wrap at mid-height of the column, Figure 3-22, to enable assessment of the confinement efficiency and distribution of FRP stresses.

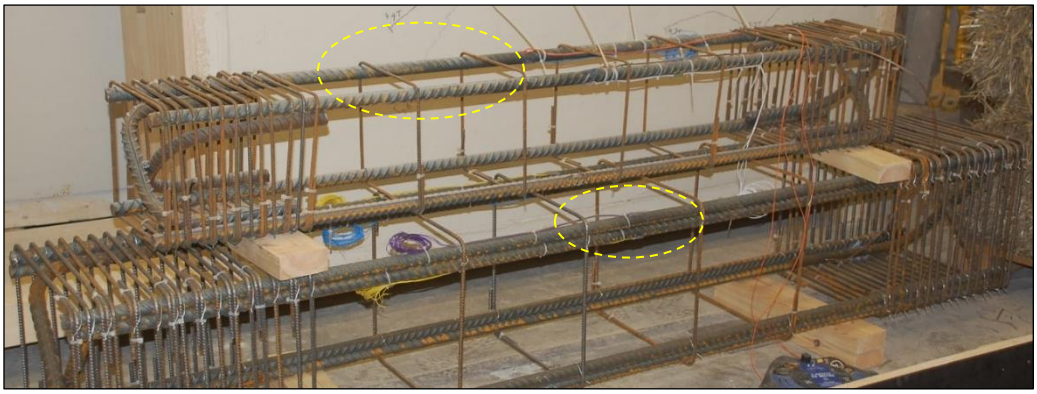

Figure 3-21: Strain gauge location on the longitudinal steel rebar, highlighted in yellow

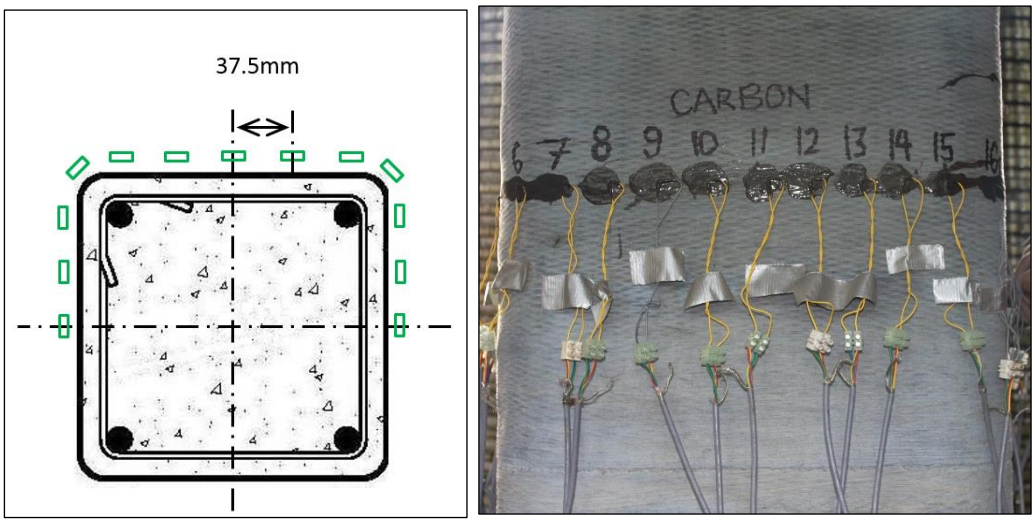

Figure 3-22: Strain gauge locations around the perimeter of the FRP jacket (distance between gauges always 37.5mm, regardless of specimen cross-sectional dimensions)

Preparation of the base material for application of strain gauges varied between CFRP and steel. The surface of the CFRP had to be gently removed using sand paper until fibres were just visible and then cleaned with a non-acidic/gentle product. Steel-mounted gauges required a small area of the bar to be ground flat for application, this area was cleaned thoroughly and the surface neutralised. The application process of the gauge for CFRP and steel was:

1. The strain gauge and terminal pad were aligned, glue applied to the base of both and placed on the cleaned surface and held for around 60 seconds ensuring a combination of pressure and heat.
2. Wires were soldered to contact points on the terminal pad and allowed to cool.
3. The gauges were checked with a multimeter to ensure that the correct resistance (120.2 Ohms) was present. If a gauge in a critical position had stopped working on the CFRP prior to test set-up, it was replaced.
4. The wires were threaded through straws and the gauge sealed with a coating of protective liquid padding.

The number of failed gauges mounted on the steel was 2% of the total number applied to the reinforcing steel.

LINEAR VARIABLE DISPLACEMENT TRANSDUCERS (LVDTS)

LVDTs were selected to measure the specimen displacement in the longitudinal and lateral directions.

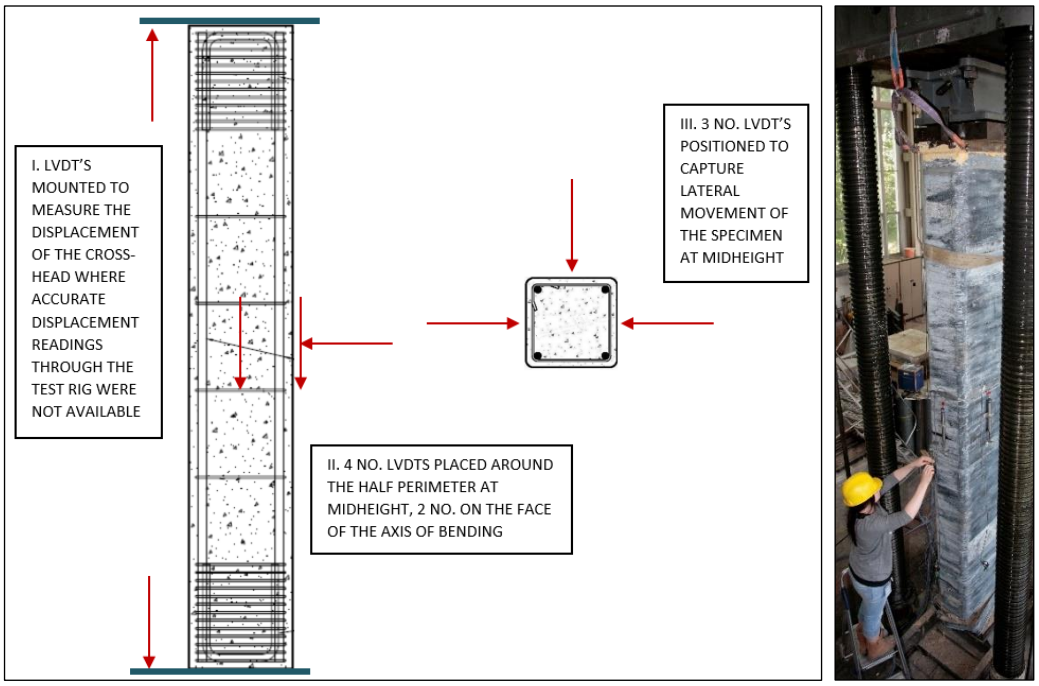

Figure 3-23: LVDT locations on the specimen, measuring: i. crosshead displacement, ii. vertical displacement and iii. lateral movement

LVDTs were fixed to the face of the specimen on half of the column, using the axis of symmetry, Figure 3-23. The lateral deflection was determined from LDVT measurements on opposite sides of the column; the compression face and the tension face, both at mid-height. Testing at the BRE required LVDTs to be used to monitor the movement of the cross-head as the in-built reader was lacking in accuracy.

3.4.3.2. TESTING – UNIVERSITY OF BATH

Specimens were tested on a 2,000kN Dartec rig at the University of Bath. The applied load was measured using a load cell within the test machine.

Pre-test set-up included painting exposed concrete with a white wash, marking up the column with identifying instrumentation locations, checking strain gauges and gluing on

clamps. The rig was set-up with the correct jaws (for pinned loading). The test procedure was as follows:

SPECIMEN POSITIONING

1. The specimen was manoeuvred into position, ensuring that it was sitting on the platen with the centre-line of the specimen exactly at the predetermined eccentricity to generate the established strain profile over the cross-section.
2. To ensure that the specimen did not move within the rig, a dental plaster mix was prepared and applied to the bottom plate. The specimen was checked to ensure it was level and then allowed to set so creating a smooth flat surface for load transfer between specimen and jaws, see Figure 3-24. This was repeated for the top platen.

Figure 3-24: Specimen Positioning – Steps 1 & 2; application of dental plaster mix, positioning of the specimen, checking position accuracy

INSTRUMENTATION

3. Once the specimen was positioned correctly, the LVDTs were positioned in the required locations around the rig. On the small-scale specimens, horizontal deflection was also established with LVDTs at three heights on the column; the bottom of the test region, at mid-height and at the top (1, 2 and 3 on Figure 3-23). This allowed the additional P-delta effects generated by the CFRP wrap to be observed.
4. The logging cables from the data recording equipment were linked up to the protruding wires from the strain gauges.

5. Instrumentation was tested to verify it was reading accurately and replaced if necessary.

TESTING

6. A preload of approximately 5kN for small-scale specimens was applied allowing removal of supporting stubs and shims and to initiate logging of data.
7. A monotonic, displacement controlled load was applied.
8. When predetermined loads were attained, the columns were checked visually for concrete cracking and where safe to do so, the column was marked up, and repeated until specimen failure.

Post-test analysis was performed, discussed in detail in Section 3.4.5.

3.4.3.3. TESTING – BUILDING RESEARCH ESTABLISHMENT

Medium- and large-scale specimens were tested on either the Avery Denison 5,000kN rig or the Amsler 10,000kN rig. Mechanical difficulties with the Amsler rig necessitated the use of the 5,000kN rig to ensure testing was completed in the given timescale. The test procedure followed the same principles used on the small-scale specimens. Additional safety measures were essential, especially with the manoeuvring of the specimens requiring the use of a crane; and when working at height to secure the column and fix the instrumentation. The load applied using both rigs at the BRE was monotonic and displacement controlled using visual gauge measurements in the absence of computerised monitoring and controls that are found on more modern machines. Displacement readings relative to the load were taken using LVDT's mounted on the top and bottom platens.

3.4.4. POST TEST ANALYSIS PROCEDURE

Post-test analysis of the specimens helped ensure detailed assessment of the failure behaviour, especially as it was not always immediately evident and also required examination of the debonded area of the FRP jacket. As the necessary safety constraints did not allow for detailed examination of the development of cracks and other defects on the specimens during testing, each specimen was observed from a safe distance and images

taken whilst it was still standing in the rig, then thoroughly examined after removal of the load.

Debonding of the FRP from the concrete was established using the coin tap method. The specimen was marked up with a 20mm grid (size arbitrary) and each square tapped with a coin. Where a hollow sound returned, it was marked with a cross, to visibly demonstrate the debonded area, Figure 3-25. The CFRP was then cut down the length of the column, exposing the areas still bonded to the concrete.

Figure 3-25: Debonding check, i. grid mark up, ii. debonded areas highlighted with 'X' after tap test

The results from the experimental test programme are detailed in Chapter 4.

3.5. CONCLUDING REMARKS

Design and construction methodology of the specimens was adhered to where feasible to minimise variations between tests. However compromises were necessary due to the use of different test locations and the methods of construction for small-, medium-, and large-scale specimens. This resulted primarily from space and cost constraints. The primary variable in the construction was the concrete strength which varied significantly due to the mix being over-strengthened by the external contractors' supplied mix. This was observed and quantified by establishing the 28 day compressive cube strength of the concrete. Within the scope of the laboratory tests described in this chapter, all of the significant characteristics of the materials involved and their interaction with one another have been established and recorded to allow full comprehension of the test results, specifically how and why the confinement behaviour occurs. Furthermore, full adherence to design codes and guidance was implemented where feasible and if deviated from, it has been noted.

CHAPTER 4

EXPERIMENTAL TEST RESULTS

4.1. INTRODUCTION

This chapter presents the results obtained from the experimental test programme detailed in Chapter 3. As an overview, the results demonstrate positive behaviour in terms of an increase in axial strength capacity for the FRP-confined specimens, and gives further insight into the cross-sectional confinement through FRP mounted strain gauge readings that confirm postulated behaviour. However general behaviour on occasion diverges from that postulated; specifically, the peak load for FRP-confined specimens does not always exceed the peak unconfined load. Detailed analysis of this behaviour is further detailed in Sections 4.2 to 4.4, for size effect, load eccentricity and cross-sectional aspect ratio parameters respectively.

In terms of unconfined specimen behaviour, prismatic RC columns subjected to a combination of axial or axial-flexural loads under low levels of longitudinal strain, demonstrate proportional transverse strain (Poisson's Ratio), thus initially behave elastically. Therefore they have a reasonably linear load-displacement path, diverging slightly before peak stress is achieved, as softening is initiated which occurs fully after peak stress. Failure occurs shortly after, with the column shedding approximately 80% of the peak load. This was the case with all unconfined specimens that reached peak load, hence the analysis of the results focuses on the behaviour of the FRP-confined specimens, and the capacity increase attainable with respect to the corresponding unconfined specimens.

The test results are evaluated initially with respect to TR55 (2005) and then compared against TR55 (2011) to evaluate the current guidance against large-scale results. In some

instances, aspects of TR55 (2011) are used before the full comparison to investigate specific detail that is not addressed in TR55 (2005).

4.2. EXPERIMENTAL SERIES SC – SIZE EFFECT

Series SC comprises of specimens of square cross-section, subject to an axial load, to address the effect of size on the potential increase in strength capacity of the FRP-confined columns. Owing to the nature of the specimen casting (detailed in Chapter 3) normalisation of the results with respect to concrete compressive cube strength is favourable for comparison and graphical presentation. Fundamentally, FRP-confinement of specimens demonstrates an evident increase in capacity as shown in Table 4-1.

Table 4-1: Series SC (Size Effect) – Summary of load, moment and FRP strain results

SPECIMEN ID	X-SEC	PREDICTED LOAD	PEAK LOAD	LATERAL DEFLECTION (@ PEAK)	MOMENT (FROM LATERAL DEFLECTION @ PEAK)	FRP STRAIN (PEAK | FAILURE)	CONFINEMENT EFFECTIVENESS
	mm	kN	kN	mm	kNm		
SC1	150 | 150	816	766	0.08	0.1	-	1.27
SC2		995	936	5.83	5.5	0.22 | 0.50	
SC3	300 | 300	2548	2443	1.76	4.4	-	1.80
SC4		3486	3617	8.49	30.7	0.18 | 0.90	
SC5 †	450 | 450	7811	9112	2.39	21.9	-	NOT DETERMINED
SC6		7548	7364	1.17	55.3	1.60 | 0.95	

† Specimen did not reach peak load, experiment had to be prematurely halted

Testing of unconfined specimen SC5 was terminated prematurely as the 10,000kN capacity of the test rig was close to being realised with minimal evidence of imminent failure. SC5 was initially designed using a 30MPa concrete compressive cube strength but the external concrete mix exceeded this (50% higher strength than specified). Adjustment of initial design calculations to take the higher concrete strength into consideration predicted a failure of 7811kN, however this was far exceeded (a variation of 14%). There is no evidence of this happening with unconfined specimens studied in the literature reviewed in Chapter 2. Large-scale FRP-confined specimen SC6 also deviated from the postulated behaviour.

The predicted versus peak load of the FRP-confined specimens has a maximum 6% variation. Generally, the specimens reach peak strength marginally less than the predicted load. All specimens were subject to pure axial load thus theoretically no moment should be evident. In all specimens, a small lateral deflection at mid-height is recorded thus generating a small moment, conceivably due to slight misalignment on the platens or P-Delta effects intrinsic in the construction of the specimen. As the size of the specimen increases, the P-Delta effects generate an additional moment, thus it is imperative to address the specimen slenderness with changes in size and FRP confinement level.

FRP strain at peak and failure load presented in Table 4-1 is the maximum reading from the accurately measuring gauges mounted at mid-height around the specimen. The FRP strain at peak load is significantly less than at failure for small- and medium-scale specimens. The pattern of increasing strain from peak to failure is not evident in the large-scale specimen, due to the failure mode. Unusually, SC6 reaches far higher strains at peak load than the other specimens reach at failure, due to the location of FRP failure generating localised areas of higher FRP strain away from the mid-height gauges. Furthermore the strain at failure is less than the ultimate strain of 2% (as defined in Table 3-8).

During testing, rupture strain was rarely achieved, with strain measurements at mid-height not fully describing the localised behaviour of the FRP-confinement at the area of rupture. Looking at Figure 4-1 for SC4, failure occurred very close to mid-height of the specimen hence the strain is anticipated to be closer to the FRP ultimate strain of 2%. It follows that when measuring hoop strain of FRP confined concrete it is vital to take measurements exactly at the point of failure to capture the true failure strain (Harries & Carey, 2003). Furthermore, a lesser strain at rupture than the FRP coupon ultimate strain correlates with experimental results addressing the change in corner radius from sharp corners to circular [Barrington et al. (2011)] illustrating that the FRP failure strain decreases with decreasing corner radius hence an ultimate strain of 2% is not achievable.

Confinement effectiveness of the small- and medium-scale specimens relative to their unconfined equivalent increases with specimen size. Confinement effectiveness of the large-scale specimen is not determined as the unconfined test was halted prematurely. Excluding the large-scale specimens, the trend shows that as size increases, confinement effectiveness increases, but due to the unexpected results from the FRP-confined large-scale specimen, this requires further verification. As one of each specimen was tested, rather than

assume that there was a lower confinement occuring for large-scale specimens, additional testing of large-scale specimens is necessary.

The FRP-confined specimens failed through rupture of the FRP jacket, illustrated in Figure 4-1. During testing their initial behaviour followed that of the unconfined RC specimens, exhibiting a linear load-displacement path. After approximately 70% loading, micro-cracking of the FRP jacket could be heard. The behaviour of the FRP-confined specimen then began to deviate from the corresponding unconfined specimen while the concrete continued to expand laterally engaging fully the FRP jacket, thus transitioning from elastic to plastic behaviour in the concrete as the FRP jacket held the concrete in tension. Peak load was achieved, and then plateaued with a slight decrease until failure when a large portion of this load was shed (specimens SC2 and SC4).

Figure 4-1: Series SC – Failure modes, top row from left; small-scale SC1 and SC2, middle row from left, medium-scale SC3 and SC4, bottom row from left, SC5 and SC6

As previously stated, specimen SC5 did not reach failure and post-test examination found the only evidence of loading in a hair-line crack at the base of the column. The load-displacement path is linear until termination of the test hence is it difficult to ascertain at what load failure would have likely occurred, especially as there was very little cracking of the concrete to be heard in comparison with the other unconfined specimens.

Large-scale FRP-confined specimen, SC6, behaves unusually. The specimen follows an initial linear elastic stress-strain path until the FRP jacket engages before peak load but fails shortly after, at the base of the specimen in close proximity to a corner. Consequently there is no evidence of the FRP engaging fully to plateau after peak load and thus produce the postulated bilinear response. As this is not anticipated, the load was reapplied to establish if it was just a local anomaly, but again the specimen could not maintain the load. When performing post-test examination, failure was evident at the base of the specimen, through buckled steel reinforcement, along with crushed concrete in proximity, evident under the very small area of fractured FRP.

Failure of SC2 also occurs in the bottom region but due to FRP rupture as opposed to failure of the concrete or steel. Maximum strain in the FRP jacket at failure is 0.9%, and the determined FRP rupture strain is 2%, thus the behaviour at mid-height is not representative of the anticipated maximum FRP strain. This behaviour is corroborated with SC4, and although rupture occurs at mid-height, the FRP strains again are localised and not picked up to the full extent in the gauges. Evidence of this occurring with other researchers is not available due to the lack of large-scale specimens but it not apparent in smaller specimen results either.

4.2.1. STRESS-STRAIN BEHAVIOUR

The postulated stress-strain relationship is evident in small- and medium-scale FRP-confined specimens, with the behaviour tracing the initial linear elastic path (stiffness) of the corresponding unconfined specimen, and deviating once the maximum compressive strength of unconfined concrete, f_{c0}, is reached. The FRP jacket engages and the behaviour transitions with the stress in the specimen continuing in relatively linear form to the ultimate confined concrete strength, f_{ccd}, where it peaks then drops off, Figure 4-2.

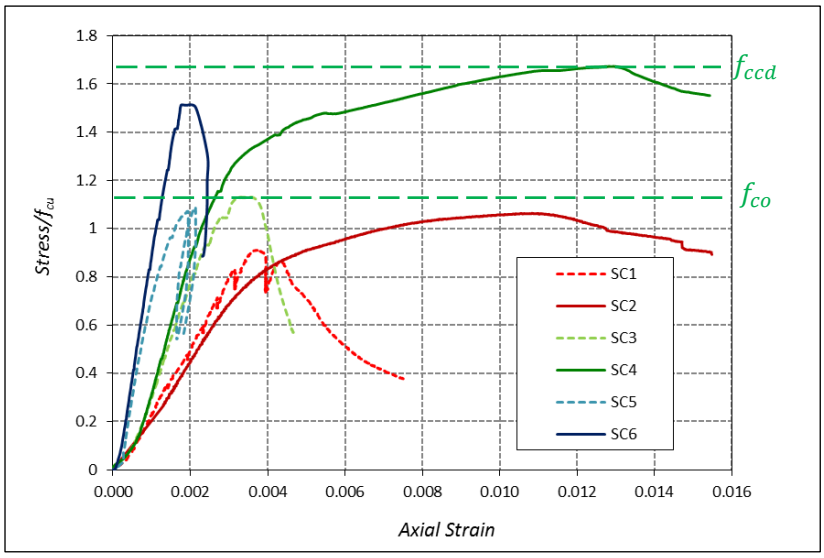

Figure 4-2: Series SC – Stress-strain behaviour (stress is normalised with respect to concrete compressive cube strength)

Taking the medium-scale specimen, SC4, as an example study, the stages evident in the FRP-confined stress-strain plot are:

1. The initial path of unconfined concrete (the concrete modulus of elasticity) is equal to E_c and the FRP-confined specimens track this. The effect of confinement is insignificant before the unconfined concrete compressive peak strength, f_{co}, is reached. This is the first linear portion of the typical FRP-confined concrete bi-linear stress-strain curve.
2. The transition zone occurs where the concrete deviates from elastic behaviour of the unconfined specimen and starts to soften as cracks form, and the concrete laterally dilates against the FRP jacket. This is not as visibly defined as in Figure 2-1 but when comparing against the linear portion of the unconfined specimen up to peak load, it is apparent in the gradually changing slope of the FRP-confined specimen.
3. The FRP jacket is fully activated and the confining stress is linearly proportional to the load from the transition zone until peak stress, but with a reduced stiffness as compared to that of unconfined concrete. It has generally been agreed that if this second part of the bilinear plot is ascending, the confinement is adequate and if it is descending then additional confinement is required. Hence the second portion of the bi-linear curve is ascending to peak load, thus there is adequate FRP-confinement.

4. A further small post-peak load plateau occurs demonstrating the ductility of the column until a sudden shed in load or where the test has been stopped as it has been deemed unsafe to continue. This stage is not evident in results presented by other researchers, and it is not quantified whether this is due to the test being stopped immediately after achieving peak load or it just not occurring.

Thus, the effect of FRP-confinement is dual; the peak strength increases due to the ability of the jacket to contain the nonlinear dilation of the concrete; and a post-peak pseudo-ductile plateau develops from the containment of the concrete and reinforcement providing an increase in the ductility and strength capacity of the specimen. A variation in behaviour from established theory is evident in SC6 as peak load is at the transition zone and the behaviour effectively mimics that of unconfined concrete. This is reasonable when taking into consideration that failure initiated in the reinforced concrete causing localised failure before the FRP potentially reaches peak load and maintains it on the pseudo ductile plateau until failure.

Table 4-2: Series SC – Stiffness of the stress-strain curves, for concentrically loaded specimens

	UNCONFINED	**FRP-CONFINED**
SMALL-SCALE (150 | 150)	6.29	4.97
MEDIUM-SCALE (300 | 300)	21.38	22.38
LARGE-SCALE (450 | 450)	45.94	76.71

The initial stiffness of small- and medium-scale FRP-confined specimens follows that of the equivalent unconfined specimen. Significantly, there is a marked difference between the small-, medium- and large-scale specimens, with the stiffness increasing with size, refer to Table 4-2. This change in stiffness has not been apparent in previous research and as such, it is postulated that it relates to the size effect, as all aspects of geometry were proportionally scaled (refer to Chapter 3), including the geometry, ratio of longitudinal steel, and the number of FRP wraps. Further study into medium- and large-scale testing would shed more light on this aspect and confirm reasoning.

4.2.2. EFFECT OF CONFINEMENT UPON SPECIMEN SLENDERNESS

The maximum lateral deflection recorded at mid-height of the specimen is detailed in Table 4-1, with FRP-confined specimens demonstrating a larger lateral deflection than the

equivalent unconfined specimen. Large-scale specimens have not followed behavioural trends, and due to the previous explanation of the unusual results, it was deemed reasonable to ascertain that this is not the inherent behaviour, so results are omitted from general comparison and assumptions. From the lateral deflection, an insight into the P-Delta effects of the specimens can be obtained.

In design, a purely axial load was assumed whereas in reality a small bending moment was induced, demonstrated by the mid-height lateral deflection reading from an LVDT, attributable to either a slightly off perfect alignment of the specimen and/or inherent geometric imperfections. When establishing the slenderness of a specimen, λ, BS EN 1992-1-1:2004 is referred to as the industry standard for unconfined concrete columns. The slenderness of FRP-confined columns is not addressed in TR55 (2005) and as such, to gain an understanding of the slenderness effects, TR55 (2011) is referred to. The slenderness is anticipated to have a greater effect with FRP-confined than the unconfined equivalent, as seen with the larger lateral deflection readings and as such, the critical slenderness, λ_{crit}, is determined using a process is based upon the work of Teng and Jiang (2009).

Table 4-3: Series SC – Slenderness data

SPECIMEN ID	X-SEC DIMENSIONS	CRITICAL LENGTH	APPLIED ECCENTRICITY	SLENDERNESS †1 λ	CRITICAL SLENDERNESS †2 λ_{crit}
	mm	mm	mm		
SC2	150 | 150	925	0	21.20	9.17
SC4	300 | 300	1850	0	21.20	7.94
SC6	450 | 450	2400	0	18.33	7.84

†1 In accordance with BS EN 1992-1-1:2004
†2 In accordance with TR55 (2011)

Referring to BS EN 1992-1-1:2004, the slenderness of SC4 is 21.20, and this is used to establish the critical slenderness, for which the limiting slenderness, λ_{lim}, is taken from BS EN 1992-1-1:2004.

$$\lambda_{lim} = 20\,A\,B\,C/\sqrt{n} \qquad (4\text{-}1)$$

where: $A = 1/(1 + 0.2\varphi_{ef}$ (if the effective creep ratio φ_{ef} is not known, *A = 0.7*)

$B = \sqrt{1 + 2\omega}$, where the mechanical reinforcement ratio $\omega = (A_s f_{yd})/(A_c f_{cd})$

$C = 1.7 - r_m$, (if the moment ratio r_m is not known, *C = 0.7*)

$n = N/(A_c f_{cd})$

From Equation 4-1, the critical slenderness $\lambda_{crit}$was taken from TR55 (2011):

$$\lambda_{crit} = \frac{\lambda_{lim}}{\frac{f_{ccd}}{f_{c0}}(1 + 0.06\,\rho_\varepsilon)} \qquad (4\text{-}2)$$

where: ρ_ε is the strain ratio, $\frac{\varepsilon_{h,rup}}{\varepsilon_{c2}}$ ($\varepsilon_{c2} = 0.002$, as per BS EN 1992-1-1:2004 for $f_{ck} < 50MPa$)

If $\lambda > \lambda_{crit}$, the specimen is considered slender, hence SC4 is slender. Consequently strengthening significantly increases load capacity without necessarily increasing the flexural ability. As all specimens when using the criteria in BS EN 1992-1-1:2004 are considered slender, failure through buckling or a decrease in strength capacity for greater slenderness is anticipated. Referring to TR55 (2011), the advice on design of slender specimens is to take into consideration an additional second-order nominal moment encompassing the potential P-Delta effects at the design stage.

The initial design of these specimens to TR55 (2005) did not consider second order effects, however through post-test analysis it is evident that for a column confined with FRP, the potential for buckling and second-order effects increases and this has a subsequent reduction on the axial capacity of the specimen. Furthermore, the stiffness of the specimen can greatly influence the P-Delta effects, and as this varies with specimen size, it is imperative to consider not just the applied eccentricity to the column but these P-Delta effects when evaluating the results.

4.2.3. INTERACTION BEHAVIOUR

The interaction diagram represents the theoretical behaviour of a column through progression of applied loading from pure axial to pure bending, Figure 4-3. Development of the interaction curves is based on principles of equilbrium and strain compatilbilty, equivalent to that of an unconfined concrete column. For the FRP-confined specimens, the behaviour of the additional confinement is taken into account through the stress distribution, and these points can be found on the interaction curve detailed in TR55 (2011). It must be noted that this analysis here is as detailed below, and does not follow the methodology stated in TR55 (2011). This comparison is presented in Section 4.5.

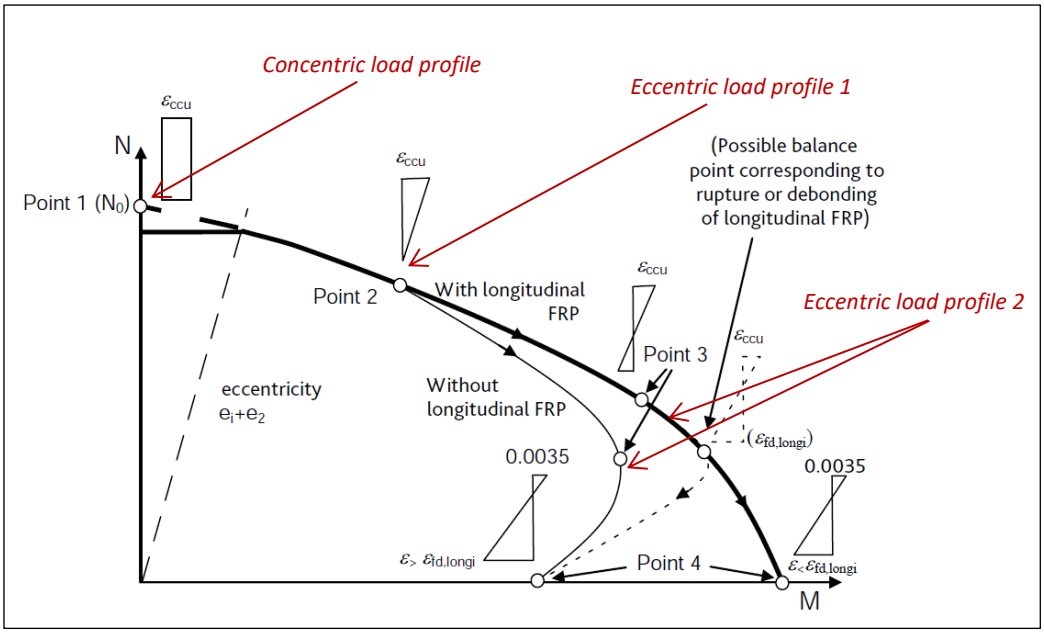

Figure 4-3: Interaction diagram annotated with strain profiles adopted for experimental testing [TR55 (2011)]

The strain profiles selected for experimental testing correspond to points 1, 2 and 3 in Figure 4-3. These points are characterised by:

1. A pure axial load is applied to the specimen, generating uniform axial compressive strain.
2. An axial-flexural load is applied to generate maximum compressive strain at the top of the specimen and zero axial strain at the bottom, at the tensile face.
3. An axial-flexural load is applied to generate a balanced failure with the maximum axial compressive strain at the top face and a corresponding tensile strain at the

bottom, tensile face. This generates yielding in both top and bottom reinforcing steel.

The established curves, alongside the test specimen behaviour determine the actual activity. As there is a large deviation in concrete compressive cube strength from the design strength of 30MPa, development of the interaction diagrams take the 28 day compressive cube strength of the concrete using the design method described in Chapter 3.

The load profile adopted in this series of tests is concentric only, so in theory there should be no moment. However from Table 4-1 and examination of the slenderness effects, it is apparent that potential P-Delta effects need to be considered and as such, the impact of this on the axial versus moment interaction diagrams for small-, medium- and large-scale specimens can be seen in Figure 4-4, Figure 4-5, and Figure 4-6 respectively.

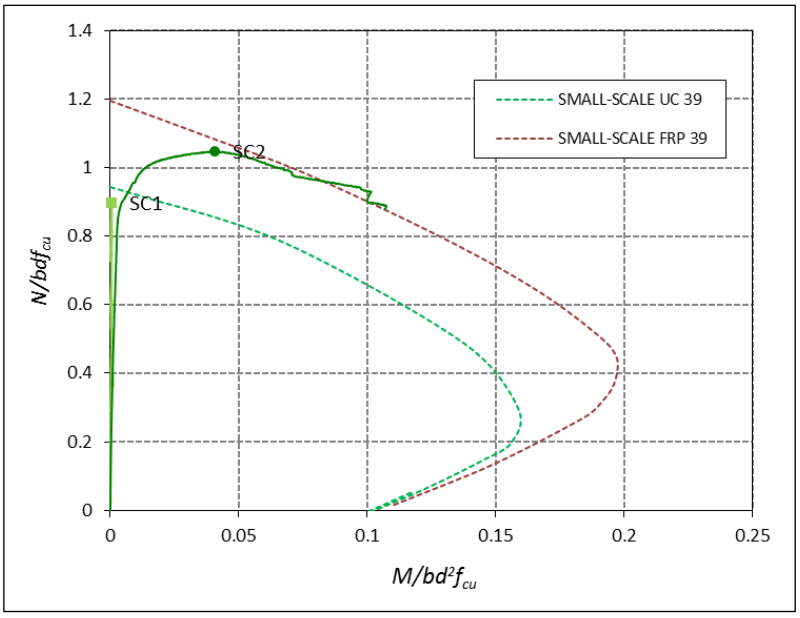

Figure 4-4: Series SC – Interaction diagram for small-scale specimens with a concrete compressive cube strength of 39MPa (peak load highlighted)

Small-scale specimens' peak load is in close proximity to their associated interaction curve. For unconfined SC1, the prediction of behaviour is reasonably accurate and no moment evident. However for FRP-confined SC2, the post-peak load demonstrates considerable moment for a theoretical pure axial load. After deviation from the first portion of the bilinear stress-strain curve (shortly before peak load) as the FRP jacket engages, the P-Delta effects identified for confined columns transpire and increase post-peak load, following the

interaction curve for increasing moment until failure. Thus, combined with the information on the slenderness established in TR55 (2011), the additional nominal second-order moment need to be incorporated into design.

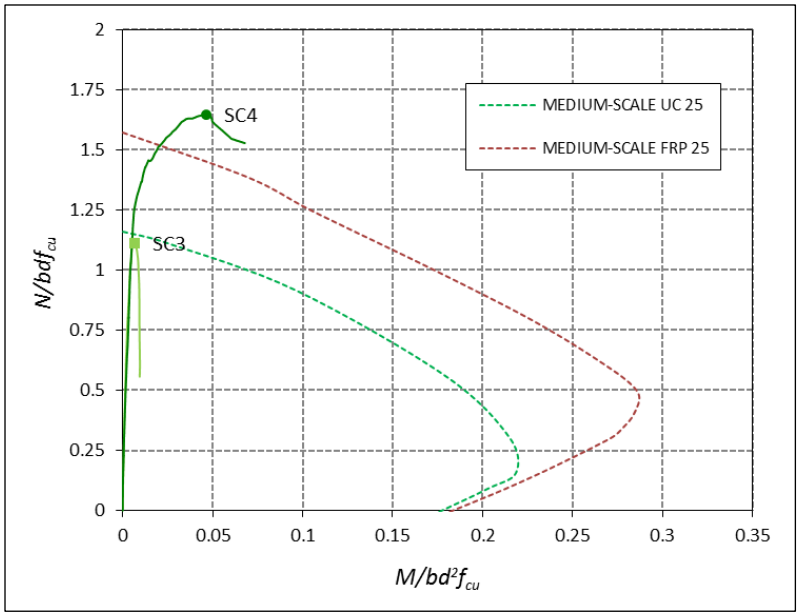

Figure 4-5: Series SC – Interaction diagram for medium-scale specimens with a concrete compressive cube strength of 24.4MPa (peak load highlighted)

Medium-scale specimens present similar trends to small-scale specimens. Unconfined SC3 exhibits a slight bending moment, but not enough to affect the axial capacity. FRP-confined SC4 exceeds the confined curve in terms of both moment and axial capacity, and follows the same trend post-peak as SC2. In terms of the increase in axial capacity, the additional capacity was underestimated in design, within aspects such as FRP overlap, and application. The overall behaviour of SC4 demonstrates additional moment effects not evident in SC3 and again post-peak load, following the curve for greater moment until failure.

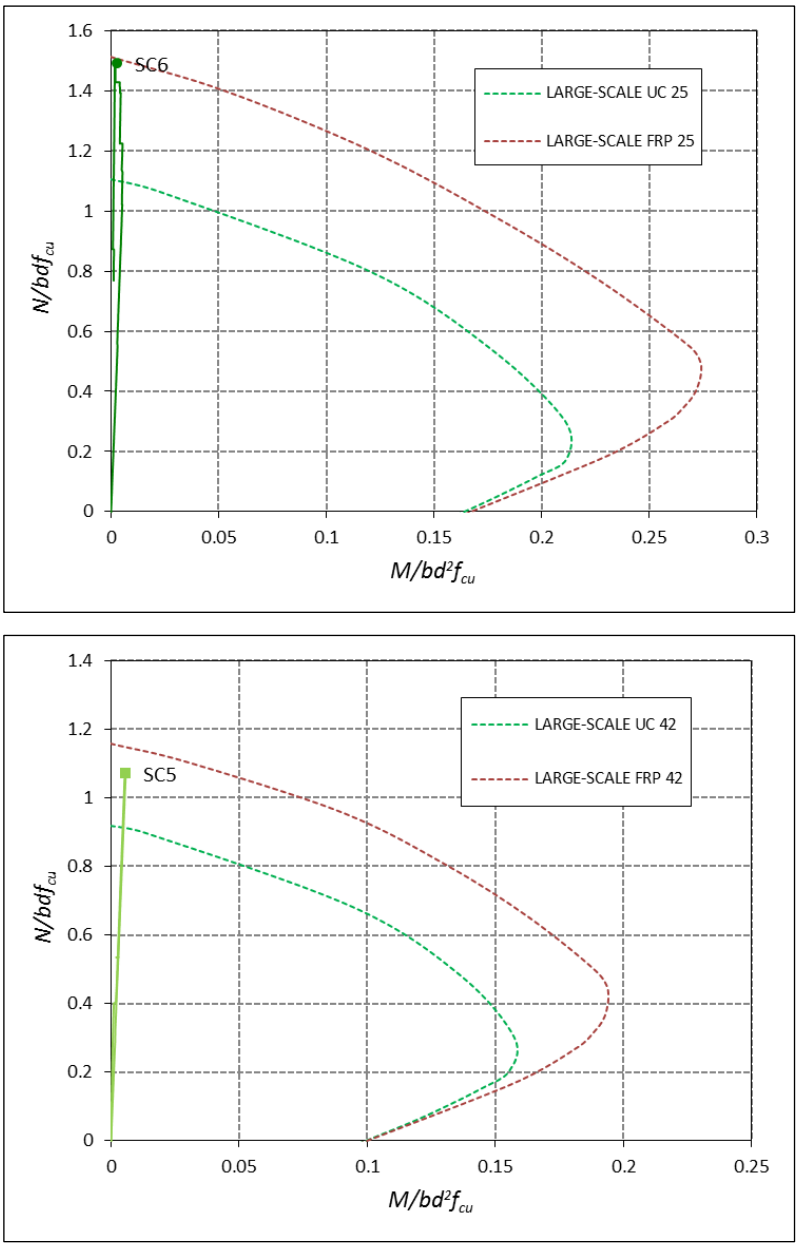

Figure 4-6: Series SC – Interaction diagrams for large-scale specimens from top; concrete strength of 24.4MPa and 42.0MPa (peak load highlighted)

Large-scale specimens do not demonstrate the same behaviour as small- and medium-scale specimens. Unconfined SC5 exceeds the anticipated axial capacity by 14%, before premature halting of the test, but is still less than SC6. FRP-confined SC6 is accurately predicted for the axial capacity, however there is no evidence of a bilinear stress-strain curve (Figure 4-2), and as there is no additional moment, it does not follow the confined curve until failure.

Considering the small- and medium-scale plots together (large-scale excluded due to the erroneous results), the importance of addressing the additional moment developed due to the FRP-confinement is evident, especially when including a flexural aspect in the load application.

4.2.4. FRP JACKET BEHAVIOUR

Specimen axial and lateral strains were measured at the top and mid-height of the column respectively using LVDTs. Evaluating the axial-to-lateral strain with respect to the normalised stress, demonstrates that the confined specimens exhibit an increase in strength capacity and ductility over their unconfined equivalent (the exception being the large-scale results), refer to Figure 4-7. Both axial and lateral strains show a bilinear response, with an ascending second portion for the axial strain, and slightly descending second portion, after peak load for lateral strain.

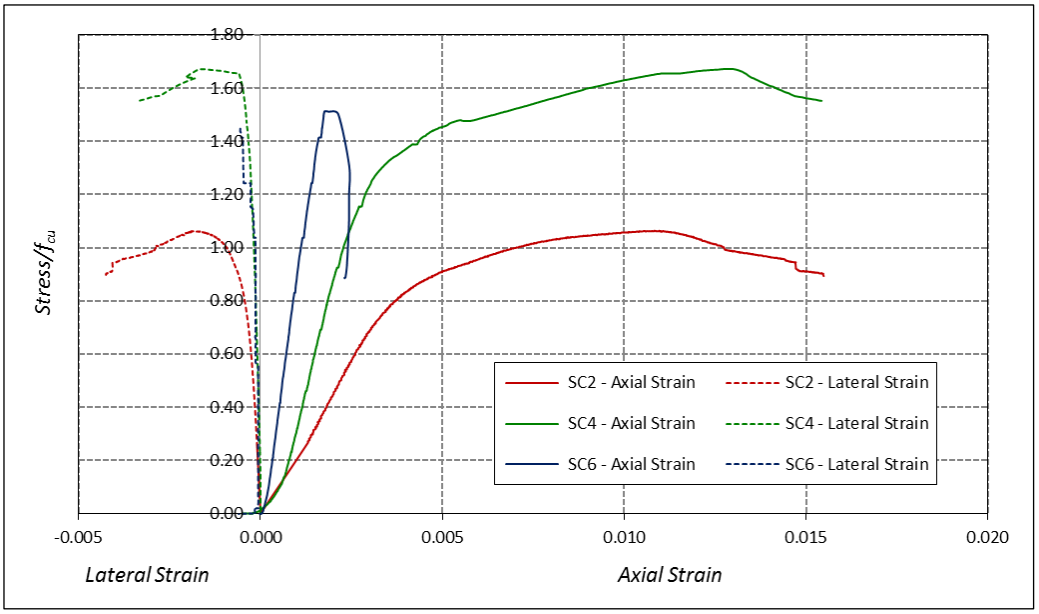

Figure 4-7: Series SC – Axial-to-lateral strain for small-, medium-, and large-scale concentrically loaded specimens (normalised with respect to concrete compressive cube strength strength)

Failure of SC6 occurred at the base of the specimen, consequently the FRP jacket did not fully engage and laterally restrain the concrete, so no bilinear stress-strain response occurred. Furthermore, the gauge mounted at mid-height of the specimen stopped reading accurately prior to failure so the full lateral behaviour could not be presented.

Lateral strains in the FRP jacket were captured at mid-height of the specimen, with gauges arranged around half of the cross-section in view of the symmetry in loading (although there are two axis of symmetry in concentric columns, half of the column was deemed appropriate to pick up potential bending in the specimens). These lateral strains recorded are presented in Figure 4-8 for the small-, medium- and large-scale specimens.

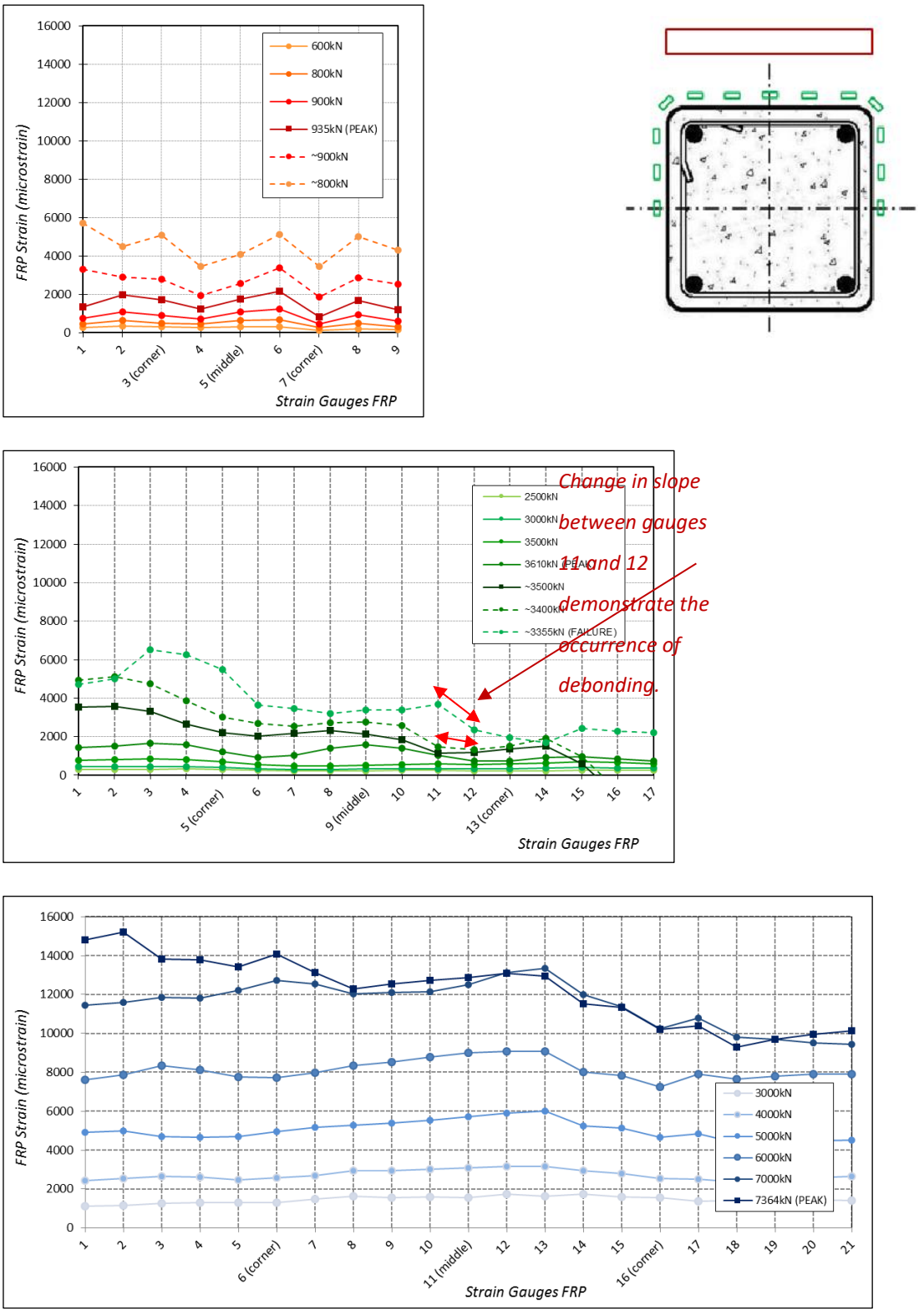

Figure 4-8: Series SC – FRP strains measured around half of the specimen cross-section at mid-height; from top to bottom; SC2, SC4 and SC6

Strain readings at failure are only marked on some of the plots, due to a FRP mounted gauge occasionally failing totally or giving an erroneous reading, displaying negative or compressive readings (as demonstrated with gauges 16 and 17 on SC4). These readings are either attributable to failure of the gauge, or cross-sectional warping deformation generating the high negative readings towards the end of the test. In circumstances where a FRP mounted gauge experiences failure or an overload message mid test; where feasible valid readings from the closest working strain gauges were used to evaluate behaviour until failure.

The magnitude of the strains were similar in small- and medium-scale specimens. The highest strain in the FRP jacket is approximately 0.6% for small-scale SC2, significantly lower than the rupture strain of 2%. Failure of the specimen occurred in the bottom portion of the column, far from the middle, thus the gauges may not register the full strain in the FRP. For SC4, the failure strain was the same, but the location of failure was approximately 100mm below mid-height. This demonstrates that the failure in these specimens is localised, presumably first influenced by local failure of the concrete as crushing of the aggregate and cracking occur. A discrepancy noted is the strain gauges located on the corner read unexpectedly low strain values due to bending of the gauge affixed to the FRP, registering more than the pure, direct tensile strain, as seen with Wang et al. (2012) where the strains were consistently lower in the corners. Wang et al. (2012) had only mounted one gauge between the corners, hence a lot of the FRP behaviour was not necessarily captured.

Had strain gauges been affixed around the region of failure, a lateral strain pattern similar to that of specimens SC2 and SC4 would be expected but potentially of larger magnitude. Lateral failure strains are significantly less than the rupture strain of the FRP established in the coupon tests and this has not been commonly reported elsewhere. These FRP strain plots still give an insight into the mechanics of confinement with the strain readings in close proximity to the corners giving an approximation of the cruciform shape over the cross-section. The overall, slight variation in strain readings over the cross-section is due to a slight movement over to the higher compressive stress side from the influence of additional second order effects. The full FRP coupon strain was not achieved in all tests, correlating with results from Barrington et al. (2011), where a variation of up to 57% for different sized corner radii was evident. Furthermore, Bisby & Take (2009) found saw hoop strain variation of up to 50% over the height of a circular column.

Thus a more detailed understanding of the FRP failure strain in the hoop direction and the relationship to FRP coupon strain, relating to the ratio of the corner radius to side length is required and then incorporated into design.

4.2.4.1. DEBONDING OF THE FRP JACKET

Debonding of the FRP jacket is determined from post-test examination of the specimen alongside interpretation of the results. The FRP strain plots in Figure 4-8 illustrate debonding occurrence where there is a significant variation of the slope between two adjacent gauges. Specifically, this is evident in the SC4, at approximately 3,500kN post-peak loading, where the bond between the FRP and concrete is beginning to break down and debond before failure. Post-test analysis and mark up of the specimen corroborates this, Figure 4-9.

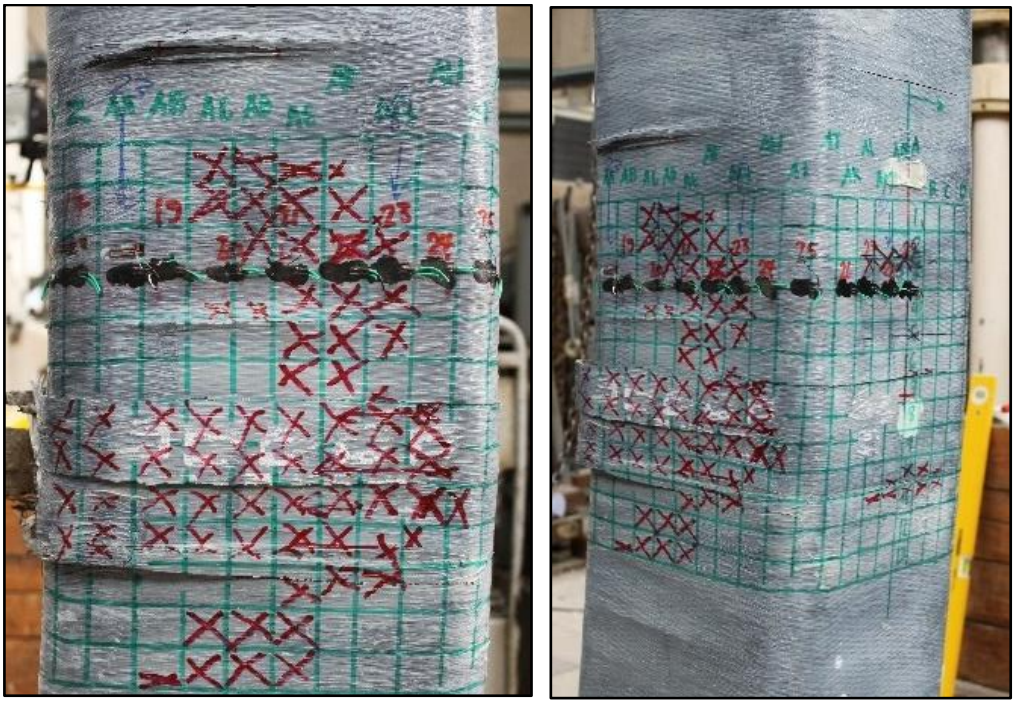

Figure 4-9: Series SC – Debonding mark-up of medium-scale SC4; 'X' marked areas of the grid signify breakdown of the FRP-concrete bond

Debonding of the FRP jacket is only recognised and incorporated into design calculations in TR55 (2011) and not in TR55 (2005), identifying that the confining stress varies around the cross-section, even for concentric loading. The variation in strain readings between FRP gauges leads to the generation of shear stress in the FRP-concrete bond and is presented in Figure 4-10 for SC4. Specimen SC4 is singled out for further examination due to the

promising pattern of FRP strain readings, although low in magnitude show evidence of debonding and failure close to specimen mid-height.

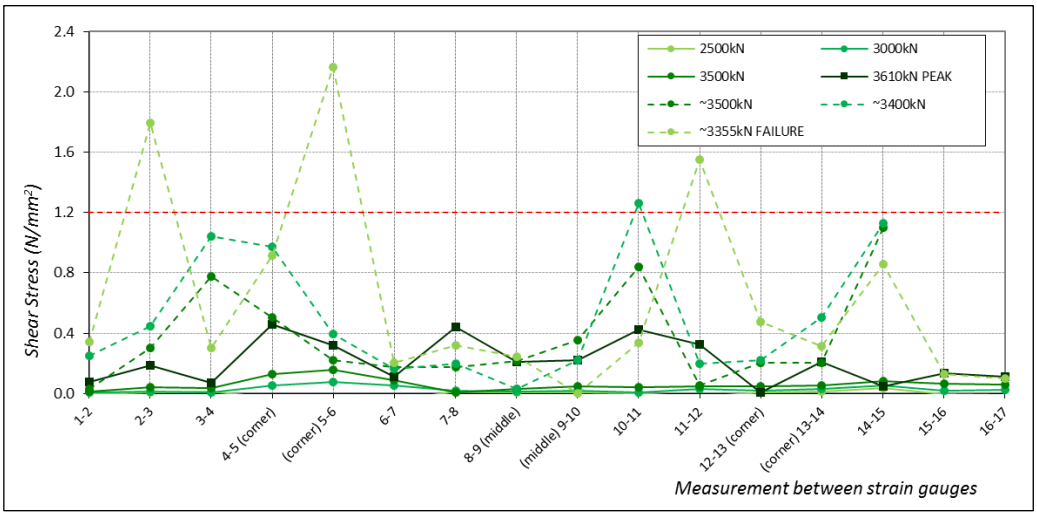

Figure 4-10: Series SC – FRP shear stress between strain gauges for medium-scale SC4

The red dashed line in Figure 4-10 highlights the limiting shear stress as advised by TR55 (2011) Equation 8.21:

$$\tau_{lim,c} = 0.8\,\frac{f_{ctk}}{\gamma_{mc}} \qquad (4\text{-}3)$$

where: f_{ctk}, the characteristic concrete tensile strength is established from BS EN 1992-1-1:2004 Table 3.1

γ_{mc}, partial safety factor for concrete, taken as 1.0 for research purposes

Thus for SC4, the unconfined concrete cube strength, $f_{cu} = 24.4MPa$, the corresponding cylinder strength $f_{ck} = 19.5MPa$ and from BS EN 1992-1-1:2004 Table 3.1, the mean axial tensile strength of concrete, f_{ctm} and the characteristic concrete tensile strength, f_{ctk} are established:

$$f_{ctm} = 0.3\,{f_{ck}}^{2/3} = 2.2MPa \qquad (4\text{-}4)$$

$$f_{ctk} = 0.7\,f_{ctm} = 1.5MPa \qquad (4\text{-}5)$$

Thus the limiting shear stress is $\tau_{lim,c} = 1.2\,\text{N/mm}^2$. Table 4-4 details the FRP sections between gauges that exceeded the limiting shear stress.

Table 4-4: Series SC – FRP shear stress for medium-scale SC4 exceeding the limiting shear stress, from Figure 4-10

STRAIN GAUGE ID	LOAD	SHEAR STRESS	FRP STRAIN %	GAUGE DEBONDED? (DETERMINED THROUGH PHYSICAL EXAMINATION)
	kN	N/mm²		
2-3	3355 (FAILURE)	1.79	0.58	NO
(CORNER) 5-6	3355 (FAILURE)	2.16	0.46	YES
10-11	3500 (POST-PEAK)	1.26	0.20	YES
11-12	3355 (FAILURE)	1.15	0.30	YES

Debonded areas on concentrically loaded specimens tend to be governed by an additional element of lateral deflection, and as such, debonding is on the side of the cross-section of relatively higher compressive stress. Referring to Figure 4-8, the areas of debonding signified by the change in gradient are evident and correlate with that found on the physical check. No debonding was found to occur at the convex corners, where the confinement over the cross-section is generated. As SC4 did not experience particular bending and migration of the compressive region, a weak spot in the FRP-concrete bond could generate debonding.

Both Series SC experimental results and experimental testing of Barrington et al. (2011) (presented in Table 2-2) highlight that the FRP coupon ultimate strain is rarely achieved. TR55 (2011) states that the maximum strain in the FRP jacket is usually less than the ultimate strain, and noted that as the ratio of the corner radius to the side length decreases, as does the rupture strain. Thus from TR55 (2011) Equation 8.16, the rupture strain for prismatic columns can be established as:

$$\varepsilon_{h,rup} = \varepsilon_{fd}\left[0.46\left(\frac{2R_c}{h}\right) + 0.14\right] \qquad (4\text{-}6)$$

The FRP ultimate strain was established as $\varepsilon_{fd} = 0.02$ from coupon tests detailed in Section 3.4.1.2, and the rupture strain from Equation 4-6 above, $\varepsilon_{h,rup} = 0.0053$ for specimen SC4, approximately one quarter of the ultimate strain. This correlates with the typical 25% to 40% of the design strain capacity for practical corner radii for prismatic specimens identified in TR55 (2011). Furthermore, as rupture occurred near the mid-height gauges on the specimen, this illustrates that the FRP strain in Figure 4-8 to be closer to the maximum capacity of the wrap than originally thought when comparing with the FRP ultimate strain.

TR55 (2011) Equation 8.22 develops further on this by addressing the debonding strain of a specimen. This takes the shear stress into consideration due to the variation in stress along the specimen sides. Thus debonding strain becomes:

$$\varepsilon_{h,rup} = \varepsilon_{h,debond} = \tau_{lim,c} \frac{(h-2R_c)}{t_f E_{fd}} \quad (4\text{-}7)$$

Hence for SC4, $\tau_{lim,c} = 1.2\,\text{N/mm}^2$, thus $\varepsilon_{h,debond} = 0.003$. From Table 4-4, the strain corresponding to the identified debonded areas, exceeds the debonded strain in some locations. The FRP strain reading between gauges 10-11 is less than this, having propagated from the debonded area next to it. Thus the ultimate capacity of FRP does not reasonably represent the maximum strain of the FRP when used for strengthening prismatic specimens, and to be reliable for use in analytical modelling, consideration of rupture and debonding strain, Equations 4-6 and 4-7 respectively, is necessary.

Rocca et al. (2005) experienced debonding with FRP-confined prismatic specimens (Series C, C2 & C3, 457 x 457mm cross-section, 1016mm height, 2 and 4 wraps of FRP respectively) but do not detail the extent to which it occurred hence assessment against the results presented here and TR55 (2011) guidance is not feasible.

It is imperative to take debonding of the FRP jacket into consideration as once the bond has broken down between the concrete and FRP, there is absolutely no generation of confinement in this area. Size appears to have an impact on debonding as it is not as evident in the small-scale specimen tested or studied research, thus the effect magnifies with size increase.

4.2.5. COMPARISON WITH OTHER RESEARCH ON SIZE EFFECT

Research directly relevant for comparison with the large-scale axially loaded specimens is detailed below (refer to Table 2-2 for full information on specimens, only specific aspects discussed here relevant to experimental findings):

- *Rocca et al. (2005)*
  Series C, E, and F are axially loaded prismatic columns of 450x450mm, 300x300mm and 300x300mm cross-section respectively. Series E and F differ in height, Series F

of a more comparable height with the specimens presented here. There are three specimens in each, unconfined and FRP-confined with 2 and 4 plies.

- *Wang et al. (2012)*

  Small- and medium-scale specimens are presented, subjected to axial monotonic or axial cyclic loading with varying number of FRP plies.

- Song et al. (2013)

  Medium-scale prismatic specimens of RC, under eccentric loading, concentric tests used plain concrete. Specimens are 250x250mm cross-section, height of 1500mm with variation in load eccentricity of 20mm, 60mm, 100mm and 150mm for specimens SSR-1, SSR-1, SSR-3 and SSR-4 respectively.

The benefit of FRP strengthening of medium-scale specimens is corroborated by Rocca et al. (2005), demonstrating a 7% and 11% increase in capacity for large-scale (Series C) and medium-scale (Series F) specimens. Rocca et al. (2005) have not assessed the medium-scale specimens (Series E – shorter columns) as the unconfined specimen (E1) failed prematurely hence comparison was not made. Interestingly, Rocca et al. (2005) identified that the medium-scale specimens have the greatest strength capacity increase, however, height variation needs to be considered.

Generally with an increase in specimen size, the stiffness of the specimen pre-peak loading increases. Results presented by Rocca et al. (2005) allowed for comparison of the stiffness, and are roughly presented in Figure 4-11.

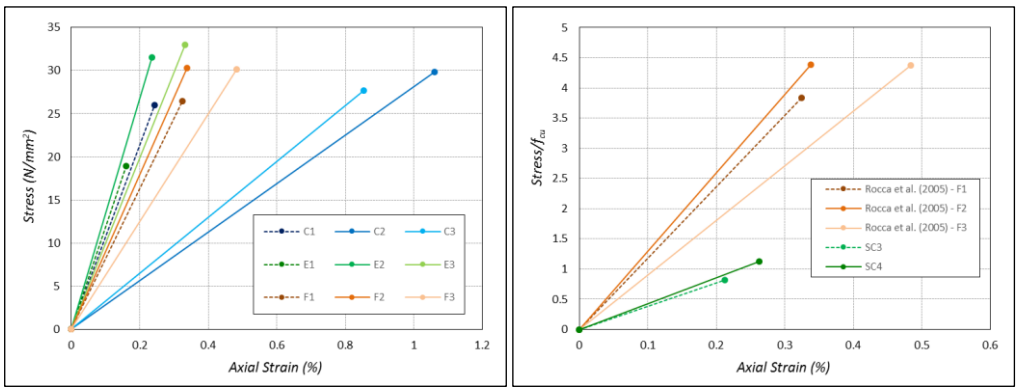

Figure 4-11: Summary of stiffness from peak stress and axial strain, from left; Rocca et al. (2005) Series C, E and F, and comparison of Rocca et al. (2005) Series F with medium-scale specimens (normalised with respect to concrete compressive cube strength)

A direct comparison can be made between Rocca et al. (2005) Series C and E, 450 and 300mm respectively of the same height (1m, short), where a significant decrease in stiffness occurs as the number of FRP plies increases. This appears to be an erroneous result with respect to Series E and F. When looking at Series F, the taller medium-scale specimens, the stiffness of all, unconfined and FRP-confined specimens is reasonably similar.

Rocca et al. (2005) Series F have been plotted alongside SC3 and SC4 in Figure 4-11. This is still not an accurate representation as the peak stress and peak axial strain have been plotted for Rocca et al. (2005) which actually occurred in the transition zone so slightly reducing the stiffness. It is evident that specimen height has an impact on the stiffness of the specimen and without a more extensive database, it is difficult to determine conclusively the relationship between stiffness and size effect. Rocca et al. (2005), conversely to the results of Series SC, for the short specimens (Series C and E) the medium-scale specimens (E) had a greater stiffness than the large-scale specimens (C). Thus further study into size effect to ascertain the behaviour and the predicted increase in stiffness with size is necessary.

Wang et al. (2012) applied monotonic and cyclic loading to specimens of the same size, and the specimens subject to cyclic loading reached a slightly lower stress but experienced higher axial strains as unloading/reloading can postpone failure of columns.

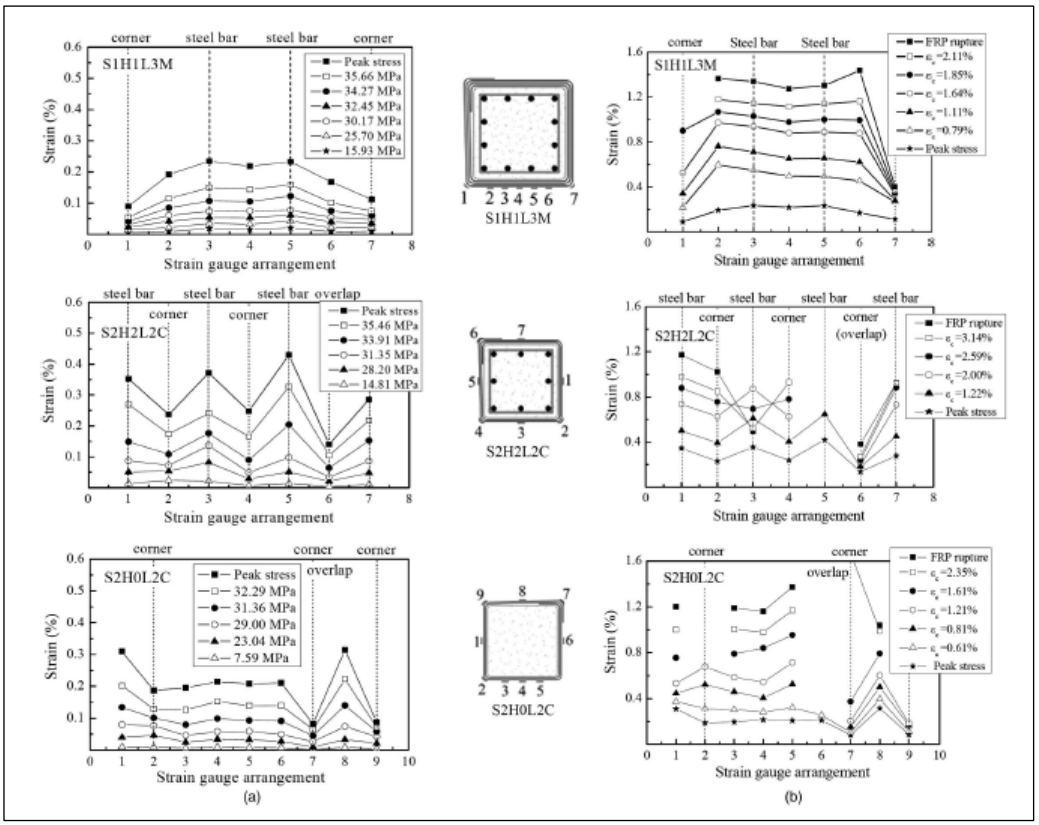

Figure 4-12: Typical hoop strain distributions on CFRP wrap; a. pre-peak behaviour, b. post-peak behaviour [Wang et al. (2012)]

Specimens presented in Figure 4-12 are S1H1L3M (305x305mm cross-section), S2H2L2C (204x204mm cross-section), and S2H0L2C (204x204mm cross-section with no steel reinforcement) and the strains are all seen to increase after peak load (for further detail refer to Table 2-2). Failure of the specimens in relation to the strain gauge location is not specified but as photographs of the failure methods show rupture over a large portion of the middle section, it is assumed that it has occurred here. The plots correlate well with Series SC in that the compressive region has not moved to a particular side and looking at an averaged strain between gauges, it is reasonably flat. The FRP strains at peak load in Wang et al. (2012), specimens SC2 and SC4, are in the region of 0.3%, however at failure there is a more significant divergence, as in the tests analysed by Wang et al. (2012) the positions of gauges are closer to or directly on the FRP rupture region.

Lastly, the primary focus of Song et al. (2013) is eccentrically loaded specimens, with comparison against concentrically loaded medium-scale specimens. Post-test break down of the specimen reveals the effectively confined concrete, Figure 4-13.

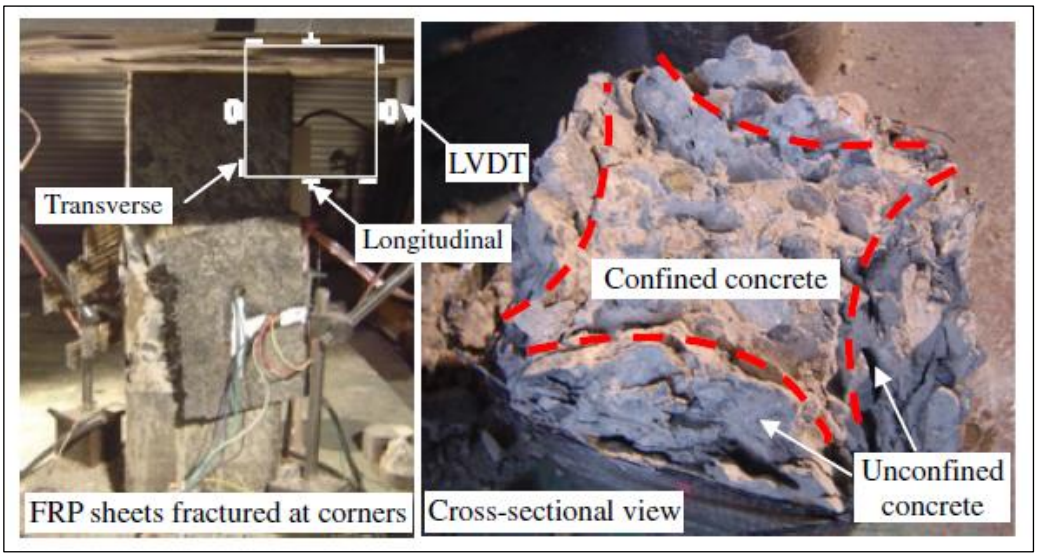

Figure 4-13: Typical failure mode of square concentrically loaded FRP-strengthened plain concrete column, identifying the confined area [Song et al. (2013)]

4.2.6. EXPERIMENTAL SERIES SC SUMMARY

For an accurate overview of specimen behaviour in Series SC, only the small- and medium-scale specimens are considered. Large-scale results are omitted as SC5 did not reach failure and SC6 failure method was in the reinforced concrete, thus does not represent realistic behaviour in the FRP jacket.

FRP-confinement of the concentrically loaded specimens provides an increase in axial strength capacity and a larger increase in axial strain capacity. Failure of FRP-confined specimens occurred through sudden rupture of the FRP jacket. Specimens show a bilinear stress-strain response, with an ascending second portion, thus demonstrating that the confinement level is reasonable.

An additional induced moment is evident in lateral displacement readings, from the inherent P-Delta effects. Specimen design to TR55 (2005) did not take this into consideration, and as the specimens have been established as being slender, this is imperative to capture in future design methodology.

FRP strains readings show the general behaviour over half of the FRP jacket but do not pick up rupture strains accurately due to location of failure elsewhere. Even though the FRP jacket is under global tensile strain, the high strains at failure are local, and not registered.

Post-test examination highlights the extent of debonding in medium- and large-scale specimens, on the flat sides between corners, which is reflected in the FRP strain plots. The FRP strains in all the specimens are less than the FRP coupon strains, as anticipated, and also due to rupture of the FRP occurring away from the strain gauges mounted at mid-height of the specimen.

Debonding is evident in the FRP strain curves and post-test analysis for the medium-scale specimen, so it is essential to consider this in the design stages, especially when the effect could be exacerbated with an increase in size and/or cross-sectional aspect ratio due to the longer flat sides allowing for greater potential of debonding.

As the large-scale specimens did not fail through FRP rupture, further testing to check for size effect and corroborate the results with other research is highly recommended.

4.3. EXPERIMENTAL SERIES SE – LOAD ECCENTRICITY

Experimental Series SE comprises of square specimens subjected to eccentric loading (including specimens from Series SC for comparison). The objective is to address the change in behaviour, as the load eccentricity is increased from a base case of concentric loading (comparison with Series SC) and in doing so to establish the subsequent change in strength capacity. When eccentric load is applied, the FRP-confinement increases the strength capacity where comparable with an unconfined specimen, refer to Table 4-5.

Table 4-5: Series SE (Load Eccentricity) – Summary of load, moment and FRP strain results

SPECIMEN ID	X-SEC	PREDICTED LOAD	PEAK LOAD	LATERAL DEFLECTION (@ PEAK)	MOMENT (FROM LATERAL DEFLECTION @ PEAK)	FRP STRAIN (PEAK | FAILURE)	CONFINEMENT EFFECTIVENESS
	Mm	kN	kN	mm	kNm		
SC1	*150 | 150*	*816*	*766*	*0.08*	*0.1*	-	*1.27*
SC2		*995*	*936*	*5.83*	*5.5*	*0.22 | 0.50*	
SE1	150 | 150	696	774	2.7	13.7	-	1.11
SE2		851	812	3.0	14.6	0.12 | 0.84	
SE3		257	184	10.9	21.8	-	2.21
SE4		540	249	11.5	29.8	0.11 | 0.68	
SC4	*300 | 300*	*3480*	*3617*	*8.49*	*30.7*	*0.18 | 0.90*	*1.80*
SE5	300 | 300	3729	4200	4.7	230.1	0.14 | 1.18	N/A
SE6		2434	970	21.8	241.2	0.05 | 0.10	N/A
SC6	*450 | 450*	*7562*	*7364*	*1.17*	*55.3*	*1.60 | 0.95*	*NOT DETERMINED*
SE7	450 | 450	8110	9120	2.8	341.3	0.43 | 1.04	N/A
SE8		3633	2287	26.9	814.1	0.10 | 0.75	N/A

In terms of predicted versus peak load, the specimens follow two patterns. Firstly, ECC1 profiles (SE1 (unconfined), SE2, SE5 and SE7) achieve close to or exceed the predicted load. Secondly, specimens with ECC2 load profile (SE3 (unconfined), SE4, SE6 and SE8) reach peak load significantly lower than predicted, but perform well in terms of post-peak deformation capacity, demonstrating a beneficial aspect of the FRP strengthening, although the axial strength capacity is particularly low.

In Series SC, the moment calculated from the lateral deflection increases with confinement and size which is corroborated in Series SE and furthermore, the moment sustained at peak load increases with load eccentricity too. This behaviour is anticipated, due to the initial moment is induced in the applied loading. Lateral strains at peak load are still significantly lower than the FRP coupon rupture strain, and an assessment of the FRP strain diagrams demonstrates an increase in strain after peak load. However this is reasonable as seen in Series SC when the rupture strain is evaluated with respect to TR55 (2011), and found to be approximately 25% of the coupon test.

Confinement effectiveness is only measureable for the small-scale specimens as they have an unconfined equivalent to compare with. Solely looking at these specimens, for ECC1 this is similar to the concentric specimen, but as the load eccentricity increases, the effect of confinement significantly increases due to the flexural ability of the specimen, generating larger strains in the FRP jacket, seen in the second portion of the bilinear stress-strain curve (also witnessed by Mirmiran et al. (1998), Fitzwilliam and Bisby (2010)).

FRP-confined specimens subject to eccentric load do not always fail through rupture of the FRP jacket. The initial behaviour is similar to the unconfined RC specimens as per Series SC thus exhibiting a linear load-displacement path until the FRP jacket engages as peak strength approaches. Peak load is achieved in all specimens and then the variation is evident, in the duration that the specimen could maintain a similar loading increasing, hence higher strains in the FRP. The specimens fail though FRP rupture if bending is not dominant, Figure 4-14, Figure 4-15, and Figure 4-16.

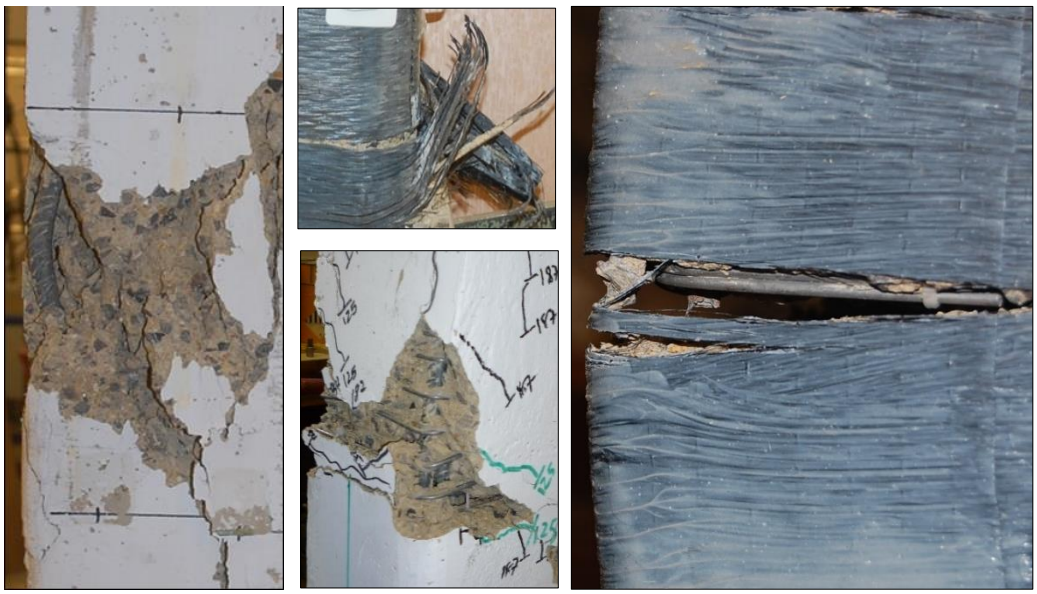

Figure 4-14: Series SE – Failure modes of small-scale specimens, from left; small-scale SE1, SE2, SE3, and SE4

Figure 4-15: Series SE – Failure modes of medium-scale specimens, from left, SE5 and SE6

Figure 4-16: Series SE – Failure modes of large-scale specimens, from left, SE7 and SE8

All FRP-confined specimens in Series SE fail through one of two failure methods.

- The first failure method, rupture of the FRP jacket occurs on the specimens with a small eccentric loading profile (ECC1), with a sudden loud bang and dust from the FRP and concrete being expelled from the area that ruptured. This is reflected in the loading as a large portion is shed. This failure behaviour is experienced by specimens SE2, SE5 and SE7.
- The second failure method, columns with large eccentricities fail though bending of the specimen at mid-height, generating yielding in the rebar which subsequently snaps on the tension side of the cross-section before there was a chance of the FRP to reach rupture strain (less than the FRP coupon strain as explained in the previous section). The mechanical aspect of this failure is similar to the unconfined equivalent in the small-scale specimens. The FRP can be seen to have cracked in some areas but this tended to be separation along the grain of the fibre as opposed to perpendicular to the fibres for rupture. The size of this crack in the medium- and large-scale specimens is approximately 20mm. This failure occurs in specimens SE4, SE6 and SE8.

During testing, micro-cracking of the FRP jacket was evident, along with lateral curvature in the specimens occurring gradually after peak load was achieved. Song et al. (2013) experienced the same behaviour with eccentrically loaded medium-scale specimens, and found compression to be the controlling method of failure. For FRP-confined specimens however, the FRP does not carry the load as initially anticipated. In many cases, only after the specimen reaches peak load and starts to deform plastically, does the FRP engage and

start to confine the concrete, maintaining a large portion of the applied load at post-peak strength. Further analysis of this is found in Section 4.3.4.

Post-test analysis through controlled destruction of the specimens indicates that the postulated behaviour of the FRP indeed differs from the actual behaviour as the FRP is not fully engaged over the length of specimens as per small-scale tests. Instead the behaviour is localised, with around half of the FRP jacket engaging, thus extrapolation of small-scale results/behaviour is not advised.

Inclusion of a flexural component in the load leads to an increasingly lower axial strength capacity of the specimen. To ascertain the effect of eccentricity with increasing size, the peak load of he concentrically and eccentrically loaded specimens was normalised with respect to the concrete strength and plotted against each other in size groups, Figure 4-17. This plot demonstrates the increase in load capacity between unconfined and FRP-confined specimens (orange and dark blue bars respectively) and as the eccentricity of load is applied and increases, the peak load reduces (medium and light blue bars). However this is not truly representative as it does not take into consideration the moment in the specimen.

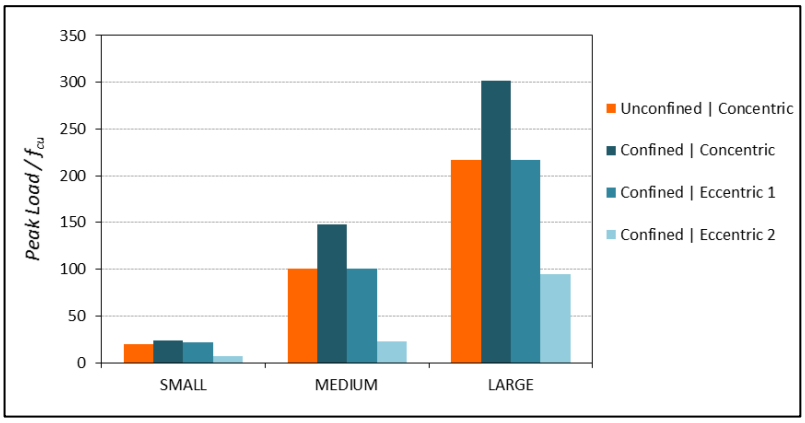

Figure 4-17: Series SE – Comparison of strength capacity increase for concentric and eccentric load profiles of each size category, see Table 3-1 for specimen scaling detail (peak load normalised with respect to concrete compressive cube strength)

Generally, Figure 4-17 demonstrates that in terms of axial peak load only, when comparing unconfined to confined, ECC1 profiles maintain the same loading as an equivalent sized and concentrically loaded, unconfined specimen whilst exhibiting a significant increase in deformability, this is evident in the stress-strain results in the following Section 4.3.1. These

results are presented for specimens scaled in all aspects, including the number of FRP plies around the specimen.

4.3.1. STRESS-STRAIN BEHAVIOUR

The postulated bilinear stress-strain relationship is evident in all FRP-confined specimens. The behaviour for ECC1 again traces the initial stiffness of the corresponding unconfined specimen, and deviates at this point from the Series SC specimens, reaching the maximum compressive strength of unconfined concrete, f_{c0}. There is a descending second branch of the bilinear curve as failure testifies the activation of the FRP, Figure 4-18. As the load eccentricity increases, the stiffness of the initial portion of this reduces.

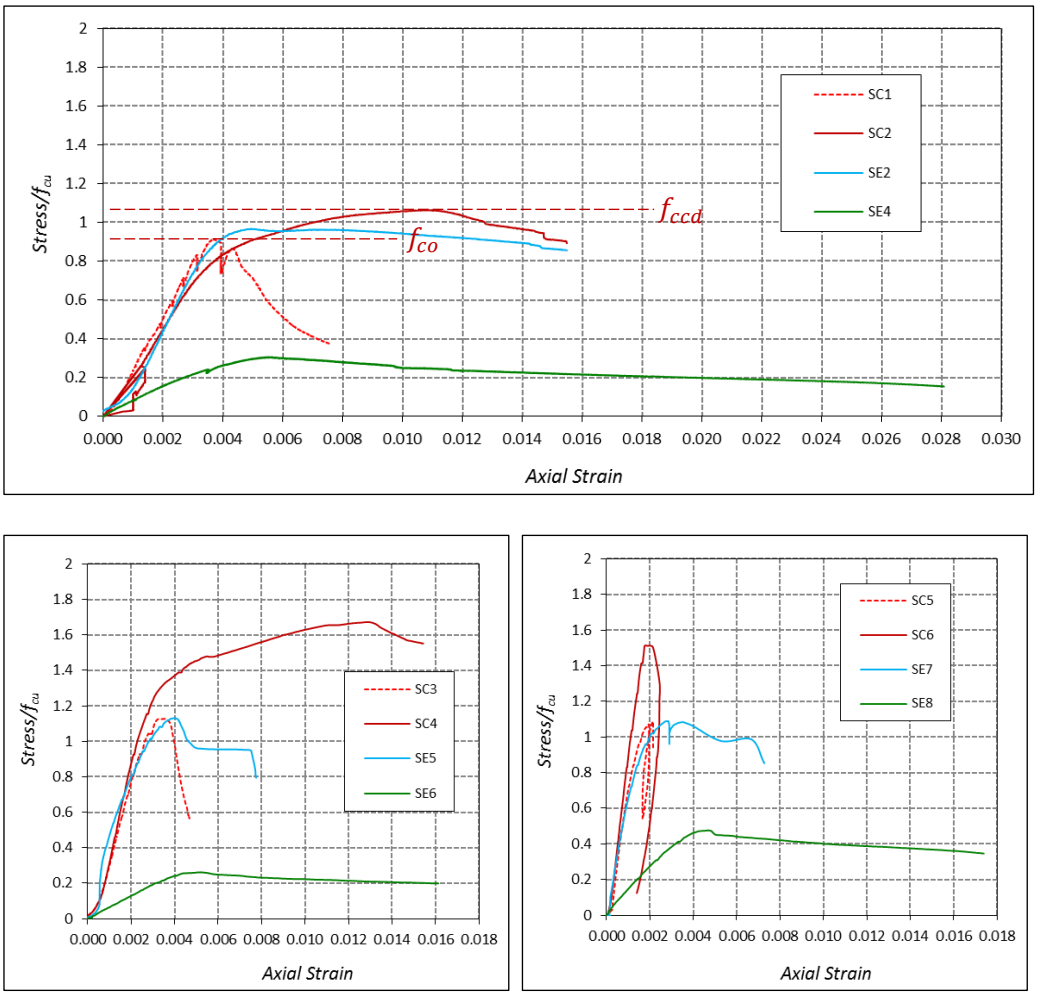

Figure 4-18: Series SE – Stress-strain behaviour, top row; small-scale, bottom row from left; medium-scale and large-scale (stress normalised with respect to concrete compressive cube strength)

The stress-strain curves for concentric and eccentric specimens vary, particularly with the axial strain at failure. Small-scale SE2 (ECC1) maintains the stiffness of the concentrically loaded unconfined specimen as anticipated, and reaches similar strain levels to SC2 of 1.5%, before rupture of the FRP occurs. The bilinear curve is gradually descending post-peak load, hence additional FRP plies would mitigate the insufficient level of confinement. In terms of ECC2 profile, SE4, the post peak portion of the bilinear curve reaches large strains, effectively reaching the ultimate strain.

Medium-scale SE5 and large-scale SE7 (ECC1) follow the stiffness of the unconfined specimen, reaching peak stress, then descending in second portion of the bilinear curve before early failure, relative to the axial strains of SE2. Thus it is imperative that without further testing to examine the behaviour, and small-scale eccentrically loaded results are not scaled up as the strain achieved is lower in the larger specimens when failure is by means of FRP rupture. For the medium- and large-scale specimens, SE6 and SE8, with load profile ECC2, very similar behaviour is evident, regardless of size, in the shape of the descending bilinear stress-strain curve and the failure strain of around 1.6%. These eccentrically loaded specimens demonstrate plastic behaviour post-peak load, and show an increasing ductility with larger applied eccentricity.

When evaluating the stiffness of the eccentrically loaded specimens there are two main patterns, Table 4-6.

Table 4-6: Series SE – Stiffness of the stress-strain curves, for comparison of concentrically and eccentricity load specimens

	CONCENTRIC	**ECCENTRIC PROFILE NO. 1**	**ECCENTRIC PROFILE NO. 2**
SMALL-SCALE (150 | 150)	4.97	1.60	0.94
MEDIUM-SCALE (300 | 300)	22.38	19.04	2.94
LARGE-SCALE (450 | 450)	76.71	44.15	11.48

Firstly, as with Series SC, the stiffness of the specimen increases with size, regardless of the applied eccentricity. Secondly, there is reducing stiffness with increasing eccentricity, as the part of the cross-section in compression reduces and as such, the lateral displacement is greater, leading to a corresponding increase in lateral strain. This has not been prominent in other literature and demonstrates the potential in axial-flexural strengthening.

4.3.2. EFFECT OF CONFINEMENT UPON SPECIMEN SLENDERNESS

The maximum lateral deflection at mid-height of the specimen is detailed in Table 4-4, with an increase in mid-height deflection evident with increasing applied load eccentricity. As an axial-flexural load is applied in Series SE, the moment is known to be much larger and as such, there is potential for greater P-Delta effects. The specimen slenderness is significant due to the non-proportional increase in lateral deflection with increasing load eccentricity, and this is presented in Table 4-7.

Table 4-7: Series SE – Slenderness Data

SPECIMEN ID	X-SEC DIMENSIONS	CRITICAL LENGTH	APPLIED ECCENTRICITY	SLENDERNESS †1 λ	CRITICAL SLENDERNESS †2 λ_{crit}
	mm	mm	mm		
SE2	150 | 150	925	15	21.2	10.2
SE4	150 | 150	925	108	28.6	15.9
SE5	300 | 300	1850	32	21.2	10.3
SE6	300 | 300	1850	226	28.1	16.1
SE7	450 | 450	2400	35	18.3	10.2
SE8	450 | 450	2400	325	25.2	16.5

†1 In accordance with BS EN 1992-1-1:2004
†2 In accordance with TR55 (2011)

The critical slenderness of all FRP-confined columns is less than the slenderness of the equivalent unconfined specimen when checked in accordance with BS EN 1992-1-1:2004. Again, due to the lower critical slenderness, it can be seen that it is imperative to consider additional second order effects in the specimen design as advised by TR55 (2011).

4.3.3. INTERACTION BEHAVIOUR

For Series SE, load profiles ECC1 and ECC2 were identified as per Figure 4-3. A theoretical moment is established in the design stage, and due to this pre-existing moment, the potential is for larger secondary effects. The lateral deflection results, Table 4-5, and the slenderness results, Table 4-7, demonstrate that the potential P-Delta effects need to be considered and as such, the axial versus moment interaction diagrams for small-, medium-

and large-scale specimens are presented in Figure 4-19, Figure 4-20, and Figure 4-21 respectively.

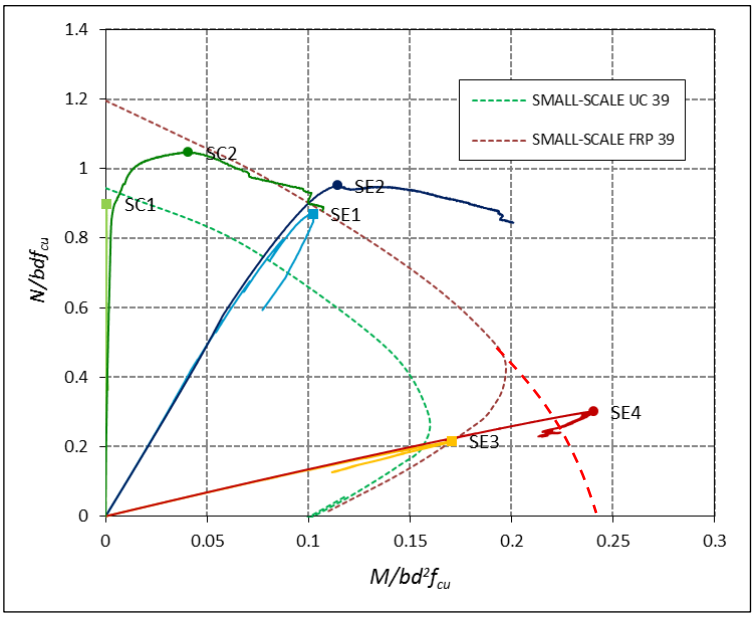

Figure 4-19: Series SE – Interaction diagram for small-scale specimens with a concrete compressive cube strength of 39MPa (peak load highlighted)

The small-scale unconfined specimens SE1 and SE3 both exceed the unconfined interaction curve, reaching the FRP-confined interaction curve. FRP-confined SE2 follows the same path to peak load as the corresponding unconfined specimen and marginally exceeds the confined interaction curve at peak load. As with Series SC confined specimens, a considerable moment is evident and this is furthered when combined with P-Delta effects after peak loading, increasing in moment capacity although reducing in axial capacity until failure.

FRP-confined SE4 (ECC2), exceeds the confined interaction curve. Following the guidance of TR55 (2011) for analysis of the curve exceedance, instead of modelling the maximum moment at a balance point at which the concrete crushing and steel yielding is assumed to occur concurrently (thus as the neutral axis depth increases, the moment capacity starts to reduce), but instead as FRP is included, the FRP strain is still increasing with the neutral axis depth reducing. Further from this point, the failure is limited to the tensile behaviour as the tensile strain is now larger than the compressive strain on the top face. Thus once this

extended curve is included as per Figure 4-3 (and demonstrated in Figure 4-19 with a dashed red line), the exceedance is minimal.

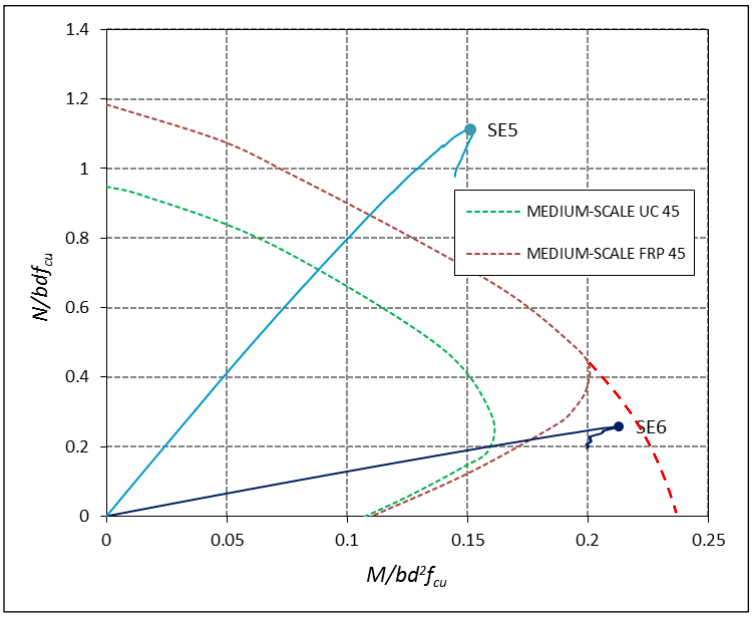

Figure 4-20: Series SE – Interaction diagrams for medium-scale specimens with a concrete compressive cube strength of 42.0MPa (peak load highlighted)

Medium-scale FRP-confined SE5 far exceeds the anticipated axial strength capacity. Confined SE6 (ECC2) is similar to that of the small-scale specimens in that the confined curve does not reflect the moment capacity until inclusion of the extended curve taking into consideration the FRP strains defined in TR55 (2011). For this higher load eccentricity there is less of a moment tail after peak load as the peak load is at the latter part of the second phase of the bilinear curve.

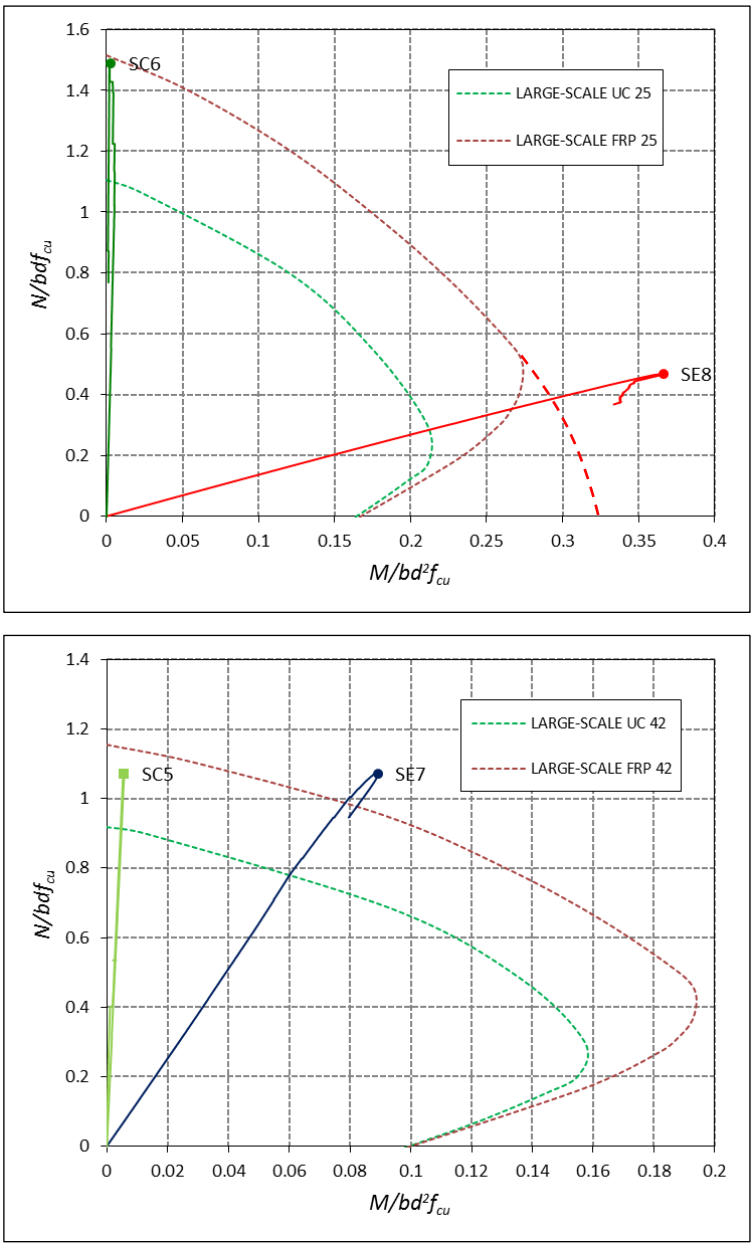

Figure 4-21: Series SE – Interaction diagrams for large-scale specimens, from left; concrete compressive cube strength of 24.4MPA, and a concrete compressive cube strength of 42.0MPa (peak load highlighted)

Large-scale confined specimens SE7 and SE8 both exceed the confined interaction curves. SE7 is marginally over with minimal moment after peak loading, but SE8 far exceeds it due to the additional P-Delta effects allowing the specimen to maintain a large portion of the load for a long time (refer to Figure 4-18 for stress-strain behaviour).

Results from the interaction curves are sporadic, and there is consistent underestimation of the eccentrically loaded FRP-confined specimens' axial strength capacity, especially as the specimen experiences a larger moment. Thus, the interaction curves have not adequately taken into account the P-Delta effects on the FRP-confined columns. Although design was to TR55 (2005), the results demonstate that it is advisable to use the extended curve for larger eccentricities as defined in per TR55 (2011).

4.3.4. FRP JACKET BEHAVIOUR

The axial and lateral strain of the specimens is measured at the top and mid-height of the column respectively. Axial-to-lateral strain is evaluated with respect to the normalised stress and demonstrates that the eccentrically loaded FRP-confined specimens exhibit a bilinear response, slightly decreasing in the second portion for axial and lateral strain after peak load (signified by the transition point). Concentric specimens demonstrate an ascending bilinear curve for axial strain, also evident in the experimental work of Hadi and Widiarsa (2012).

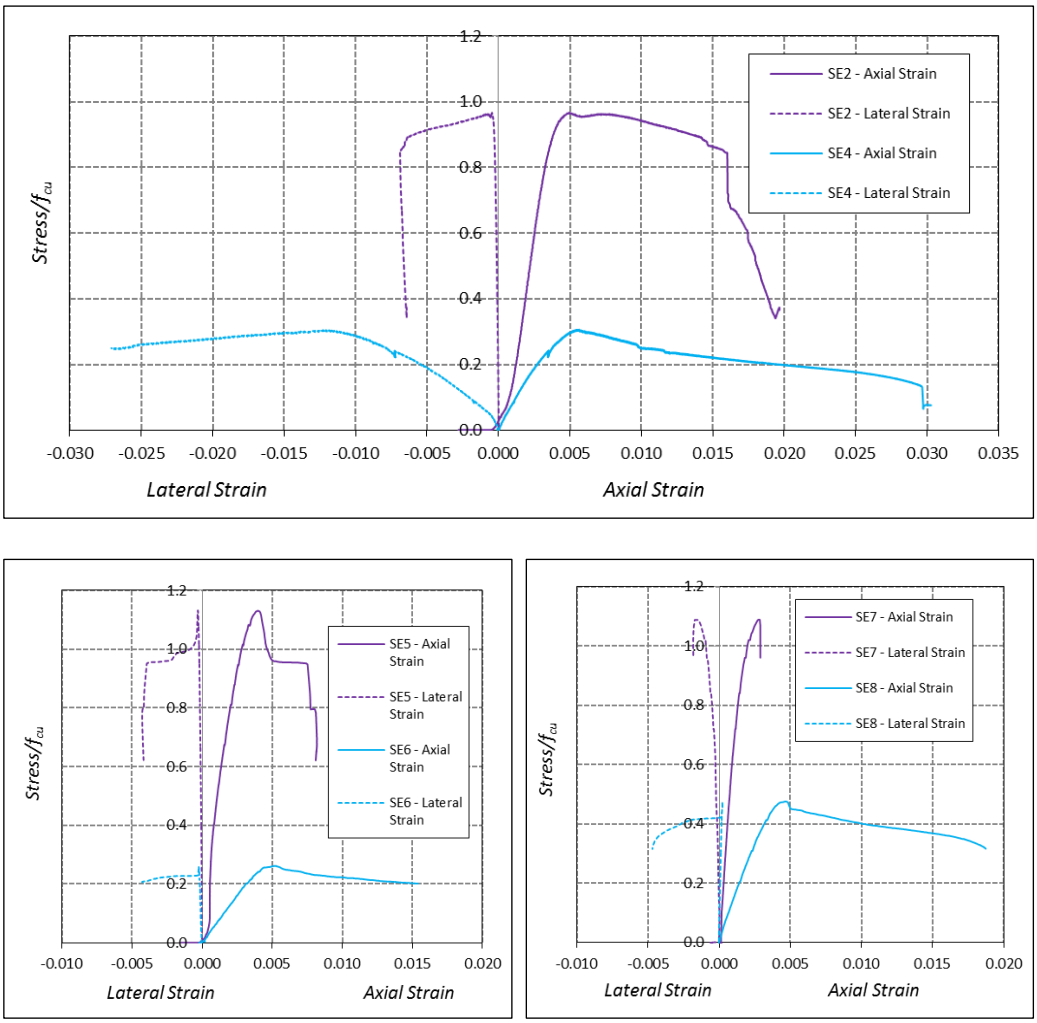

Figure 4-22: Series SE – Axial-to-lateral strain for small-, medium-, and large-scale concentrically and eccentrically loaded specimens; top row, small-scale, bottom row from left; medium-scale and large-scale (normalised with respect to concrete compressive cube strength)

Small-scale specimens exhibit a bilinear axial and lateral strain response, with increasing strain magnitude and eccentricity. Medium-scale results are positive, both axial and lateral plots achieving peak strain and a plateau of increasing strain with relatively constant stress. Large-scale specimens SE7 and SE8 display results in good correlation with medium-scale specimen of equivalent load profiles.

The normalised axial stress for all specimens under ECC1 loading is similar, as it is for ECC2 loading profile. As the load eccentricity increases, the axial capacity that the specimen can sustain is substantially less and the strains demonstrate post-peak plateauing due to the improved deformation capability.

A further insight into the FRP jacket behaviour is obtained from the FRP strain readings captured at mid-height of the specimens, presented in Figure 4-23 and Figure 4-24 for ECC1 and ECC2 respectively.

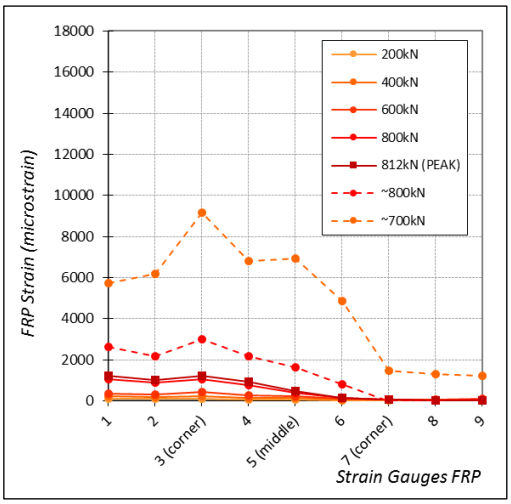

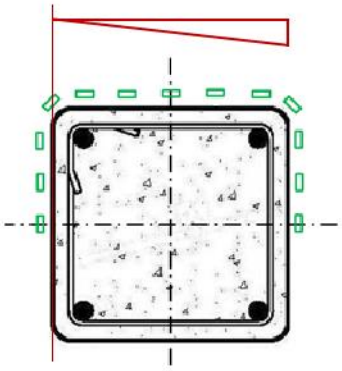

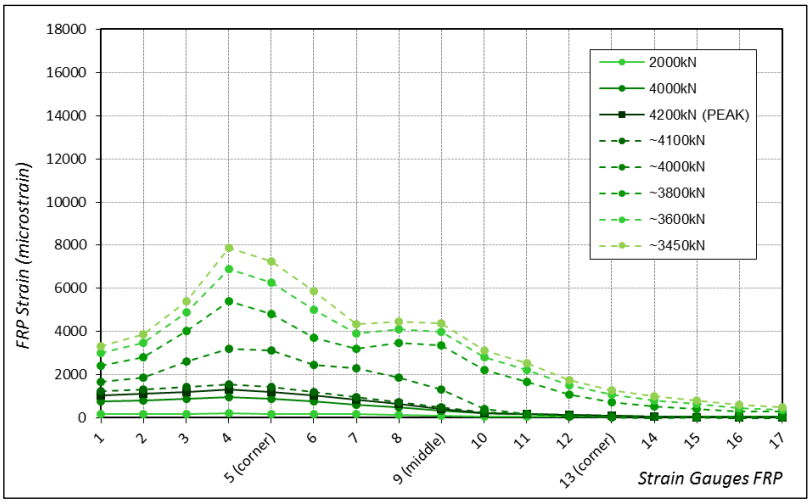

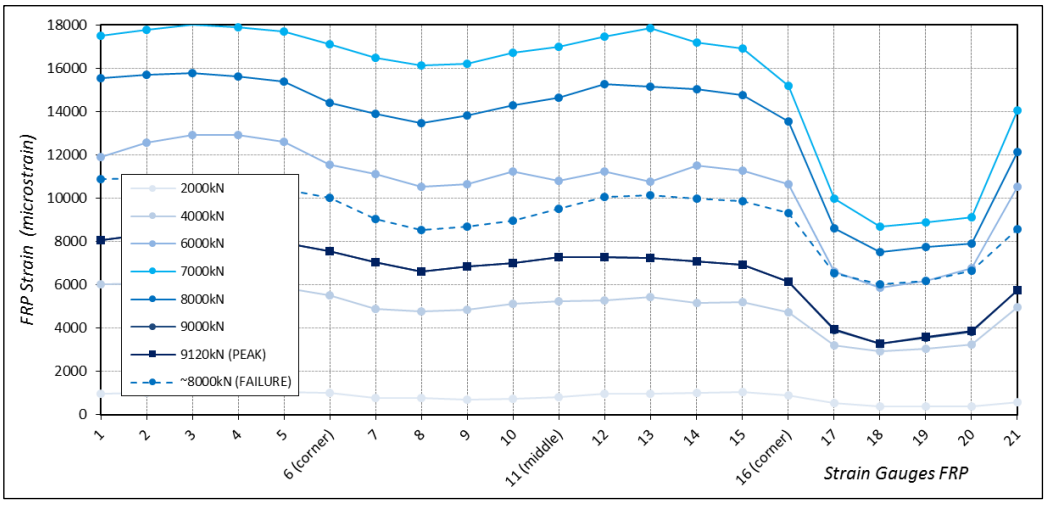

Figure 4-23: Series SE – FRP strains measured around half of the specimen cross-section at mid-height, with ECC1 load profile; from top to bottom; SE2, SE5 and SE7

The FRP strain plots for ECC1 vary from the concentric profile presented in Series SC as it is evident from the overall strain gradient in the FRP jacket that the effectively confined area is moving to the area of higher compressive stress on the left-hand side of the cross-section. In theory, at this point the strain on the right-hand side is designed to reduce to zero, and as such, a small confining force at the corner of the specimen is generated, producing a lower to negligible strain on the right hand side. In small-scale SE2 and medium-scale SE4, this profile is particularly apparent, with the magnitude of the strains around 0.8%. Failure of the specimen is localised.

Large-scale SE7 has high strains almost reaching the ultimate strain of 2%. Failure of the specimen occurred at mid-height, giving a good behavioural representation of FRP jacket. The movement of the profile over to the compressive side of the column is less apparent due to the strain readings in gauge 21, these are erroneous readings from a faulty gauge.

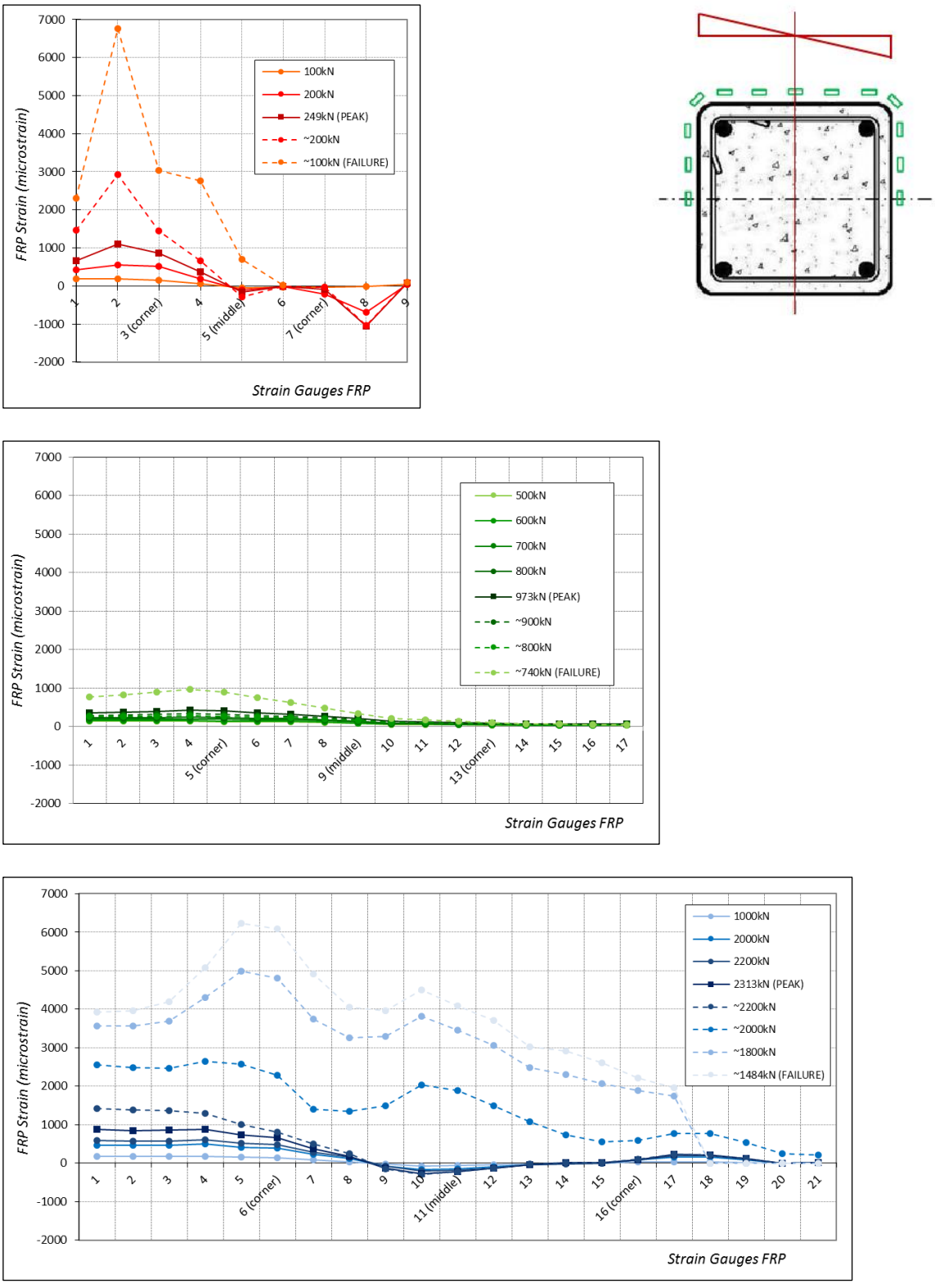

Figure 4-24: Series SE – FRP strains measured around half of the specimen cross-section at mid-height, with ECC2 load profile; from top to bottom; SE4, SE6 and SE8

With ECC2 load profile application, the FRP strains move further over to the compressive side of the cross-section reducing significantly on the tensile side.

Small-scale SE4 and large-scale SE8 have clear movement over to the compressive side. The strain on the tensile side of the specimen (right hand side) is significantly lower than that of the compressive side, thus the compressive region covers half of the cross-section, and as such the force generated at the corners on the right hand side is minimal. The predicted cruciform shape for the ECC2 loaded specimens is pulled into the compressive side and the lack of strain at the tensile corners, allows for the generation of a bar across the compressive side of the cross-section as shown in Figure 2-3.

Strain magnitude is less than the ultimate strain for all specimens. Failure occurred through yielding of the steel rebar as opposed to FRP rupture, thus the FRP jacket did not generate high strains. Negative strains registered are due to failure of the gauge as compression in FRP is not feasible for SE4. SE8 also registered negative strain readings in middle of the face, and are attributable to the flat side not experiencing much strain in the FRP jacket until peak load is achieved and the FRP engages properly.

Over the cross-section the area of interest is where the strains drop to zero, tending to move closer to the middle of the cross-section with larger applied load eccentricity, suggesting that there is no strain in the corners and as such, minimal confinement at this point. Hence the postulated belief that the effectively confined area moves into the compressive section of the columns is validated.

4.3.4.1. DEBONDING OF THE FRP JACKET

Debonding is very evident within the FRP strain results for specimens SE4 and SE8, and this was corroborated by the physical post-test examination and analysis, Figure 4-25.

Figure 4-25: Series SE – Debonding mark-up of medium- and large-scale specimens; 'X' marked areas of the grid signify breakdown of the FRP-concrete bond; top row from left, medium-scale SE5, SE6 (front), SE6 (back); bottom row from left; large-scale SE7, SE8 (side view with front), SE8 (back view)

As debonding is evident in concentrically loaded specimens, it is postulated that it becomes more prominent with eccentric loading due to the greater variance in the FRP strain gradient along the flat sides. The shear capacity is again determined as per TR55 (2011) using FRP strain measurements around the cross-section, and is presented in Figure 4-23 and Figure 4-24, for specimens SE5 and SE6. (These medium-scale specimens are singled out for further examination due to the evidence of debonding and failure close to mid-height).

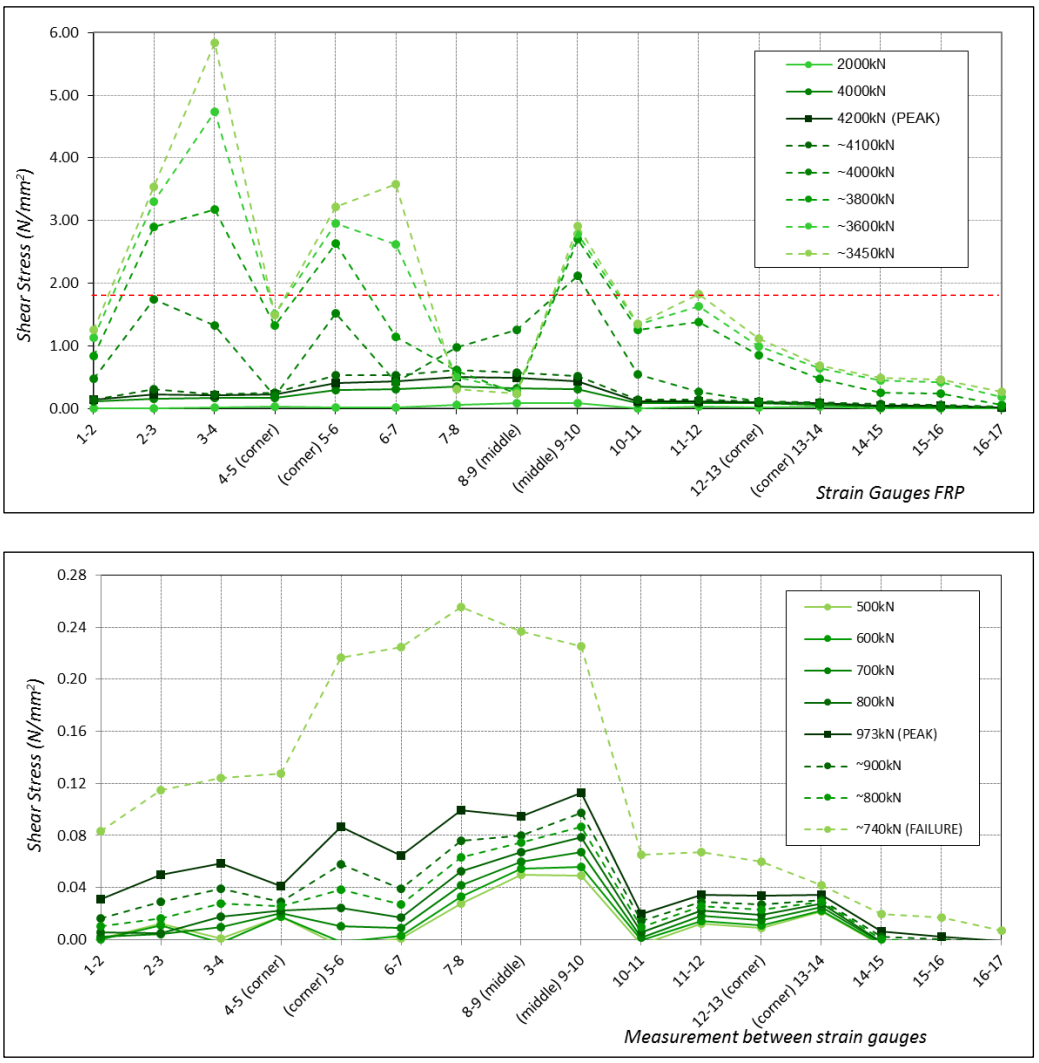

Figure 4-26: Series SE – FRP shear stress between strain gauges for medium-scale specimens, from top; SE5 (EEC1) and SE6 (EEC2)

The limiting shear stress for both specimens is $\tau_{lim,c} = 1.75\,\text{N/mm}^2$, established from Equation 4-3. Table 4-8 details the areas between gauges that exceed this limiting shear stress for specimen SE5.

Table 4-8: Series SE – FRP shear stress for medium-scale SE5 (ECC1) exceeding the limiting shear stress, from Figure 4-26

GAUGE ID	LOAD	SHEAR STRESS	FRP STRAIN %	DEBONDED? (DETERMINED THROUGH PHYSICAL EXAMINATION)
	kN	N/mm²		
2-3	3800 (POST-PEAK)	2.90	0.23	YES
3-4	3800 (POST-PEAK)	3.18	0.29	NO
(CORNER) 5-6	3600 (POST-PEAK)	2.95	0.43	NO
6-7	3600 (POST-PEAK)	2.61	0.35	YES
(MIDDLE) 9-10	3800 (POST-PEAK)	2.12	0.28	YES
11-12	3450 (POST-PEAK)	1.83	0.22	YES

FRP strains in specimen SE6 are small and as such the limiting shear stress is not reached. Looking at Figure 4-25 for SE5, debonding has occurred where the FRP gauges are mounted. This is only on the sides where the strain gradient varies as the cross-section goes from compression to tension. Furthermore, as one small area debonds, if there is a less than perfect concrete-FRP bond, debonding below the limiting shear stress can progress into areas in close proximity, and this propagation, post-peak load, was evident from the cracking sounds as loading and deformation continued.

The area of debonding was more extensive below the mid-height point of specimen SE5, see Figure 4-27.

Figure 4-27: Series SE – Alternative view of debonding mark-up with respect to failure location on medium-scale; from left; SE5 (ECC1) and SE6 (EEC2)

Debonding was witnessed extensively in the medium- and large-scale specimens over the mid-height region where failure occurred. From Figure 4-27 it can be seen that the debonded section is never at the corners and instead debonding is on the flat sides between the corners, irrespective of the load eccentricity. Debonding is more significant for eccentrically loaded specimens, especially on the two sides of varying FRP strain profile.

4.3.5. COMPARISON WITH OTHER RESEARCH – AXIAL-FLEXURAL LOADING

The research relevant for comparison for eccentrically loaded specimens are (refer to Table 2-2 for full information on specimens, only crucial aspects relevant to testing are discussed here):

- *El Maaddawy (2009)*
  Small-scale prismatic specimens of RC, under various eccentric load profiles with large corbels for load application. However there are no concentric specimens for comparison against. FRP wrapping was partial and full. Additional secondary moment has been taken into consideration.

- *Hadi and Widiarsa (2012)*
  Small-scale square specimens, 200x200mm cross-section eccentrically loaded, corner radius of 34mm. Short specimens. High modulus concrete. FRP was applied fully and with additional strips on some specimens.

- *Song et al. (2013)*
  Medium-scale prismatic specimens of RC, under eccentric loading, concentric tests used plain concrete. Specimens are 250x250mm cross-section, height of 1500mm with variation in load eccentricity of 20mm, 60mm, 100mm and 150mm for specimens SSR-1, SSR-1, SSR-3 and SSR-4 respectively.

The failure method of specimens with a large eccentric profile is the same as for ECC2 profiles in Series SE, in that the steel yields and rupture of the FRP does not occur. El Maaddawy (2009) tested small-scale specimens with very large corbels on each end, see Figure 2-7. These specimens of equivalent loading to ECC1 and ECC2, underwent failure though yielding of the steel reinforcement in tension. This is peculiar for ECC1, but the size of the corbels may have generated a greater pull on the longitudinal rebar. El Maaddawy (2009) used corbelled ends on specimens where the point of load application did not require it.

Song et al. (2013) identified that as the load eccentricity increased, effectiveness of the FRP-confinement of the specimen decreased, while the specimen was able to maintain a lower axial load, Figure 4-28. Although the strengthening effect decreases with increasing load eccentricity, the deformability of the columns notably improves.

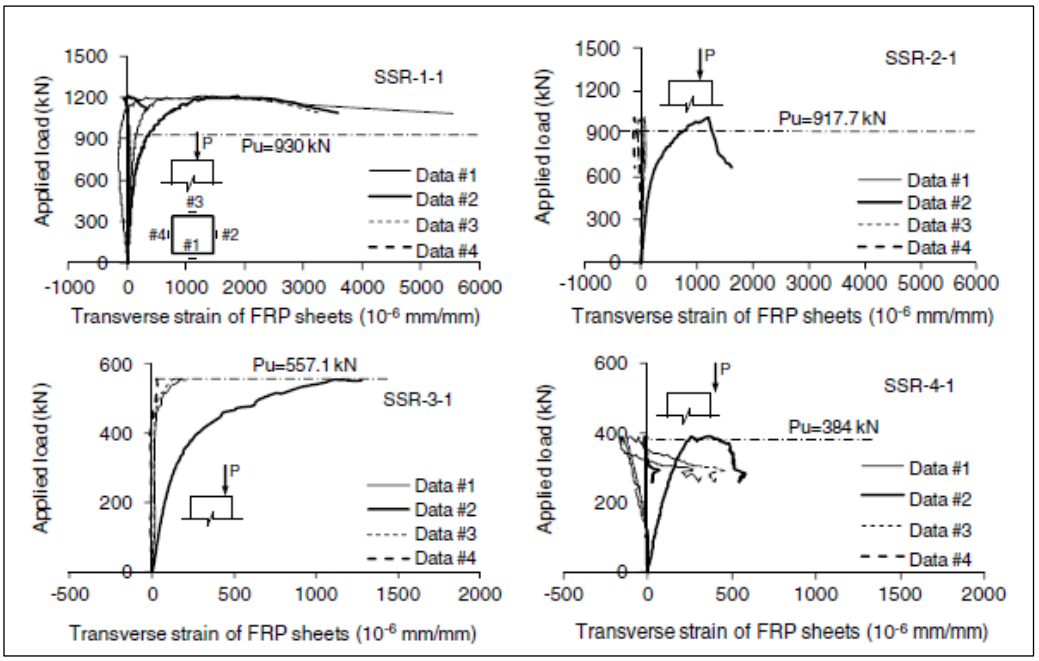

Figure 4-28: Transverse strains for square specimens subject to increasing load eccentricity [Song et al. (2013)]

The behaviour of the effectively confined area was studied by Song et al. (2013) and similar results were found. As the compressive area of the cross-section reduced in size with increasing eccentricity, it zeroed out when the load eccentricity was equal to or greater than half of the cross-sectional height.

In terms of the ideal number of FRP plies to use, Hadi and Widiarsa (2012) saw a slight decrease in load capacity for the same displacement level when the number of plies reduced. Lateral deflection was evident and although comparable the columns were small (200x200mm cross-section), and still experienced second order effects. This was mitigated slightly with the inclusion of FRP straps at set intervals on some specimens, wrapped unidirectionally around the specimen, on top of one layer of FRP. For a large applied load eccentricity, the FRP straps produced higher ductility than those with similar number of full FRP wraps without compromising on the axial capacity. This could be a feasible, cost-effective alternative of reinforcement.

4.3.6. EXPERIMENTAL SERIES SE SUMMARY

Series SE investigates increasing load eccentricity on square specimens. As the load eccentricity increases, the axial capacity decreases as anticipated. The flexural capacity significantly increases with greater load eccentricity. Failure methods of the specimens took two forms; FRP rupture for ECC1, and yielding of the longitudinal steel and cracking of the FRP for ECC2.

A bilinear stress-strain response of eccentrically loaded specimens occurred, and for load profile ECC1, the second portion is ascending. With increasing eccentricity, this second linear portion descends, hence additional FRP plies would be beneficial, either as full wraps or straps. Fundamentally, as the applied load eccentricity increases, the strength capacity of the column decreases too, but the lateral deflection in the column increases.

Higher FRP strains are measured in the FRP jacket on the compressive side of the specimen cross-section and the force generated in the opposite corners reduces. This demonstrates the movement of the effectively confined area into the region of higher compressive stress. Another aspect highlighted is the necessity to consider debonding. Through analysis of the shear stress from the FRP strains and post-test analysis, debonding of the FRP is more apparent and extensive, even below the limiting shear stress determined from TR55 (2011). Thus the combination of increasing size and axial-flexural load can cause the breakdown of the FRP-concrete bond, so with larger eccentricities, potentially the only FRP-concrete bond is at the corners on two sides of the specimens.

4.4. EXPERIMENTAL SERIES RC/E – CROSS-SECTIONAL ASPECT RATIO

Experimental Series RC/E comprises of rectangular cross-sections of varying aspect-ratio subject to both concentric and eccentric loading (specimens from Series SC are included for comparison). The objective is to evaluate the change in confinement and cross-sectional behaviour with the increase in cross-sectional aspect ratio and subsequently the behaviour when eccentrically loaded in the minor or major axis of a specific cross-sectional aspect ratio.

Table 4-9: Series RC/E (Aspect Ratio) – Summary of load, moment and FRP strain results

SPECIMEN ID	X-SEC	PREDICTED LOAD	PEAK LOAD	LATERAL DEFLECTION (@ PEAK)	MOMENT (FROM LATERAL DEFLECTION @ PEAK)	FRP STRAIN (PEAK | FAILURE)	CONFINEMENT EFFECTIVENESS
	mm	kN	kN	mm	kNm		
SC3	*300 | 300*	*2548*	*2443*	*1.76*	*4.4*	*-*	*1.80*
SC4		*3486*	*3617*	*8.49*	*30.7*	*0.18 | 0.90*	
RC1	300 | 450	4810	3958	3.21	12.7	-	0.84
RC2		5232	4434	2.30	10.2	0.47 | 0.49	
RC3	300 | 600	6424	6527	1.93	12.6	-	0.63
RC4		6627	6124	2.03	12.5	0.91 | 0.87	
RE1	300 | 600	5972	5637	1.42	302	0.58 | 0.36	n/a
RE2		2526	1934	3.70	612	0.18 | 0.78	n/a
RE3	600 | 300	4474	6303	16.7	307	1.59 | 0.65	n/a
RE4		2196	1411	53.0	708	0.05 | 0.64	n/a
RC5	300 | 750	8038	8000	2.55	20.4	-	0.50
RC6		7651	6593	5.17	34.1	1.20 | 0.03	

Firstly, for concentrically loaded specimens, FRP-confined predicted load overestimates the capacity of the specimen, due to assumptions in the design using TR55 (2005). Secondly, the eccentrically loaded specimens are also overestimated, especially for ECC2, as seen in Series SE.

A moment is evident at mid-height on all specimens, reasonably small for concentrically loaded and increasing with load eccentricity. Loading on the minor axis generates far greater

mid-height deflections than on the stiffer major axis. The bending at mid-height in RE4 is approximately 150mm at failure and surpassed the length of the LVDT. Hence the additional second order moment is prominent with changing cross-sectional aspect ratio with greater prominence as this increases.

FRP strain at peak and failure loads is variable. Concentrically loaded RC2 and RC4 have little difference in the strain between peak and failure, whereas the failure mechanics of RC6 indicate a massive reduction in FRP strain just before failure. The behaviour in Series RE is even more sporadic, which potentially is related to the failure behaviour using ECC1 and ECC2 profiles, and analysis of the FRP strains over the cross-section is required.

Confinement effectiveness is only established for Series RC as each FRP-confined specimen had an unconfined equivalent. As the cross-sectional aspect ratio increases, the effectiveness of the FRP-confinement reduces due to the longer flat sides between the corners that are not generating any confinement, thus reducing the effectively confined area.

The failure methods of the specimens are as previous tests in Series SC and SE. The unconfined specimens fail through buckling of the steel followed by spalling of the concrete, and as the cross-sectional aspect ratio of the column increases, the momentum behind the steel buckling increases. Due to the large amount of energy released during failure, the vigour with which the concrete spalled from the column increased and the load was dropped. Series RC FRP-confined specimens all failure followed the rupture of the FRP in the end sections of the specimens. Series RE specimens, if they did not fail in this manner, they failed through yielding and snapping of the steel rebar at mid-height which coincided with the FRP snapping apart along the line of the fibres on the tension face. These specimens were able to sustain load long after hairline cracks appeared in the FRP, see Figure 4-29.

Figure 4-29: Series RC – Failure modes, clockwise from top; RC1 (300x450), RC2 (300x450), RC4 (300x600), RC6 (300x750), RC5 (300x750) and RC3 (300x600)

Figure 4-30: Series RE – Failure methods, clockwise from top; RE1 (300x600), RE2 (300x600), RE4 (600x300), RE3 (600x300)

Of the FRP-confined specimens, FRP failure does not occur close to mid-height and the location of the FRP strain gauges. Specimen RE4, loaded on the minor access did not fail in the testing rig, but was stopped after it was deemed unsafe to continue due to the angle that the specimen was sitting in the jaws. Peak load had been achieved. With load being removed in a controlled manner, the specimen then fell out of the rig, illustrating the extent to which it could bend and deform.

4.4.1. STRESS-STRAIN BEHAVIOUR

The stress-strain behaviour for Series RC and Series RE specimens are addressed in separate figures. Firstly in Series RC, all columns are concentrically loaded thus they are compared with concentrically loaded square specimens of 300mm cross-section, SC3 and SC4, Figure 4-31. Secondly, Series RE eccentrically loaded specimens are compared with the 300x600 concentrically loaded specimen RC4, Figure 4-32.

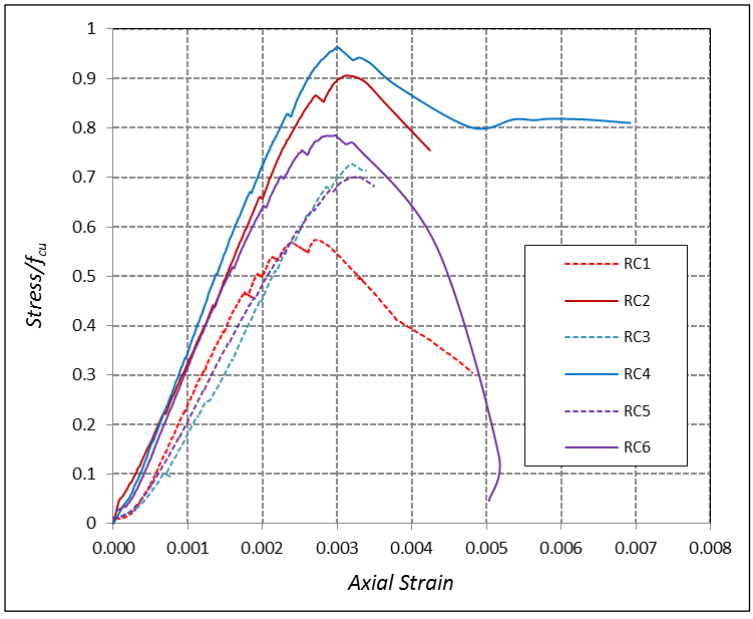

Figure 4-31: Series RC – Stress-strain behaviour for concentrically loaded specimens (normalised with respect to concrete compressive cube strength)

FRP-confined specimens have a similar stiffness and exceed the peak strength of the unconfined counterpart. The stress-strain plot is bilinear, descending in the second portion for all FRP-confined specimens. The descending part of the stress-strain curve is reasonable steep in comparison with the FRP-confined specimens in Series SC and SE, showing a lack of

deformation capacity. Thus for the larger aspect ratios, additional FRP plies are required for adequate strengthening. The increase in cross-sectional aspect ratio does not have an effect on the stiffness of the specimens, when concentrically loaded.

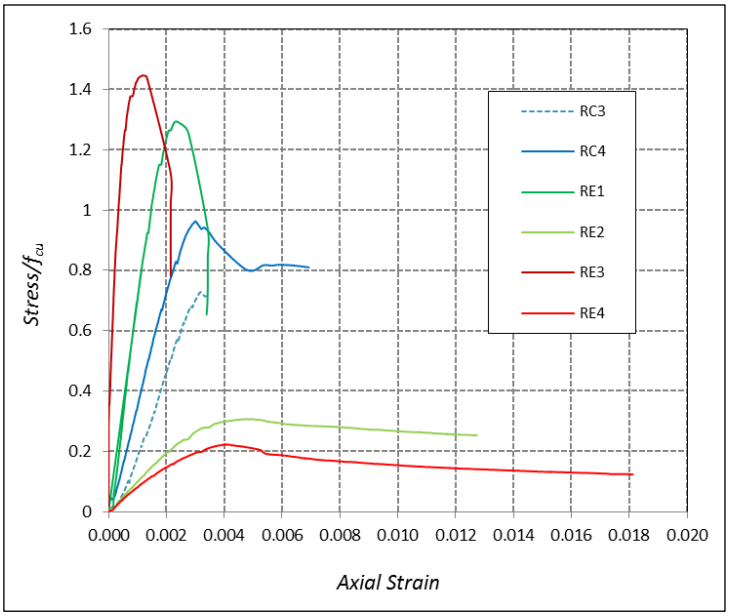

Figure 4-32: Series RE – Stress-strain behaviour for eccentrically loaded specimens (normalised with respect to concrete compressive cube strength)

The behaviour of Series RE specimens in the minor and major axes is promising with an increase in ductility evident with ECC2 profile. A reduction in stiffness mimics that found in Series SE for ECC2 loading. Replicated patterns of behaviour are evident in the stiffness of the ECC1 profiles, and exceed that of ECC2 profiles, regardless of major or minor axis loading. Specimens RE1 and RE3, (ECC1) gave erroneous results with a reverse effect with the increased load capacity and stiffness, over the unconfined specimen. Examination of relevant literature has not shown similar behaviour to drawn a reasonable conclusion for the deviation.

The specimen stiffness for Series RC and RE is presented in Table 4-10.

Table 4-10: Series RC/E – Stiffness of the stress-strain curves, for evaluation of concentrically and eccentrically loaded specimens of rectangular aspect ratio

	UNCONFINED	CONCENTRIC	ECCENTRIC PROFILE NO. 1	ECCENTRIC PROFILE NO. 2
AR (300 | 450)	22.48	31.45	-	-
AR (300 | 600) MAJOR	20.87	24.14	97.75	3.49
AR (300 | 600) MINOR	*AS ABOVE*	*AS ABOVE*	38.60	5.10
AR (300 | 750)	19.84	27.20	-	-

There are two evident patterns, firstly as the cross-sectional aspect-ratio increases in size, the stiffness does not change particularly for concentrically loaded specimens. Secondly, looking at the concentric and ECC2 results, the stiffness reduces with increasing eccentricity regardless of major or minor axis loading, correlating with Series SE. Lastly, there is a discrepancy in the results, the stiffness of the ECC1 specimen increases relative to the concentric specimen, contrary to that found with Series SE.

4.4.2. EFFECT OF CONFINEMENT UPON SPECIMEN SLENDERNESS

The maximum lateral deflection was recorded using a LVDT at mid-height of the specimen is detailed in Table 4-9, with FRP-confined specimens with larger load eccentricity demonstrating the largest deflection at mid-height. Concentrically loaded specimens have followed behavioural trends with the increasing cross-sectional aspect ratio, marginally increasing critical slenderness.

Table 4-11: Series RC/E – Slenderness data

SPECIMEN ID	X-SEC DIMENSIONS	CRITICAL LENGTH	APPLIED ECCENTRICITY	SLENDERNESS †1 λ	CRITICAL SLENDERNESS †2 λ_{crit}
	mm	mm	mm		
RC2	300 | 450	2450	0	28.1	9.26
RC4	300 | 600	3200	0	36.8	9.96
RC6	300 | 750	3750	0	36.8	10.3
RE1	300 | 600	3200	35	36.8	13.9
RE2	300 | 600	3200	385	36.8	11.3
RE3	600 | 300	3200	27	36.8	17.6
RE4	600 | 300	3200	365	43.2	10.4

†1 In accordance with BS EN 1992-1-1:2004
†2 In accordance with TR55 (2011)

The critical slenderness of the all concentrically and eccentrically loaded FRP-confined columns is less than the slenderness of the equivalent unconfined specimen, thus FRP-confinement causes greater slenderness of the specimen, as the strengthening significantly increases load capacity without increasing the flexural ability. All specimens when checked against BS EN 1992-1-1:2004 are considered slender in design.

The dominance of P-Delta effects in Series RE increases the slenderness of FRP-confined specimens, particularly those loaded on the minor axis. Specimens RE3 and RE4 maintained load, decreasing slightly with massive displacement in the axial direction. However the peak load that is achieved and the reducing load maintained post-peak does not prove this to be beneficial in increasing the strength capacity of the specimen.

Again the test results demonstrate that it is imperative to take into consideration not just the applied eccentricity to the column but the P-Delta effects when evaluating the results, as illustrated in Figure 4-33. The lateral deflection at mid-height exceeded the movement of the LVDT, and failure was through yielding of the longitudinal steel, not FRP rupture. Thus for specimens with a large eccentric loading, design should take into consideration the steel capacity and lessen the advantage on strength capacity of wrapping with FRP.

Figure 4-33: Series RE – FRP-confinement on the ductility of specimen RE4, before and during testing

Beneficial effects of FRP-confinement were evident in the previously performed test by other researchers for ductility, emphasising the importance slenderness when considering FRP-confinement. Chaallal and Shahawy (2000) found that at ultimate peak strength, the section strains and hence, curvature in the unconfined specimen is more uniform over the length than the confined specimen which feature localised peaks of section strains. The layout of instrumentation in this series of experiments cannot verify this.

4.4.3. INTERACTION BEHAVIOUR

In this series of tests, both concentrically and eccentrically loaded specimens are tested, along with varying cross-sectional aspect ratio, the results are addressed for Series RC, 300x450mm and 300x750mm cross-sections separately and, then Series RC and RE, for the 300x600mm cross-section.

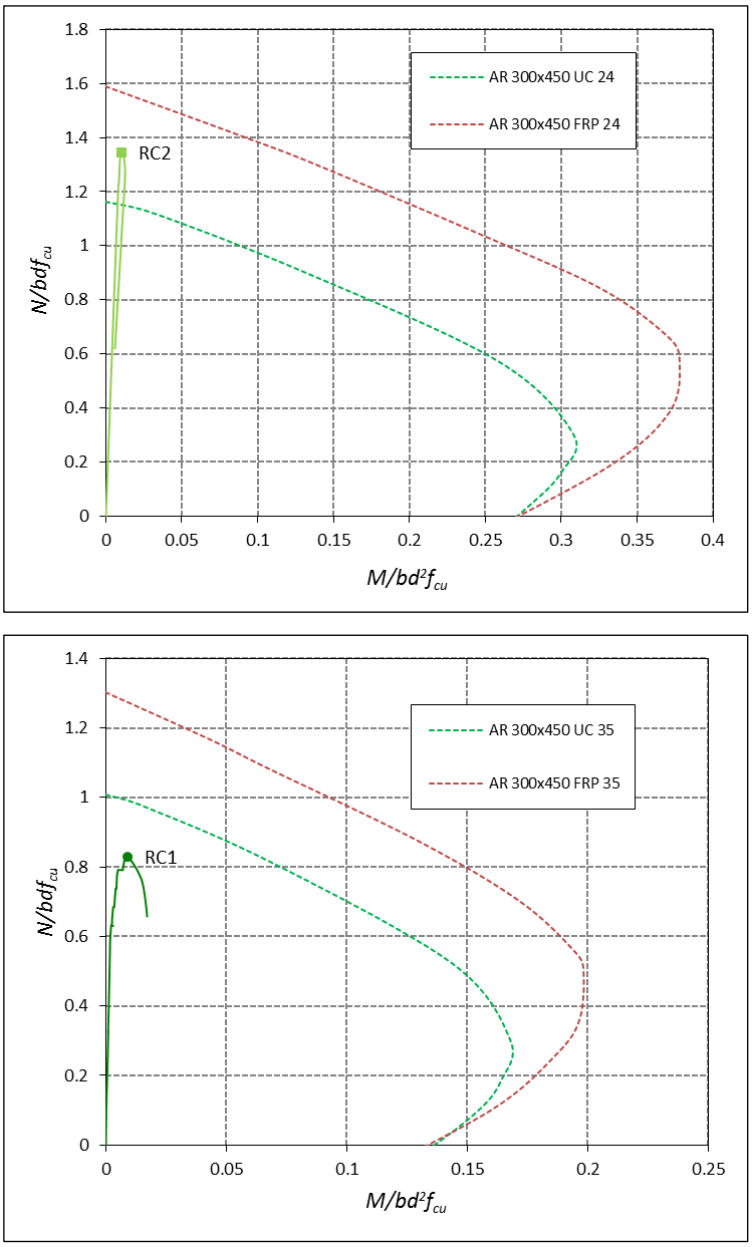

Figure 4-34: Series RC – Interaction diagram for 300x450 cross-sectional aspect ratio specimens; from top; with a concrete compressive cube strength of 24.4MPa and 35.3MPa (peak load highlighted)

RC1 does not reach the unconfined interaction curve or exhibit much influence from P-Delta effects, with a reasonable size moment generated from 75% of peak load until failure. Specimen RC2 also does not reach the reach confined curve and has little moment relative to RC1. Both RC1 and RC2 do not attain assumed peak capacity and experienced different degrees of moment, but not enough to explain the reduction in axial strength capacity.

Specimens of cross-sectional dimension 300x600mm are presented together in Figure 4-35.

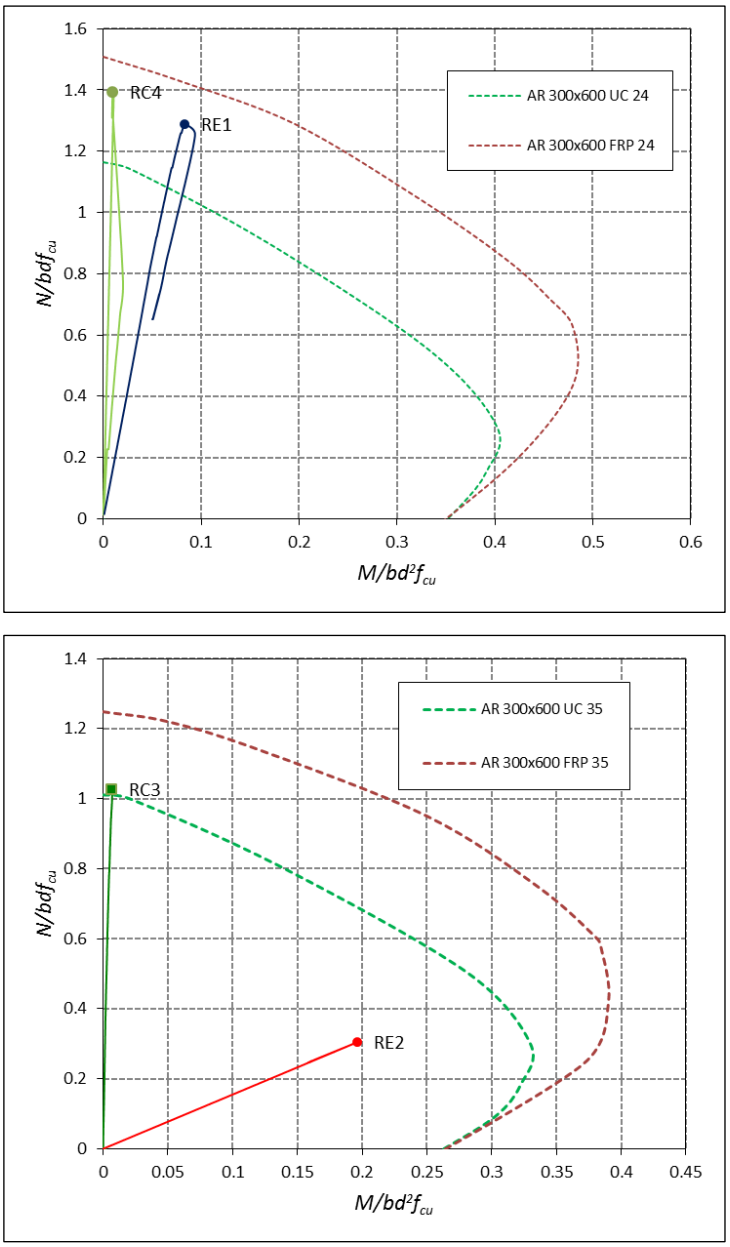

Figure 4-35: Series RC/E – Interaction diagram for 300x600 cross-sectional aspect ratio specimens with concentric and eccentric loading in the major axis; from top; with a concrete compressive cube strength of 24.4MPa and 35.3MPa (peak load highlighted)

Series RC specimens RC3 and RC4 both are close to the associated interaction curve and show little moment, less so than for RC2, the 300x450mm cross-section. There is no evidence of the specimen following the curve with moment after peak load as seen with Series SC.

The eccentrically loaded specimens on the major axis, RE3 and RE4 are not as postulated. RE1 reaches the confined curve with less moment than predicted in the initial interaction diagram from TR55 (2011), Figure 4-3. This diagram has had varied results in terms of magnitude of axial and moment capacity achieved but with all specimens in Series SC and SE, the path to the point on reaching the curve as anticipated. RE2, the larger eccentricity does not reach the unconfined curve, far less the confined curve and as such there is no evidence of a requirement for an extended curve as with Series SE.

The variation in cross-sectional aspect ratio results, suggests that the method of calculating the effectively confined concrete and FRP influence in TR55 (2005) does not explain that for rectangular specimens sufficiently according to the results and analysis of this experimental series.

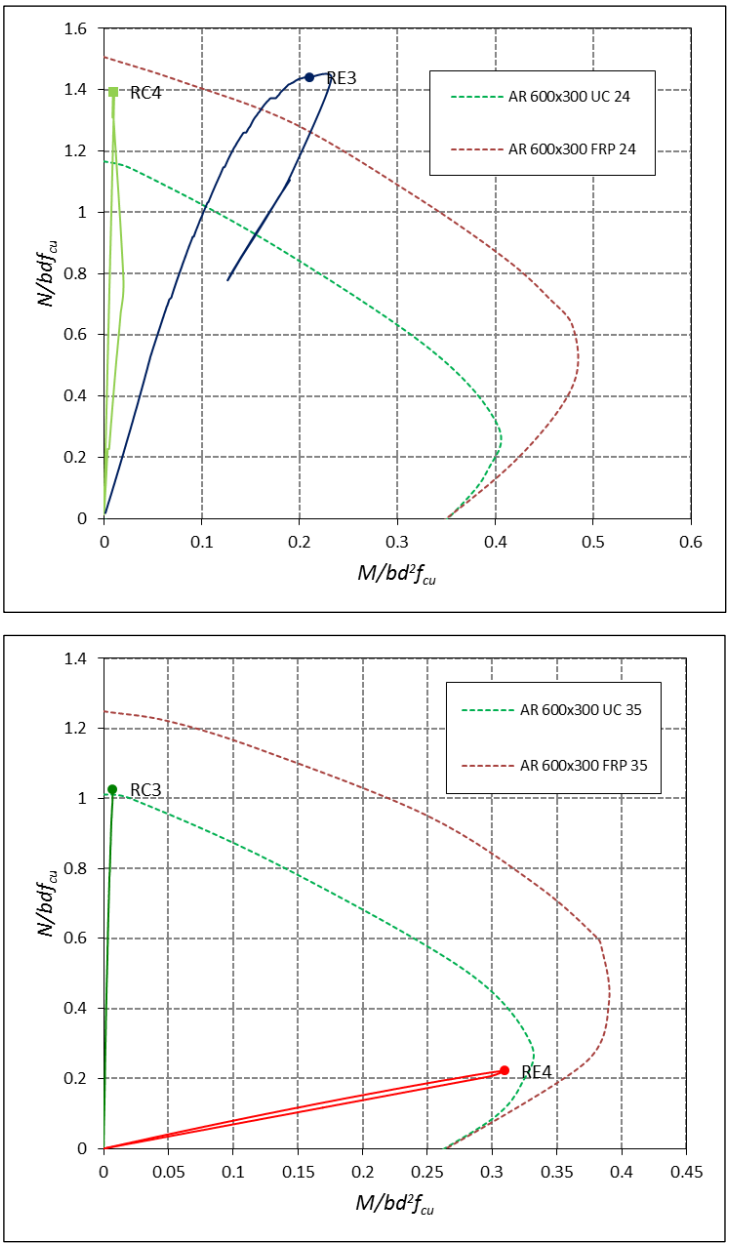

Figure 4-36: Series RC/E – Interaction diagram for 300x600 cross-sectional aspect ratio specimens with concentric and eccentric loading in the minor axis; from top; with a concrete compressive cube strength of 24.4MPa and 35.3MPa (peak load highlighted)

Specimen RE3 has similar behaviour to the loading on the major axis in that the path to the confined curve is not as anticipated as it again reaches the curve with far less moment than designed for. The variation here is that there is some evidence of a moment in the specimen post peak load. RE4 again does not reach the confined curve. During testing, the lateral deflection at failure was around 150mm but the LVDT did not capture this. Had this

increased moment been captured by the instrumentation, it would have meant that RE4 would have exceeded the confined curve.

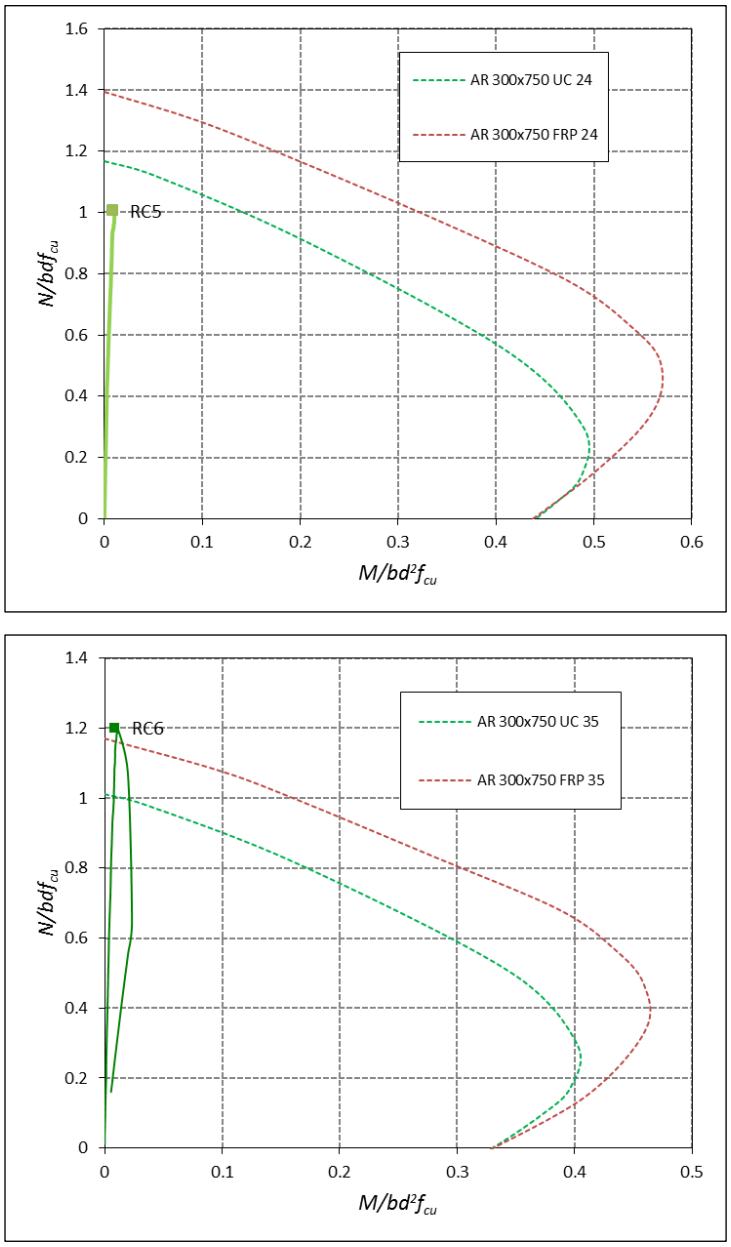

Figure 4-37: Series RC – Interaction diagram for 300x750 cross-sectional aspect ratio specimens; from top; with a concrete compressive cube strength of 24.4MPa and 35.3MPa (peak load highlighted)

Concentrically loaded specimens RC5 and RC6 have the largest cross-sectional aspect ratio of 300x750mm. They display results very similar to the other concentrically loaded specimens in this series, with an axial capacity similar to the design and little moment.

Series RC displays similar behaviour for all FRP-confined specimens with axial load close to or on the confined curve and little moment from P-Delta effects evident. Series RE varied greatly in the results, suggesting that the confined behaviour was not captured adequately in TR55 (2005) design process adopted.

4.4.4. FRP JACKET BEHAVIOUR

The axial and lateral strain in the specimen is measured using LVDTs at the top and mid-height of the column. When looking at the axial-to-lateral strain after the stress is normalised, the concentrically loaded specimens display similar behaviour regardless of the cross-sectional aspect ratio for concentric loading, Figure 4-38.

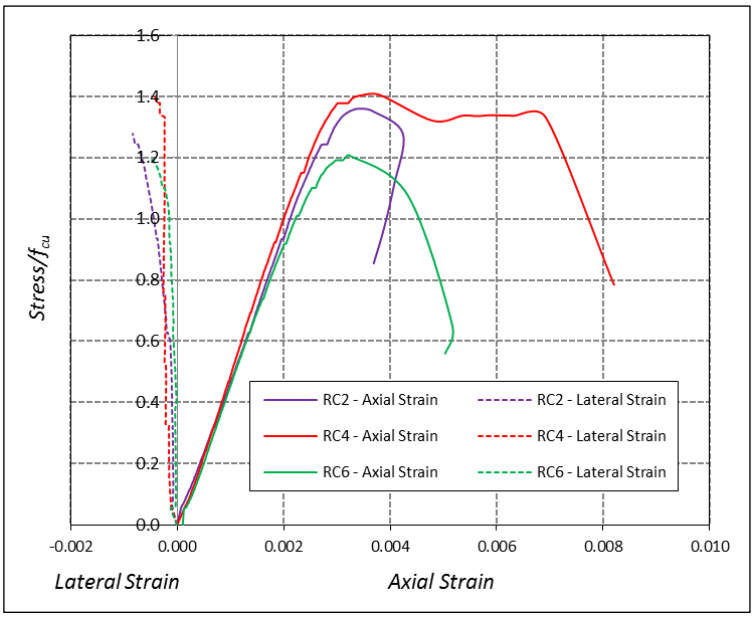

Figure 4-38: Series RC – Axial-to-lateral strain for concentrically loaded rectangular specimens with varying cross-sectional aspect ratio (normalised with respect to concrete compressive cube strength)

Axial stress-strain curves do not follow the bilinear stress-strain response, showing little capacity after peak load. FRP-confinement for rectangular specimens, needs to be increased to be effective. These specimens have very little lateral moment and consequently little deformation capacity.

Series RE axial-to-lateral strain is shown in Figure 4-39. The bilinear form was evident again, but only for the ECC2 profile in the major and minor axes.

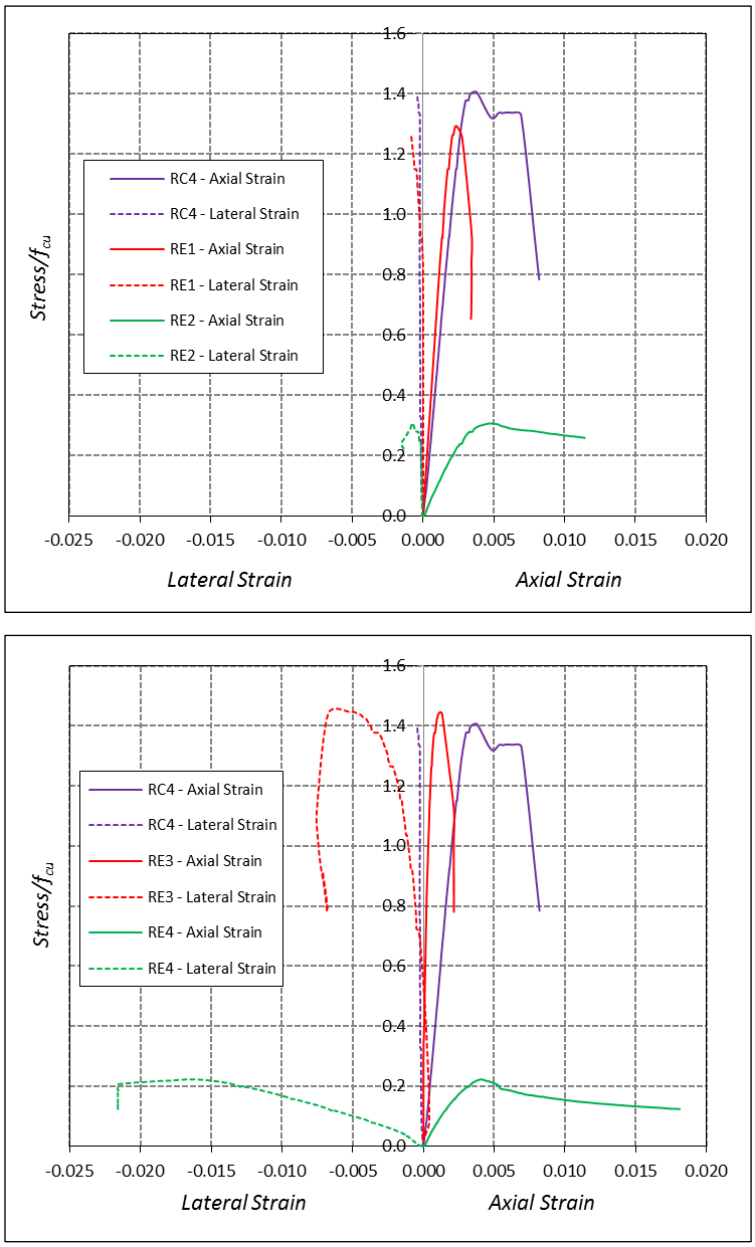

Figure 4-39: Series RE – Axial-to-lateral strain for eccentrically loaded rectangular specimens with 300x600mm cross-section; from left, loaded on the major axis and loaded on the minor axis (normalised with respect to concrete compressive cube strength)

The behaviour of ECC1 profile in both the major and minor axes is similar to the Series SE and again while the load eccentricity is small, the descending second portion of the bilinear stress-strain curve is due to inadequate confinement. RE2 (major axis loading) and RE4 (minor axis loading) have a bilinear response and although the axial capacity is small, there is large deformation capacity, especially when loaded on the minor axis. Furthermore,

specimens eccentrically loaded in the minor axis show significantly higher lateral strains with the bending of the specimen.

To further examine this behaviour of the FRP jacket, the strains in the FRP specimens measured around mid-height of half of the column are presented in Figure 4-40, Figure 4-42 and Figure 4-43 for Series RC, Series RE (major axis loading) and Series RE (minor axis loading) respectively.

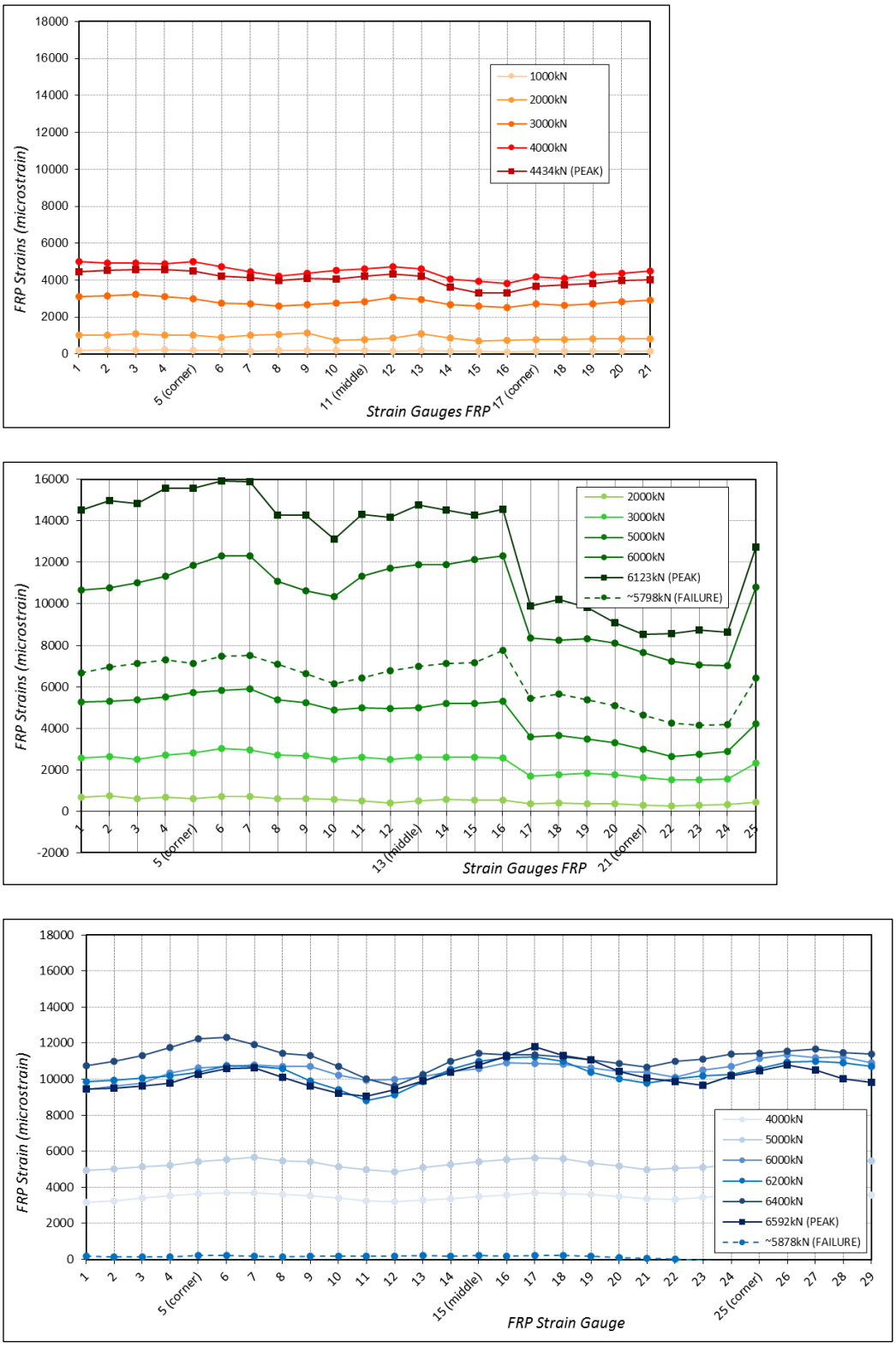

Figure 4-40: Series RC – FRP strains measured around half of the specimen cross-section at mid-height; from top to bottom; RC2, RC4 and RC6

Specimens RC2 and RC4 demonstrate strain behaviour similar to Series SC, in that the strains are level across the section and no evidence of movement to into an area of greater compressive stress. There is minimal change in slope hence it would suggest that there is no evidence of debonding, however this does not corroborate with post-test analysis, where slight debonding was apparent away from mid-height of the specimen. Failure was localised at the top of the specimen. Definition between peak and failure in terms of FRP strains is not evident as there is little of a bilinear response.

Specimen RC4 shows a little movement of the effectively confined area over to the compressive side of the specimen, and with the change in slope, there is evidence of debonding, Figure 4-41. This debonding, as with RC2 and RC4, is very localised. In the debonded area, the long flat sides are fully debonded between the corners, and to a lesser extent on the short sides.

Figure 4-41: Series RC – Debonding mark-up of RC4; 'X' marked areas of the grid signify breakdown of the FRP-concrete bond, illustrating the localised debonding

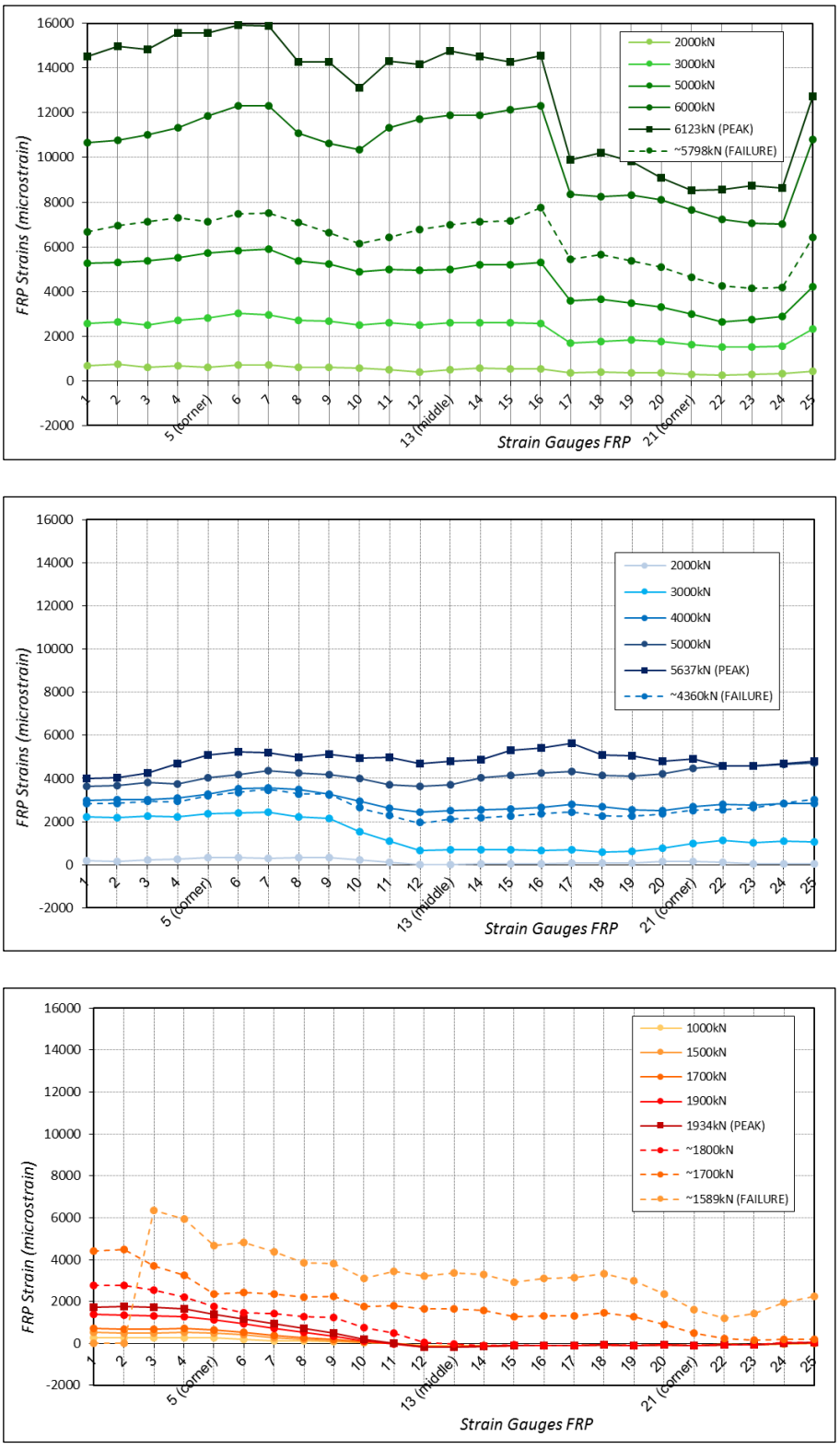

Figure 4-42: Series RE – FRP strains measured around half of the specimen cross-section at mid-height, with major axis load profile; from top; RC4 (included for comparison), RE1 and RE2

FRP strains around the cross-section of the specimens from Series RE were expected to follow similar patterns to Series SE, in terms of the strains being greater on the compressive side and demonstrating the moment of the effectively confined area. Looking at Figure 4-42, there is slight movement in RE2 but this is particularly small considering the applied ECC2 load profile. These FRP gauges did not pick up strain readings that reflected the behaviour in the FRP wrap.

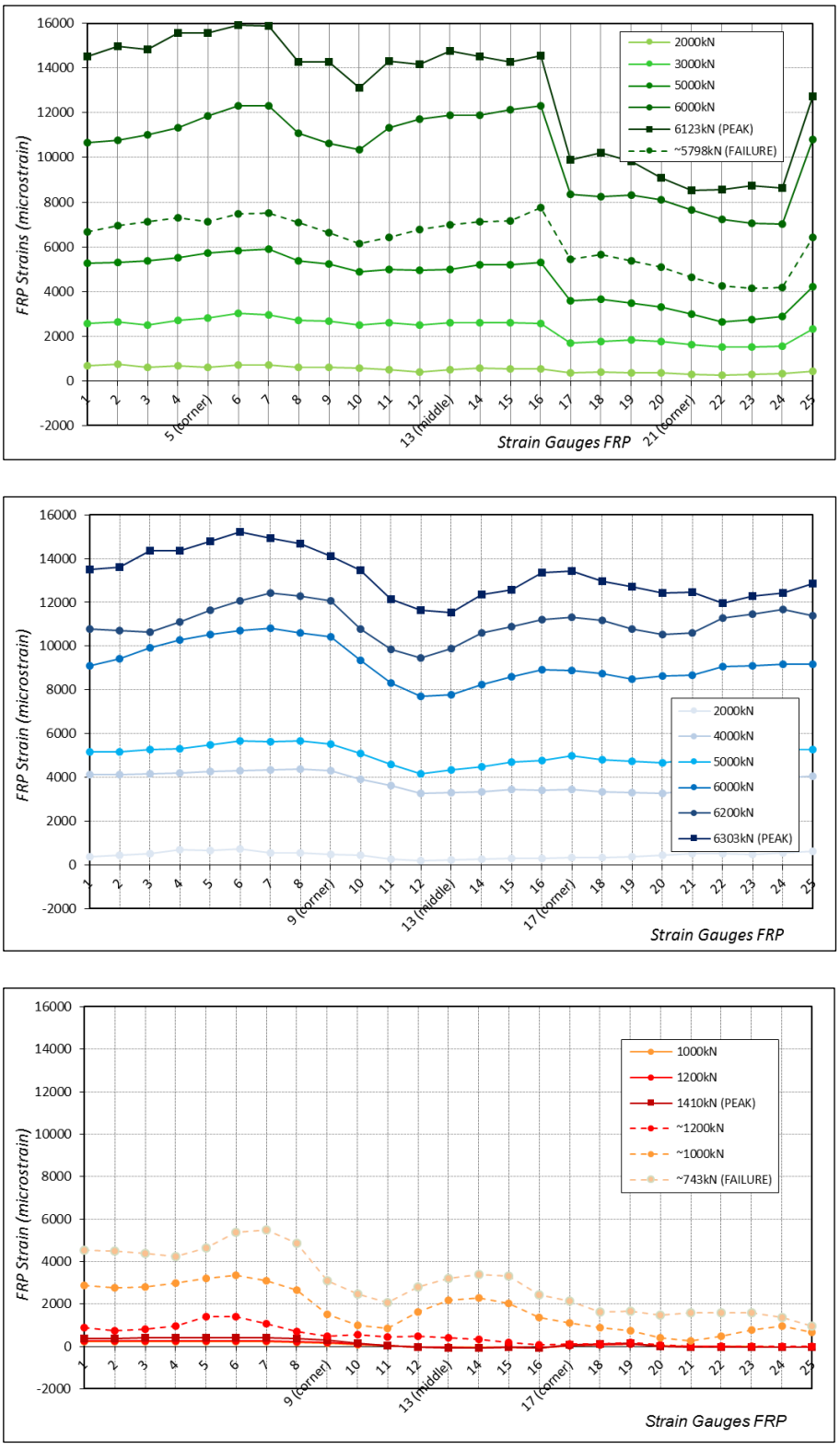

Figure 4-43: Series RE – FRP strains measured around half of the specimen cross-section at mid-height, with major axis load profile; from top; RC4 (included for comparison), RE3 and RE4

Series RE, subjected to loading on the minor axis has similar behaviour in the FRP strain plots, Figure 4-43, as for Series RE, major axis loading, with localised behaviour not reflected in the mid-height strain gauges readings. Again, ECC2 profile shows slight movement of the effectively confined area to the area of highest compressive stress, shown with the high strains.

To adequately capture the FRP jacket behaviour of these specimens would require a considerably more instrumentation on the tensile steel reinforcement as well as the FRP jacket to negate missing localised failure.

4.4.4.1. DEBONDING OF THE FRP JACKET

The large side dimension of the cross-section, especially on the eccentrically loaded specimens, was subject to debonding to the extent that a shallow bubble formed as the ping of the concrete-FRP bond breaking down over the whole side was heard and this was subsequently visible to the naked eye on closer inspection of the area of this acute debonding. This dramatic effect of during testing was hard to capture in an image and so is shown after examination and mark-up, Figure 4-44.

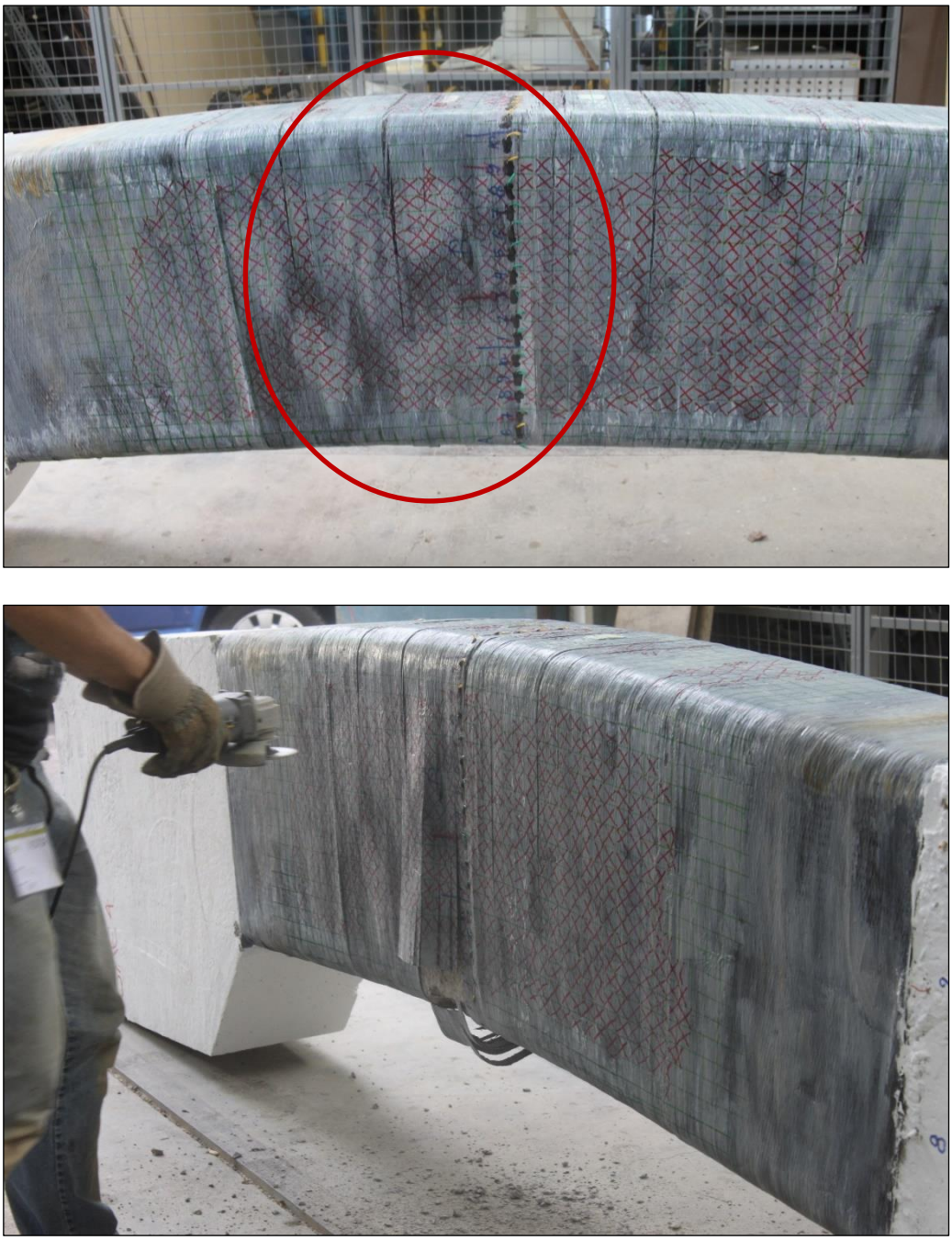

Figure 4-44: Series RE – Debonding and post-test analysis of RE2 ECC2 loading on the major axis, from top; marked area of debonding that 'popped' out during testing, and post-test analysis of the FRP jacket around the debonded areas

The major axis however did not demonstrate such obvious results due to the stiffness of the cross-section relative to the minor axis. In Figure 4-44, the technician (Will Bazely) is about to cut the FRP. In specimens with large flat sides with debonded sections like this, the FRP began to split when post-test cutting commenced, as a large amount of residual energy was

still contained. Even though the FRP fully debonded along the flat sides, the bond at the corners was still thoroughly intact. Furthermore for safety reasons, it is important to ensure that if debonding does occur, that the FRP will still not then split, and release the contained energy through sudden and rapid movement away from the column.

The shear stress has been established from the FRP strains and Figure 4-45 shows the areas where the limiting shear stress is exceeded in specimen RE2.

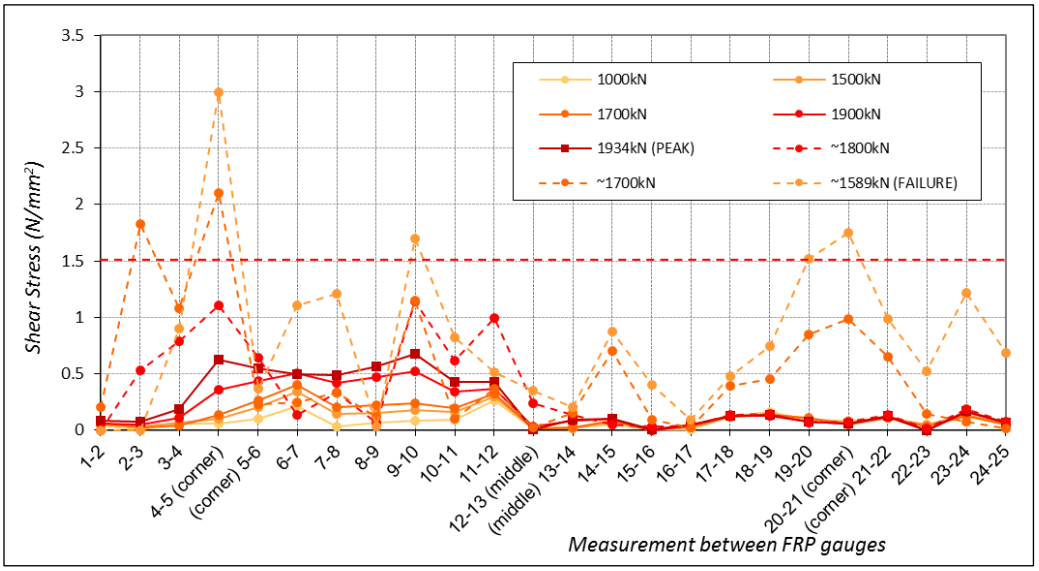

Figure 4-45: Series RE – FRP shear stress between strain gauges for RE2 (major axis loading)

Thus for RE2, an unconfined concrete cube strength of 35.3MPa, the limiting shear stress is $\tau_{lim,c} = 1.5\text{N/mm}^2$. Table 4-12 details the areas between gauges that exceeded this limiting shear stress.

Table 4-12: Series RE – FRP shear stress for RE2 (ECC2 loading in the major axis) exceeding the limiting shear stress, from Figure 4-45

GAUGE ID	LOAD	SHEAR STRESS	FRP STRAIN %	DEBONDED? (DETERMINED THROUGH PHYSICAL EXAMINATION)
	kN	N/mm²		
2-3	1800 (POST-PEAK)	1.83	0.41	YES
4-5 (CORNER)	1800 (POST-PEAK)	2.10	0.28	YES
9-10	1589 (FAILURE)	1.70	0..35	YES
19-20	1589 (FAILURE)	1.52	0.27	YES
20-21 (CORNER)	1589 (FAILURE)	1.75	0.20	YES

Debonding on RE2 was found to be a lot more extensive than the shear stress plot demonstrates. The large section that debonded just before failure could still be taking strain between the corners, hence a change in readings would not be registered in the gauges.

Debonding along the long side of a rectangular specimen was found on all specimens. As the eccentricity increases, the localisation of the debonding decreases and it covers more of the specimen. This is more of a problem with loading in the major axis, where the long sides are seen to be debonded from corner to corner for a large vertical distance along the specimen.

4.4.5. COMPARISON WITH OTHER RESEARCH – CROSS-SECTIONAL ASPECT RATIO

The work that has been identified as relevant for comparison here are as follows (refer to Table 2-2 for full information on specimens, only some aspects discussed here relevant to testing):

- *De Luca et al. (2011)*
  Medium-scale specimens of aspect ratio from 1.0 to 1.45 with a corner radius of 25.4mm. However reinforcement is using GFRP confinement. Medium to high modulus concrete. Concentric loading applied.

- *Micelli and Modarelli (2013)*
  Cross-sectional aspect ratio of 1:2 small- and medium-scale. Numerous tests omitted from comparison including GFRP and hollow centre SHORT specimens. All specimens using plain concrete. Concentric loading only.

- *Wu and Wei (2010)*
  Short/prism size of varying cross-sectional aspect ratio from 1:1 to 1:2 with a 20mm corner radius. Plain concrete only, with an unconfined compressive cube strength of 30MPa. Concentric loading only.

Wu and Wei (2010) found that the effect of the increasing cross-sectional aspect ratio generated a descending second portion of the bilinear curve. For the large aspect ratios, the stress-strain response also changed from initial linear and strain-hardening response to a strain-softening response, and to mitigate this happening at a smaller cross-sectional aspect ratio, a thicker FRP jacket is required. This correlates with all specimens in Series RC and RE as the confinement has been found to be inadequate for all. For Series RE, FRP straps over FRP full confinement could mitigate too many plies of FRP along the whole length of the column.

In terms of FRP strain results, Wu and Wei (2010) found that the strain distribution is significantly less when looking at peak load as opposed to failure, which does not correlate due to the localised behaviour that was not captured in Series RC/E specimens. It is difficult to ascertain if the maximum FRP strain at peak load decreases with cross-sectional aspect ratio as well, as the results are not truly representative of what happens in the region of FRP rupture.

De Luca et al. (2011) addressed concentrically loaded columns of rectangular cross-section and found that confinement effectiveness is higher for square cross-sections than for rectangular cross-sections, thus decreases as the side aspect ratio of the specimen increases. These specimens were wrapped with glass FRP thus the numerical results have to consider the different properties of the material.

Micelli and Modarelli (2013) looked at rectangular prisms concentrically loaded. These very short specimens did not experience much of a descending portion of the bilinear stress-strain curve, as such demonstrating that the height and the subsequent slenderness are important factors in the behaviour and as such, the design.

The data available for comparison with Series RC/E is sparse if all aspects that do not corroborate with the parameter selection in this research are removed. To evaluate rectangular specimens further, it is essential that larger specimens are tested to establish a

wider database, encompassing the effects of the long side, debonding, and the second order effects from the height.

4.4.6. EXPERIMENTAL SERIES RC/E SUMMARY

In Series RC/E, two main aspects were studied; firstly, the effect of increasing cross-sectional aspect ratio under concentric loading, and secondly, the effect of load eccentricity on rectangular columns.

In terms of the concentrically loaded specimens, an increase in axial strength capacity is evident and this increase has minimal change with increasing aspect ratio. Generally FRP-confinement enhances the axial and ductile capacity of the specimen but as the cross-sectional aspect ratio increases, the strength gain decreases until becoming insignificant after an aspect ratio of 1:2. This has been established on short specimens and this effect is not as apparent as confinement effectiveness is still evident for cross-sectional aspect ratio 1:2.5 (300x750mm). The behaviour followed that of the concentrically loaded FRP-confined specimens leading to a belief that there is a size effect. To confirm or mitigate this, further testing is essential.

When the 300x600 specimens were loaded eccentrically in the major axis, the specimen with ECC1 load profile followed the same behavioural pattern as for concentric and large-scale specimens. The large eccentricity did modify the behaviour back into a bilinear response but this was of minimal gain in strength capacity.

Specimens eccentrically loaded in the minor axis showed a significant increase in ductility, evident in the bilinear response. This increase was so great that the ECC2 load profile specimen was bending to such an extent that it caused it to slip from its mountings on the test rig. However, the benefit in terms of strength enhancement was minimal and in this case, bilinear fibre wrap would be necessary to provide more axial support and resistance to the bending.

The significant behaviour in all of the FRP-confined specimens was the occurrence of debonding, which became more vigorous along the long flat sides with increased load eccentric.

4.5. COMPARISON WITH TR55 (2011) DESIGN METHODOLOGY

TR55 (2005) has been superseded by TR55 (2011), as detailed in Section 2.7.3. The approach to design of FRP-confined prismatic specimens has evolved significantly and as such provides a far more detailed design basis. Integral in the design of specimens to TR55 (2011) are aspects that through use in analysis in Sections 4.2 to 4.4, have been found to be of a critical influence in the test series, such as the actual maximum strain capacity in the FRP relative to the established FRP ultimate strain and debonding of the FRP jacket. Thus the specimens presented in this chapter are compared against TR55 (2011) to ascertain the reliability of the code for design of FRP-confined prismatic columns of realistic size and loading.

The design methodology presented in TR55 (2011) allows for the influence of debonding, FRP rupture and variation in strain over the cross-section to be considered. It advises that there is little benefit in using the design methodology for specimens that:

- Have a cross-sectional aspect ratio greater than 1:1.15
- Have corner radii less than 20mm
- Have a load eccentricity so large at the steel yields in tension

Some specimens in the test matrix in this study exceed the advisory limitations for design in terms of the cross-sectional aspect ratio and applied load eccentricity profile ECC2. However, it is useful to evaluate the design method presented for specimens outside this range to ascertain if it is a conservatism for construction purposes.

Referring to the TR55 (2011) interaction diagram presented in Figure 4-3, four strain profiles of varying axial load and moment combinations are considered to produce the interaction diagram for a specific cross-section size and concrete strength. These four interaction points are illustrated in Figure 4-46.

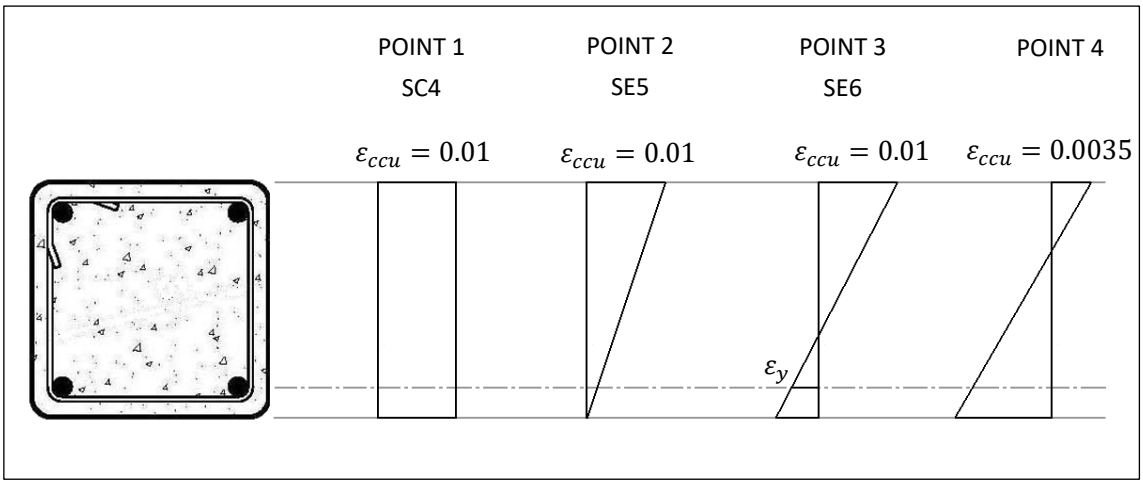

Figure 4-46: Strain profiles for generation of the interaction diagram

The strain profiles above correspond to the experimental test matrix and are described by TR55 (2011) as follows:

1. *SC4 – Concentric loading (Series SC)*
   "A pure axial load is applied to the specimen thus generating uniform axial compressive strain."

2. *SE5 – Eccentric profile 1 (Series SE)*
   "An axial-flexural load is applied to generate maximum compressive strain at the top of the specimen and zero axial strain at the bottom, at the tensile face."

3. *SE6 – Eccentric profile 2 (Series SE)*
   "An axial-flexural load is applied to generate a balance failure with the maximum axial compressive strain at the top face and a corresponding tensile strain at the bottom, tensile face. This generates yielding in both top and bottom reinforcing steel."

Interaction point 4 does not represent any specimens in the experimental test series presented however for completeness of the interaction curves, this theoretical interaction point has been established, representing the point on the moment axis that equates to zero axial force.

The process establishing this interaction curve is illustrated in a flow chart detailed in TR55 (2011) Section 8.9.4 and shown in Figure 4-47.

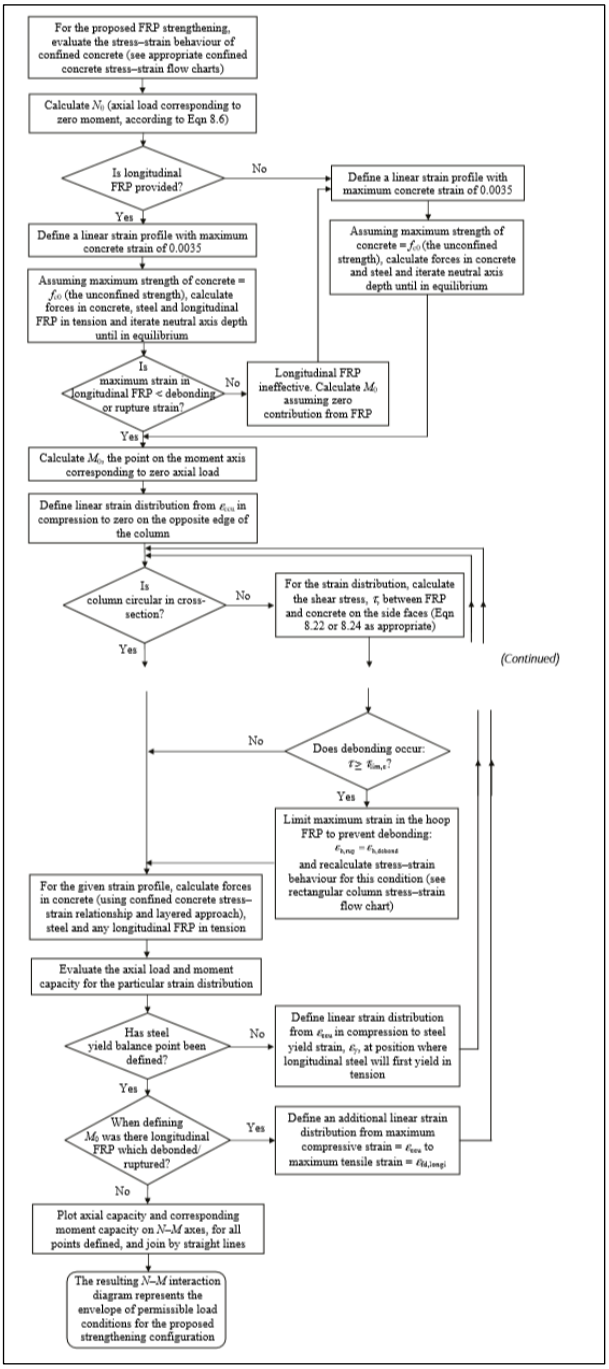

Figure 4-47: TR55 (2011) flow chart for establishing N-M interaction diagram for prismatic columns

Further flow charts in TR55 (2011) also detail; stress-strain behaviour of FRP confined concrete rectangular/square columns (Section 8.9.2), and column strengthening – combined axial load, N, and moment, M (Section 8.9.3) for reference as required.

4.5.1. INTERACTION BEHAVIOUR FOR MEDIUM-SCALE SPECIMENS

Initial specimen design in Chapter 3 was for medium-scale specimens, hence design to TR55 (2011) is demonstrated for medium-scale specimens with presentation of all results in Section 4.5.2. The actual compressive cube strength of the specimen SC4 is used as opposed to the design strength and the behaviour is compared with the established interaction curve in accordance with TR55 (2011).

TR55 (2011) advises that the following are necessary for design of axially loaded columns:

- Slip does not take place between the FRP and the concrete
- The maximum allowable compressive strain in the concrete is 0.01 or ε_{ccu}, whichever is less
- Confinement provided by any existing hoop steel is ignored

Furthermore "the stress-strain response for unconfined concrete follows the idealised curve for concrete presented in current codes and standards, with $\gamma_c = 1.5$." This is neglected in this design as it is important to get realistic representation of the behaviour.

The four interaction points necessary for establishing the interaction diagram are evaluated as in Sections 4.5.1.1 to 4.5.1.4.

4.5.1.1. INTERACTION POINT 1 – CONCENTRICALLY LOADED SPECIMEN (ID SC4)

Point 1 on the interaction curve represents uniform strain over the cross-section, thus the axial capacity is calculated in terms of the maximum confined strength and the corresponding strain.

The rupture strain as seen in Section 4.2.4.1 is be significantly lower than the FRP ultimate strain, and more representative of the actual FRP behaviour, hence TR55 (2011) takes this into consideration through Equation 4-6. Following determination of the rupture strain, the confined strength (TR55 (2011) Equation 8.18) can then be derived as follows:

$$\frac{f_{ccd}}{f_{c0}} = 1 + 5.25\,(k_e\,\rho_k - 0.01)\,\rho_\varepsilon \qquad (4\text{-}8)$$

where: $\rho_k \geq \frac{0.01}{k_e}$ must be satisfied to ensure sufficient stiffness

The axial capacity of the specimen, N_0, is a function of the concrete capacity detailed in Equation 4-8 and the longitudinal steel capacity:

$$N_0 = A_{c,net} f_{ccd} + A_s f_{yk}/\gamma_s \quad (4\text{-}9)$$

where: γ_s is the material partial safety factor of steel and taken as 1.0 for design

Thus the axial capacity for medium-scale concentrically loaded specimen SC4 is 3776kN for a concrete compressive cube strength, $f_{cu} = 24.4$N/mm^2.

Theoretically this concentrically loaded specimen should experience no moment and as such there should be no applied eccentricity of load. However, the results presented earlier in this chapter demonstrate a lateral deflection in all specimens, so it is important to consider the effect of these imperfections. This is addressed in Section 8.2.4 through methodology based on the nominal curvature method defined in BS EN 1992-1-1.

The additional nominal second order moment, M_2, is defined in TR55 (2011) Equation 8.10:

$$M_2 = Ne_2 \quad (4\text{-}10)$$

And the peak second-order lateral deflection, e_2, is defined in TR55 (2011) Equation 8.11:

$$e_2 = K_r K_\varphi \frac{1}{r_o} \frac{l_0^3}{10} \quad (4\text{-}11)$$

To establish this lateral deflection, the following equations are defined as:

$$K_r = \left(\frac{n_u - n}{n_u - 0.4}\right) \leq 1.0 \quad (4\text{-}12)$$

$$K_\varphi = 1 + \beta\varphi_{ef} \quad (4\text{-}13)$$

where: φ_{ef} is the effective creep coefficient as specified by BS EN 1992-1-1 Section 5.8.4, which states that for if λ < 75, the effect of creep can be ignored and taken as 0

$$n = \left(\frac{N}{A_c f_{ccd}}\right)$$

$$\frac{1}{r_o} = \left(\frac{f_{yd}}{E_s\ 0.45d}\right)$$

When applying the formulae to determine the additional second order moment, an anomaly was observed between TR55 (2011) Section 8.2.4 and its source document, BS EN 1992-1-1 Section 5.8.8.3 (3) for the definition of n_u. Equations 4-14a and 4-14b define n_u for TR55 (2011) and BS EN 1992-1-1 respectively and the source Equation 4-14b has been adopted for this analysis.

$$n_u = \left(1 - \frac{A_s f_{yd}}{A_c f_{ccd}}\right) \quad (4\text{-}14a)$$

$$n_u = 1 + \omega \quad (4\text{-}14b)$$

where: $\omega = \frac{A_s f_{yd}}{A_c f_{ccd}}$

Inclusion of the imperfections generates an additional moment, M_2, of 0kNmm to give an applied moment, $M_{applied}$, of 0kNmm and subsequently does not reduce the axially capacity of the specimen. If a reduction in capacity was evident, it can be evaluated once the interaction diagram is established for this series. The adjusted eccentricity, e_2, is 0mm. Refer to Appendix A for the detailed calculations.

4.5.1.2. INTERACTION POINT 2 – ECCENTRICALLY LOADED SPECIMEN (ID SE5)

With the addition of a flexural component to the load, shear stresses develop between the concrete and the FRP along the flat side between the corners, and if this flat side is long enough, debonding can occur. Debonding is taken into consideration as per Equation 4-6. If the FRP debonding strain is less than the FRP rupture strain, this is used in place of the FRP rupture strain as once debonding has occurred, the stiffness of confinement reduces significantly and as such, the there is less effective strength enhancement.

To encompass a small load eccentricity (point 2 on the interaction curve, Figure 4-3), a compressive strain distribution of zero to $\varepsilon_{cc,max} = 0.01$ over the cross-section is adopted. It is assumed that the strain in the FRP can reach rupture strain on the compressive side, and consequently the opposite edge is unstressed. The flexural component is taken into consideration through evaluation of the shear stress and the FRP rupture/debonding strain. The shear stress is defined in TR55 (2011) Equation 8.22 as:

$$\tau = t_f E_{fd} \frac{\varepsilon_{h,rup}}{(h-2R_c)} \leq \tau_{lim,c} \quad (4\text{-}15)$$

If this limit is not satisfied, the FRP debonding strain as identified in Equation 4-7 needs to be calculated for use in place of the FRP rupture strain.

The stress-strain relationship is included through use of the appropriate equation from TR55 (2011) Equations 8.12 and 8.13 as satisfies the mentioned criteria:

$$f_{cc} = E_{cm}\varepsilon_{cc} - (E_{cm} - E_2)^2\,\varepsilon_{cc}/4f_{c0} \quad \text{for} \quad 0 \le \varepsilon_{cc} \le \varepsilon_t \qquad (4\text{-}16)$$

$$f_{cc} = f_{c0} + E_2\varepsilon_{cc} \quad \text{for} \quad \varepsilon_t \le \varepsilon_{cc} \le \varepsilon_{ccu} \qquad (4\text{-}17)$$

Once this stress-strain relationship has been established, the force in the concrete and any compressive force in the steel is included (any compressive force in the FRP is ignored). From this the axial load and corresponding moment are calculated. The effect of imperfections is calculated as per interaction point 1 and included with the initially defined moment.

Thus for a $f_{cu} = 42.0$N/mm^2 (corresponds to SE5), the axial capacity of specimen SE5 is 3935kN with a moment of 67399kNmm. Inclusion of the effect of imperfections increases the moment to 72490kNmm and the applied load eccentricity is subsequently 18.4mm.

4.5.1.3. INTERACTION POINT 3 – ECCENTRICALLY LOADED SPECIMEN (ID SE6)

At point 3 on the interaction diagram, the maximum moment capacity is reached when steel yielding dominates the column behaviour. The maximum tensile strain in concrete is $\varepsilon_{cc,max} = 0.01$ to a strain in the lower longitudinal steel equal to the yield strain. This is approximately similar to design using the strain in the concrete on this side as 0.0035. The process for establishing axial load and moment replicates that at interaction point 2, with an adaptation to Equation 4-15 for shear and Equation 4-7 for debonding to take into consideration the longitudinal steel and a portion of the FRP being in tension.

Thus the shear stress is now established as per TR55 (2011) Equation 8.24 and has to satisfy the following limit:

$$\tau = t_f E_{fd}\,\frac{\varepsilon_{h,rup}}{(x - R_c)} \le \tau_{lim,c} \qquad (4\text{-}18)$$

And the debonding strain is as per TR55 (2011) Equation 8.25 if the shear stress exceeds the limiting shear stress:

$$\varepsilon_{h,rup} = \varepsilon_{h,debond} = \tau_{lim,c}\frac{(x-R_c)}{t_f E_{fd}} \quad (4\text{-}19)$$

Using a concrete compressive cube strength of $f_{cu} = 42.0$N/mm^2 for specimen SE6, the axial capacity is 2053kN with a moment of 214746kNmm. The effect of imperfections is calculated as per interaction point 1 and included with the initially defined moment. Thus the resulting moment is 260962kNmm, with an applied load eccentricity of 127mm.

4.5.1.4. INTERACTION POINT 4 – MOMENT ONLY (NO EQUIVALENT SPECIMEN)

In the test matrix established in Chapter 3, there is no specimen that corresponds to point 4 of the interaction curve, representing pure moment with no axial component hence it is calculated and presented only for completeness of the interaction diagram.

The neutral axis depth is iterated until longitudinal forces in the column are in equilibrium and the concrete confinement is negligible, thus the concrete strain capacity is limited to $\varepsilon_{cc,max} = 0.0035$. The corresponding concrete stress is taken as f_{c0}. The strain distribution from the point of FRP rupture or debonding to a maximum compressive strain limit of 0.01 generates the required balance point. The effect of imperfections on the axial capacity is included in the applied moment and eccentricity as per interaction point 1.

4.5.1.5. MEDIUM-SCALE INTERACTION BEHAVIOUR

The design load, moment and eccentricity for the medium-scale specimens is presented in Table 4-13, for a concrete compressive cube strength of 24.4MPa and 42.0MPa for specimen SC4, and specimens SE5 and SE6 respectively.

Table 4-13: Medium-scale load, moment and eccentricity data to TR55 (2011)

SPECIMEN ID	DESIGN LOAD	DESIGN INITIAL MOMENT	INITIAL ECCENTRICITY	ADDITIONAL SECOND ORDER MOMENT	ADJUSTED MOMENT	ADJUSTED ECCENTRICITY
	kN	kNmm	mm	kNmm	kNmm	mm
SC4	3776	0	0	0	0	0
SE5	4270	72374	17	2725	75100	18
SE6	2053	241746	118	23292	265038	127

The interaction diagram for medium-scale specimens of concrete compressive cube strengths of 24.4MPa and 42.0 MPa is presented in Figure 4-48, alongside the behaviour of the test specimens.

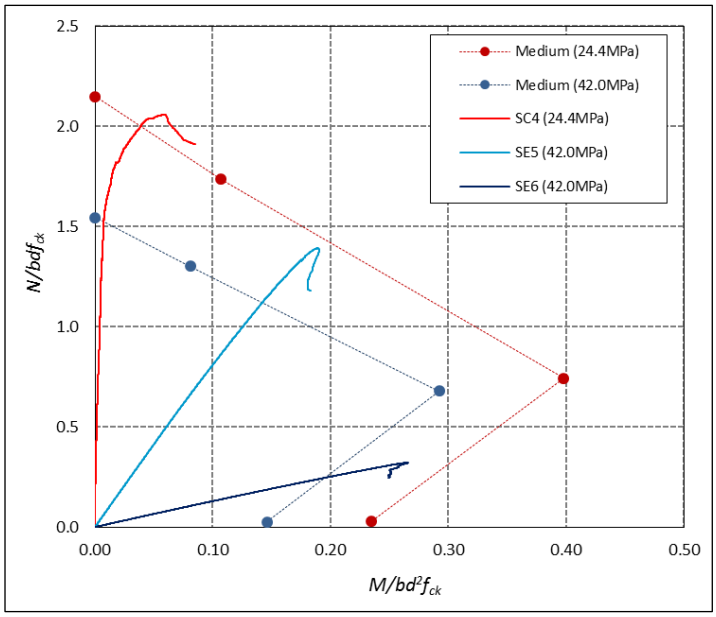

Figure 4-48: Interaction behaviour established in accordance with TR55 (2011) – medium-scale specimens

The axial capacity of concentrically loaded SC4 is suitably estimated in TR55 (2011) design process, but the moment is not taken into consideration as well, and the subsequent reduction in axial capacity has not occurred. In specimen SE5 (ECC2), the predicted axial capacity reasonably close, but again the moment is substantially underestimated. Specimen SE6 (ECC2) had an applied load profile representing the steel approximately balanced and as such dominating behaviour however this in reality is past the balance point, hence the discrepancy in axial capacity. The moment capacity is similar to that determined for

interaction point 3, hence this point requires further investigation. It is recommended from the offset in TR55 (2011) that the design methodology is not used for specimens where the longitudinal steel has yielded, and these results demonstrate that it is imperative to heed this advice. Furthermore design factors have been omitted that would reduce the estimated axial capacity.

In comparison with that presented in Sections 4.2 and 4.3 for medium-scale concentrically and eccentrically loaded specimens respectively, TR55 (2011) design methodology provides a more accurate overall representation and comprehensive methodology. In the previous design, refer to Figure 4-5 and Figure 4-20, for SC4 (interaction point 1) and SE5 (interaction point 2) the axial capacity was greatly underestimated thus once design factors had been applied there would have been little room for an achievable increase in capacity to warrant use of the technique for strengthening.

It is necessary to consider that the interaction diagrams were based loosely on the information available in TR55 (2005) and from general stress-strain design practice. Thus TR55 (2011) is already a more meticulous design methodology to follow and can be develop with further insight into behaviour as the test database for medium- and large-scale specimens expands.

4.5.2. COMPARISON WITH EXPERIMENTAL RESULTS

Using the TR55 (2011) methodology presented in Section 4.5.1, all FRP-confined specimens presented in Table 3-1 have been evaluated. The variation in predicted load between design methodology using TR55 (2005) presented in Chapter 3, the updated TR55 (2011) design calculations, and actual peak load achieved in testing is detailed in Table 4-14. Further information on TR55 (2005) design and results can be found in Table 4-1, Table 4-5 and Table 4-9 for Series SC, Series SE and Series RC/E respectively.

Table 4-14: TR55 (2011) design calculation comparison

SERIES	SPECIMEN ID	INITIAL DESIGN PREDICTED LOAD	DESIGN PREDITED LOAD TR55 (2011)	PEAK LOAD	TR55 (2011) vs PEAK LOAD VARIATION %	RUPTURE STRAIN	DEBONDING STRAIN
		kN	kN	kN			
SC	SC2	995	1108	936	15.5	0.0053	N/A
	SC4	3486	3776	3617	4.20	0.0053	N/A
	SC6	7548	8225	7364	10.5	0.0053	N/A
SE	SE2	851	982	812	17.3	0.0053	0.0041
	SE4	540	460	249	45.8	0.0053	0.0028
	SE5	3729	4270	4200	1.65	0.0053	0.0044
	SE6	2434	2053	970	52.8	0.0053	0.0030
	SE7	8110	9344	9120	2.40	0.0053	0.0044
	SE8	3633	2993	2287	23.6	0.0053	0.0022
RC/E	RC2	5232	5106	4434	13.2	0.0044	N/A
	RC4	6627	6489	6124	5.62	0.0040	N/A
	RE1	5972	6091	5637	7.46	0.0040	0.0072
	RE2	2526	4634	1934	52.3	0.0040	0.0068
	RE3	4474	5721	6303	-10.2	0.0040	0.0031
	RE4	2196	3339	1411	57.8	0.0040	0.0027
	RC6	7651	7892	6593	16.5	0.0038	N/A

TR55 (2011) in all but one instance overestimates the axial capacity. The specimens highlighted in red were subject to ECC2 load profile and as such, TR55 (2011) advises not to use the design procedure for this case, as evident with the 23.6% to 57.8% exceedance over the actual peak load. For square specimens with concentric or ECC1 loading, this is a closer representation of the behaviour than TR55 (2005) guided design, illustrated in Figure 4-49. As FRP-confinement of RC columns is primarily for an increase in axial capacity in the UK, this has been presented.

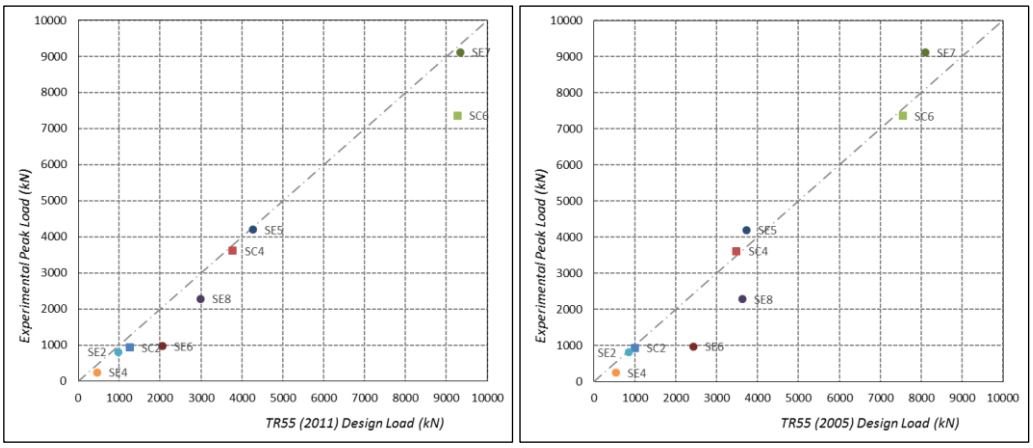

Figure 4-49: Series SC & SE – from left, TR55 (2011) Design Load vs Actual Peak Load and TR55 (2005) Design Load vs Actual Peak Load

Comparison of the two plots, highlights that there is less scatter by TR55 (2011) design, and omission of SC6 (large-scale) is necessary as this specimen failed through steel buckling, and not in the FRP.

Series RC/E addresses changing cross-sectional aspect ratio and use of the TR55 (2011) design methodology does not give an improvement on the prediction the peak axial load, see Figure 4-50. Behaviour of both ECC2 loaded specimens was dominated by steel yielding, which subsequently developed column ductility. To represent this adequately, the axial capacity needs to be considered in combination with this. Through analysis of the axial capacity of rectangular specimens, there is a room for improvement in design for large aspect ratios and as such, the guidance may not be the best to be used, as specified for this.

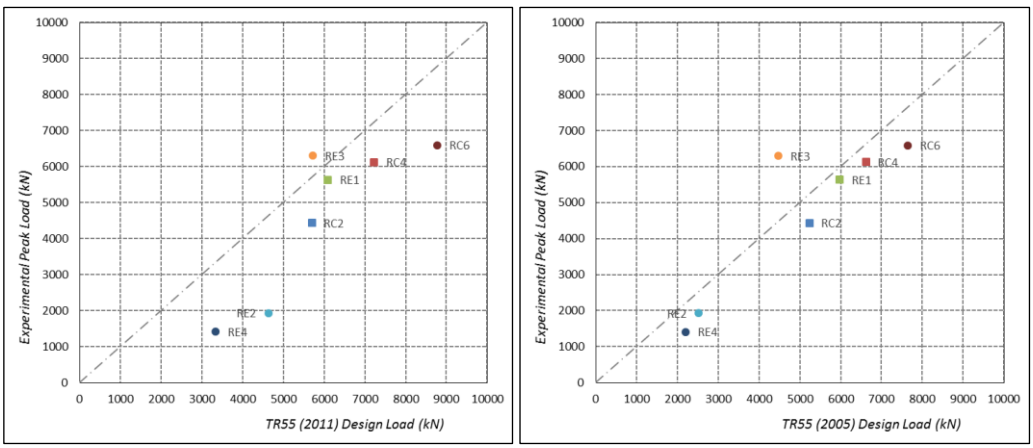

Figure 4-50: Series RC/E – from left, TR55 (2011) Design Load vs Actual Peak Load and TR55 (2005) Design Load vs Actual Peak Load

The cross-sectional aspect ratio of specimen RC2 is within the advised limits of use for design by TR55 (2011) but the methodology as detailed in Chapter 3 gave a more reasonable prediction. However this is one specimen only, and to ascertain if the prediction is better using the TR55 (2005) version of the guidance, more reference specimens are required.

The FRP rupture strain is significant in the determination of the specimen capacity and is approximately 20-30% of the FRP ultimate strain, reducing with increasing cross-sectional aspect ratio. As the debonding strain is a function of the shear stress, this varies with the neutral axis, and as such reduces with increasing load eccentricity. In most instances, this is less than the rupture strain. Hence, the likelihood of debonding increases with increasing aspect ratio, further decreasing the axial capacity.

Further assessment looking at the interaction diagrams to consider the moment capacity established is necessary and presented in Sections 4.5.2.1 and 4.5.2.2.

4.5.2.1. INTERACTION BEHAVIOUR – SERIES SC & SE

To fully evaluate the prediction of load from TR55 (2011) against the experimental behaviour of the specimens, interaction diagrams for all tested specimens were created. The interaction diagrams for the remaining specimens in Series SC and SE are presented in Figure 4-51 and Figure 4-52 for small-scale and large-scale respectively.

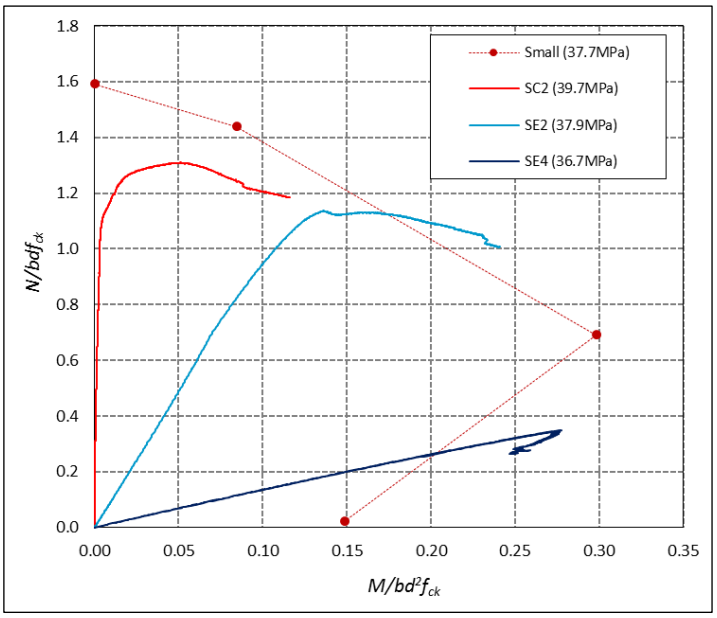

Figure 4-51: Interaction behaviour established in accordance with TR55 (2011) – Small-scale specimens

Axial capacity over-estimation is evident again in small-scale results, with a greater moment than anticipated in SC2 (CON) and SE2 (ECC1), subsequently reducing the axial capacity. There is a trend of over-estimation of ECC2 profile axial capacity and design of SE4 must have been look beyond the point of longitudinal steel yielding as the axial capacity is not reached as the moment has a greater impact on the specimen than originally thought.

The interaction action curves developed for reference against TR55 (2005) are shown in Figure 4-4 and Figure 4-19 for concentric and eccentric loading, and illustrate a closer axial prediction for SC2 and SE2 but the moment capacity is not estimated well. Thus, TR55 (2011) design includes procedure to incorporate additional second order moments which are significant, thus is a more representative design procedure.

The large-scale interaction behaviour according to TR55 (2011) design process is presented in Figure 4-52.

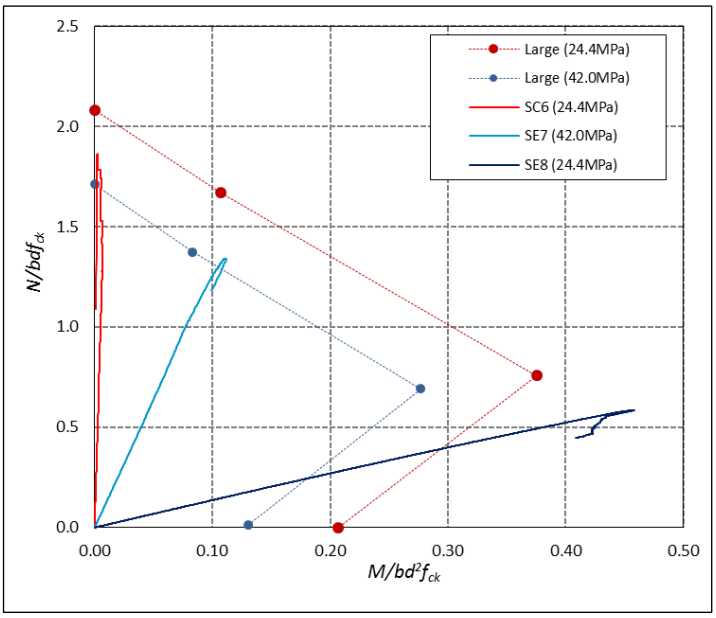

Figure 4-52: Interaction behaviour established in accordance with TR55 (2011) – Large-scale specimens

SC6 reaches close to the predicted axial load with no moment, as is evident in Figure 4-6. SE7 again is close to the predicted axial load capacity, with little post-peak ductility occurring. Significant exceedance of the interaction curve can be seen with SE8 and again the axial capacity is not achieved due to the moment, or lateral deflection influencing the results. The previous analysis can be seen in Figure 4-21.

Interaction behaviour in small- and large-scale specimens correlates with the medium-scale behaviour in Figure 4-48. In terms of concentrically and eccentrically loaded FRP-confined square columns, the results have consistently shown that there is an over-estimation of the axial capacity, as the effect of the lateral deflection and subsequent moment has not been encompassed. The ECC2 profile has been advised not to be addressed using the TR55 (2011) methodology and this should be heeded.

4.5.2.2. INTERACTION BEHAVIOUR – SERIES RC/E

Interaction diagrams for the specimens in Series RC/E are presented. Concentrically loaded specimen RC2, with cross-sectional dimensions of 300x450mm (aspect ratio of 1:1.5) is presented in Figure 4-53. This is within the advised limits of use for TR55 (2011).

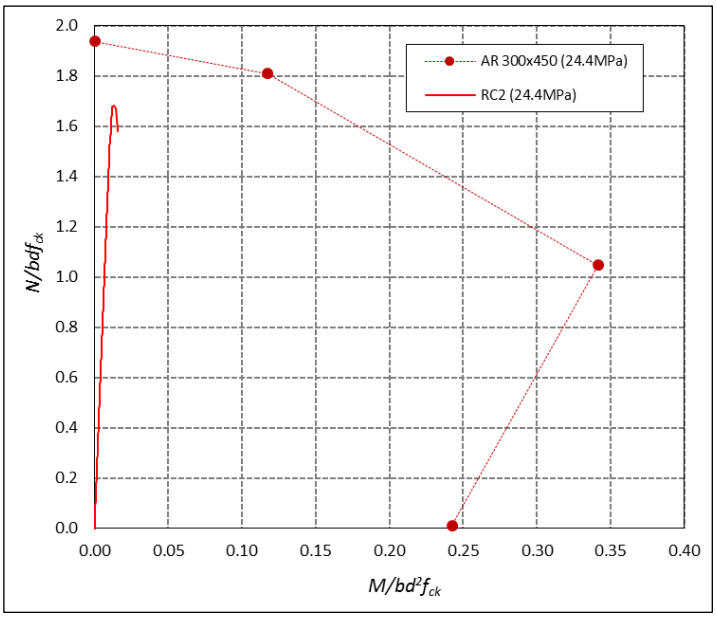

Figure 4-53: Interaction behaviour established in accordance with TR55 (2011) – 300x450 aspect ratio specimens

The axial capacity of RC2 is overestimated following TR55 (2011) design methodology, with little lateral deflection and moment in the test specimen to justify the reduction in axial capacity. Comparison with TR55 (2005) design in Figure 4-34 shows that it is equally overestimated. No specimens of this aspect ratio were tested to evaluate behaviour under eccentric loading.

The 300x600mm cross-section specimens loaded concentrically and eccentrically on the major axis are presented in Figure 4-54. It must be noted that the aspect ratio of this prismatic specimen of 1:1.5 is not within the range advised for use of this guideline.

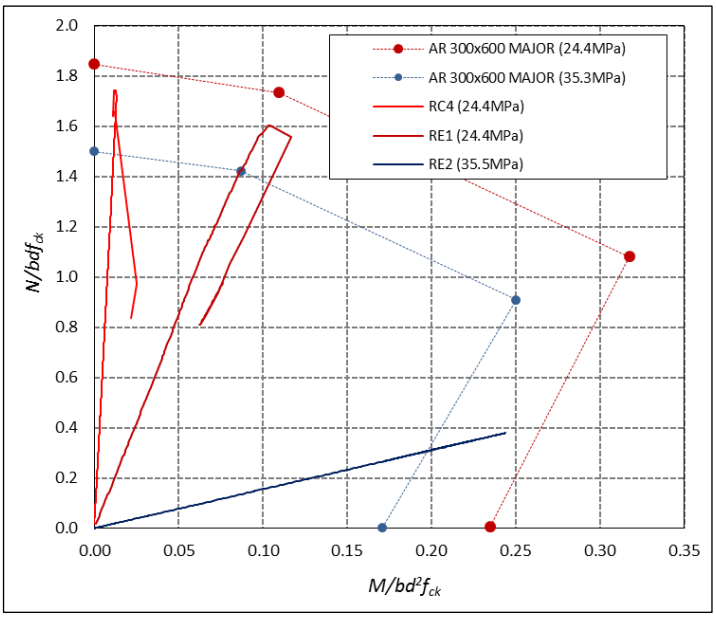

Figure 4-54: Interaction behaviour established in accordance with TR55 (2011) – 300x450 aspect ratio specimens with major axis loading

Again, in all instances the axial capacity is overestimated, and the moment combination with axial are very reasonable for concentric and ECC1 loading profiles. Comparison with Figure 4-35 shows a slightly closer prediction with RC4 and RE1, but the significant improvement is in the moment prediction of RE2. However, as seen with other specimens, the ECC2 axial capacity prediction is consistently lower than anticipated.

Specimens of cross-sectional dimensions 300x600mm are loaded on the minor axis are presented along with concentrically loaded specimen RC4 in Figure 4-55.

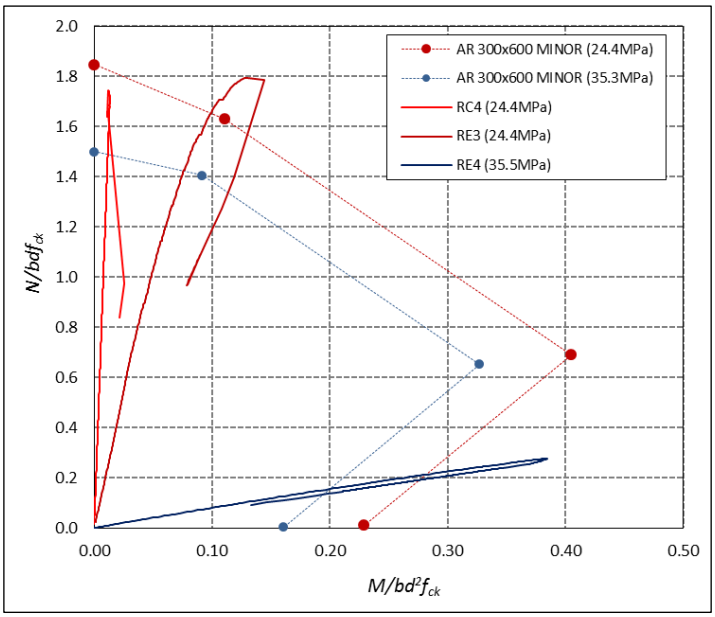

Figure 4-55: Interaction behaviour established in accordance with TR55 (2011) – 300x600 aspect ratio specimens with minor axis loading

Both the eccentrically loaded specimens differ from their corresponding points 2 and 3 on the interaction curve. The predicted axial capacity for RE3 is less than achieved in testing, and the path to peak load demonstrates good applied eccentricity and lateral deflection combination to produce the design strain profile over the section. The predicted axial capacity of RE4 is consistently twice the actual capacity in testing and the moment, as dominated by steel behaviour, exceeds the design curves. Evaluating against Figure 4-36 it is evident that design prediction is more reasonable as an under estimation of capacity.

Interaction behaviour for the 300x750 cross-section, aspect ratio of 1:2.5 is shown in Figure 4-56.

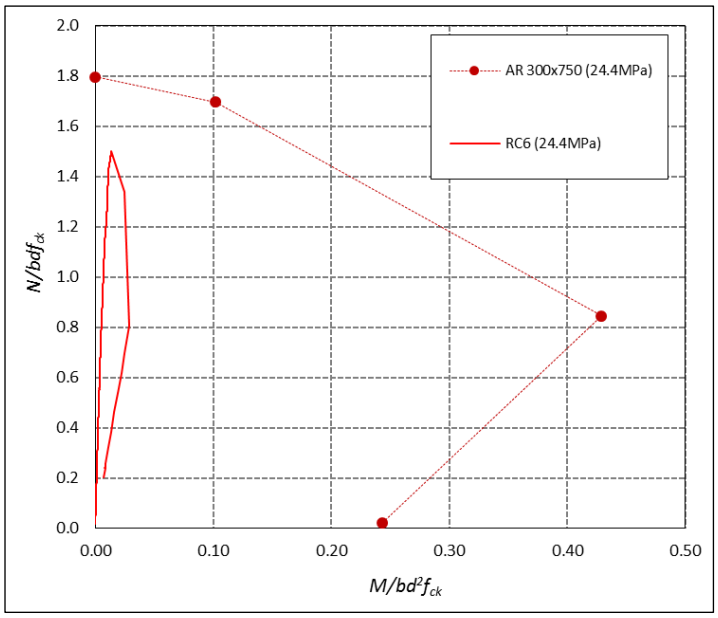

Figure 4-56: Interaction behaviour established in accordance with TR55 (2011) – 300x750 aspect ratio specimens

RC6 prediction is overestimated for axial behaviour unlike in Figure 4-37. The cross-sectional aspect ratio is far greater than the maximum aspect ratio advised for use of this guideline.

For rectangular cross-sections, the guidance is regularly over-estimating the axial capacity, with less consistency in behaviour to be confident of the use. However there is limited repetition of tests here and as such, the advice not to use the guidance for aspect ratios greater than 1:1.15 should be adhered to until further research can shed light onto the behaviour and help understand application of the TR55 (2011) design methodology to specimens that do not adhere to the limits of use.

4.5.3. TR55 (2011) COMPARISON SUMMARY

The purpose of this comparison of test results with TR55 (2011) methodology was to establish if it is a close representation of the behaviour for concentrically and eccentrically loaded, square and rectangular columns. The results are positive for specimens that are within the recommended limits of use.

It became apparent that in Series SC and SE (square specimens) the axial capacity is overestimated consistently for load profiles concentric and ECC1. Profile ECC2 was consistently around 50% less than the predicted axial capacity but the true effect of the

lateral deflection and subsequent moment applied to the specimen may not be fully captured. Realistically, when looking at the initial design, the specimen likely has a profile between interaction points 3 and 4 as the additional second order moments were not address in the initial design.

Representation is reasonable, axial capacity is overestimated but this is consistent over the specimens. Moment is more reasonably established. Results are consistent for specimens within the recommendation of the limits of the guidance. Beyond these limits, it is more sporadic and requires further evaluation specifically, the axial capacity for ECC2 profiles. Moment is done well and axial could be considered.

Also, the actual profile of the specimens is not as originally designed in Chapter 3 as the lateral deflection is present in all and reasonably large with increasing eccentricity and perhaps does not reduce the axial capacity enough in the design.

4.6. CONCLUDING REMARKS

To conclude the chapter on experimental testing, the key observations found from analysis of the results are:

- *STRENGTH CAPACITY*

  FRP-confinement of square and rectangular columns when concentrically loaded provides an increase in strength capacity. It is more effective for square specimens than rectangular specimens, due to the increased proportion of the cross-sectional area being effectively confined.

- *SLENDERNESS*

  Analysis of the results revealed that although no moment was directly applied on concentrically loaded specimens, the residual P-Delta effects were apparent and should be taken into consideration at the design stage for FRP-confined specimens as this will affect the axial strength capacity of the specimen. The slenderness effect reduced with increasing cross-sectional aspect ratio.

- *AXIAL-FLEXURAL LOADING*

  Applying a flexural element with the axial loading, reduced the axial capacity of the column but the deformation capacity substantially increased. In terms of FRP wrapping, the confinement provided in the experimental series proved to be insufficient in some cases, but to negate this, FRP straps as opposed to full layers would help increase the capacity of the specimens with a lower cost aspect.

- *FRP STRAIN CAPACITY*

  The FRP maximum strain measured in the gauges was substantially lower than the FRP ultimate strain established from the coupon tests in Chapter 3. Through analysis of the medium-scale specimens, the maximum rupture strain as detailed in TR55 (2011) gave a reasonable estimation, which tends to be 25% to 40 % below the ultimate strain. This needs to be taken into consideration in design. Furthermore, TR55 (2011) identified the debonding strain through use of the limiting shear stress, which is a further reduction on the FRP maximum strain, and again correlated well with the results.

- *DEBONDING*

  Debonding occurred in all medium- and large-scale specimens to varying degrees, where failure occurred through rupture of the FRP jacket, becoming more pronounced with the larger specimens that had the greater flat side dimensions. As the entire flat area of the sides between the corners was susceptible to become completely debonded, this leaves no redundancy if accidental rupture was to be generated. Thus, consideration in design and modelling is required as the debonding strain is lower than the maximum strain.

- *TR55 (2011) DESIGN GUIDANCE COMPARISON WITH RESULTS*

  Fundamentally, TR55 (2011) is a reasonable representation of the behaviour when using within the recommended criteria. Outside these criteria consideration needs to be paid to the results, especially the stated axial capacity. Further large-scale testing will expand the experimental data base and as such allow for the guidance to cover a greater variance in cross-section thus be developed beyond the current set limitations.

CHAPTER 5

ANALYTICAL MODELLING

5.1. INTRODUCTION

This chapter details the analytical model developed to better capture the behavioural mechanics over the prismatic cross-section of the FRP-confined specimens presented in Chapter 4. The existing models for prismatic columns are considered and ultimately, the model from TR55 (2005) from which experimental design was established, is adapted to reflect the increased knowledge on the behaviour of the effectively confined area, with additional reference to the latest version, TR55 (2011).

The adaptions to the model take the form of an altered confinement effectiveness factor, k_s. The adaption of the shape factors then enables the shape and loading profile of the prismatic columns to be considered more accurately. Furthermore, as the effect of applied load eccentricity has been seen to be significant in experimental results, (Chapter 4) the movement of the effectively confined area is reflected through the inclusion of the shear stress generated in the flat sides of the FRP jacket between the curved corners.

5.2. BACKGROUND

The confinement mechanics of a prismatic cross-section are relatively complex in nature when compared with a circular cross-section, and the general assumptions on the confinement provided by the FRP jacket to the concrete core tends to take one of two forms:

1. The cross-section is assumed have an effectively confined area, with the remainder of the cross-section outside this area, assumed to be fully unconfined. The shape of

this effectively confined area is based on arbitrary assumptions with the confinement forming a cruciform shape along the diagonals and as such, the areas in close proximity to the flat sides of the column are unconfined.

2. An effective circular cross-section of diameter *D* is assumed for the prismatic cross-section, thus the prismatic section is understood to be in a state of uniform biaxial confinement and the formulae are adapted to produce a confinement level suitable for this shape.

In this research, the first approach, which assumes a cruciform-shaped effectively confined area is deemed more appropriate than the second approach, as there is a greater opportunity to accurately capture the behaviour when a flexural element to the load is included.

5.2.1. EFFECTIVELY CONFINED AREA

Utilising the first approach detailed above, the effective confinement of a concentrically loaded prismatic specimen has a parabolic stress profile distribution assumed over the cross-section. The major concentration of the stresses arising from the FRP jacket is at the corners, with stresses of reducing magnitude distributed along the diagonals. This has been corroborated with FEM demonstrating the stress concentration reducing with increasing distance from the corners, Figure 2-20. The level of confinement provided outside this cruciform shape, by the flat sides of the specimen, is negligible if present, hence it is assumed to be of no confinement at all for analysis, Figure 5-1.

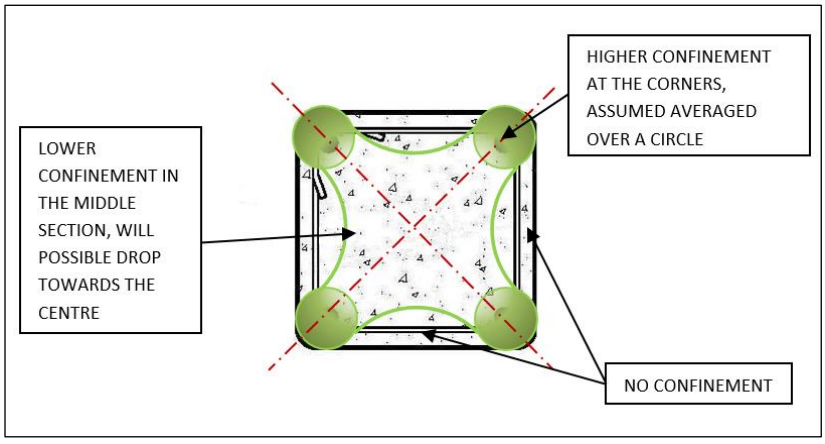

Figure 5-1: Postulated shape of the effectively confined area for a concentrically loaded specimen of square cross-section

In reality, the load is never purely axial, as a flexural element exists in the loading whether intentional or induced by an additional second order moment, and as such the distribution of confinement over the cross-section varies. As the eccentricity of the load increases, it is postulated to move into the area of higher compressive stress, Figure 5-2. The cruciform shape adapts to the uneven strain distribution in the FRP jacket, and the change in stress concentration at the corners while not explicitly known, is still found to be the area of highest stress concentration with respect to FEM, Figure 2-21.

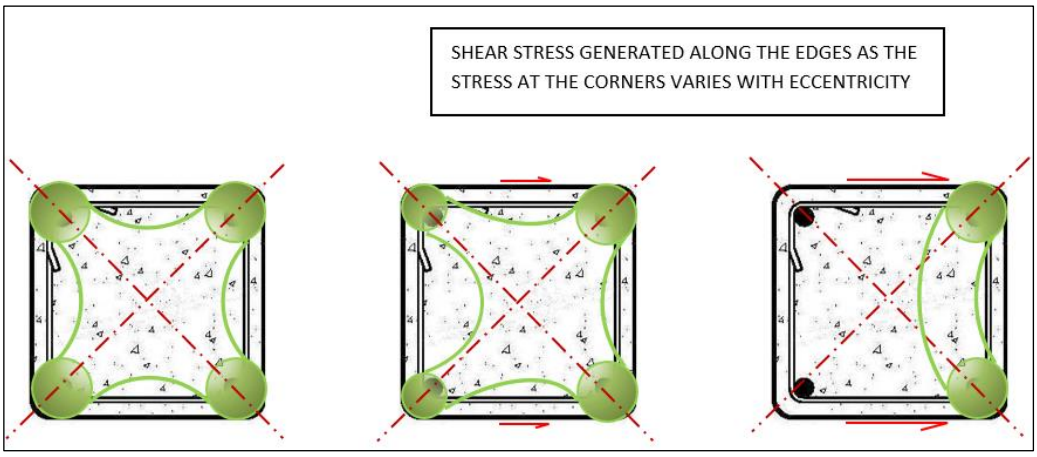

Figure 5-2: Postulated evolution of the effectively confined area with increasing load eccentricity, corresponding to experimental loading profiles; concentric, ECC1 and ECC2

The strain profiles selected for experimental testing corresponds to interaction points 1, 2 and 3, as detailed in Figure 4-3. These points are characterised by:

1. A pure axial load is applied to the specimen generating uniform axial compressive strain around the FRP jacket. This shape of the effectively confined area for this is seen in the left hand image of Figure 5-2.
2. An axial-flexural load is applied to generate maximum compressive strain at the top of the specimen and zero axial strain at the bottom, at the tensile face (ECC1). This is illustrated in the middle image of Figure 5-2.
3. An axial-flexural load is applied to generate a balance failure with the maximum axial compressive strain at the top face and a tensile strain in the yielded longitudinal steel at the bottom (ECC2). This is depicted in the right hand image of Figure 5-2.

In the experimental testing presented in Chapter 4, as the applied load eccentricity on the specimen increased, the strain in the FRP jacket generated at the corners reduces on the

lower compressive stress/tensile stress side of the cross-section. Taking the medium-scale FRP-confined square specimens (SC4, SE5 and SE6) from Series SC and SE, this is visualised in Figure 4-8, Figure 4-23 and Figure 4-24 for the concentric, ECC1 and ECC2 loading profiles. Analysis of the FRP strain in close proximity of the corners, validates that the highest stress present is in the corners on the compressive side of the specimen. The variation in strain between the corners consequently induces shear stress in the concrete-FRP bond between the corners on the flat sides of the column. The magnitude of the shear stresses are established and guidance from TR55 (2011) gives a methodology for determining the limiting shear stress, see Equation 4-3, and an estimation from this shows the likely occurrence of debonding.

Hence the aspects to be addressed in evaluation of the effectively confined area are:

1. The magnitude of the stress over the cross-section, with specific consideration at the corners where the concentration is highest
2. The division of the cross-section for the different magnitudes of stress, specifically:
    a. Division between the effectively confined area and non-confined area
    b. Division of the effectively confined area for varying magnitude of stress

Where a flexural element is also included, the following aspects also need to be determined:

3. The development of shear stresses in the FRP between the corners and the spread of these stresses over the cross-section
4. The movement of the effectively confined area into the compressive side of the specimen, specifically with respect to the shape that forms and the change in magnitude of the stresses

Taking all aspects above into consideration, the theoretical stress in each defined area over the cross-section is determined and compared with experimental results for validation of the proposed methodology.

5.2.2. THE CONFINEMENT EFFECTIVENESS FACTOR

The confinement effectiveness factor has been adopted in many design-oriented stress-strain models, to encompass the shape effect from the prismatic specimen. The value taken for the confinement effectiveness, *k*, can be adapted to accurately reflect the experimental

results of the author or others works. From TR55 (2005), the fundamental definition for failure stress for hydrostatic pressure defined by RIchart et al. (1928) and detailed in Equation 2-2, is adapted using the confinement effectiveness constant *k*, for establishing the confined strength:

$$f_{ccd} = f_{co} + k\, f_r \tag{5-1}$$

Where the confined pressure for a circular section is given by:

$$f_r = \frac{2\, f_{fd}\, t_f}{D} \tag{5-2}$$

The value adopted for *k* varies with researchers and tends to take either a nonlinear form, defined in terms of f_l/f'_{co} or just f_l, or a constant, normally between 2.0 and 3.3 [Mirmiran and Shaahawy (1997), Razvi and Saatcioglo (1999), Harries and Kharel (2002), Marques et al. (2004) and Lam and Teng (2007)]. TR55 (2005) recommends use of Equation 39 which uses a failure criterion based on confinement stiffness as opposed to confinement pressure, established by Lillistone and Jolly (2000), to overcome the lack of correlation with the lateral strains. The advantage of this is that the failure criterion does not require prior knowledge of the lateral expansion of the concrete core. Thus for circular columns they suggest:

$$f_{ccd} = f_{c0} + 0.05 \left(\frac{2t_f}{D}\right) E_{fd} \tag{5-3}$$

where: E_{fd} is the design elastic modulus of FRP.

To incorporate the prismatic shape and the varying confinement, TR55 (2011) Equation 47 is recommended:

$$f_{cc} = f_{co} + 2.0\, g_s\, f_r \tag{5-4}$$

Where g_s is the shape factor considering the ratio of effective area to cross-sectional area:

$$g_s = \frac{b}{h}\frac{A_e}{A_g} \tag{5-5}$$

And the equivalent confining pressure, f_r, uses $D = \sqrt{(b^2 + h^2)}$ as defined by Lam and Teng (2003) in Equation 5-2. For a detailed explanation of this, refer to Chapter 3, Equations 3-10 to 3-14.

The approach of using a shape factor to define the ratio of the confined area to that of the gross area, was also used by Pessiki et al. (2001), establishing *k* as:

$$k_e = 1 - \frac{2}{3}\left[\frac{\left(1-2\frac{r}{b}\right)^2}{1-(4-\pi)\left(\frac{r}{b}\right)^2}\right] \quad (5\text{-}6)$$

This definition for the shape factor here is for square cross-sections but it gives opportunity to consider rectangular shaped cross-sections.

5.2.3. TR55 (2011) VARIATION IN DESIGN APPROACH

The latest edition of TR55 (2011) differs from TR55 (2005), assuming a simpler average confining stress rather than establishing the effectively confined area. This approach, when combined with equilibrium models and based on Darby et al. (2011) and Karam and Tabbara (2005) gives an effectiveness factor which is specified as:

$$k_e = \frac{R_c}{b}\left(1 + \frac{b}{h}\right) \quad (5\text{-}7)$$

And this is used as per description in Section 2.7.3.

TR55 (2011) considers axial flexural loading through assuming a variation of stresses over the cross-section as a simple average of the stresses leading to a conservative overestimation in design. An interaction diagram is created using a four step process, defining load states from pure axial load to pure moment with zero axial load. This diagram takes the shear capacity and additional second order moment of the column into consideration but it is quite an arduous process if numerous specimens of varying geometry and load profiles are to be designed.

5.3. PROPOSED ANALYTICAL MODEL

The proposed analytical model addresses in a simple manner, purely axially loaded columns and then deals with the addition of a flexural element of loading by taking into account the shear stress generated along the flat sides between the curved corners. Key assumptions made with the analytical model are that:

- For concentric loading, the bond between the concrete and the FRP remains perfect, hence debonding is negated at this point
- The tensile strength of the concrete is neglected
- Confinement generated from reinforcing steelwork is neglected
- Plane sections remain plane

Medium-scale specimens have been selected as the most appropriate set for initial model development as the failure modes experienced were as predicted, and the FRP gauges performed as expected, i.e. reasonable strains, shown in Figure 4-8, Figure 4-23, and Figure 4-24 for concentric, ECC1 and ECC2 load profiles respectively. Furthermore, Series RC/RE, addressing the effect of axial and axial-flexural loaded specimens of varying cross-sectional aspect ratio are medium-scale, with the short side length always 300mm, leading to a reasonable comparison.

The assumptions on the shape of the effectively confined area generated from FEM plots have been verified with the experimental results, as the strains present at the corners of the FRP jacket were investigated. Gauges were mounted on either side of the corners from which the force in the FRP jacket was established, allowing for determination of a force vector generated at the corners. From this force vector, the parabolas of the effectively confined area were determined and plotted, originating from the ends of the flat sides, and forming the effectively confined area, Figure 5-3.

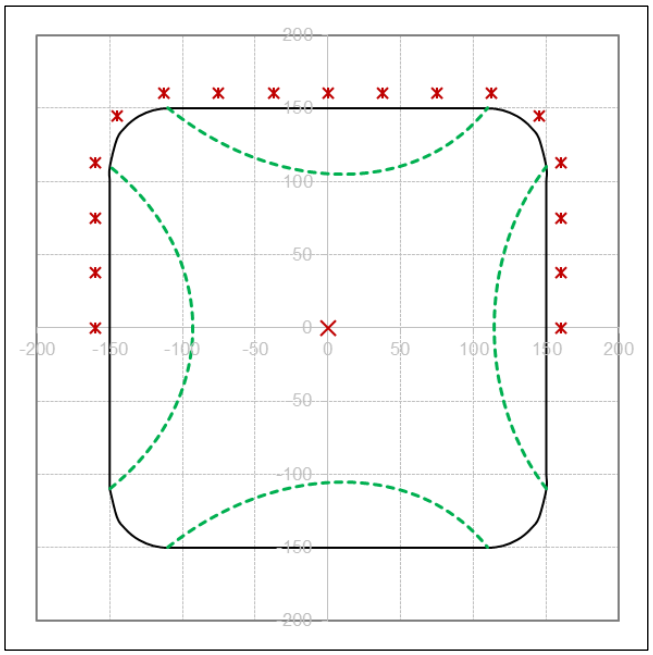

*Figure 5-3: Effectively confined area, generated from the FRP strains at the gauges adjacent to the corners for medium-scale specimen SC4 (X marks position of applied load, * marks the position of the strain gauges)*

The effectively confined area for a concentrically loaded specimen takes a cruciform shape as postulated. The angle of the parabolas from the flat sides of the cross-section are not exactly 45 degrees due to the inherent P-Delta effects in the specimen, causing a slight eccentricity of loading. This lack of symmetry over the y-axis, due to the lateral deflection identified in Table 4-1, is small enough to ignore for initial development. Thus the postulated cruciform shape can be assumed for establishing the confinement effectiveness factor for model development.

5.3.1. THE CONFINEMENT EFFECTIVENESS FACTOR

In prismatic columns, measurement of the FRP strain around the cross-section in experimental testing revealed that strains are highest at the corners, which has been corroborated by others [Al-Salloum (2007), Barrington et al. (2011), Pham and Hadi (2014)] and the stress subsequently can be assumed to be distributed in a cruciform shape along the diagonals, as per Figure 5-3. This further varies as eccentric loading is applied and the effective confinement migrates into the area of higher compressive stress, but the strains are still higher at the corners located on the compressive side of the cross-section.

To address the division of confinement and non-confinement over the cross-section and the associated levels of stress within the confined area, the concentrically loaded column is addressed first. In order to establish the model, the average confined strength of the cross-section is defined by Equation 5-4, assuming a reasonable value for *k*:

$$f_c = f_{co} + k\sigma_{av} \tag{5-8}$$

where: σ_{av} is the in-plane average stress at preselected points over the cross-section

The average in-plane stress is established directly from experimental strain gauge readings situated at the mid-height of the specimen. The strain components are used to determine the stress over parabolas on the diagonals of the cross-section. Further to this, the out-of-plane stress over the cross-section is established using Equation 5-4 and corroborated with the peak stress of the specimen from experimental testing. Thus an initial confinement effectiveness factor is established.

From the FEM stress plots of the cross-section, the three areas for different levels of stress were approximated. These three areas and their associated confinement levels are; the four corners as concentrically loaded so similar distribution over the two axis of symmetry (high confinement), the cruciform shape between the corners (medium confinement), and the remaining unconfined areas (no confinement). These are superimposed on the FEM stress plot, Figure 5-4.

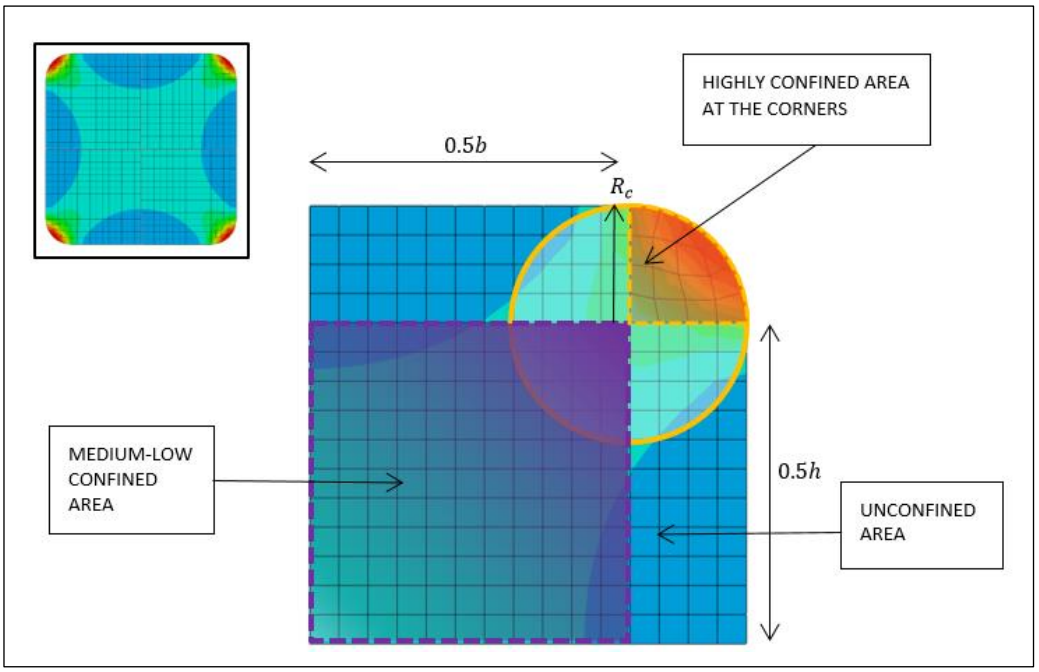

Figure 5-4: Approximation of areas of confinement for a concentrically loaded column

To break this down, the areas are established as:

1. *CORNER REGION*

   High confinement is assumed to be one quarter of the circle formed from the corner radius, as the entire area of the circle has been shown to be a gross overestimation in FEM. The level of stress in this area is taken to be equal to that of a circular column due to the curvature of the corner radius, thus for the cross-section:

$$A_{c,high} = \pi {R_c}^2 \quad (5\text{-}9)$$

   And the stress in this area, equal to a small circular column is:

$$f_{ccd,high} = [1 + 3.5\,(\rho_k - 0.01)\,\rho_\varepsilon]\,f_{c0} \quad (5\text{-}10)$$

2. *CRUCIFORM REGION*

   Medium confinement is assumed, taken as a square from the central point of the circle defined by the corner radius. The level of confinement in this region is one third of the corner stress:

$$A_{c,med} = (h - 2R_c)(b - 2R_c) \quad (5\text{-}11)$$

   Where the stress is equated as:

$$f_{ccd,med} = f_{co} + 2.0\, g_s\, f_r \quad (5\text{-}12)$$

3. *UNCONFINED REGION*

   Unconfined region is assumed due to the proven negligible confinement outside the effectively confined area. The area is the remainder of the cross-section and is calculated as follows:

$$A_{uc} = 2(h - 2R_c)R_c + 2(b - 2R_c)R_c \quad (5\text{-}13)$$

   The stress in the unconfined region is not included for assessment of confinement purposes.

For the concentrically loaded medium-scale specimen SC4, the ratio of high confinement (corner stress) to the remainder of confinement over the cross-section is 6%.

Using data from the FRP strain gauges to establish the confinement effectiveness factor to encompass the stress distribution over the cross-section for different levels of confinement was found to be *k=2.7* (Refer to Appendix C for full methodology and associated figures).

5.3.1.1. ADAPTION TO ACCOUNT FOR AXIAL LOAD ECCENTRICITY

To account for flexural loading applied to the column, the FRP strains from specimens SE5 and SE6, load profiles ECC1 and ECC2 respectively, are evaluated to ascertain the movement of the effectively confined area, Figure 5-5. The location of the applied load is marked, alongside the calculated eccentricity when taking the measured mid-height lateral deformation into consideration (this was not incorporated in the initial design procedure adopted from TR55 (2005)).

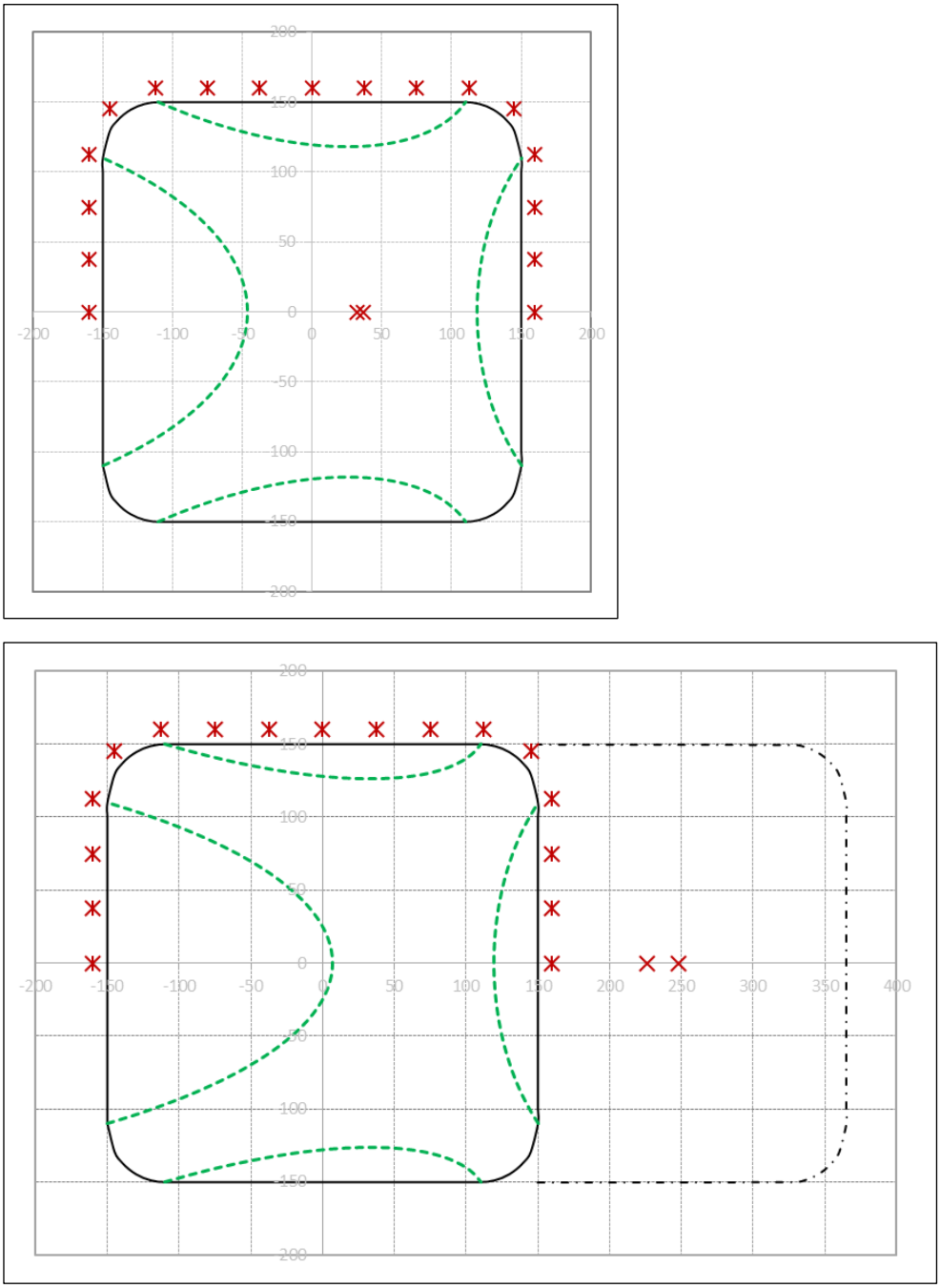

Figure 5-5: Postulated effectively confined area, generated from the FRP strains at the gauges adjacent to the corners for medium-scale specimens; from top SE5 (ECC1) and SE6 (ECC2) (applied load eccentricity signified by 'X' closest to the origin, and other included the lateral deformation measured at mid-height)

A key assumption in the generation of the concentric model is that the forces at the corners are applied at 45 degree angle before division into the components. From Figure 5-5, the distribution of the stress in the corner in the area of higher compressive is of a reasonably similar shape to the concentric model thus the assumption of generation of forces at the corner at an angle of 45 degrees for determination of the high confinement area is reasonable, as corroborated by the FEM model, Figure 2-21. This generalisation is deemed acceptable as there is high stress is over a small area and it is not distributed further with changing eccentricity. The distribution of medium confinement however differs significantly.

With eccentric loading, shear stresses are generated along the flat sides of the column, Figure 5-6. To capture the effect from the applied load eccentricity, it is necessary to look at the strain variation between the corners and assess the development of the shear stresses. This shear stress is limited by the rupture strain if debonding does not occur first.

The shear stresses established are based on the assumption that the area of confinement over the cross-section moves with the neutral axis and as such, the shear stresses move similarly. For ease of modelling, the shear stress takes a linear form, shown in Figure 5-6 for the strain profile ECC1, with the neutral axis at the end of the cross-section, and for ECC2, the neutral axis moving approximately one third along the cross-section.

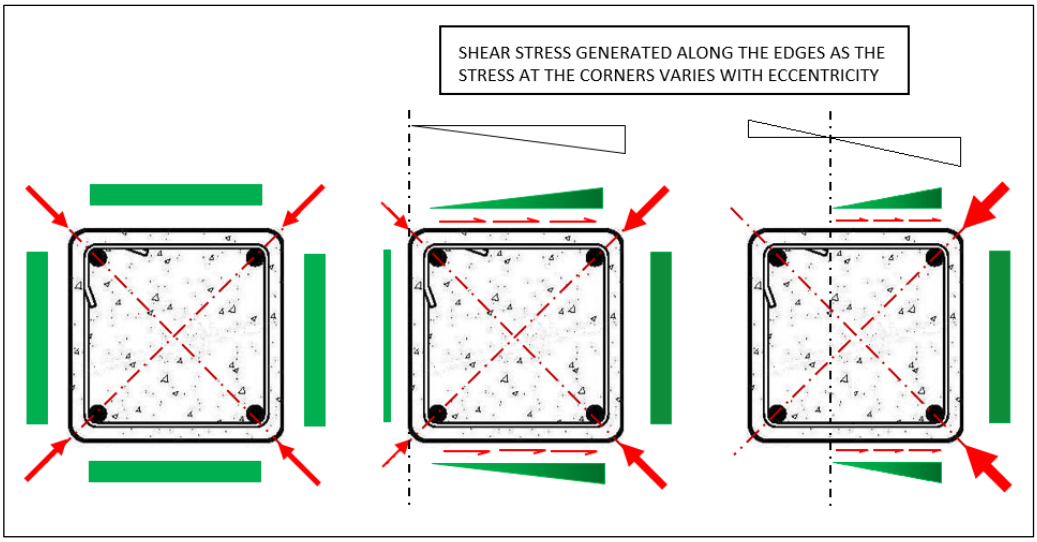

Figure 5-6: Stress distribution around the cross-section, changing with increasing load eccentricity

The average shear stress between the gauges in close proximity to the corners is:

$$\tau_{av,frp} = n_f t_f \frac{\sigma_{g1} - \sigma_{g2}}{x_g} \quad (5\text{-}14)$$

where: σ_{g1} and σ_{g2} are the stresses established from the strain readings of selected gauges

$x_g = 37.5$mm, the distance between the gauges

A further assumption is that the distribution of the shear stresses from one side of the cross-section to the other, parallel with the neutral axis can be assumed to be of a block form as opposed to parabolic for ease of modelling with greater load eccentricity. This is primarily due to the magnitude of shear being significantly lower than the stresses in the corners so is considered adequate.

The FEM stress results are presented in Figure 5-7 and the method for determining the area and corresponding stress are presented below.

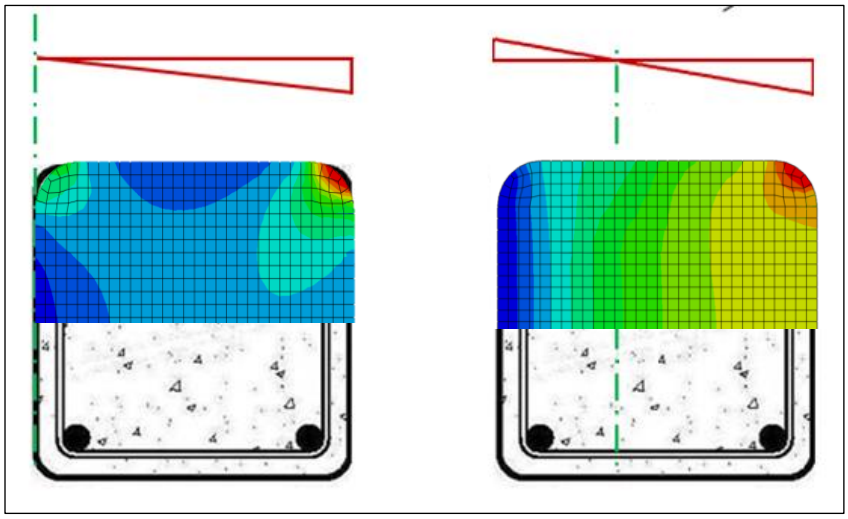

Figure 5-7: FEM stress distribution for eccentrically loaded specimens, from left; ECC1 and ECC2

To establish the magnitude of the stresses for the different areas of confinement, the three areas defined for a concentrically loaded specimen are again adopted for load profile ECC1, illustrated on the left side of Figure 5-7. These become:

1. *CORNER REGION – HIGH CONFINEMENT*

   The corner stress is as per that of the concentric specimen but only applied to the corners in the region of higher compressive stress, that is the top corners of Figure 5-8. Although the cruciform shape incorporates the bottom corners, the stress level has appreciably reduced here.

   The depth of this section is equal to the radius of the corner as with the concentrically loaded specimens.

$$A_{c,high} = \frac{\pi {R_c}^2}{2} \quad (5\text{-}15)$$

   The level of stress applied at the point is the same as Equation 5-10.

2. *CRUCIFORM REGION – MEDIUM CONFINEMENT*

   The cruciform area, (no longer necessarily taking the shape of a regular cruciform) is defined relative to the neutral axis. This effectively takes into account the movement of the confinement between the corners.

   The depth from the top of the section is *0.66x.*

$$A_{c,med} = (b - 2R_c)(h - (h - x)) \quad (5\text{-}16)$$

   The stress definition now incorporates the shear stress generated at the sides of the cross-section and takes the form of TR55 (2011) Equation 8.4:

$$f_{ccd,med} = [1 + 5.25\,(k_e\rho_K - 0.01)\rho_\varepsilon]/f_{c0} \quad (5\text{-}17)$$

   This equation applies when the confinement stiffness ratio $\rho_K \geq 0.01$, ad where insufficient confinement is generated, this approach is not advised.

3. *UNCONFINED REGION*

   The unconfined region is that below the medium confinement to the neutral axis depth.

$$A_{uc} = A_g - A_{c,high} - A_{c,med} \quad (5\text{-}18)$$

   The unconfined areas are again omitted from the confined stress calculation.

This adequately captures the confinement levels when compared with the experimental test results for specimen SE5 and the stress block for design purposes is adapted as per Figure 5-8.

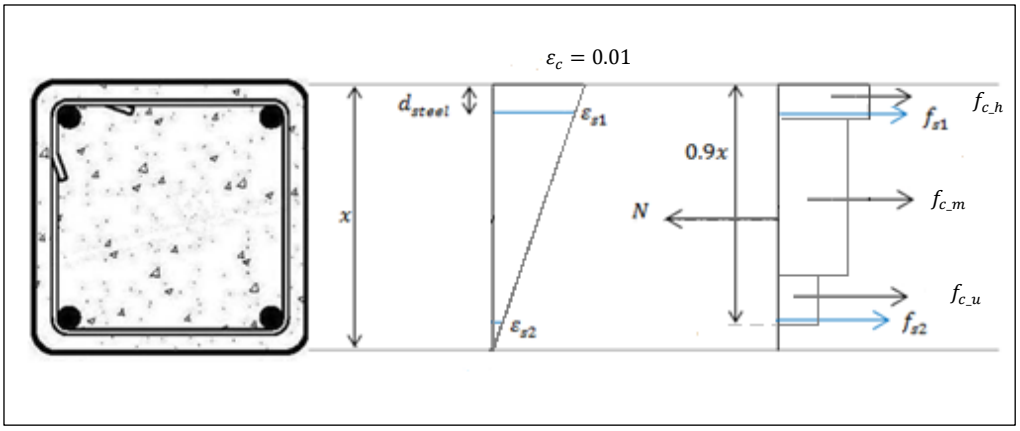

Figure 5-8: Adapted stress block for confinement areas

When the effectively confined area reaches approximately half the cross-section as with profile ECC2, Figure 5-5, the magnitude of the stresses for the different areas of confinement, need a slightly different approach than that specified for ECC1. With reference to the FEM stress result on the right hand image of Figure 5-7, the stress at the corners is still high, but with an area, rectangular in shape between the two corners. On the tensile side of the specimen there is minimal confinement, hence the area and stress are defined as:

1. *CORNER REGION – HIGH CONFINEMENT*

   The corner stress is as per that of the concentric specimen but only applied to the corners in the region of higher compressive stress, the top corners of as per Figure 5-8. The bottom corners are now fully below the neutral axis.

   The depth of this section is equal to the radius of the corner.

$$A_{c,high} = \pi {R_c}^2 + (b - 2R_c)R_c \qquad (5\text{-}19)$$

   The stress definition is as applied in Equation 5-10.

2. *CRUCIFORM REGION – MEDIUM CONFINEMENT*

   The cruciform area, (no longer necessarily taking the shape of a cruciform) is defined relative to the neutral axis and 0.75 of the area up to the top. This

effectively takes into account the movement of the confinement between the corners.

The depth from the top of the section is *0.66x*

$$A_{c,med} = (b - R_c)\, h \quad (5\text{-}20)$$

The stress definition is as applied in Equation 5-17.

3. *UNCONFINED REGION*

The unconfined region is the remainder below the neutral axis.

$$A_{uc} = h\,(b - x) \quad (5\text{-}21)$$

The unconfined areas are again omitted from the confined stress calculation.

The results have been checked against medium-scale specimen SE6 and show good correlation with the peak stress. Furthermore, specimens with profile ECC2 from the test matrix detailed in Table 3-1 are adequately predicted using this method.

Several researchers assume that the angle of the parabolas from the effectively confined area is 45 degrees from the sides of the section for all prismatic cross-sections [Lam and Teng (2003), Marques et al. (2004)] which is reasonable for purely axial loading. However, from the combination of FEM and analytical modelling suggests that this is only the case for the high confinement at the corners and instead, the lower confinement areas follow the vector found from the strains.

5.4. MODEL COMPARISON WITH EXPERIMENTAL TEST RESULTS

The analytical model was created using data from medium-scale specimens then checked and iterated against other test specimens in Series SC and SE. To verify the model, the predictions are checked against the experimental results from all test series.

As comparison is made with the experimental peak load, the results presented are established for the FRP strains measured at peak load. The FRP failure strains were also evaluated in development of the model.

5.4.1. EXPERIMENTAL SERIES SC – SIZE EFFECT

Series SC consisted of specimens of square cross-section of varying size, subject to concentric load only. The confinement behaviour has been ascertained to follow that of a cruciform shape over the cross-section due to the even generation of forces at the corners of the specimen. Thus, due to the two axis of symmetry, the prediction of peak load in the analytical model is reasonably accurate. The results of the prediction can be seen in Table 5-1.

Table 5-1: Series SC – Analytical model axial capacity prediction and comparison

SERIES ID	SPECIMEN ID	LOAD PROFILE	CONCRETE STRENGTH	EXPERIMENTAL PEAK LOAD	PREDICTED LOAD (ANALYTICAL)	VARIATION %
			N/mm^2	kN	kN	
SC	SC2	CON	39.7	936	902	-3.77
	SC4	CON	24.4	3617	3426	-5.58
	SC6	CON	24.4	7364	7122	-3.40

The variation between the experimental peak load and the predicted capacity established in the analytical model is sufficiently low to provide confidence in the first stage of the modelling process. The axial capacity is slightly underestimated, which although not ideal, is better than an over prediction. The predicted axial capacity from the analytical model is plotted against the experimental peak load in Figure 5-9.

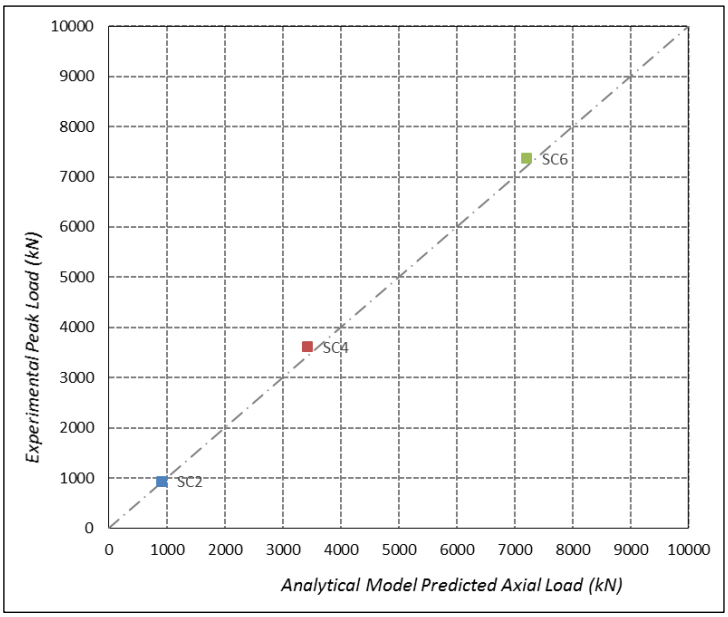

Figure 5-9: Series SC – Comparison of analytical model predicted axial capacity against experimental testing peak load

The concentrically loaded specimens have the theoretical benefit of symmetry but lateral deflection measured at mid-height of the column illustrates the need for inclusion of the additional secondary moment, thus generating small shear stress between the FRP jacket and the concrete on the flat sides.

5.4.2. EXPERIMENTAL SERIES SE – LOAD PROFILE

To encapsulate the behaviour of the eccentrically loaded specimens, the shear and potential debonding along the side of the specimens was incorporated into the model, so modelling the movement of the cruciform shaped effectively confined area into the region of higher compressive stress. Thus Series SC is included as there is a small shear stress evident along the sides due to the additional secondary moment apparent in the lateral deflection. Series SC and SE are presented in Table 5-2.

Table 5-2: Series SC & SE – Analytical model axial capacity prediction and comparison

SERIES ID	SPECIMEN ID	LOAD PROFILE	CONCRETE STRENGTH	EXPERIMENTAL PEAK LOAD	PREDICTED LOAD (ANALYTICAL)	VARIATION %
			N/mm²	kN	kN	
SC	SC2	CON	39.7	936	884	-5.88
	SC4	CON	24.4	3617	3357	-7.75
	SC6	CON	24.4	7364	7096	-3.78
SE	SE2	ECC1	37.9	812	784	-3.57
	SE4	ECC2	36.7	249	212	-17.5
	SE5	ECC1	42.0	4200	3749	-12.0
	SE6	ECC2	42.0	970	842	-15.2
	SE7	ECC1	42.0	9120	8744	-4.30
	SE8	ECC2	24.4	2287	1743	-31.2

Inclusion of the shear stress generated along the sides of the specimen lead to a greater variance between the analytical model and test results. Similarly with the initial design and design comparison with TR55 (2011), the axial capacity prediction for load profile ECC1 demonstrates greater accuracy as the dominant behaviour is in the FRP and concrete. Results show that for ECC2, the prediction is not as accurate as the steel capacity is not considered. In terms of progression, this should be included in the model as this dominates behaviour and causes failure, not the FRP jacket. The scatter of these results is presented in Figure 5-10.

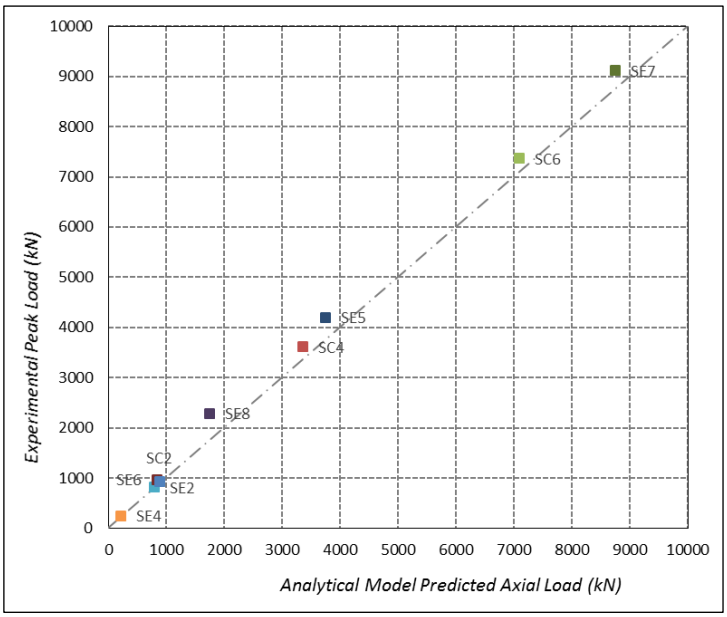

Figure 5-10: Series SC & SE – Comparison of analytical model predicted axial capacity against experimental testing peak load

Development of the model alongside TR55 (2011) would allow for a more detailed representation of the FRP jacket and concrete interaction behaviour as the eccentric load is applied thus better capturing the impact of the shear stress.

5.4.3. EXPERIMENTAL SERIES RC/E – CROSS-SECTIONAL ASPECT RATIO

The specimens in Series RC/E vary in terms of the cross-section aspect ratio as well as the applied load profile. For specimens subject to eccentric loading, the load has been applied on the major and minor axes. This analytical model developed using medium-scale square specimens has been compared against all specimens in Series RC/E, but the output does not capture the behaviour as accurately as in Series SC and SE. The comparison of predicted axial capacity against the experimental result is presented in Table 5-3.

Table 5-3: Series RC/E – Analytical model axial capacity prediction and comparison

SERIES ID	SPECIMEN ID	LOAD PROFILE	CONCRETE STRENGTH	EXPERIMENTAL PEAK LOAD	PREDICTED LOAD (ANALYTICAL)	VARIATION %
			N/mm²	kN	kN	
RC	RC2	CON	24.4	4434	4125	-7.49
	RC4	CON	24.4	6124	5264	-16.3
	RE1	ECC1	24.4	5637	5115	-10.2
	RE2	ECC2	35.5	1934	2652	27.1
	RE3	ECC1	24.4	6303	5437	-15.9
	RE4	ECC2	35.5	1411	1757	19.7
	RC6	CON	24.4	6593	5627	-17.2

The variation in behaviour is more sporadic and greater with increasing aspect ratio. With inclusion of a load eccentricity, the capacity is initially underestimated for load profile ECC1 and then grossly overestimated for load profile ECC2. The graphical presentation in Figure 5-11 shows a greater movement away from the dashed line.

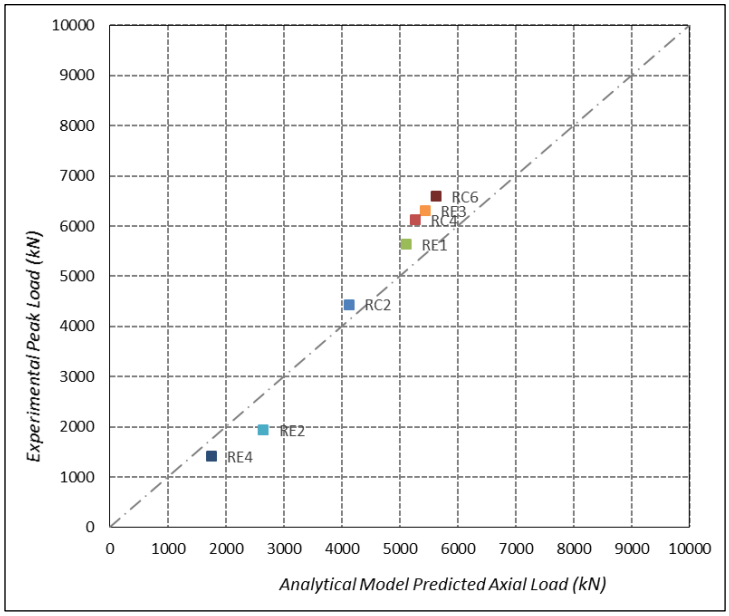

Figure 5-11: Series RC/E – Comparison of analytical model predicted axial capacity against experimental testing peak load

Fundamentally, the use of the confinement effectiveness factor in the presented form does not incorporate the confinement mechanics of the rectangular cross-section adequately enough, thus the factor needs to address the change in cross-sectional dimensions.

5.5. COMPARISON AGAINST OTHER RESEARCH

To evaluate the accuracy of the model, it has been appraised against the results of research performed by Rocca et al. (2005) Hadi and Widiarsa (2012), Wang et al. (2012) and Song et al. (2013) for specimen parameters of size, load eccentricity and cross-sectional aspect ratio. Refer to Table 2-2 for full details of the test specimens. Furthermore, as the UK design guidance was updated post testing, the later version TR55 (2011) is also assessed against the results.

Song et al. (2013) postulated that the shape and movement is as the experimental testing and FEM have illustrated in this thesis. An assumption also made for ease of modelling was that the angle of the parabolas is at 45 degrees to the corner/edge connection, Figure 5-12.

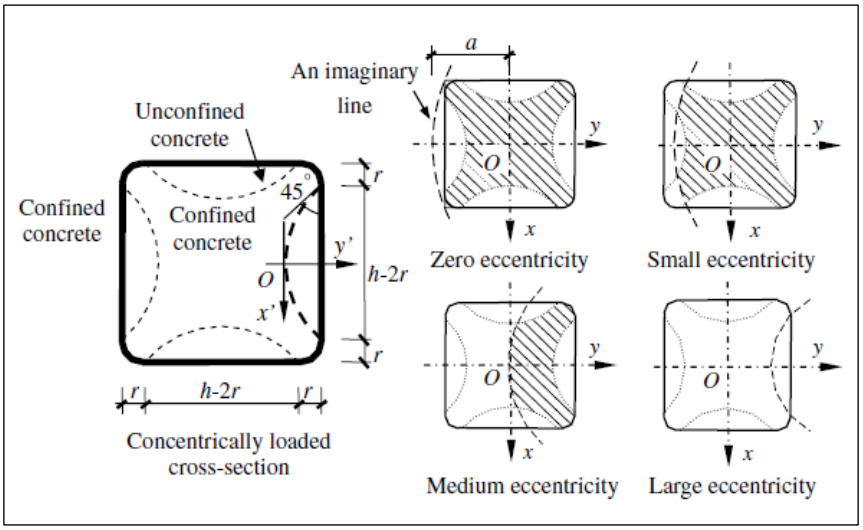

Figure 5-12: Effectively confined area and movement with applied eccentricity [Song et al. (2013)]

For medium eccentricities, Song et al. (2013) also saw the effectively confined area move to the compressive half of the cross-section, Figure 5-12 and defined this using a parabola:

$$y = \frac{x^2}{h-2r} + a \qquad (5\text{-}22)$$

In Equation 5-22, *a* is the intercept of the cutting line on axis y and is determined by:

$$a = \begin{cases} -\frac{h^2}{4(h-2r)} - \frac{h}{2} & e_0 = 0 \\ Linear\ interpolation & 0 < e_o < \frac{h}{2} \\ \frac{h}{2} - \frac{1}{4(h-2r)} & e_o = \frac{h}{2} \end{cases} \quad (5\text{-}23)$$

The model is a reasonable representation but would benefit from consideration of the likelihood of debonding and the effect on the strain in the FRP jacket.

It is imperative to be selective with the strain readings selected for use and the location along the height of the column that these are taken from. Barrington et al. (2011) demonstrated that as there is a variation in hoop strains with height, it is not always appropriate to validate confinement models using hoop strain measurements from isolated point strain readings, instead finding a more valid statistical basis with more detailed knowledge of the variability of hoop strains, for selection of strains where there is a choice.

5.6. CONCLUDING REMARKS

The FRP-confined concrete model for prismatic columns explicitly accounts for interaction of the FRP and concrete when taking into consideration the flat sides of the cross-section.

The model has been developed and evaluated for concentrically loaded specimens first, then the movement of the effectively confined area and shear stress that is generated is taken into account. The model is presented in terms of the subdivided confined stress and the area that it applies to. To get to this stage, a shape factor has been applied to the cross-sectional area to generate the out-of-plane stress.

Comparison with test results of the medium- and large-scale square specimens especially, show reasonable correlation of the results, and the model can be judged conservative as in some instances of load application using ECC2 profile, it slightly overestimates the results.

Further development of this model is necessary for a more realistic representation to consider debonding that has extensively occurred on the medium- and large-scale tests. Through further research, TR55 (2011) has moved away from the use of a shape factor in

the design methodology. Thus it would be beneficial to use the experimental results presented here to fit the models used behind this guidance and check their viability with large-scale testing.

CHAPTER 6

DISCUSSION AND CONCLUSIONS

6.1. INTRODUCTION

This chapter summarises the research undertaken and presented in this thesis. It details the aspects that would benefit from further insight to ensure a detailed understanding of the behaviour of large-scale FRP-confined prismatic RC columns when subject to a variety of loading.

The principal aim of this research as identified in Chapter 1, was to ascertain if a reasonable gain in strength capacity is achievable with FRP-confinement of realistically sized and loaded prismatic RC columns. This research aim is divided into detailed objectives, specifically:

1. To establish the effect of column size upon the increase in strength capacity and the failure modes of FRP-confined prismatic columns
2. To establish the effect of cross-sectional aspect ratio and load eccentricity upon the evolution of the effectively confined area, and the resulting strength enhancement of FRP-confined prismatic columns
3. To develop a rational model for predicting the strength of realistically dimensioned FRP-confined prismatic columns subject to concentric and eccentric loading capturing the mechanics of the behaviour.

This chapter discusses and summarises the results from the experimental testing, finite element modelling, and analytical modelling. An overview of the results demonstrate that the behaviour of the confinement mechanics over the cross-section of the prismatic column is found to be in agreement with the postulated views presented in Chapter 2.

6.2. EXPERIMENTAL METHODOLOGY AND RESULTS

An experimental test matrix was set up to assess realistically sized and loaded FRP-confined prismatic specimens. Throughout testing and in analysis of the results, it was pertinent to establish lessons, to adapt design and construction methodology, with the potential to improve results and further develop understanding in future testing.

Specimens were designed according to the now superseded TR55 (2005) and as a result of this, there is a slightly different approach to design with regard to certain aspects in its replacement TR55 (2011). The most fundamental change for the aims of this thesis is that the second order moments are not taken into consideration in initial design to TR55 (2005). Through analysis of the lateral deflection, it is imperative to take this into account in design, even for theoretically concentrically loaded specimens.

TR55 (2011) approaches the design of rectangular specimens in a different manner to TR55 (2005), omitting the overlapped section of the effectively confined area in the middle for large cross-sectional aspect ratios. This updated method more accurately captures the predicted strength capacity, especially for specimens subject to an eccentric load.

With regard to the construction of the specimens there was a large variation in the concrete strength from the external mixes, indicating further monitoring and control over the contractors would have been beneficial. The large volume of concrete required restricted production of the concrete to external contractors. A 30MPa mix was specified, and after concrete cube tests at 14 days, it became apparent that the contractor had provided an excessively strong mix, as is typical in the construction industry. With hindsight, best practice would have been to design the mix alongside the contractor and state the precise quantities of each part to control the strength and slump of the mix.

6.2.1. EXPERIMENTAL RESULTS – STRENGTH CAPACITY

An increase in strength capacity for FRP-confined columns when compared with their unconfined equivalent was presented in Chapter 4. However this increase varies significantly when taking into consideration the geometry of the cross-section and the nature of the load profile applied.

Medium-scale concentrically loaded specimens had a maximum 48% increase in capacity, and an ascending bilinear stress-strain response, illustrating that the confinement level was adequate. Increasing the cross-sectional aspect ratio, cause the gain in axial strength capacity to reduce and there was no longer a clear bilinear stress-strain response. The long flat sides of these specimens have an impact, reducing the effectively confined area and as such, a greater level of confinement than an equivalent sized square cross-section is necessary to generate the same strength capacity gain and to avoid degradation before FRP rupture. Thus confinement is far more effective for square columns than rectangular columns, as the aspect ratio increases it reduces the strength gain and the effectiveness of confinement until an aspect ratio greater than two sees no significant increase, Wu and Wei (2010). The proven increases in axial strength capacity appear reasonable, however once safety factors are taken into consideration in design guidance the combination of FRP amount, architecture and method may not be viable until optimal strengthening levels of FRP are determined, thus, although an increase in capacity is available, it requires further development.

When addressing the effect of size, it was apparent that the results of small-scale testing should not be scaled up, as the strength capacity can be significantly overestimated, because the small-scale specimens do not exhibit the behaviour of large-scale specimens to the same extent. This is evident in debonding of the FRP from the concrete, visible with large-scale testing to the eye but only slightly evident upon closer inspection of some small-scale specimens.

Application of a flexural element to the applied load reduces the gain in axial strength capacity in FRP-confined specimens, while demonstrating more ductile behaviour. The stress-strain behaviour of these specimens with increasing eccentricity exhibits an extensive post-peak plateau, maintaining the vast proportion of the load for a long duration before failure occurs, dropping a large portion of the load. The inclusion of bidirectional fibres, mounted longitudinally, has been seen to aid with increasing axial strength capacity when large load eccentricities are applied [Fitzwilliam and Bisby (2010)].

Slenderness of the FRP-confined specimen was pertinent. In the experimental testing, the lateral movement far exceeded what was expected in medium- and large-scale specimens. Furthermore, this has occurred in small-scale specimens to an extent, Chaallal and Shahawy (2000) and El Maaddawy (2009), with localised peak strains experienced. With the large-

scale, eccentrically loaded specimens, failure was at mid-span, hence these localised strains were captured. Fundamentally, the addition of the FRP jacket increases the slenderness of the specimen and the subsequent second order effects, thus it should be considered at the design stage.

6.2.2. EXPERIMENTAL RESULTS – CONFINEMENT MECHANICS

The prismatic specimens were assessed for concentric and eccentric loading on square and rectangular cross-sections. The development of the effectively confined area for a concentrically loaded square cross-section was first addressed and the variation in shape and movement the loading profile was adapted. Lastly, the cross-sectional aspect ratio was changed from square to rectangular.

The ultimate strength of rectangular/square columns cannot be predicted accurately without considering the reduction in the confining pressure due to the shape effect, which depends on the geometry of the confined concrete section. The cross-section geometry has a major role in the levels of confinement achievable and as such, the mechanics of confinement have been studied in detail. The experimental, FEM and analytical modelling are all in agreement over the shape and movement of the effectively confined area.

The postulated shape and movement of the effectively confined area of square columns was verified first though a nominal depth FEM model of the cross-section and then from the FRP strain gauge readings from the experimental results. Both have demonstrated that from the strain in the FRP wrap, the confining forces in the corners generate a cruciform shape along the diagonals, for concentrically loaded specimens. FEM highlighted that the largest concentration of stress is at the corners, decreasing towards the centre of the specimen. The region next to the flat sides provides minimal, if any confinement so for ease of modelling, it is assumed to be unconfined.

A postulated size effect in prismatic specimens was the initial reason for this research and has been realised in experimental testing, thus scaling of the small-scale results to predict the behavioural mechanics is not feasible.

6.2.2.1. EFFECTIVELY CONFINED AREA OF SQUARE CROSS-SECTION

The cruciform shape of a concentrically loaded square column is not largely influenced by size effect, with the experimental results corroborating the FEM findings. The variation comes with realistic loading where an element of moment is present due to P-Delta effects, and inherent imperfections in the specimen. This is unavoidable in reality, and is brought into consideration with TR55 (2011).

Even columns that in theory are only loaded axially, the impact of including even a small flexural component to the load causes the effectively confined area to migrate into the region of higher compressive stress. The variation in confinement pressure in the FRP jacket over the cross-section causes the confining forces to differ over the load axis, and if this is large enough, with minimal resistance on the flat sides between the corners, shear stress is generated, potentially debonding the flat sides from the concrete. Firstly, with lower eccentricities the effectively confined area is seen to maintain a shape similar to the cruciform, with the main part of the shape in the compressive region. Then as the eccentricity increases, the effectively confined area eventually is solely generated between the two corners in this higher compressive stress region and as such, no confinement results from the FRP jacket at the other corners. Measured strain from the FRP gauges drops towards zero at this point on the larger eccentric specimens only.

6.2.2.2. EFFECTIVELY CONFINED AREA OF RECTANGULAR CROSS-SECTION

Looking at the cruciform shape of the concentrically loaded square specimen, as the cross-sectional aspect ratio increases, the effectively confined area reduces due to the long flat sides. The flat sides provide no confinement thus there is a greater portion of the cross-section of low confinement between the highly stressed regions of the corners and as such these specimens are not as effective. With the application of an eccentric load, the confinement efficiency is further reduced as the high stresses at the corners, and the medium level between them is proportionally less of the cross-sectional area when compared with an equivalent sized square specimen. This is further compounded with minor axis loading.

Debonding of the FRP along the flat sides of the specimen becomes more prominent with increasing aspect ratio. All specimens in the experimental testing experienced debonding,

to a varied extend. Concentrically loaded specimens debonded locally, reflecting especially if a slight misalignment of load, or P-Delta generated moment was evident. As the load eccentricity increased, the extent of the debonded area was more severe, but still localised to the mid-span area, and extending from corner to corner. With an increased aspect ratio, this was heard to "ping" off the flat surface of the specimen for a large area. Thus debonding is significant and verifies the assumption that the concrete on the flat sides is unconfined.

6.2.2.3. MODELLING OF THE EFFECTIVELY CONFINED AREA OF PRISMATIC COLUMNS

A simple model was proposed to capture the formation and the movement of the effectively confined area, specifically with respect to the application of eccentric loading on prismatic columns. The model captures the behaviour of the specimens as per the experimental analysis of the strains at mid-height and the FEM. However, many aspects still require addressing in order to predict the behaviour with complete accuracy. Most importantly is the effect of debonding on the mechanics of behaviour. Debonding initiated long before failure of the specimen, evident by the pinging noises from the FRP, but this always occurred after application of peak load and is not represented fully in any behavioural modelling.

It is imperative to note that the reduced tensile characteristics of the FRP have not been analysed in detail and as such the analytical model would benefit from inclusion of further research in this area. As this is closely related to the failure strain, as from experimental results, failure occurs at strain levels below the ultimate strain defined in standard tensile test results. The failure of the specimens were unfortunately in the majority of the tests, away from the mid-height strain gauges, thus the full effect was not captured and it cannot be assumed as an accurate representation of the actual state of stress in the FRP jacket at failure.

6.2.3. RESEARCH INTO FRP RUPTURE STRAIN

Through analysis of pertinent research relating to FRP-confinement of prismatic specimens and the experimental results is presented in Chapter 4, the impact of the selected strain to represent the actual rupture strain is significant. This was not accurately measured in Chapter 4, as the failure location occurred away from the mid-height gauges.

Through analysis of the experimental results, the rupture strain of FRP (identified through flat coupon tests detailed in Chapter 3), is considerably greater relative to the rupture strain measured when failure occurred near the FRP strain gauges. To ascertain a more reasonable FRP failure strain, split-disk testing would have provided potentially more accurate representation as they are generally found to be lower results, Chen et al. (2011). Furthermore, as the corner radius increases, the rupture strain increases [Wang and Wu (2008)] thus the FRP strain is also dependent on the ratio of the corner radius to the side length.

The impact of rupture strain on cross-sectional aspect ratio was evaluated by Wu and Wei (2010) and as the cross-sectional aspect ratio increased over two, the FRP rupture strains were no longer identical or close to those between 1-2 cross-sectional aspect ratio. Thus the rupture strain is a function of the shorter side length and corner radius in these specimens.

An aspect to take into consideration is that Harries and Carey (2003) highlighted that if the strain measurement is not exactly at the strain concentration point where a crack exists, the average jacket strain reading is much lower than the actual material strain capacity which is only reached at the stress concentration as was highlighted with the experimental testing in Chapter 4.

The approach of TR55 (2011) found the maximum strain in the FRP jacket, as 25% to 40% of the ultimate rupture strain and this was evaluated against the results of the experimental study, corroborating the finding. Furthermore, the debonding strain, being lower than the maximum strain, again illustrated close agreement. Thus, through recent data capture techniques such as GeoPIV, adopted by Barrington et al. (2011) and greater understanding of the strain behaviour and debonding of the jacket, a more reasonable estimation of the FRP jacket behaviour can be assumed.

6.3. DESIGN GUIDANCE

Additional assessment of the experimental results was performed against the updated TR55 (2011) design guidance and this illustrated a number of key points, specifically:

- The axial capacity of the specimens was generally overestimated but the degree to which this occurred was not large
- The moment capacity of the specimens was more reasonably captured and when considered within the recommended limits, this can provide an accurate representation
- Specimens that were out of the limits for use of the design guidance were not reasonably estimated and the results sporadic thus use of TR55 (2011) for design is not recommended without a specific case by case review and adaptation where necessary

TR55 (2011) guidance when used within the limits specified gave promising results. This is especially so when the use of the design factors are included and will lower the theoretical axial capacity. Extension of the design guidance will open up many more areas, especially columns of larger cross-sectional aspect ratios but as it stand at the moment, the results are not good and use of the guidance for this is not advisable.

6.4. CONCLUSIONS

To conclude this research, two major areas have been addressed; potential gain in strength capacity for FRP-confinement, and the confinement mechanics over the prismatic cross-section.

6.4.1. AXIAL STRENGTH CAPACITY

The increase in axial strength capacity available through FRP-confinement of the specimens is less than for an equivalent circular column. Through testing, it was confirmed that size effect is a major issue as demonstrated by the post-test analysis/destruction of the specimens. Contrary to previously postulated FRP behaviour, the FRP had not engaged over

the length of specimens as per small-scale tests and instead, the behaviour was localised, with only sections of the FRP engaging.

In terms of axial strength gain, experimental results show that a 48% maximum increase for the medium-scale specimens can be obtained for concentric loading. This does not exactly correlate with other research and when comparing, the geometry and material data is rarely an exact match, especially with larger specimens. Parameters which are often varied include; corner radius, number of FRP plies, FRP fibre orientation, and concrete strength. As this database of parameter variations increases, then patterns of behaivour can be confirmed. The specimens presented here give a thorough analysis of the behaviour when concentrically loaded.

The gain in strength capacity reduces with increased load eccentricity and/or increasing aspect ratio. In terms of load eccentricity, although axial capacity is not greatly increased, the flexural capacity is, with specimens able to maintain a vast proportion of the peak load before failure. It was seen from the descending second portion of the stress-strain curves that using the same amount of FRP as on the concentric specimens (which had ascending second portion) does not provide adequate confinement. Thus more FRP plies, or straps over the minimal FRP jackets is a feasible alternative to full wraps.

Increasing the aspect ratio of the column yields similar results in that the level of confinement is inadequate and this is compounded if an eccentricity of load is applied. When strengthening, the large, flat sides require consideration as debonding was commonly found over the area from corner to corner.

6.4.2. CONFINEMENT MECHANICS

The confinement mechanics over the cross-section of the specimens were as postulated. Thus the results, originating from the FRP strains have demonstrated that the effectively confined area forms a cruciform shape from the corners. When including a load eccentricity, the change in FRP strains between the corners, along with the established shear stress, moves the effectively confined area in to the compressive region, until the confinement is provided by two corners only for large eccentricities.

6.4.3. DESIGN GUIDANCE

The update of TR55 (2005) to TR55 (2011) incorporates aspects of the results thus when design is performed using TR55 (2011) and compared with the experimental results, there is good agreement for specimens within the defined limitations. For specimens exceeding the stated limitations, design based on TR55 (2011) is recommended but with detailed design to reviewed pertinent literature.

A fundamental aspect that was not covered in design by TR55 (2005) was the slenderness of the specimens. Through measured lateral deflection at mid-height, specimens have some P-Delta effects, and this is greater for square cross-sections and increasing load eccentricity. It is imperative to include the potential second order moments at design stage, as is done in the more recent TR55 (2011).

To conclude, the novel experimental tests have yielded a vast amount of data on the behaviour of realistically sized and loaded specimens. Interpretation of this data has demonstrated that there is great potential in strengthening of RC columns with FRP. However, as the test database is still limited, there is currently little confidence in the technique within industry. Thus, with further research into realistically sized and loaded RC prismatic columns, FRP-confinement of existing columns will be a beneficial strengthening technique in the future.

6.5. FUTURE RESEARCH

Further work following on from this research that is considered necessary for this FRP-confinement strengthening technique to become viable in industry is:

- *FRP – FIBRE ORIENTATION*
  Orientation of the fibres on large-scale specimens, especially with an applied load eccentricity, should be addressed. If there was a portion of fibres included in the longitudinal direction, on top of that in the hoop direction, this could allow for the increase in strength capacity whilst still providing the ductility enhancement.

- *LARGE-SCALE EXPERIMENTAL TESTING*

  Further large-scale would be beneficial as the FRP-confined specimen in the test matrix did not fail through the expected rupture of the FRP. In this set of testing, there was only one of each specimen, and as such there was no way of comparing results to ascertaining the size effect over the medium-scale specimens.

- *LARGE CROSS-SECTIONAL ASPECT RATIO*

  Currently, the relevant design guidance, TR55 (2011) is still conservative in terms of the maximum recommended cross-sectional aspect ratio. The experimental results demonstrated the varied response, especially with increasing load eccentricity on the minor axis. The benefit in confinement using a standard number of FRP plies was in the ductility increase as opposed to strength capacity.

- *PARAMETER VARIATION*

  Size effect that has become apparent in the results, suggests that varying some of the parameters already studied for small-scale specimens, including the number of FRP plies or the use of additional FRP straps in the hoop direction, would perhaps be more beneficial

- *EXTREME SITUATIONS*

  Extreme loading on specimens including marine, earthquake and fire has been addressed. However there is limited data on the fatigue endurance of specimens. The results of this testing, although not performed with the focus on cyclic loading or fatigue could be used alongside other testing that focuses on ductility, primarily for the earthquake regions. The combination of the results could hold a greater insight into the behaviour, if all data was available for analysis.

The research presented and the future suggestions show a great potential for FRP-confinement of RC prismatic columns, can be used for development of design guidance, to cover a broader spectrum of columns for strengthening and generate greater belief in the technique in industry.

REFERENCES

A

ACI440.2R-02: 2002, Guide for the Design and Construction for Externally Bonded FRP Systems for Strengthening Concrete Structures. *American Concrete Institute*.

Al-Salloum, Y.A., 2007. Influence of edge sharpness on the strength of square concrete columns confined with FRP composite laminates. *Composites: Part B*, **38**, pp. 640-650.

B

Barrington, J., Dickson, D., Bisby, L. & Stratford, T. 2011. Strain Development and Hoop Strain Efficiency in FRP Confined Square Concrete Columns. *American Concrete Institute*, **49** (9), pp. 9.1-9.20

Binici, B., 2005. An analytical model for stress-strain behaviour of confined concrete. *Engineering Structures*, **27**, pp. 1040-1051.

Bisby, L., Ranger M., 2010. Axial-flexural interaction in circular FRP-confined reinforced concrete columns. **24**, pp. 1672-1681

Bisby, L.A., Take, W.A., 2009. Strain Localizations in FRP Confined Concrete: New Insights. *Proceedings of the ICE - Structures and Buildings*, **162** (5), pp. 301-309

BS8110-1: 1997. Structural use of concrete. Code of practice for design and construction BSI

C

Campione, G., Miraglia, N., 2003. Strength and strain capacities of concrete compression members reinforced with FRP. *Cement and Concrete Composites*, **25**, pp. 31-41.

Chaallal, O., Shahawy, M., Hassan, M., 2003. Performance of axially loaded short rectangular columns strengthened with carbon fiber-reinforced polymer wrapping. *Journal of Composites for Construction*, **7** (3), pp. 200-208.

Chakrabarti, A., Chandra, A., Bharagava, P., 2008. Finite element analysis of concrete columns confined with FRP sheets. *Journal of Reinforced Plastics and Composites*, **27** (12), pp. 1349-1373.

Chen, J.F., Li, S.Q., Bisby, L.A., Ai, J., 2011. FRP rupture in the split-disk test. *Composites: Part B*, **42**, pp. 962-972

Chun, S.S., Park, H.C., 2002. Load carrying capacity and ductility of RC columns confined with carbon fiber reinforced polymer, *Proceedings Third International Conference on Composites in Infrastructure*

Cole, C., Belarbi, A., 2001. Confinement characteristics of rectangular FRP-jacketed RC Columns. *Proceedings, Fifth International Symposium on Fiber Reinforced Polymers for Reinforced Concrete Structures, Cambridge, UK*, 16th-18th July, pp. 823-832.

CSA, 2002. Design and Construction of Building Components with Fibre-Reinforced Polymers. S806-02 *Canadian Standard Association*

Csuka, B., Kollár L.P., 2012. Analysis of FRP confined columns under eccentric loading. *Composite Structures*, **94**, pp. 1106-1116.

Cusson, D., Paultre, P., 1995. Stress-Strain Model for Confined High-Strength Concrete. *Journal of Structural Engineering*, **121** (3), pp. 468-477.

D

Darby, A. P., Coonan, R. M., Ibell, T. J., Evernden, M., 2011. FRP confined square and rectangular columns under concentric and eccentric loading. *Proceedings of Advanced Composites in Construction (ACIC 2011)*, Warwick 2011

De Luca, A., Nardone, F., Matta, F., Nanni, A., Lignola, G.P., Prota, A., 2011. Structural evaluation of full-scale FRP-confined reinforced concrete columns. *Journal of Composites for Construction*, **15** (1), pp. 112-123.

Doran, B., Köksal, H.O., Turgay, T., 2009. Nonlinear finite element modelling of rectangular/square concrete columns confined with FRP. *Materials and Design*, **30**, pp. 3066-3075.

E

El Maaddawy, T., 2009. Strengthening of eccentrically loaded reinforced concrete columns with fiber-reinforced polymer wrapping system: Experimental investigation and analytical modelling. *Journal of Composites for Construction*, **13** (1), pp. 13-24.

F

Fam, A.Z., Flisak, B., Rizkalla, S.H., 2003. Experimental and analytical modelling of concrete-filled fiber-reinforced polymer tubes subjected to combined bending and axial loads. *ACI Structural Journal*, **100** (4), pp. 399-509.

Fam, A.Z., Rizkalla, S.H., 2001. Confinement model for axially loaded concrete confined by circular fiber-reinforced polymer tubes. *ACI Journal Structural*, **98** (4), pp.451-461.

Fardis, M.N., and Khaili, H.H., 1982. FRP-encased concrete as a structural material. *Magazine of Concrete Research,* **34**, pp. 191–202.

Fib, 2001. Externally Bonded FRP Reinforcement for RC Structures. *Fédération International du Béton*

Fitzwilliam, J., Bisby, L.A, 2010. Slenderness Effects on Circular CFRP Confined Reinforced Concrete Columns. *Journal of Composites for Construction*, **14** (3), pp. 280-288.

H

Hadi, M.N.S., 2006a. Behaviour of FRP wrapped normal strength concrete columns under eccentric loading. *Composite Structures*, **72**, pp. 503-511.

Hadi, M.N.S., 2006b. Comparative study of eccentrically loaded FRP wrapped columns. *Composite Structures*, **74**, pp. 127-135.

Hadi, M.N.S., Widiarsa, I.B.R., 2012. Axial and flexural performance of square RC columns wrapped with CFRP under eccentric loading. *Journal of Composites for Construction*, **s** (6), pp. 640-648.

Hajsadeghi, M., Alaee, F.J., Shahmohammadi, A., 2011. Investigation on behaviour of square/rectangular reinforced concrete columns retrofitted with FRP jacket. *Journal of Civil Engineer and Management*, **17** (3) pp. 400-408.

Harmon, T.G., Gould, P.L., Wang, E., Ramakrishnan, S., 1998. Behaviour of Confined Concrete Under Cyclic Loading. *Proceedings of the Second International on Composites in Infrastructures*, ICCI'98.

Harries, K.A, Kharel, G., 2002. Behaviour and modeling of concrete subject to variable confining pressure. *ACI Materials Journal*, **99** (2), pp. 180-189.

Harries, L.A., Carey, S.A., 2003. Shape and "gap" effects on the behaviour of variably confined concrete. *Cement Concrete Research*, **33** (6), pp. 811-890.

I

Issa, C., Karam, G., 2004. Compressive strength of concrete cylinders with variable widths CFRP wraps. *Proc., 4th International Conf. on Advanced Composite Material Structures*, ACMBS-IV, Calgary, Alberta, Canada.

J

Jiang, J.F., Wu, Y.F., 2012. Identification of material parameters for Drucker-Prager plasticity model for FRP confined circular concrete columns. *International Journal of Solids and Structures*, **49**, pp. 445-456.

Jiang, T., Teng, J.G., 2007. Analysis-oriented stress-strain models for FRP-confined concrete. *Engineering Structures*, **29**, pp. 2968-2986.

K

Karabinis, A.I., Rousakis, T.C., 2002. Concrete confined by FRP material: a plasticity approach. *Engineering Structures*, **24**, pp. 923-932.

Karabinis, A.I., Rousakis, T.C., Manolitsi, G.E., 2008. 3D finite-element analysis of substandard RC columns strengthened by fiber-reinforced polymer sheets. *Journal of Composites for Construction*, **12**, pp. 531-540.

Karam, G., Tabbara, M., 2005. Confinement effectiveness in rectangular concrete columns with FRP wraps. *ASCE Journal of Composites for Construction*, **9** (5), pp. 388–396.

L

Lam, L., Teng, J.G., 2003b. Design-oriented stress-strain model for FRP-confined concrete in rectangular columns. *Journal of Reinforced Plastics and Composites*, **22** (13) pp. 1149-1186.

Lillistone, D., and Jolly, C.K., 2000. An innovative form of reinforcement for concrete columns using advanced composites. *The Structural Engineer*, **78** (23/24), pp. 20-28.

M

Maalej, M., Tanwongsval, S., Paramasivam, P., 2003. Modelling of rectangular RC columns strengthened with FRP. *Cement & Concrete Composites*, **25**, pp. 263-276.

Manders, J.B., Priestley, M.J.N., Park, R., 1988. Theoretical stress-strain model for confined concrete. *Journal of Structural Engineer New York*, **114** (8), pp. 1804-1826

Marques, S.P.C., Marques, D.C.S.C., Silva, J.L., Cavalcante, M.A.A., 2004. Model for analysis of short columns of concrete confined by fiber-reinforced polymer. *Journal of Composites for Construction*, **8** (4), pp. 332-340.

Micelli, F., Modarelli, R., 2013. Experimental and analytical study on properties affecting the behaviour of FRP-confined concrete. *Composites: Part B*, **45**, pp. 1420-1431.

Mirmiram, A., Shahawy, M., 1996. A new concrete-filled hollow FRP composite column. *Composites: Part B*, **27**, pp. 263-268.

Mirmiram, A., Shahawy, M., Samaan, M., El Echary, H., Mastrapa, J C., Pico, O., 1998. Effect of column parameters on FRP-confined concrete. *Journal of Composites in Construction*, **2** (4), pp.175-185.

Monti, G., Nistico, N., 2008. Square and rectangular concrete columns confined by CFRP: Experimental and numerical investigation. *Mechanics of Composite Materials*, **44** (3), pp. 289-308.

Mostofinejad, D., Moshiri, N., Mortazavi, N., 2015. Effect of corner radius and aspect ratio on compressive behaviour of rectangular concrete columns confined with CFRP. *Materials and Structures*, **48**, pp. 107-122.

N

Nanni, A., 1995. Concrete repair with externally bonded FRP reinforcement: examples from Japan. *Concrete International*, **97**, pp. 22-26.

P

Papanikolaou, V.K., Kappos, A.J., 2007. Confinement-sensitive plasticity constitutive model for concrete in triaxial compression. *International Journal for Solids and Structures*, **44**, pp. 7021-7048.

Park, R., Paulay, T., 1975. Ductile reinforced concrete frames – some comments on the special provisions for seismic design of ACI 318-71 and on capacity design. *Bulletin of New Zealand Society for Earthquake Engineering*, **8** (1), pp. 70-90.

Parvin, A., Wang, W., 2001. Behaviour of FRP jacketed concrete columns under eccentric loading. *Journal of Composites in Construction*, **5** (3), pp. 146-152.

Pessiki, S., Harries, K.A., Kestner, J.T., Sausa, R., Ricles, J.M., 2001. Axial behaviour of reinforced concrete columns confined with FRP jackets. *Journal of Composites for Construction*, **5** (4), pp. 237-245.

Pham, T.M., Hadi, M.N.S., 2014. Stress prediction model for FRP confined rectangular concrete columns with rounded corners. *Journal for Composites in Construction*, **18** (1), pp. 1-10.

Popovics, S., 1973. A numerical approach to the complete stress-strain curve of concrete. *Cement and Concrete Research*, **3**, pp. 583-599.

Prota, A., Manfredi, G., Cosenza, E., 2003. Confinement of RC rectangular columns using GFRP. *FRPRCS-6: Externally Bonded Reinforcement for Confinement*. pp. 653-662

R

Ranger, M., Bisby, L., 2007. Effects of load eccentricities on circular FRP-confined reinforced concrete columns. *Proc., 8th Int. Symp. on Fibre Reinforced Polymers for Reinforced Concrete Structures (FRPRCS8)*, Patras, Greece, pp. 290-291

Razvi, S., Saatcioglu, M., 1999. Confinement model for high-strength concrete. *Journal of Structural Engineering*, **125** (3), pp. 281-289.

Rocca, S., Galati, N., Nanni, A., 2005. Experimental evaluation of FRP strengthening of real size reinforced concrete columns. *Center for Infrastructure Studies/UTC program*, University of Missouri-Rolla.

Rocca, S., Nestore, G., Nanni, A., 2009. Interaction diagram methodology for design of FRP-confined reinforced concrete columns. *Construction and Building Materials*, **23**, pp. 1502-1520

Rochette, P., Labossière, P., 2000. Axial testing of rectangular column models confined with composites. *Journal of Composites for Construction*, **4** (3), pp. 129-136.

S

Sadeghian, P., Rahai, A.R., Ehsani, M.R., 2010. Experimental study of rectangular RC columns strengthened with CFRP composites under eccentric loading. *Journal of Composites for Construction*, **14** (4), pp. 443-450.

Samaan, M., Mirmiran, A., Shahawy, M., 1998. Model of concrete confined by fiber composites. *Journal of Structural Engineering*, **124** (5), pp. 1025-1031.

Song, X., Gu, X., Li, Y., Chen, T., Zhang, W., 2013. Mechanical behaviour of FRP-strengthened concrete columns subject to concentric and eccentric compression loading. *Journal of Composites for Construction*, **17** (3), pp. 336-346.

Spoelstra, M.R., Monti, G., 1999. FRP-confined concrete model. *Journal of Composites for Construction*, **3** (3), pp. 143-150.

T

Tao, Z., Yu, Q., 2008. Behaviour of CFRP-strengthened slender square RC columns. *Magazine of Concrete Research*, **60** (7), pp. 523-355.

Teng, J.G., Chen, J.F., Smith, S.T., Lam, L., 2002. FRP-strengthened RC structures. *RC Structures*, Wiley, Chichester, UK.

Teng, J.G., Chen, J.F., Smith, S.T., Lam, L., 2003. Behaviour and strength of FRP-strengthened RC structures: A state of the art review. *Structures and Buildings*, **156** (1), pp. 51-62.

Teng, J.G., Lam, L., 2004. Behavior and modeling of fiber reinforced polymer-confined concrete. *Journal of Structural Engineering*, **130** (11), pp. 1713-1723.

Teng, J.G., Yu, T., Wong, Y.L., Dong, S.L., 2007a. Hybrid FRP-concrete-steel tubular columns: Concept and behaviour. *Construction and Building Materials*, **21**, pp. 846-854.

Teng, J.G., Huang, Y.L., Lam. L., Ye, L.P., 2007b. Theoretical model for fiber-reinforced polymer-confined concrete. *Journal of Composites for Construction*, **11** (2), pp. 201-210.

Teng, J.G., Jiang, T., Lam, L., Luo, Y.Z., 2009. Refinement of a design-oriented stress-strain model for FRP-confined concrete. *Journal of Composites for Construction*, **13** (4), pp. 269-278.

Thériault, M., Neale, K. W., Claude, S. (2004). FRP-confined circular concrete columns: Investigation of size and slenderness effects. *Journal of Composites in Construction*, **8** (4), pp. 323–331.

Toutanji, H., Han, M., Gilbert, J., Matthys, S., 2010. Behaviour of large-scale rectangular columns confined with FRP composites. *Journal of Composites for Construction*, **14** (1), pp. 62-71.

TR55 2nd Edition: 2005, Design Guidance for Strengthening Concrete Structures using Fibre Composite Material. *The Concrete Society*

TR55 3rd Edition: 2011, Design Guidance for Strengthening Concrete Structures using Fibre Composite Material. *The Concrete Society*

Turgay, T., Köksal, H.O., Polat, Z., Karakoç, C., 2009. Stress-strain model for concrete confined with CFRP jackets. *Materials and Design*, **30**, pp. 3243-3251.

Turgay, T., Polat, Z., Köksal, H.O., Doran, B., Karakoç, C., 2010. Compressive behavior of large-scale square reinforced concrete columns confined with carbon fiber reinforced polymer jackets. *Materials and Design*, **31**, pp. 357-364.

V

Vermeer, P.A., de Borst, R., 1984. Non-associated plasticity for soils, concrete and rock. *Heron*, **29**, pp. 1-64.

W

Wang, L.M., Wu, Y.F., 2008. Effect of corner radius on the performance on CFRP-confined square concrete columns: Test. *Engineering Structures*, **30** (2), pp. 493-505

Wang, Z., Wang, D., Smith, S., Lu, D., 2012. CFRP-confined square RC columns. I: Experimental Investigation. *Journal of Composites for Construction*, **16** (2), pp. 150-160.

White, D.J., Take, W.A., Bolton, M.D., 2003. Soil deformation measurement using particle image velocimetry (PIV) and photogrammetry. *Géotechnique*, **53** (7), pp. 619-631

William, K.J., Warnke, E.P., 1974. Constitutive model for the triaxial behaviour of concrete. *Seminar on: Concrete Structures subject to triaxial stresses*,

Wu, Y.F., Wei, Y.Y., 2010. Effect of cross-sectional aspect ratio on the strength of CFRP confined rectangular concrete columns. *Engineering Structures*, **32** (1), pp 32-45

Wu, Y.F., Zhou, Y.W., 2010. A unified strength model based on Hoek-Brown failure criterion for circular and square columns confined by FRP. *Journal of Composites for Construction*, **14**, pp. 175-184.

X

Xiao, Y., Wu, H., 2000. Compressive behaviour of concrete confined by carbon fibre composite jackets. *Journal of Materials in Civil Engineering*, **12** (2), pp. 139-146.

Y

Yang, X., Wei, J., Nanni, A., Dharani, L.R., 2004. Shape effect on the performance of carbon fiber reinforced polymer wraps. *Journal of Composites for Construction*, **8** (5), pp. 444-451.

Youssef, M.N., Feng, M,Q, Mosallam, A.S., 2007. Stress-strain model for concrete confined by FRP composites. *Composites: Part B*, **38**, pp. 614-628.

Yu, T., Teng, J.G., Wong, Y.L., Dong, S.L., 2010. Finite element modelling of confined concrete-II: Plastic-damage model. *Engineering Structures*, **32**, pp. 680-691.

APPENDIX A – SPECIMEN DESIGN

CONTENTS:

A-1 – DESIGN CALCULATIONS – CONCENTRICALLY LOADED UNCONFINED SPECIMEN

CONCENTRICALLY LOADED UNCONFINED SPECIMEN – PAGE 1 OF 1

DESIGN OF AN UNCONFINED CONCENTRICALLY LOADED SPECIMEN

THIS CALCULATION DETAILS THE DESIGN OF SPECIMEN SC3 (MEDIUM-SCALE) FOR A NOMINAL CONCRETE STRENGTH

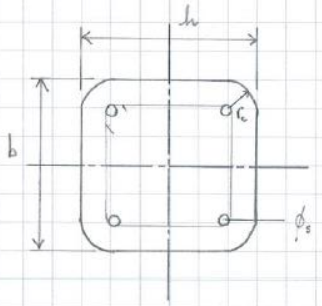

b = 300 mm
h = 300 mm
r_c = 40 mm
n_s = 4
ϕ_s = 25 mm

f_{cu} = 30 N/mm²
f_{yd} = 580 N/mm²

AREA CONCRETE, $A_g = bh - (4r_c^2 - \pi r_c^2)$
$= 300 \times 300 - (4 \times 40^2 - \pi 40^2)$
$= 88627\ mm^2$

AREA STEEL, $A_s = 4\pi r_s^2 = 4 \times \pi \times 12.5^2$
$= 1963\ mm^2$

AXIAL CAPACITY OF THE COLUMN:

$N = 0.67 f_{cu} A_g + f_{yd} A_s$
$= 0.67 \times 30 \times 88627 + 580 \times 1963 = 2920\ kN$

A-2 – DESIGN CALCULATIONS – ECCENTRICALLY LOADED UNCONFINED SPECIMEN

ECCENTRICALLY LOADED UNCONFINED SPECIMEN – PAGE 1 OF 2

DESIGN OF AN UNCONFINED ECCENTRICALLY LOADED SPECIMEN

THIS CALCULATION DETAILS THE DESIGN OF A THEORETICAL SPECIMEN, MEDIUM-SCALE WITH LOAD PROFILE ECC2

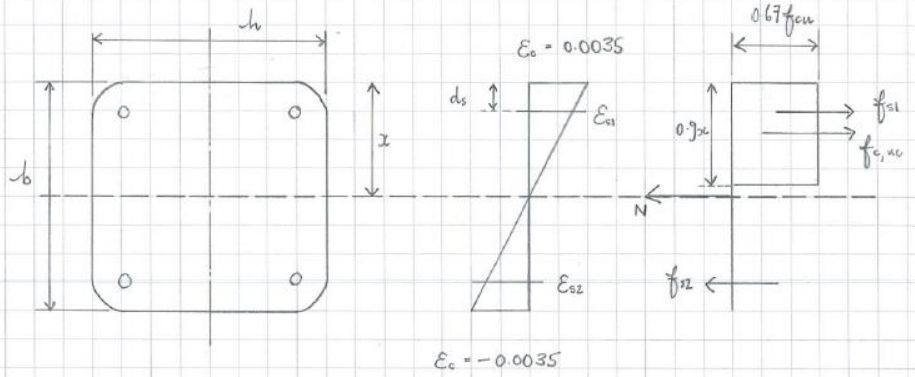

$b = 300\,mm$
$h = 300\,mm$
$r_c = 40\,mm$
$n_s = 4$
$\phi_s = 25\,mm$

$f_{cu} = 30\,N/mm^2$
$f_{yd} = 580\,N/mm^2$
$E_s = 200$

$A_g = 88627\,mm^2$
$A_s = 1963\,mm^2$

$d_{Gnc} = b - x + 0.1x + 0.45x$
$= 233mm$

$d_{s1} = b - d_s = 247.5mm$
$d_{s2} = d_s = 52.5mm$

TESTING OF STEEL REBAR $\phi 25$ SAMPLES ESTABLISHED YIELD AT $\varepsilon = 0.0029$

LONGITUDINAL STEEL CAPACITY :

$$\varepsilon_{s1} = -\varepsilon_{s2} = \frac{\varepsilon_c}{x}(x - d_s) = \frac{0.0035}{150}(150 - 52.5) = \pm 0.0023$$

$\therefore$ STEEL NOT YIELDED

$$f_{s1} = -f_{s2} = \frac{A_s}{2}\varepsilon_{s1} E_s = \frac{1963}{2} \cdot 0.0023 \cdot 200 = 447\,kN$$

ECCENTRICALLY LOADED UNCONFINED SPECIMEN – PAGE 2 OF 2

CONCRETE CAPACITY :

$f_{c,ue} = h \cdot 0.9x \cdot 0.67 f_{cu} = 300 \times 0.9 \cdot 150 \times 0.67 \cdot 30 = 814\ kN$

HENCE THE MAXIMUM CAPACITY OF THE SPECIMEN :

$N = f_c + f_{s1} + f_{s2} = 814 + 447 - 447 = 814\ kN$

AND ASSOCIATED MOMENT :

$M = f_{c,ue} d_{c,ue} + f_{s1} d_{s1} + f_{s2} d_{s2} - N x$

$= 814 \times 233 + 447 \times 247.5 - 447 \times 82.5 - 814 \times 150 = 154,265\ kNmm$

HENCE LOAD TO BE APPLIED AT ECCENTRICITY :

$e_i = \frac{M}{N} = \frac{154\,265}{814} = 190\ mm$

AS $e_i > 0.5h$, A CORBEL IS REQUIRED AT EACH END OF THE SPECIMEN FOR APPLICATION OF LOAD

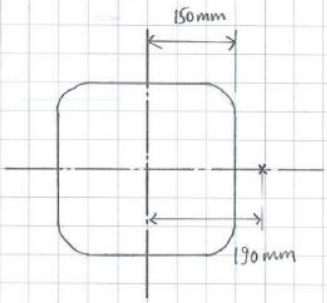

A-3 – DESIGN CALCULATIONS – CORBEL DESIGN FOR ECCENTRIC LOADING

CORBEL DESIGN FOR ECCENTRIC LOADING – PAGE 1 OF 2

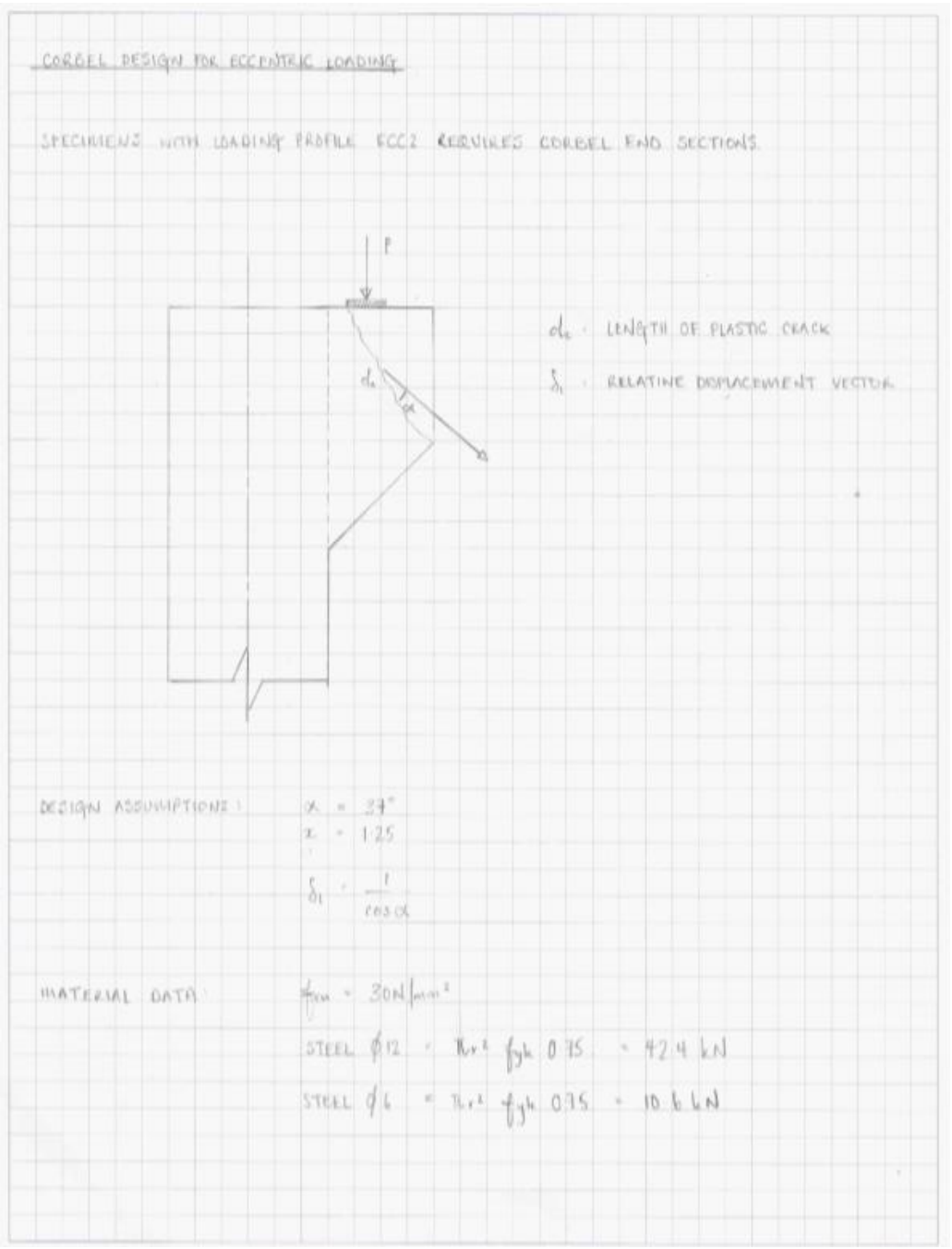

CORBEL DESIGN FOR ECCENTRIC LOADING – PAGE 2 OF 2

LOAD TO BE SUSTAINED :

$P.\delta_1 = b\, d_1 \frac{1}{2}(1 - \sin\alpha) \times f_{cu}\,\delta$

$= 300 \times 387 \times \frac{1}{2}(1 - \sin 37) \times 125 \times 30 \times 0.5$

$= 935.6\ kN$

LOAD IN STEEL :

SHAPE CODE 66 10 @ ϕ12 = 424 kN

LOAD IN CONCRETE :

f_c = 814 kN

THUS TOTAL CAPACITY > PEAK DESIGN LOAD CORBEL DESIGN SATISFACTORY

* NOTE : AS CAPACITY > DESIGN LOAD FOR SLS, OK TO BE USE

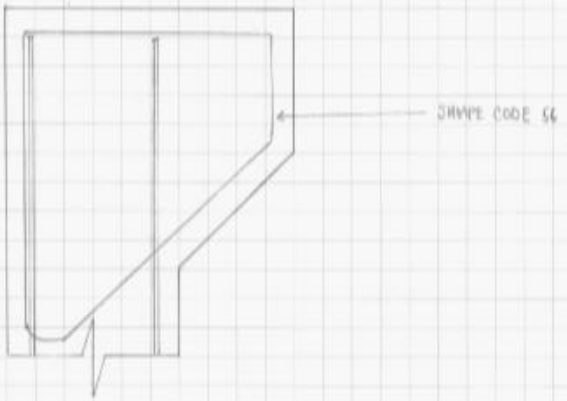

A-4 – DESIGN CALCULATIONS – CONCETNRICALLY LOADED FRP-CONFINED SPECIMEN

CONCENTRICALLY LOADED FRP-CONFINED SPECIMEN – PAGE 1 OF 2

DESIGN OF A FRP-CONFINED CONCENTRICALLY LOADED SPECIMEN

THIS CALCULATION DETAILS THE DESIGN OF FRP-CONFINED SPECIMEN SC4 (MEDIUM-SCALE) TO DESIGN GUIDANCE TR55 (2005)

b = 300 mm
h = 300 mm
r_c = 40 mm
n_s = 4
ϕ_s = 25mm
n_f = 4
t_f = 0·16mm

f_{cu} = 30 N/mm²
f_{co} = 0·67 f_{cu} = 20·1 N/mm²
f_{yd} = 580 N/mm²
f_{fd} =

ρ_{sc} = 0·22
A_g = 88627mm²

FOR DESIGN TO TR55 (2005) IT IS ASSUMED THAT THE FOLLOWING CRITERIA ARE SATISFIED:

- LOADING IS ESSENTIALLY CONCENTRIC
- THE SMALLER EDGE DIMENSION IS NO GREATER THAN 200mm
- THE ASPECT RATIO IS NO GREATER THAN 1:1·5
- THE CORNER RADIUS IS AT LEAST 40mm

FROM TR55 (2005), RATIO OF EFFECTIVE AREA TO GROSS AREA, EQUATION 44:

$$\frac{A_e}{A_g} = \frac{1 - [(h-2r_c)^2 + (b-2r_c)^2 - 3A_{ol}]/(3A_g) - \rho_{sc}}{1-\rho_{sc}}$$

WHERE A_{ol} IS:

$2b = 2 \cdot 300 = 600$ & $h - 2r_c = 300 - 2 \cdot 40 = 220$

$\therefore \quad 2b > h - 2r_c \quad \therefore \quad A_{ol} = 0$

THUS:

$$\frac{A_e}{A_g} = \frac{1 - [(300-2\cdot40)^2 + (300-2\cdot40)^2 - 3\cdot0]/(3\cdot88627) - 0.22}{1-0.22} = 0.63$$

CONCENTRICALLY LOADED FRP-CONFINED SPECIMEN – PAGE 2 OF 2

SHAPE FACTOR, EQUATION 45 :

$$g_s = \frac{b}{h}\frac{A_e}{A_g} = \frac{300}{300} \times 0.63 = 0.63$$

AND EQUIVALENT CONFINING PRESSURE (EQUATION 46) :

$$f_r = \frac{2 f_{fd} t_f}{\sqrt{h^2 + b^2}} = \frac{2 \times 2676 \times (4 \times 0.16)}{\sqrt{300^2 + 300^2}} = 8.1 \text{ N/mm}^2$$

FROM g_s & f_r, STRENGTH OF COLUMN (EQUATION 47) :

$$f_{cc} = f_{co} + 2 g_s f_r$$

$$= 20.1 + 2 \cdot 0.63 \cdot 8.1 = 30.24 \text{ N/mm}^2$$

THUS THE AXIAL CAPACITY IS :

$$N = f_{cc} A_g + f_{yd} A_s$$

$$= 30.24 \cdot 88627 + 580.1963 = \underline{3779 \text{ kN}}$$

A-5 – DESIGN CALCULATIONS – ECCENTRICALLY LOADED FRP-CONFINED SPECIMEN

ECCENTRICALLY LOADED FRP-CONFINED SPECIMEN – PAGE 1 OF 3

DESIGN OF H FRP-CONFINED ECCENTRICALLY LOADED SPECIMEN

THIS CALCULATION DETAILS THE DESIGN OF SPECIMEN SE6, MEDIUM SCALE WITH LOAD PROFILE ECC2

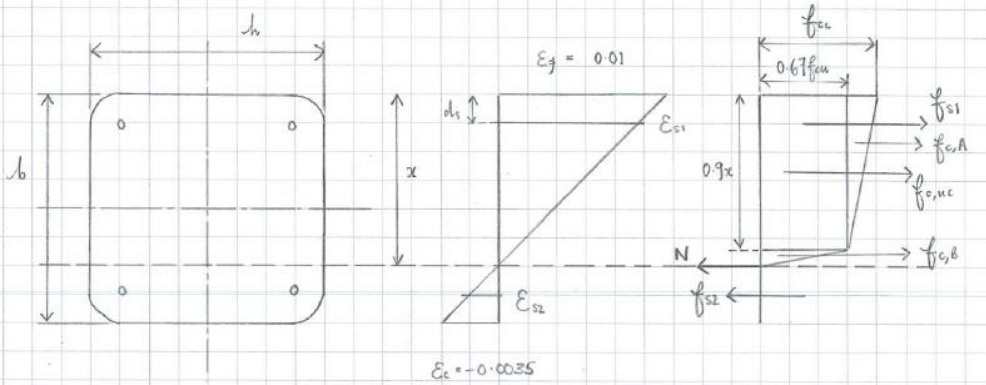

$b = 300\,mm$
$h = 300\,mm$
$r_c = 40\,mm$
$n_s = 4$
$\phi_s = 25\,mm$
$n_f = 4$
$t_f = 0.16\,mm$

$f_{cu} = 30\,N/mm^2$
$f_{yd} = 580\,N/mm^2$
$E_s =$

$A_g = 88627\,mm^2$
$A_s = 1963\,mm^2$

$x = \frac{\varepsilon_{frp}}{\varepsilon_{frp} + \varepsilon_c} \times b = 222\,mm$

$d_{c,uc} = b - x + 0.1x + 0.45x$
$= 200\,mm$
$d_{c,A} = b - x + 0.1x + \frac{2}{3} \cdot 0.9x$
$= 233\,mm$
$d_{c,B} = b - x + \frac{2}{3} \cdot 0.1x$
$= 93\,mm$

$d_{s1} = 247.5\,mm$
$d_{s2} = 52.5\,mm$

LONGITUDINAL STEEL CAPACITY

$\varepsilon_{s1} = \frac{\varepsilon_{frp}}{x}(x - d_s) = \frac{0.01}{222}(222 - 52.5) = 0.0076$ ∴ EXCEEDS YIELD

$f_{s1} = \frac{A_s}{2} f_{yd} = \frac{1963}{2} \times 580 = 569\,kN$

ECCENTRICALLY LOADED FRP-CONFINED SPECIMEN – PAGE 2 OF 3

$$\varepsilon_{s2} = \frac{\varepsilon_c}{h-x}(h-x-d_s) = \frac{0.0035}{300-222}(300-222-52.5) = 0.0011$$

$\therefore$ DOES NOT YIELD

$$f_{s2} = \frac{A_s}{2}\varepsilon_s E_s = \frac{1963}{2} \cdot 0.0011 \cdot 200 = 223\,kN$$

CALCULATION OF THE CONCRETE CAPACITY VARIES FROM THE EQUIVALENT UNCONFINED SPECIMEN WITH THE ADOPTION OF THE STRESS BLOCK.

TO ESTABLISH THE STRENGTH OF THE COLUMN, f_{cc}, THE SAME PROCESS FROM TR55 (2005) AS FOR CONCENTRICALLY LOADED SPECIMENS IS FOLLOWED, HENCE IT IS KNOWN THAT:

$$f_{cc} = 30.24\ N/mm^2$$

THUS TO ESTABLISH CONCRETE CAPACITY:

$$f_{c,uc} = h \cdot 0.9x \cdot 0.67 f_{cu} = 300 \cdot 0.9 \times 222 \cdot 0.67 \times 30 = 1206\,kN$$

$$f_{c,A} = h(0.5(f_{cc} - 0.67 f_{cu})(0.9x)) = 300(0.5(30.24 - 0.67 \times 30)(0.9 \times 222)) = 304\,kN$$

$$f_{c,B} = h(0.5(0.1x)(0.67 f_{cu})) = 300(0.5(0.1 \times 222)(0.67 \times 30)) = 67\,kN$$

HENCE THE AXIAL CAPACITY IS:

$$N = f_{c,cu} + f_{c,A} + f_{c,B} + f_{s1} + f_{s2} = 1206 + 304 + 67 + 569 - 223 = 1923\,kN$$

& MOMENT ASSOCIATED:

$$M = f_{c,uc} d_{c,uc} + f_{c,A} d_{c,A} + f_{c,B} d_{c,B} + f_{s1} d_{s1} + f_{s2} d_{s2} - N(0.5h)$$

$$= 1206 \times 200 + 304 \times 233 + 67 \times 93 + 569 \times 247.5 - 223 \times 52.5 - 1923(0.5 \times 300)$$

$$= 159806\,kNmm$$

ECCENTRICALLY LOADED FRP-CONFINED SPECIMEN – PAGE 3 OF 3

THUS THE APPLIED ECCENTRICITY IS:

$$e_i = \frac{M}{N} = \frac{159\,084}{1923} = 83 \text{ mm}$$

AS $e_i < 0.5 h_s$, CORBEL END SECTIONS ARE NOT NECESSARY. HOWEVER, IN ANTICIPATION OF VARIATIONS IN CONCRETE STRENGTH, CORBEL END SECTIONS WILL BE USED.

A-6 – TR55 (2011) DESIGN – INTERACTION POINT 1

TR55 (2011) INTERACTION POINT 1 – PAGE 1 OF 5

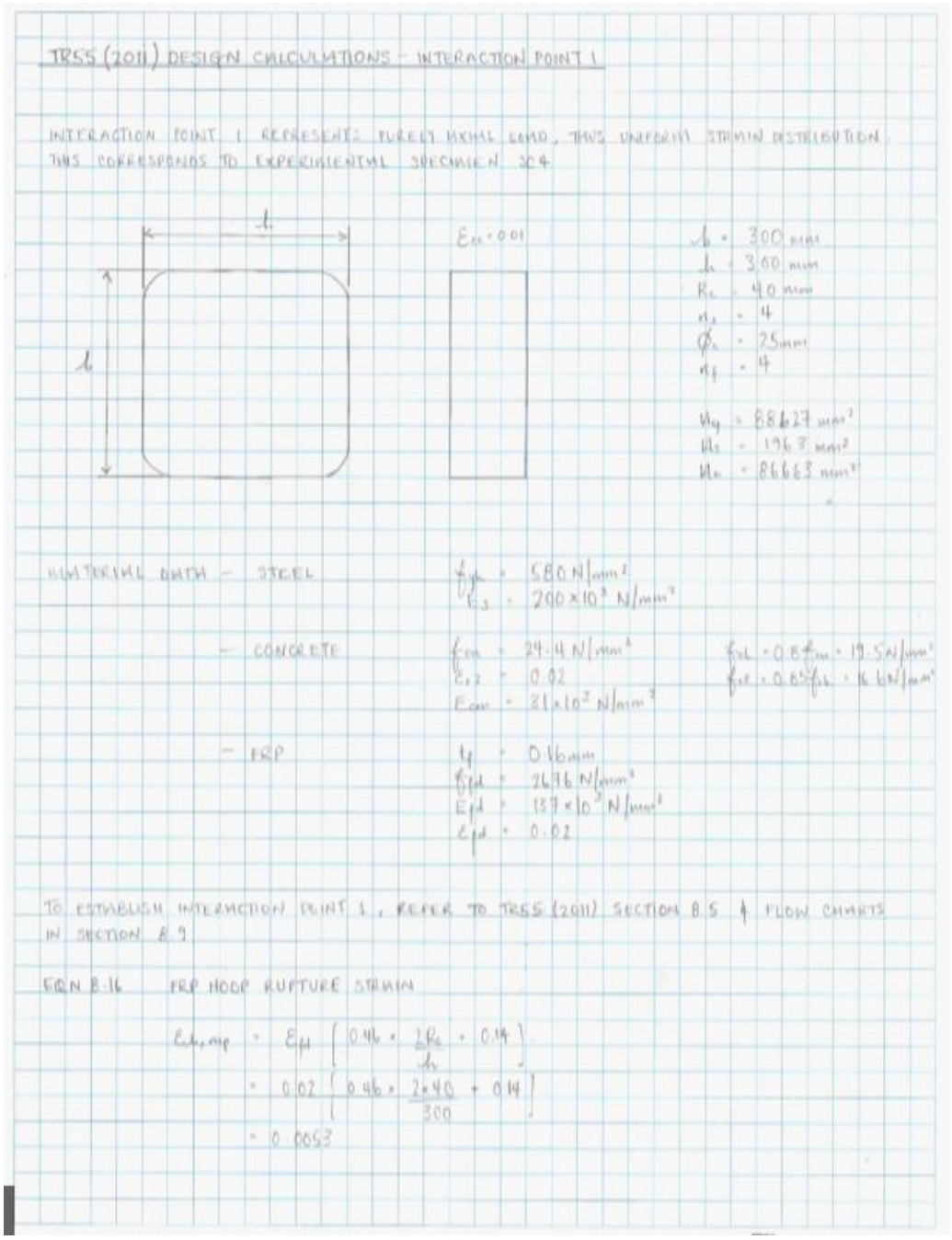

TR55 (2011) DESIGN CALCULATIONS - INTERACTION POINT 1

INTERACTION POINT 1 REPRESENTS PURELY AXIAL LOAD, THUS UNIFORM STRAIN DISTRIBUTION. THIS CORRESPONDS TO EXPERIMENTAL SPECIMEN SC4

$b = 300$ mm
$h = 360$ mm
$R_c = 40$ mm
$n_s = 4$
$\phi_s = 25$ mm
$n_f = 4$

$A_g = 88627$ mm²
$A_s = 1963$ mm²
$A_c = 86663$ mm²

MATERIAL BEHAVIOUR – STEEL

$f_{yk} = 580$ N/mm²
$E_s = 200 \times 10^3$ N/mm²

– CONCRETE

$f_{cm} = 24.4$ N/mm²
$\varepsilon_{c2} = 0.02$
$E_{cm} = 31 \times 10^3$ N/mm²

$f_{cd} = 0.85 f_{cm} = 19.5$ N/mm²
$f_{cd} = 0.85 f_{cd} = 16$ N/mm²

– FRP

$t_f = 0.16$ mm
$f_{fd} = 2696$ N/mm²
$E_{fd} = 137 \times 10^3$ N/mm²
$\varepsilon_{fd} = 0.02$

TO ESTABLISH INTERACTION POINT 1, REFER TO TR55 (2011) SECTION 8.5 & FLOW CHARTS IN SECTION 8.9

EQN 8.16 FRP HOOP RUPTURE STRAIN

$$\varepsilon_{h,rup} = \varepsilon_{fd} \left[0.46 \times \frac{2R_c}{h} + 0.14 \right]$$

$$= 0.02 \left[0.46 \times \frac{2 \times 40}{300} + 0.14 \right]$$

$$= 0.0053$$

TR55 (2011) INTERACTION POINT 1 – PAGE 2 OF 5

TR55 (2011) INTERACTION POINT 1 – PAGE 3 OF 5

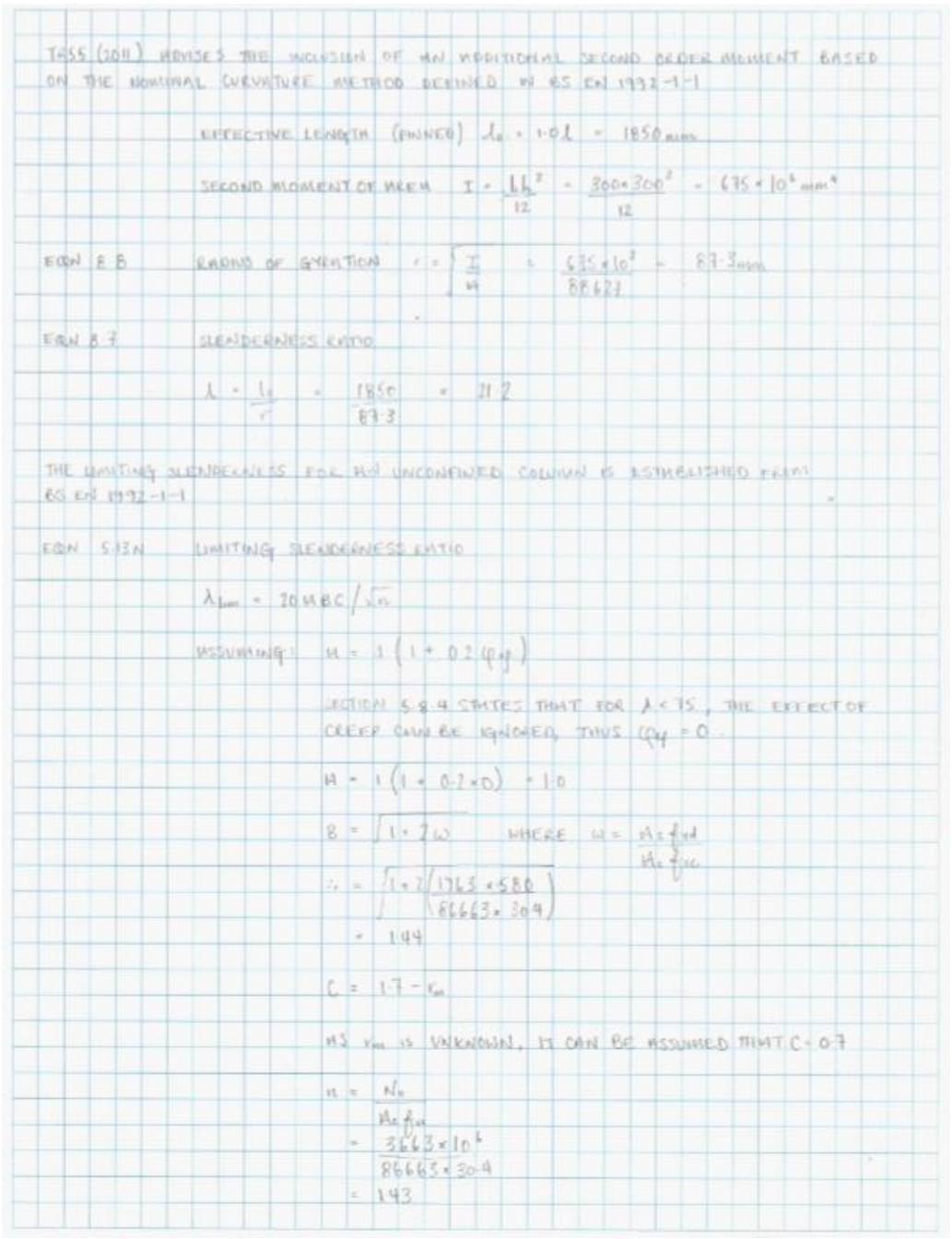

TR55 (2011) REVISES THE INCLUSION OF AN ADDITIONAL SECOND ORDER MOMENT BASED ON THE NOMINAL CURVATURE METHOD DEFINED IN BS EN 1992-1-1

EFFECTIVE LENGTH (PINNED) $l_0 = 1.0l = 1850\,mm$

SECOND MOMENT OF AREA $I = \frac{bh^3}{12} = \frac{300 \times 300^3}{12} = 675 \times 10^6\,mm^4$

EQN 8.6 RADIUS OF GYRATION $i = \sqrt{\frac{I}{A}} = \frac{675 \times 10^6}{89627} = 87.3\,mm$

EQN 8.7 SLENDERNESS RATIO

$\lambda = \frac{l_0}{i} = \frac{1850}{87.3} = 21.2$

THE LIMITING SLENDERNESS FOR AN UNCONFINED COLUMN IS ESTABLISHED FROM BS EN 1992-1-1

EQN 5.13N LIMITING SLENDERNESS RATIO

$\lambda_{lim} = 20ABC/\sqrt{n}$

ASSUMING: $A = 1\left(1 + 0.2\,\phi_{ef}\right)$

SECTION 5.8.4 STATES THAT FOR $\lambda < 75$, THE EFFECT OF CREEP CAN BE IGNORED, THUS $\phi_{ef} = 0$.

$A = 1\left(1 + 0.7 \times 0\right) = 1.0$

$B = \sqrt{1 + 2w}$ WHERE $w = \frac{A_s f_{yd}}{A_c f_{cc}}$

$\therefore = \sqrt{1 + 2\left(\frac{1763 \times 580}{86663 \times 30.4}\right)}$

$= 1.44$

$C = 1.7 - r_m$

AS r_m IS UNKNOWN, IT CAN BE ASSUMED THAT $C = 0.7$

$n = \frac{N_d}{A_c f_{cc}}$

$= \frac{3663 \times 10^3}{86663 \times 30.4}$

$= 1.43$

TR55 (2011) INTERACTION POINT 1 – PAGE 4 OF 5

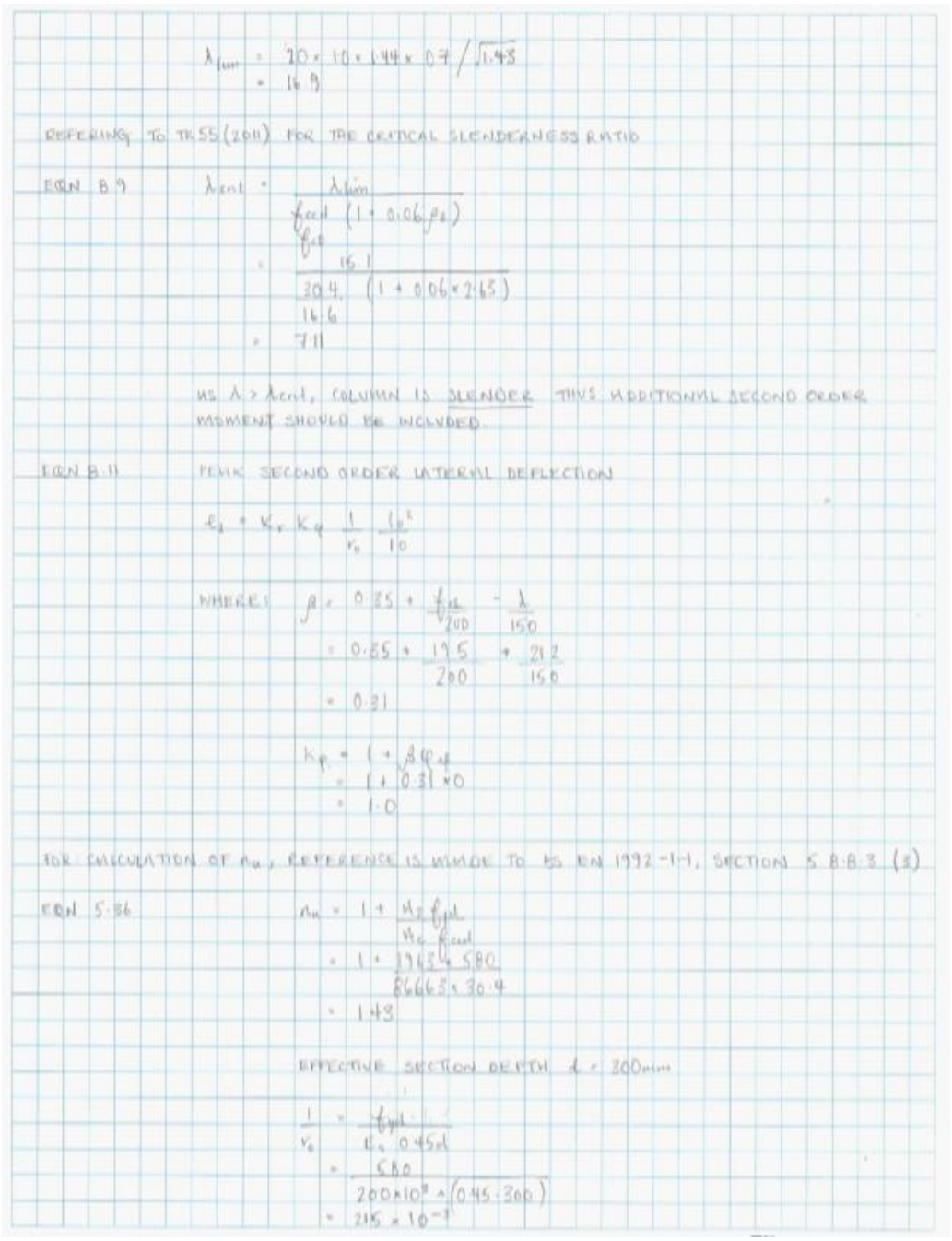

$\lambda_{lim} = 20 \times 1.0 \times 1.44 \times 0.7 / \sqrt{1.43}$

$= 16.9$

REFERRING TO TR55(2011) FOR THE CRITICAL SLENDERNESS RATIO

EQN B.9 $\lambda_{crit} = \dfrac{\lambda_{lim}}{\dfrac{f_{cd}}{f_{c0}}(1 + 0.06\beta_d)}$

$= \dfrac{15.1}{\dfrac{30.4}{16.6}(1 + 0.06 \times 2.65)}$

$= 7.11$

AS $\lambda > \lambda_{crit}$, COLUMN IS SLENDER THUS ADDITIONAL SECOND ORDER MOMENT SHOULD BE INCLUDED

EQN B.11 PEAK SECOND ORDER LATERAL DEFLECTION

$e_2 = K_r K_\varphi \dfrac{1}{r_0} \dfrac{l_0^2}{10}$

WHERE: $\beta = 0.35 + \dfrac{f_{ck}}{200} - \dfrac{\lambda}{150}$

$= 0.35 + \dfrac{19.5}{200} + \dfrac{21.2}{150}$

$= 0.31$

$K_\varphi = 1 + \beta\varphi_{ef}$

$= 1 + 0.31 \times 0$

$= 1.0$

FOR CALCULATION OF K_u, REFERENCE IS MADE TO BS EN 1992-1-1, SECTION 5.8.8.3 (2)

EQN 5.86 $K_u = 1 + \dfrac{w_2 f_{yd}}{w_c f_{cd}}$

$= 1 + \dfrac{1963 \times 580}{86663 \times 30.4}$

$= 1.43$

EFFECTIVE SECTION DEPTH $d = 300mm$

$\dfrac{1}{r_0} = \dfrac{f_{yd}}{E_s \times 0.45d}$

$= \dfrac{580}{200 \times 10^3 \times (0.45 \cdot 300)}$

$= 215 \times 10^{-7}$

TR55 (2011) INTERACTION POINT 1 – PAGE 5 OF 5

$$K_r = \left(\frac{n_u - n}{n_u - 0.4}\right) \leq 1.0$$

$$= \frac{1.43 - 1.43}{1.43 - 0.4} \leq 1.0$$

$$= 0.0 \leq 1.0 \quad \therefore \text{SATISFIED}$$

$$e_2 = 0 \times 1.0 \times 2.15 \times 10^{-3} \times \frac{1850^2}{10}$$

$$= 0.0 \text{ mm}$$

EQN 8.10 NOMINAL SECOND ORDER MOMENT IN SLENDER COLUMNS

$$M_2 = N_z e_2$$
$$= 3663 \times 10^3 \times 0.0$$
$$= 0.0 \text{ Nmm}$$

THUS THE AXIAL CAPACITY & APPLIED MOMENT ARE:

POINT 1 : AXIAL CAPACITY N_z = 3663 kN

APPLIED MOMENT : $M_{applied}$ = 0.0 kNmm

APPLIED ECCENTRICITY e_a = 0.0 mm

A-7 – TR55 (2011) DESIGN– INTERACTION POINT 2

TR55 (2011) INTERACTION POINT 2 – PAGE 1 OF 4

TR55 (2011) DESIGN CALCULATIONS – INTERACTION POINT 2

INTERACTION POINT 2 REPRESENTS A STRAIN DISTRIBUTION OVER THE CROSS-SECTION FROM ZERO STRAIN TO ε_{cu}

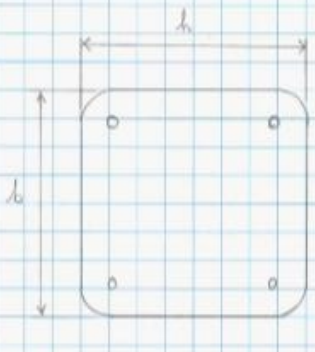

$f_{cu} = 42.0\ N/mm^2$

THUS:

$f_{ck} = 33.6\ N/mm^2$

$f_{c0} = 28.6\ N/mm^2$

REFER TO INTERACTION POINT 1 FOR GEOMETRY AND STEEL & FRP MATERIAL DATA

TO ESTABLISH INTERACTION POINT 2, REFER TO TR55 (2011) SECTION 8.5 & FLOW CHARTS IN SECTION 8.7

EQN 8.22 SHEAR STRESS

$$T = t_f E_{pl} \frac{\varepsilon_{1,mp}}{(h - 2R_o)} \leq T_{max}$$

$$= (0.16 \times 4)\ 127 \times 10^3 \cdot \frac{0.0053}{(300 - 2 \times 40)}$$

$$= 2.09$$

EQN 8.21 LIMITING SHEAR STRESS

$$T_{max} = \frac{0.8\ f_{ctk}}{\gamma_c}$$

WHERE $\gamma_c = 1.0$ ASSUMED FOR DESIGN

FROM BS EN 1992-1-1 $f_{ctm} = 0.3 f_{ck}^{2/3}$

$= 0.3 \times 33.6^{2/3} = 3.12\ N/mm^2$

$f_{ctk} = 0.7 f_{ctm}$

$= 0.7 \times 3.12 = 2.19\ N/mm^2$

TR55 (2011) INTERACTION POINT 2 – PAGE 2 OF 4

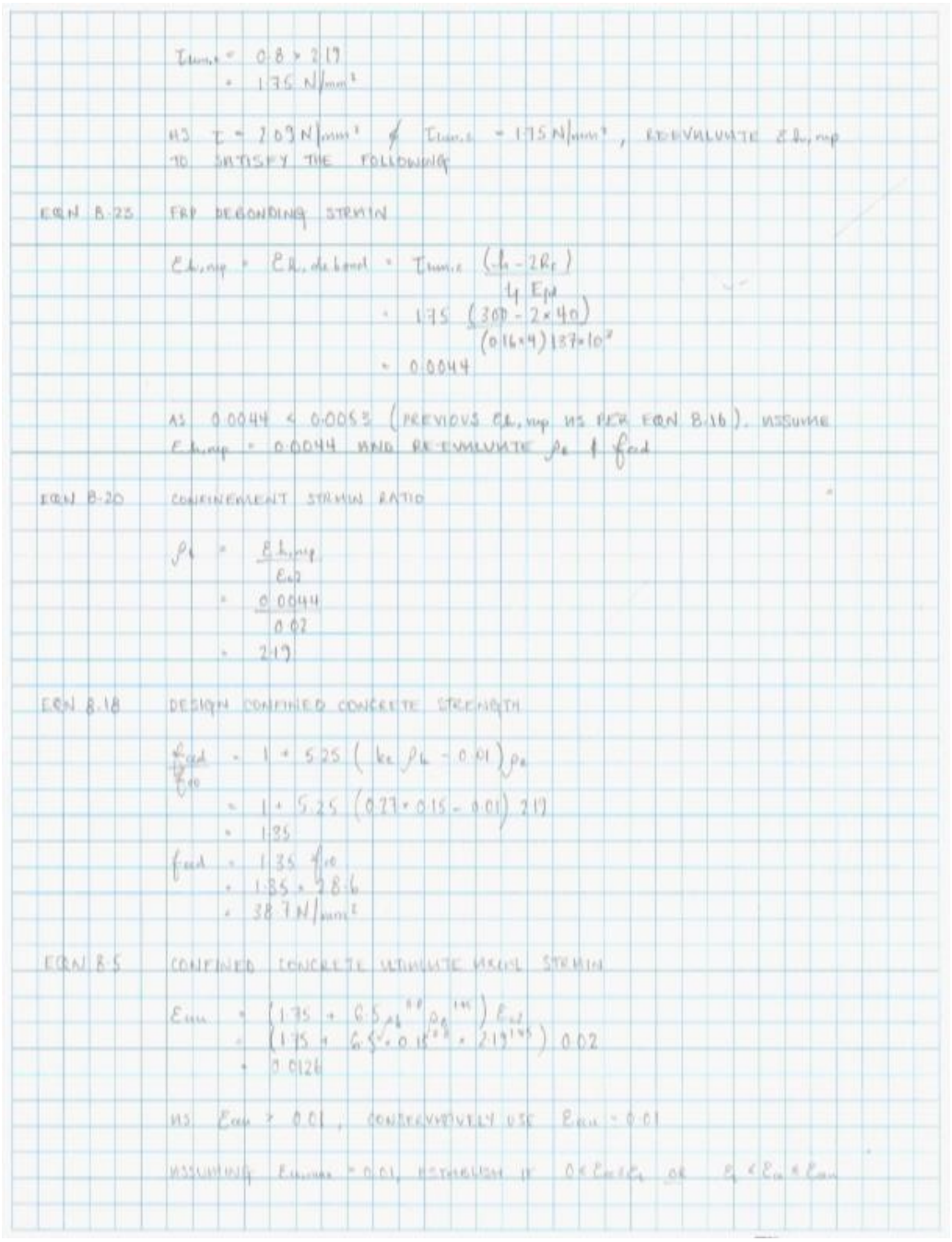

$f_{fwd} = 0.8 \times 2.19$
$= 1.75\ N/mm^2$

AS $f = 2.03\ N/mm^2$ & $f_{fwd,max} = 1.75\ N/mm^2$, RE-EVALUATE $\varepsilon_{b,rup}$ TO SATISFY THE FOLLOWING

EQN B.25 FRP DEBONDING STRAIN

$\varepsilon_{b,rup} = \varepsilon_{b,debond} = f_{fwd,max} \frac{(L_b - 2R_f)}{4 E_{fu}}$
$= 1.75 \frac{(300 - 2\times 40)}{(0.16\times 4)\,137\times 10^3}$
$= 0.0044$

AS $0.0044 < 0.0053$ (PREVIOUS $\varepsilon_{b,rup}$ AS PER EQN B.16). ASSUME $\varepsilon_{b,rup} = 0.0044$ AND RE-EVALUATE ρ_e & f_{fwd}

EQN B.20 CONFINEMENT STRAIN RATIO

$\rho_\varepsilon = \frac{\varepsilon_{b,rup}}{\varepsilon_{co}}$
$= \frac{0.0044}{0.02}$
$= 2.19$

EQN B.18 DESIGN CONFINED CONCRETE STRENGTH

$\frac{f_{fwd}}{f_{co}} = 1 + 5.25 (k_e \rho_\varepsilon - 0.01) \rho_e$
$= 1 + 5.25 (0.77 \times 0.15 - 0.01)\, 2.19$
$= 1.35$
$f_{fwd} = 1.35\, f_{co}$
$= 1.35 \times 28.6$
$= 38.7\ N/mm^2$

EQN B.5 CONFINED CONCRETE ULTIMATE MASSIVE STRAIN

$\varepsilon_{cu} = \left(1.75 + 6.5 \rho_\varepsilon^{0.8} \rho_e^{1.45}\right) \varepsilon_{co}$
$= \left(1.75 + 6.5 \sqrt{0.15}^{0.8} \times 2.19^{1.45}\right) 0.02$
$= 0.0126$

AS $\varepsilon_{cu} > 0.01$, CONSERVATIVELY USE $\varepsilon_{cu} = 0.01$

ASSUMING $\varepsilon_{cu,max} = 0.01$, HOWEVER IF $0 < \varepsilon_{b,rup} < \varepsilon_{bi}$ OR $\varepsilon_{bi} < \varepsilon_{b,rup} < \varepsilon_{cu}$

TR55 (2011) INTERACTION POINT 2 – PAGE 3 OF 4

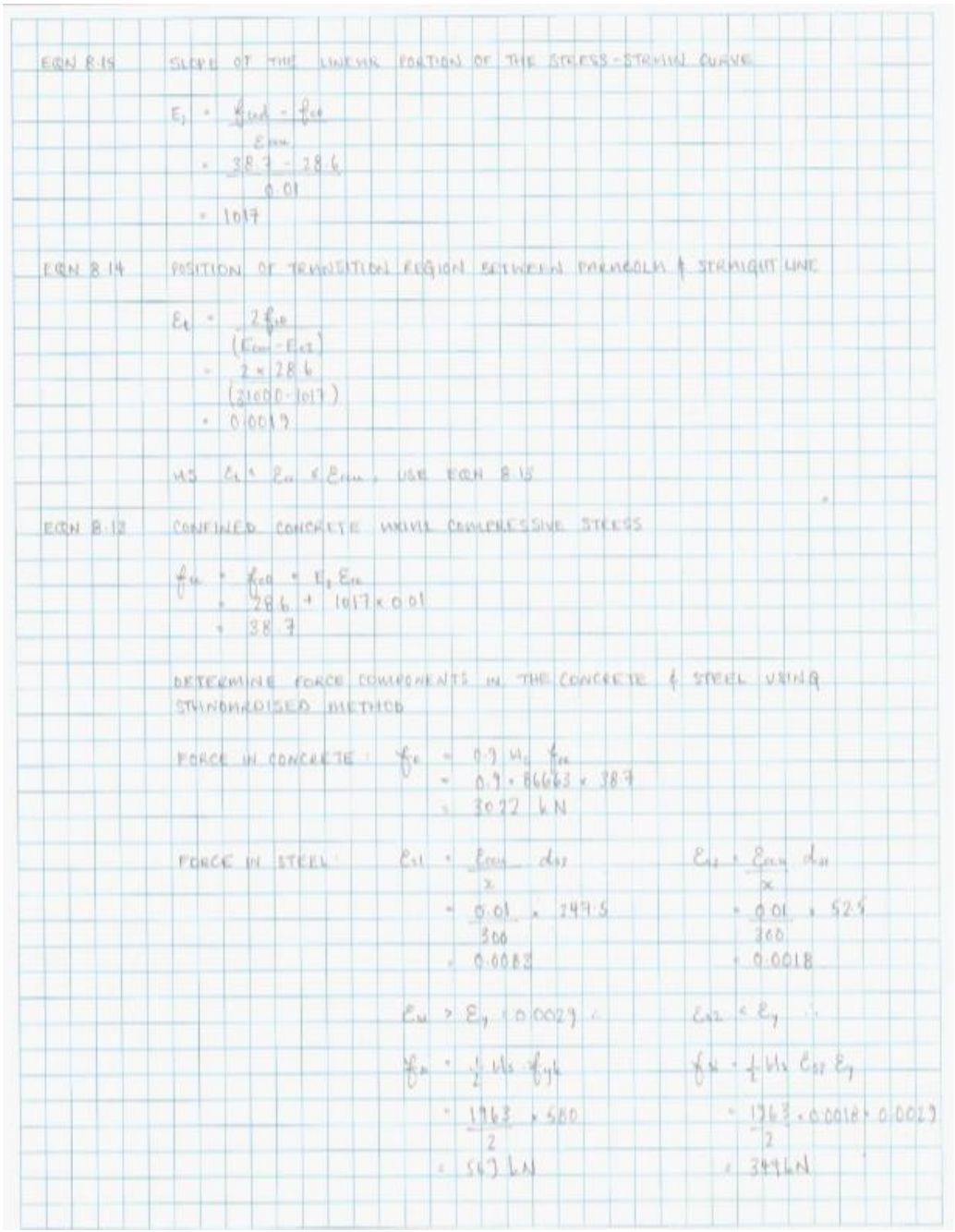

EQN 8.15 SLOPE OF THE LINEAR PORTION OF THE STRESS-STRAIN CURVE

$E_1 = \frac{f_{cu} - f_{co}}{\varepsilon_{cu}}$

$= \frac{38.7 - 28.6}{0.01}$

$= 1017$

EQN 8.14 POSITION OF TRANSITION REGION BETWEEN PARABOLA & STRAIGHT LINE

$\varepsilon_t = \frac{2 f_{co}}{(E_{cu} - E_{c2})}$

$= \frac{2 \times 28.6}{(31000 - 1017)}$

$= 0.0019$

AS $\varepsilon_t < \varepsilon_{co} < \varepsilon_{cu}$, USE EQN 8.15

EQN 8.12 CONFINED CONCRETE ULTIMATE COMPRESSIVE STRESS

$f_{cu} = f_{co} + E_1 \varepsilon_{cu}$

$= 28.6 + 1017 \times 0.01$

$= 38.7$

DETERMINE FORCE COMPONENTS IN THE CONCRETE & STEEL USING STANDARDISED METHOD

FORCE IN CONCRETE: $f_c = 0.9 \alpha_1 f_{cu}$

$= 0.9 \times 86663 \times 38.7$

$= 3022$ kN

FORCE IN STEEL: $\varepsilon_{s1} = \frac{\varepsilon_{cu}}{x} d_{s1}$ $\varepsilon_{s2} = \frac{\varepsilon_{cu}}{x} d_{s2}$

$= \frac{0.01}{300} \times 249.5$ $= \frac{0.01}{300} \times 529$

$= 0.0083$ $= 0.0018$

$\varepsilon_{s1} > \varepsilon_y$ (0.0029) $\varepsilon_{s2} < \varepsilon_y$

$f_{s1} = \frac{1}{2} \alpha_1 f_{y4}$ $f_{s2} = \frac{1}{2} \alpha_1 \varepsilon_{s2} E_y$

$= \frac{1963}{2} \times 580$ $= \frac{1963}{2} \times 0.0018 \times 0.0029$

$= 569$ kN $= 3496$ N

TR55 (2011) INTERACTION POINT 2 – PAGE 4 OF 4

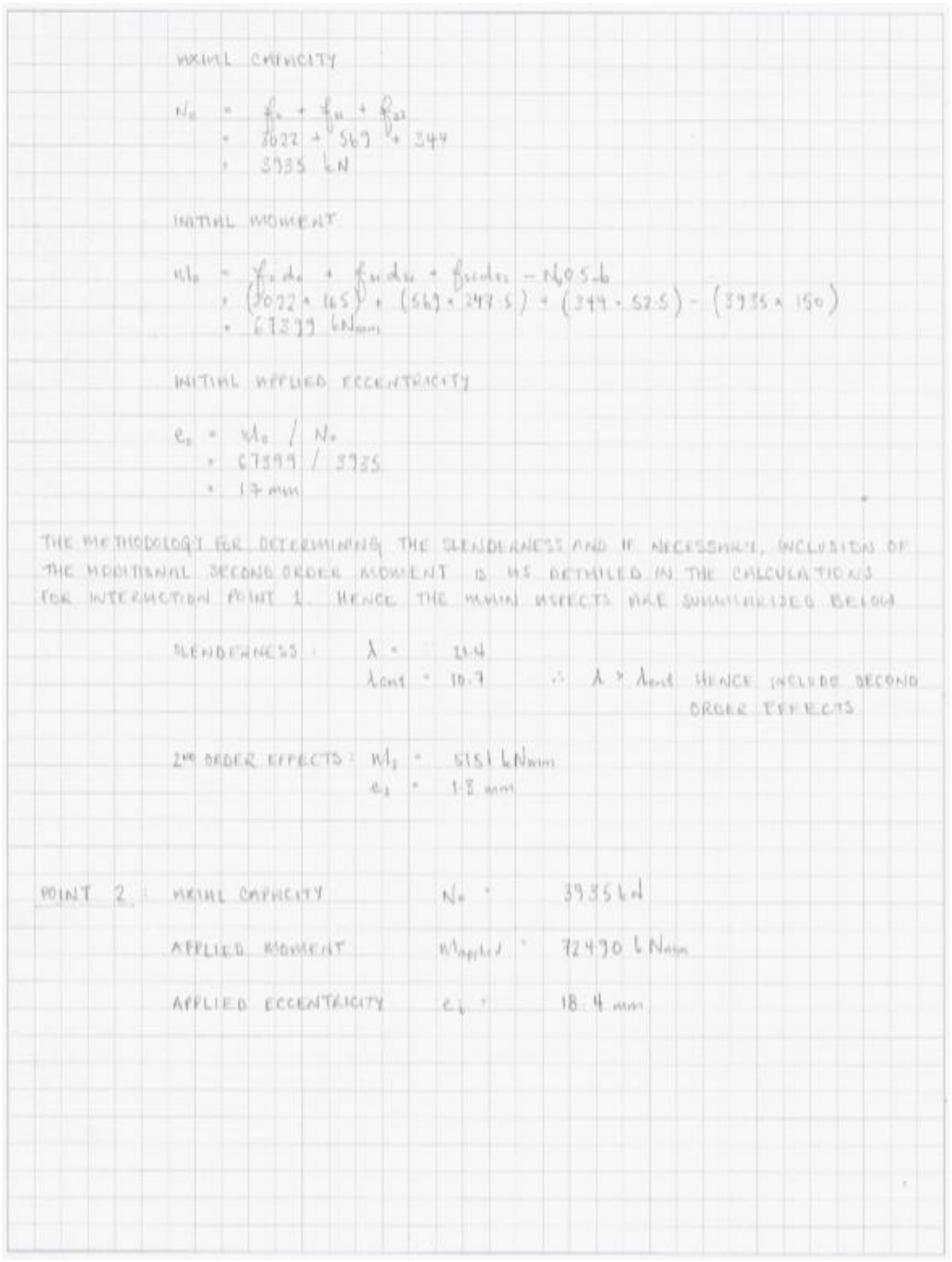

AXIAL CAPACITY

$N_o = f_{cu} + f_w + f_{sc}$
$= 3022 + 567 + 344$
$= 3935\ kN$

INITIAL MOMENT

$M_o = f_{cu} d_c + f_w d_w + f_{sc} d_{sc} - N_o 5.6$
$= (3022 \times 165) + (567 \times 247.5) + (344 \times 52.5) - (3935 \times 150)$
$= 67399\ kNmm$

INITIAL APPLIED ECCENTRICITY

$e_o = M_o / N_o$
$= 67399 / 3935$
$= 17\ mm$

THE METHODOLOGY FOR DETERMINING THE SLENDERNESS AND IF NECESSARY, INCLUSION OF THE ADDITIONAL SECOND ORDER MOMENT IS AS DETAILED IN THE CALCULATIONS FOR INTERACTION POINT 1. HENCE THE MAIN ASPECTS ARE SUMMARIZED BELOW

SLENDERNESS: $\lambda = 23.4$
$\lambda_{limit} = 10.7$ $\therefore \lambda > \lambda_{limit}$ HENCE INCLUDE SECOND ORDER EFFECTS

2ND ORDER EFFECTS: $M_2 = 5151\ kNmm$
$e_2 = 1.3\ mm$

POINT 2: AXIAL CAPACITY $N_o = 3935\ kN$

APPLIED MOMENT $M_{applied} = 72490\ kNmm$

APPLIED ECCENTRICITY $e_a = 18.4\ mm$

A-8 – TR55 (2011) DESIGN– INTERACTION POINT 3

TR55 (2011) INTERACTION POINT 3 – PAGE 1 OF 4

TR55 (2011) DESIGN CALCULATIONS - INTERACTION POINT 3

INTERACTION POINT 3 REPRESENTS THE BALANCE POINT WHERE THE TENSION STEEL YIELDS AS THE CONCRETE THUS GIVING THE MAXIMUM MOMENT CAPACITY

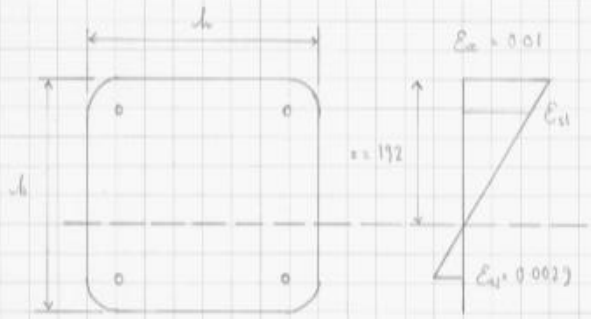

f_{cu} = 42.0 N/mm²

THUS:
f_{ck} = 33.6 N/mm²
f_{cd} = 28.6 N/mm²

REFER TO INTERACTION POINT 1 FOR GEOMETRY AND STEEL & FRP MATERIAL DATA

TO ESTABLISH INTERACTION POINT 3, REFER TO TR55 (2011) SECTION 8.5 & FLOW CHARTS IN SECTION 8.9

EQN 8.14 SHEAR STRESS

$$\tau = f_y E_{pd} \frac{\varepsilon_{b,mp}}{(x - d_s)} \leq \tau_{max,c}$$

$$= (0.16 \times 187 \times 10^3) \frac{0.0053}{(192 - 40)} \leq 1.75$$

$$= 3.03 \not\leq 1.75$$

AS τ = 3.03 $\not\leq$ $\tau_{max,c}$ = 1.75 N/mm², RE-EVALUATE $\varepsilon_{b,mp}$ TO SATISFY THE FOLLOWING

EQN 8.25 FRP DEBONDING STRAIN

$$\varepsilon_{b,mp} = \varepsilon_{b,debond} = \tau_{max,c} \frac{(x - d_s)}{f_y E_{pd}}$$

$$= 1.75 \frac{(192 - 40)}{(0.16 \times 4) 187 \times 10^3}$$

$$= 0.0020$$

TR55 (2011) INTERACTION POINT 3 – PAGE 2 OF 4

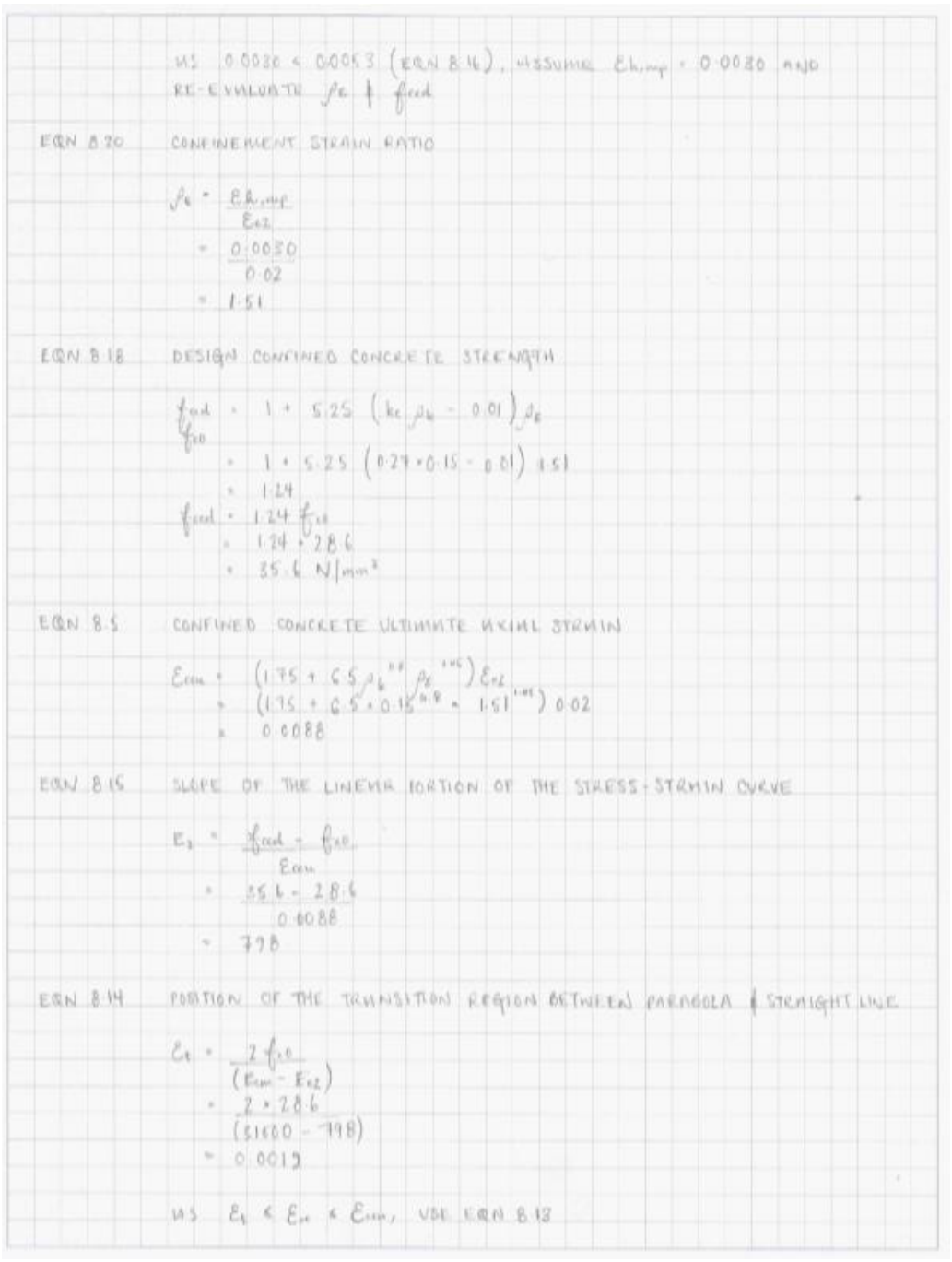

IF $0.0030 < 0.0053$ (EQN B.16), ASSUME $\varepsilon_{h,mp} = 0.0030$ AND RE-EVALUATE ρ_e & f_{cwd}

EQN B.20 CONFINEMENT STRAIN RATIO

$$\rho_e = \frac{\varepsilon_{h,mp}}{\varepsilon_{c2}} = \frac{0.0030}{0.02} = 1.51$$

EQN B.18 DESIGN CONFINED CONCRETE STRENGTH

$$\frac{f_{cwd}}{f_{cd}} = 1 + 5.25\left(k_e \rho_k - 0.01\right)\rho_e$$

$$= 1 + 5.25\left(0.29 \times 0.15 - 0.01\right) 1.51$$

$$= 1.24$$

$$f_{cwd} = 1.24 f_{cd} = 1.24 \times 28.6 = 35.6\ N/mm^2$$

EQN 8.5 CONFINED CONCRETE ULTIMATE AXIAL STRAIN

$$\varepsilon_{cu} = \left(1.75 + 6.5 \rho_k^{0.8} \rho_e^{1.45}\right)\varepsilon_{c2} = \left(1.75 + 6.5 \times 0.15^{0.8} \times 1.51^{1.45}\right) 0.02 = 0.0088$$

EQN 8.15 SLOPE OF THE LINEAR PORTION OF THE STRESS-STRAIN CURVE

$$E_2 = \frac{f_{cwd} - f_{cd}}{\varepsilon_{cu}} = \frac{35.6 - 28.6}{0.0088} = 798$$

EQN 8.14 PORTION OF THE TRANSITION REGION BETWEEN PARABOLA & STRAIGHT LINE

$$\varepsilon_t = \frac{2 f_{cd}}{(E_{cm} - E_{c2})} = \frac{2 \times 28.6}{(31400 - 798)} = 0.0019$$

AS $\varepsilon_t < \varepsilon_c < \varepsilon_{cu}$, USE EQN B.13

TR55 (2011) INTERACTION POINT 3 – PAGE 3 OF 4

EQN 8.13 CONFINED CONCRETE AXIAL COMPRESSIVE STRESS

$f_{cc} = f_{c0} + E_2 \varepsilon_{cc}$
$= 28.6 + 798 \times 0.01$
$= 36.5\ N/mm^2$

DETERMINE FORCE COMPONENTS IN THE CONCRETE & STEEL USING STANDARDISED METHOD

FORCE IN CONCRETE: $f_c = 0.9 n_c f_{cc}$
$= 0.9 \times 86663 \times 36.5$
$= 2053\ kN$

FORCE IN STEEL: $\varepsilon_{s1} = \frac{\varepsilon_{cm}}{(h - d_{s1})} \times (d_{s1} - d_{s1})$ $\varepsilon_{s2} = -0.0029$
$= \frac{0.01}{(300 - 52.5)} \times (247.5 - 52.5)$
$= 0.0073$

$\varepsilon_{s1} > \varepsilon_y = 0.0029$ $\therefore$ $\varepsilon_{s2} = \varepsilon_y$

$f_{s1} = \frac{1}{2} n_s f_{yk}$ $f_{s2} = \frac{1}{2} n_s f_{yk}$
$= \frac{1963 \times 580}{2}$ $= \frac{1963 \times 580}{2}$
$= 569\ kN$ $= -569\ kN$

AXIAL CAPACITY

$N_0 = f_c + f_{s1} + f_{s2}$
$= 2053 + 569 - 569$
$= 2053\ kN$

INITIAL APPLIED MOMENT

$M_0 = f_c d_c + f_{s1} d_{s1} + f_{s2} d_{s2} - N_0 0.5 b$
$= (2053 \times 214) + (569 \times 247.5) + (-569 \times 52.5) - (2053 \times 150)$
$= 214796\ kNmm$

INITIAL APPLIED ECCENTRICITY

$e_0 = M_0 / N_0$
$= 214796 / 2053$
$= 118\ mm$

TR55 (2011) INTERACTION POINT 3 – PAGE 4 OF 4

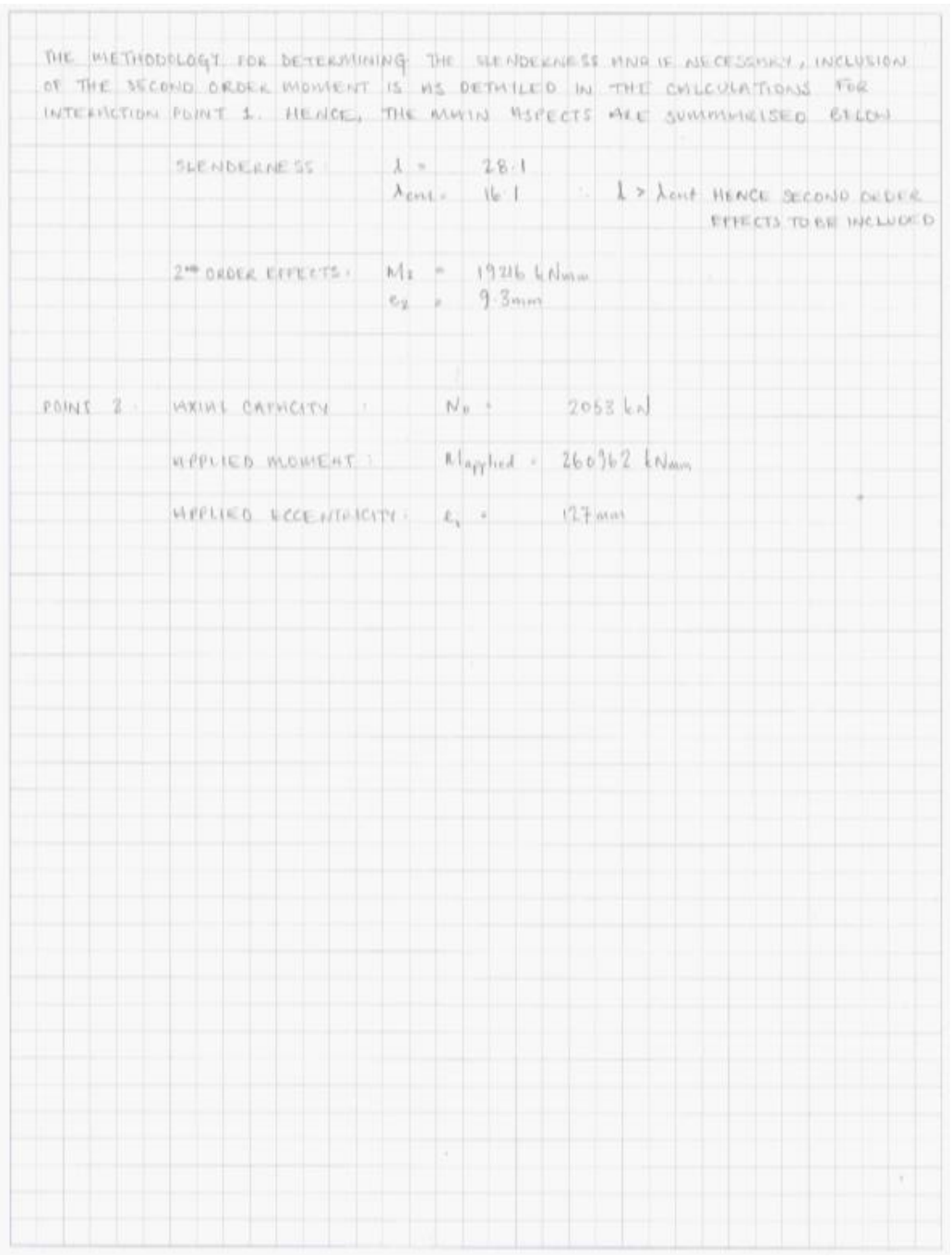

THE METHODOLOGY FOR DETERMINING THE SLENDERNESS AND IF NECESSARY, INCLUSION OF THE SECOND ORDER MOMENT IS AS DETAILED IN THE CALCULATIONS FOR INTERACTION POINT 1. HENCE, THE MAIN ASPECTS ARE SUMMARISED BELOW

SLENDERNESS: λ = 28.1, λ_{limit} = 16.1 ∴ $\lambda > \lambda_{limit}$ HENCE SECOND ORDER EFFECTS TO BE INCLUDED

2ND ORDER EFFECTS: M_2 = 19216 kNmm, e_2 = 9.3mm

POINT 2:

AXIAL CAPACITY: N_u = 2053 kN

APPLIED MOMENT: $M_{applied}$ = 26036.2 kNmm

APPLIED ECCENTRICITY: e_x = 12.7mm

A-9 – TR55 (2011) DESIGN – INTERACTION POINT 4

TR55 (2011) INTERACTION POINT 4 – PAGE 1 OF 1

PAGE 1 OF 1

APPENDIX B – MATERIAL DATA

CONTENTS: B-1 – STEEL REINFORCEMENT BAR SCHEDULE (MEDIUM- AND LARGE-SCALE)

B-2 – FRP MATERIAL DATA SHEET

B-1 – STEEL REINFORCEMENT BAR SCHEDULE (MEDIUM- AND LARGE-SCALE)

BAR MARK	SHAPE CODE	SIZE	LENGTH	QUANTITY	R	A	B	C	D	E	F
		mm	mm		mm	mm	mm	mm	mm	mm	mm
SC3 (300x300)											
Long.	OO	25	1810	4		1810					
Stirrups	51	6	1179	30	12.5	260	260	100	100		
Ends	21	25	703	4	87	280	280	280			
SC4 (300x300)											
Long.	OO	25	1810	4		1810					
Stirrups	51	6	1179	30	12.5	260	260	100	100		
Ends	21	25	703	4	87	280	280	280			
SC5 (450x450)											
Long.	OO	25	2340	8		2340					
Stirrups	51	8	1672	36	16	388	388	100	100		
Ends	21	25	1158	4	87	420	455	420			
SC6 (450x450)											
Long.	OO	25	2340	8		2340					
Stirrups	51	8	1672	36	16	388	388	100	100		
Ends	21	25	1158	4	87	420	455	420			
SE5 (300x300)											
Long.	OO	25	1810	4		1810					
Stirrups	51	6	1179	30	12.5	260	260	100	100		
Ends	21	25	703	4	87	280	280	280			
SE6 (300x300 with corbel)											
Long.	OO	25	2410	2		2410					
Long.	OO	25	2386	2		2386					
Stirrups	51	6	1709	22	12.5	525	260	100	100		
Stirrups	51	6	1695	2	12.5	518	260	100	100		
Stirrups	51	6	1635	2	12.5	488	260	100	100		
Stirrups	51	6	1577	2	12.5	459	260	100	100		
Stirrups	51	6	1517	2	12.5	429	260	100	100		
Stirrups	51	6	1459	2	12.5	400	260	100	100		
Stirrups	51	6	1399	2	12.5	370	260	100	100		
Stirrups	51	6	1341	2	12.5	341	260	100	100		
Stirrups	51	6	1281	2	12.5	311	260	100	100		
Stirrups	51	6	1223	2	12.5	282	260	100	100		
Stirrups	51	6	1179	6	12.5	260	260	100	100		

BAR MARK	SHAPE CODE	SIZE	LENGTH	QUANTITY	R	A	B	C	D	E	F
		mm	mm		mm	mm	mm	mm	mm	mm	mm
Corbel	56	12	2164	16	24, 60 (D-A)	690	513	304	577	100	100
Corbel	56	12	2104	4	24, 60 (D-A)	690	488	304	542	100	100
SE7 (450x450)											
Long.	OO	25	2340	8		2340					
Stirrups	51	8	1672	36	16	388	388	100	100		
Ends	21	25	1158	4	87	420	455	420			
SE6 (450x450 with corbel)											
Long.	OO	25	3240	4		3240					
Long.	OO	25	3216	4		3216					
Stirrups	51	8	2322	52	16	713	388	100	100		
Stirrups	51	8	2278	2	16	691	388	100	100		
Stirrups	51	8	2232	2	16	668	388	100	100		
Stirrups	51	8	2188	2	16	646	388	100	100		
Stirrups	51	8	2142	2	16	623	388	100	100		
Stirrups	51	8	2098	2	16	601	388	100	100		
Stirrups	51	8	2052	2	16	578	388	100	100		
Stirrups	51	8	2008	2	16	556	388	100	100		
Stirrups	51	8	1962	2	16	533	388	100	100		
Stirrups	51	8	1918	2	16	511	388	100	100		
Stirrups	51	8	1872	2	16	488	388	100	100		
Stirrups	51	8	1828	2	16	466	388	100	100		
Stirrups	51	8	1782	2	16	443	388	100	100		
Stirrups	51	8	1738	2	16	421	388	100	100		
Stirrups	51	8	1692	2	16	398	388	100	100		
Stirrups	51	8	1672	6	16	388	388	100	100		
Corbel	56	12	3132	28	24, 100 (D-A)	1027	697	528	745	100	100
Corbel	56	12	3072	4	24, 100 (D-A)	1027	672	528	710	100	100
RC1 (300x450)											
Long.	OO	25	2360	6		2360					
Stirrups	51	6	1479	36	12.5	410	260	100	100		
Ends	21	25	969	6	87	430	246	430			
Links	99	6	460	36	12.5	260	100				
RC2 (300x450)											

BAR MARK	SHAPE CODE	SIZE	LENGTH	QUANTITY	R	A	B	C	D	E	F
		mm	mm		mm	mm	mm	mm	mm	mm	mm
Long.	OO	25	2360	6		2360					
Stirrups	51	6	1479	36	12.5	410	260	100	100		
Ends	21	25	969	6	87	430	246	430			
Links	99	6	460	36	12.5	260	100				
RC3 (300x600)											
Long.	OO	25	3160	8		3160					
Stirrups	51	6	1779	36	12.5	560	260	100	100		
Ends	21	25	1246	12	87	580	233	580			
Links	99	6	460	36	12.5	260	100				
RC4 (300x600)											
Long.	OO	25	3160	8		3160					
Stirrups	51	6	1779	36	12.5	560	260	100	100		
Ends	21	25	1246	12	87	580	233	580			
Links	99	6	460	36	12.5	260	100				
RC5 (300x750)											
Long.	OO	25	3710	10		3710					
Stirrups	51	6	1879	36	12.5	610	260	100	100		
Ends	21	25	1534	16	87	730	211	730			
Links	99	6	460	96	12.5	260	100				
RC6 (300x750)											
Long.	OO	25	3710	10		3710					
Stirrups	51	6	1879	36	12.5	610	260	100	100		
Ends	21	25	1534	16	87	730	211	730			
Links	99	6	460	96	12.5	260	100				
RE1 (300x600)											
Long.	OO	25	3160	8		3160					
Stirrups	51	6	1779	36	12.5	560	260	100	100		
Ends	21	25	1246	12	87	580	233	580			
Links	99	6	460	36	12.5	260	100				
RE2 (300x600 with corbel)											
Long.	OO	25	4160	4		4160					
Long.	OO	25	4136	4		4136					
Stirrups	51	6	2278	46	12.5	810	260	100	100		
Stirrups	51	6	2254	2	12.5	798	260	100	100		
Stirrups	51	6	2182	2	12.5	762	260	100	100		

BAR MARK	SHAPE CODE	SIZE	LENGTH	QUANTITY	R	A	B	C	D	E	F
		mm	mm		mm	mm	mm	mm	mm	mm	mm
Stirrups	51	6	2110	2	12.5	726	260	100	100		
Stirrups	51	6	2038	2	12.5	690	260	100	100		
Stirrups	51	6	1966	2	12.5	654	260	100	100		
Stirrups	51	6	1894	2	12.5	618	260	100	100		
Stirrups	51	6	1822	2	12.5	582	260	100	100		
Stirrups	51	6	1779	6	12.5	560	260	100	100		
Corbel	56	12	3858	12	24, 180 (D-A)	1320	798	819	841	100	100
Corbel	56	12	3798	4	24, 180 (D-A)	1320	773	819	806	100	100
Links	99	6	460	54	12.5	260	100				
RE3 (300x600)											
Long.	OO	25	3160	8		3160					
Stirrups	51	6	1779	36	12.5	560	260	100	100		
Ends	21	25	1246	12	87	580	233	580			
Links	99	6	460	36	12.5	260	100				
RE4 (300x600 with corbel)											
Long.	OO	25	4160	4		4160					
Long.	OO	25	4136	4		4136					
Stirrups	51	6	1798	64	12.5	570	560	100	100		
Stirrups	51	6	1788	2	12.5	565	560	100	100		
Stirrups	51	6	1750	2	12.5	546	560	100	100		
Stirrups	51	6	1710	2	12.5	526	560	100	100		
Stirrups	51	6	1672	2	12.5	507	560	100	100		
Stirrups	51	6	1632	2	12.5	487	560	100	100		
Stirrups	51	6	1594	2	12.5	468	560	100	100		
Stirrups	51	6	1554	2	12.5	448	560	100	100		
Stirrups	51	6	1516	2	12.5	429	560	100	100		
Stirrups	51	6	1476	2	12.5	409	560	100	100		
Stirrups	51	6	1438	2	12.5	390	560	100	100		
Stirrups	51	6	1398	2	12.5	370	560	100	100		
Stirrups	51	6	1360	2	12.5	351	560	100	100		
Stirrups	51	6	1320	2	12.5	331	560	100	100		
Stirrups	51	6	1282	2	12.5	312	560	100	100		
Stirrups	51	6	1242	2	12.5	292	560	100	100		
Stirrups	51	6	1204	2	12.5	273	560	100	100		

BAR MARK	SHAPE CODE	SIZE	LENGTH	QUANTITY	R	A	B	C	D	E	F
		mm	mm		mm	mm	mm	mm	mm	mm	mm
Stirrups	51	6	1779	6	12.5	260	560	100	100		
Corbel	56	12	3244	44	24, 65 (D-A)	1183	558	759	664	100	100
Corbel	56	12	3184	4	24, 65 (D-A)	1183	533	759	629	100	100
Links	99	6	460	116	12.5	260	100				

B-2 – FRP MATERIAL DATA SHEET

GRAFIL 34-700

Grafil 34-700 carbon fiber is a continuous, high strength, PAN based fiber. It is available in 12K and 24K filament count tows. They can be supplied in either round tow or flat tow formats. The flat tow (designated by 'WD') is the ideal fiber to use in applications where spreading is required, e.g., tape production. The round tow is used in applications where spreading is not necessarily required, e.g., braiding and weaving.

Typical Fiber Properties

Tow Tensile	Strength	700 4830	ksi MPa	SRM 16
	Modulus	34 234	msi GPa	
Typical Density		0.065 1.80	$lb.in^3$ g/cm^3	SRM 15
Typical Yield	12K	620 800	yds/lb mg/m	SRM 13
	24K	310 1600	yds/lb mg/m	SRM 13

Typical Mechanical Properties

Tensile Properties	0°	Strength	373 2572	ksi MPa	ASTM D3039 / 0°8ply
		Modulus	19.9 137	msi GPa	ASTM D3039 / 0°8ply
	90°	Strength	11.17 81	ksi MPa	ASTM D3039 / 0°16ply
		Modulus	1.34 9.2	msi GPa	ASTM D3039 / 0°16ply
Compressive Properties	0°	Strength	198 1365	ksi MPa	ASTM D3410 / 0°16ply
		Modulus	18.5 127	msi GPa	ASTM D3410 / 0°16ply
	90°	Strength	30.5 210	ksi MPa	ASTM D3410 / 0°20ply
		Modulus	1.49 10.2	msi GPa	ASTM D3410 / 0°20ply
Flexural Properties	0°	Strength	253 1745	ksi MPa	ASTM D790 / 0°16ply, L/D=32, Vf=61%
		Modulus	19.1 132	msi GPa	ASTM D790 / 0°16ply, L/D=32, Vf=61%
	90°	Strength	14.9 102	ksi MPa	ASTM D790 / 0°16ply, L/D=16, Vf=61%
		Modulus	1.28 8.8	msi GPa	ASTM D790 / 0°16ply, L/D=16, Vf=61%
ILSS	Strength		14.1 97	ksi GPa	ASTM D2344 / 0°16ply, L/D=4, Vf=59%

- 250F Epoxy Prepregs
- Resin: Mitsubishi Rayon #340 resin system
- Tensile and compressive properties are normalized to 60% fiber volume

5900 88th Street
Sacramento, CA
95828, USA
Tel: 916.386.1733
Fax: 916.383.7668
Web: www.grafil.com

ISO 9001:2000
FM 56416

APPENDIX C – ANALYTICAL MODEL

CONTENTS: C-1 – ANALYTICAL MODEL CALCULATIONS – CONCENTRIC LOADING

C-2 – ANALYTICAL MODEL CALCULATIONS – ECCENTRIC LOADING

C-1 – ANALYTICAL MODEL CALCULATIONS – CONCENTRIC LOADING

CONCENTRIC LOADING – PAGE 1 OF 2

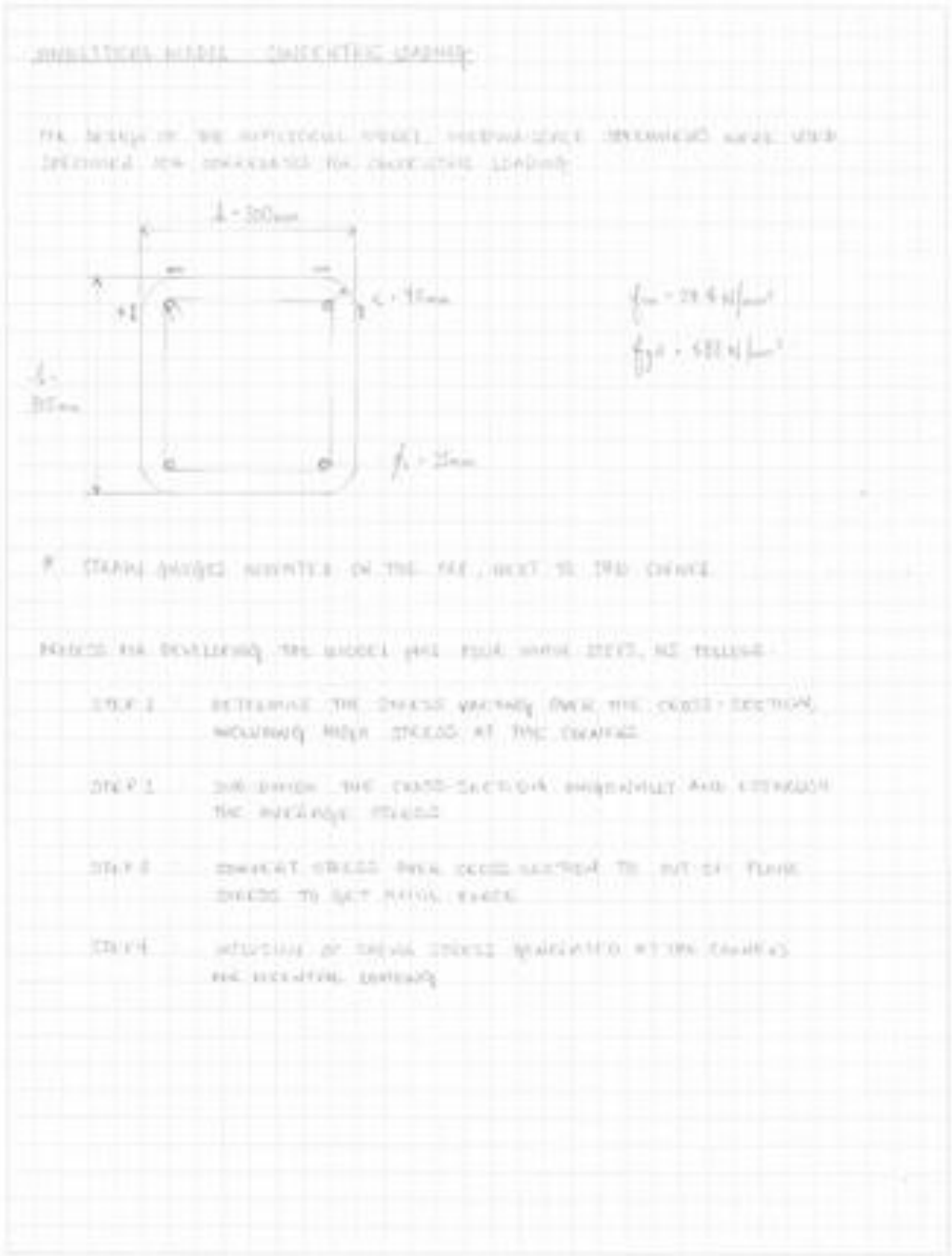

CONCENTRIC LOADING – PAGE 2 OF 2

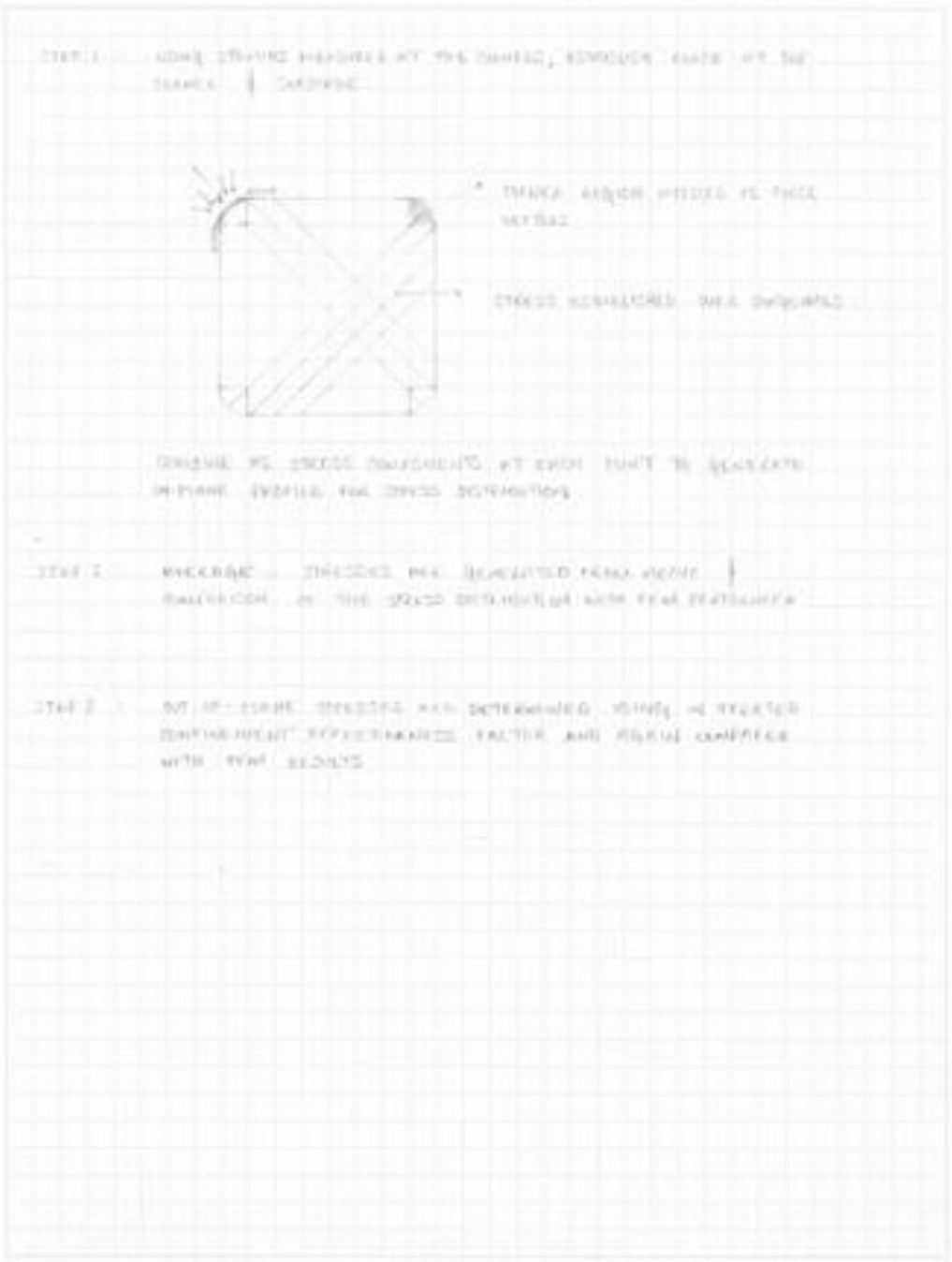

C-2 – ANALYTICAL MODEL CALCULATIONS – ECCENTRIC LOADING

ECCENTRIC LOADING – PAGE 1 OF 1

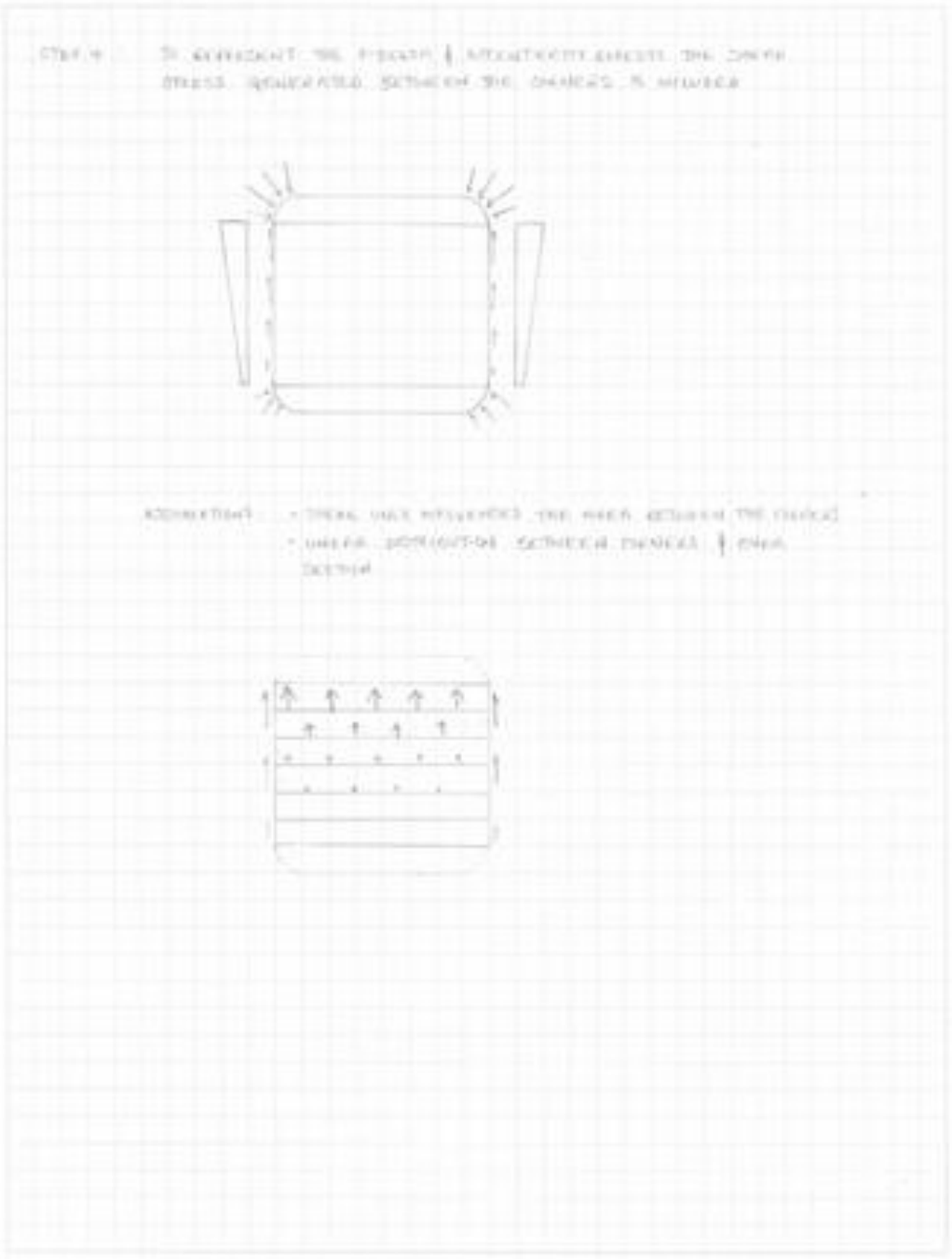

[BLANK PAGE]